UNIVERSITY OF SOUTHAMPTON

FACULTY OF SOCIAL AND HUMAN SCIENCES

School of Geography

Forecasting of Ocean State in a Complex Estuarine Environment: the Solent-Southampton Water Estuarine System

by

Niall Quinn

Thesis for the degree of Doctor of Philosophy

September 2012

UNIVERSITY OF SOUTHAMPTON

FACULTY OF SOCIAL AND HUMAN SCIENCES

SCHOOL OF GEOGRAPHY

ABSTRACT

Doctor of Philosophy

FORECASTING OF OCEAN STATE IN A COMPLEX ESTUARINE ENVIRONMENT: THE SOLENT-SOUTHAMPTON WATER ESTUARINE SYSTEM

By Niall Quinn

Coastal flooding is a natural hazard causing devastation to many regions throughout the world, induced by the coincidence of high spring tides, large storm surges and waves. To reduce the risk posed by coastal inundation, warning systems have been developed to enable preparations to an expected threat. Although current operational predictions provide invaluable warnings, uncertainty in model formulations and input datasets, can lead to errors in forecasts. In order to provide coastal managers with the best possible information with which to make decisions, recent research has begun to focus on the movement from deterministic to probabilistic forecasting, which aims to explicitly account for uncertainty in the system.

This research described the implementation of a regional tide-surge-wave model for the Solent-Southampton Water estuarine system, a region that is likely to experience increased risk of coastal flooding in the coming century. The accuracy of the model predictions were examined relative to *in-situ* measurements and those obtained from independent systems. Using the model, sources of error were examined and their effects upon the model predictions quantified, with particular reference made to the spatial variability throughout the region. In light of recent research, a probabilistic modelling approach, utilising a Monte Carlo technique used to provide a forecast capable of representing the uncertainty in the system, within a suitable time-frame for real-time flood forecasting that included an hourly Kalman filter data assimilation update.

The findings presented in this thesis will be of interest to coastal modellers working in complex estuarine environments where the influences of tide-surge-wave interactions upon model predictions are uncertain. Furthermore, the application of a computationally efficient model, presented here, will provide a useful comparison with traditional physically-based systems to those wishing to quantify uncertainty in regions where computational resources are low.

Contents

Figures

Tables

Declaration of Authorship

I, Niall Quinn

declare that this thesis and the work presented in it are my own and has been generated by me as the result of my own original research.

Forecasting of Ocean State in a Complex Estuarine Environment: the Solent-Southampton Water Estuarine System

I confirm that:

1. This work was done wholly or mainly while in candidature for a research degree at this University;

2. Where any part of this thesis has previously been submitted for a degree or any other qualification at this University or any other institution, this has been clearly stated;

3. Where I have consulted the published work of others, this is always clearly attributed;

4. Where I have quoted from the work of others, the source is always given. With the exception of such quotations, this thesis is entirely my own work;

5. I have acknowledged all main sources of help;

6. Where the thesis is based on work done by myself jointly with others, I have made clear exactly what was done by others and what I have contributed myself;

7. Either none of this work has been published before submission, or parts of this work have been published as: [please list references below]:

Signed:

Date:

Acknowledgments

I would like to thank my supervisors Prof. Peter Atkinson and Dr. Neil Wells for giving me the opportunity to work on this project, and also for their guidance, support and encouragement throughout. Thanks are also due to external contacts that have provided invaluable advice, particularly, the GEODATA group, Tammy Palmer, Ivan Haigh, Jeff Neal, Matt Wadey, Pierre Cazenave, Julian Leyland and various others I have met along the way.

This research was funded by EU Programme FP7-223913 "Semantic Sensor Grids for Rapid Application Development for Environmental Management" and Geography and Environment, University of Southampton, without which I would not have had this opportunity.

Thanks to all those who provided data and equipment for this research. In particular, Sam Roe and Robin Newman at EMU for the provision of the three buoys, Justin Dix for the bathymetry datasets, Andrew Saulter at the Met Office and Fabrice Lecornu at Previmer for the oceanographic and atmospheric datasets that were central to this research, and Simon Matthews at DHI for supplying the MIKE-21 software.

Thanks to all the other postgrads, particularly Mike, Booker, Niladri, Shawky and Hassan for the welcome (and often entertaining) stories during breaks from work, and all my other friends who have supported me through the last few years. Special thanks must be given to Kim and John who have been so supportive, especially through the final year, and of course my family who have generously helped me keep a roof over my head between the end of the funding period and the time I entered the "real" world.

Definitions and Abbreviations

ADCIRC	Advanced CIRCulation model
ANN	Artificial Neural Network
CCO	Channel Coastal Observatory
CEFAS	Centre for Environment, Fisheries and Aquaculture Science
CFL	Courant-Friedrich-Lévy
COAMPS	Coupled Ocean / Atmospheric Mesoscale Prediction System
DEFRA	Department for Environment Food and Rural Affairs
DHI	Danish Hydraulic Institute
DIA	Discrete Interaction Approximation
DIOPS	Distributed Integrated Ocean Predictions System
ECMWF	European Centre for Medium Range Weather Forecasts
ERS-2	European Remote Sensing satellite 2
FEMA	Federal Emergency Management Agency
IFREMER	Institut francais de recherché pour l'exploitation de la mer (French Research Institute for Exploitation of the Sea)
Lat.	Latitude
Long.	Longitude
MARS 2D	Model for Application at Regional Scale
MECO	Model of Estuaries and Coastal Oceans
MIKE-21 HD	MIKE-21 Hydrodynamics
MIKE-21 SW	MIKE-21 Spectral Waves
MNR	Mean Neap Range
MSR	Mean Spring Range
NOAA	The National Oceanic and Atmospheric Administration
NTSLF	National Tidal and Sea Level Facility
OD	Ordnance Datum
Pbias	Percentage Bias
POL	Proudman Oceanographic Laboratory
POLCOMS	Proudman Oceanographic Laboratory Coastal Ocean Modelling System
RMSE	Root Mean Squared Error
SAR	Synthetic Apeture Radar
SEASAT	Sea Satellite (NASA)
SHOM	Institutionnel du Service Hydrographique et Oceanographique de la Marine. (Instituational Hydrographic and Oceanographic Service of the Navy).

SI	Scatter Index
SWAN	Simulating WAves Nearshore
TGF	Tide generating force
TOPEX	TOPography Experiment (sometimes referred to as Poseidon)
WAM	Wave Action Model

Notations

Term	Description
A	Accuracy
a_h	Orbital discplacement
A_{ev}	Sub-grid scale horizontal eddy viscosity
B	Triad interaction coefficient parameter
B_F	n by 1 matrix relating the forcing term to the state vector
B_S	n by n state transition matrix associated with the forecasted state vector
c	Wave phase speed
C	Wave group phase speed
c_a, c_b, w_a, w_b	Wind stress empirical factors
c_d	Wind drag coefficient
c_{deep}	Deep water wave phase speed
C_{ds}	Whitecapping constant
c_f	Bottom stress drag coefficient
C_f	Bottom friction coefficient
CFL_{HD}	Courant-Friedrich-Lévy (CFL) number (HD model)
c_{la}	Linear wave growth constant
C_{nl}	Quadruplet interaction constant
c_{rand}	Random wave phase
Cr_{SW}	Courant-Friedrich-Lévy (CFL) number (SW model)
c_s	Smagorinsky constant
$c_{shallow}$	Shallow water wave phase speed
d	Water depth (still)
E	Energy density
ε	Ratio of density of air to water
e_f	Forecast error
e_o	Observed error
E_{tot}	Total wave energy
f	Frequency
F	Attractive force between two bodies
f_c	Friction coefficient for the current
f_{cor}	Coriolis parameter
f_w	Friction factor constant
g	Acceleration due to gravity
h	Total water depth
H	m by n measurement operator
H_m	Maximum wave height
H_s	Significant wave height
I	Identity matrix
J	Triad interaction parameter
k	Wave number
K	Kalman Gain

k_N	Gemoetric roughness size
I	Characteristic length
M	Manning number
m	Whitecapping constant
N	Action density
η	Surface elevation
O	Body of mass
O_m^M	Mass of the Moon
O_m^E	Mass of the Earth
O_r^E	Radius of the Earth
p_a	Atmospheric pressure
P_f	Covariance in the forecast error
P_o	Covaraince in the observed error
Q	n by n process noise covariance matrix describing system state errors
Q_b	Fraction of breaking waves
R	Distance between two bodies
S	Source term to the energy balance equation
$S_{d\ ij}$	Deformation rate
$S_{in,}\ S_{nl}, S_{ds,}\ S_{bot,}\ S_{surf}$	Source terms to the energy balance due to wind input, nonlinear interactions, whitecapping dissipation, bottom friction dissipation, breaking dissipation
S_m	Magnitude of discharge to point sources
S_s	Significant steepness
$S_{xy}, s_{xx}, s_{yx,}\ s_{yy}$	Radiation stress tensor components
t	Time
T_{xx}, T_{xy}, T_{yy}	Lateral stresses
T_z	Mean Period
u_*	Wind friction velocity
u, v, w	Velocity components of x, y, z directions
u_b	Flow velocity at the bottom
u_F	KF forcing term
$u_{s,}\ v_s$	Velocity of discharge into ambient water
u_w	Wind speed above the surface
u_{wb}	Rms wave orbital velocity
U_{T_b}	Friction velocity associated with bottom stress
U_{T_s}	Friction velocity associated with the surface stress
V	Variance
W	Work done (rate of energy input)
X	Ratio of the total energy in the random wave train to the energy in a wave train with the maximum possible wave height
X_a	Analysed (best guess) state
X_f	Forecasted state

x_{nl}	Nonlinear wave growth parameter
X_o	Observed state
X_t	True state
Y	Regression dependant variable
y'	Nonlinear wave growth
y'_{di}	Breaking parameter
Y_i	Regression independent variable
Z_0	Reference water level, often given as the difference between mean sea level and chart datum
z_c	Critical height
α	Linear wave growth
$\hat{\alpha}$	Overall wave steepness
α_{BJ}	Breaking constant
α_{drag}	Friction velocity constant
α_{EB}	Triad tuning parameter
β	Non-linear wave growth parameter
β_0	Regression constant
β_{drag}	Friction velocity constant
β_s	Regression slope of the independent variable
β_{tri}	Non-linear triad interaction parameter
δ	Whitecapping constant
ζ	Tidal elevation
θ	Direction
θ_a	Angle between wind direction and wave travel direction
$\theta_{E,M}$	Angle between the line joining the centre of the Earth and the Moon and the radius vector from Earth's centre to the point on the surface
θ_w	Wind direction
κ	Von Karman's constant
λ	Longitude
μ	Dimensionless critical height
ρ	Density of water
ρ_0	Reference density of water
ρ_a	Density of air
σ	Relative angular frequency
σ_{PM}	Pierson-Moskowitz frequency
τ_b	Bottom stress
τ_s	Surface wind stress
ϕ	Constituent phase relative to lunar transit of the equilibrium tide
ϕ	Latitude
ϕ^L	Phase lag of the real tide to the equilibrium tide
ω	Absolute angular frequency
Δk	Interaction phase space element
∇	Four dimensional differential operator

Chapter 1: Introduction

1.1. Background

1.1.1. The coastal flooding hazard: Causes and consequences

Coastal flooding due to extreme sea level events is a natural disaster affecting coastal communities all over the world. The costs, in terms of monetary loss and human casualties, can be devastating, killing thousands annually. For instance, The National Oceanic and Atmospheric Administration (NOAA, http://www.nhc.noaa.gov/surge/#FACTS) highlight a selection of significant inundation events impacting the USA since 1900, in most of which damage into the billions was estimated (Table 1.1). Notable examples include hurricane Ike in 2008, which led to surges of up to six meters devastating the Boliver Peninsula of Texas, and the Galvestone hurricane (1900) in which storm surge inundation was estimated to be responsible for 8,000 deaths. Hurricane Katrina in 2005 created storm surges of up to six meters, causing destruction along the Mississippi coast and the south-eastern region of Louisiana, while breaching and overtopping of levees in the New Orleans metropolitan area inundated much of the city and its eastern suburbs. Similarly, other regions, such as the Bay of Bengal, consistently suffer from storm induced coastal flooding. In just two events occurring in 1970 and 1991, 300,000 and 140,000 people, respectively, were killed (Flather, 1994).

Table 1.1. Significant storm surge events since 1900 impacting America (NOAA, http://www.nhc.noaa.gov/surge/#FACTS)*

Event	Ike	Katrina	Dennis	Isabel	Opal	Hugo	Camille	Audrey	New England	Galvestone
Date	2008	2005	2005	2003	1995	1989	1969	1957	1938	1900
Costs ($US billion)	19.3	75	2.2	3	3	8	1.4	0.15	0.31	0.3
Deaths	48	1200	42	17	50	45	256	390	600	8000

*Values given represent damages for the given hurricane event, however, in each event the storm surge was recognised as the primary hazard.

The occurrence of coastal flooding is a natural process. Where the coast is uninhabited, this is often not considered a problem. However, large urban centres and important infrastructures, such as oil refineries and nuclear power stations, are often located in coastal regions (Stern, 2007). Large flooding events in such regions can be disastrous (Smith and Ward, 1998). It is for this reason that flood risk is often defined as the product of the probability of a given flood event and the consequential damage; highlighting that there is an important human element involved (Hall *et al.*, 2006). In their study, Zang and Tooley (2003) remarked how recent land reclamation in the south east of the UK, and rapid coastal settlement developments in the south west, have led to greater risk from coastal inundation, relative to the west, which has seen less extensive development. Unfortunately, coastal areas worldwide represent some of the most densely populated regions, putting many at risk from flooding. From 1990–2008, population density increased by 32% in Gulf coastal counties of America, while half of the United States economic productivity is located within coastal zones (NOAA, http://www.nhc.noaa.gov/surge/#FACTS). Stern (2007) suggests that over 200 million people live in coastal floodplains, while two million km^2 of land and one trillion dollars' worth of assets lie less than 1 m elevation above current sea level. Furthermore, the fastest growing populations in less developed countries show very strong migratory tendencies towards coastal plain cities (Spencer and French, 1993; Hunt, 2005).

The sea conditions required to inundate an area of coast will be conditional on the form of the coast as well as any defences that may be in place. The level of the sea at a given location is conditioned by the combination of the mean sea level, tides, wave conditions and the presence of storm surges (Inter Agency Committee on Marine Science and Technology 2004). The coincidence of storm surges and high tides, together with a strong onshore wind, can raise the local sea elevation above the high tide level, leading to overtopping of defences (Zang and Tooley 2003, Hunt 2005). The difference in the two high water levels is referred to as the 'skew-surge' (Brown and Wolf 2009; Royston *et al.*, 2012).

In many regions, where the tidal range represents the largest contributor to the water surface elevations, the presence of high spring tides can be fundamental in the occurrence of coastal inundation. Tides occur daily as a result of the gravitational attraction between the Earth, Moon and Sun (Thurman, 1988; Kantha and Clayson, 2000). Spring tides are those generated when the tide generating forces of the Sun and the Moon are acting in the same direction and the solar and lunar equilibrium tides coincide, causing very large tidal ranges.

A storm surge, associated with local low pressure systems and the force of high winds upon the ocean surface, can cause further localised heightening of the sea level (Thurman, 1988). Surge magnitudes are affected by the size and track of the storm, proximity to the coast, and wind fetch and direction which push the surge up onto the

coast (Open University, 1989). In addition, in enclosed areas, the basin shape and the nearshore bathymetry can be very influential upon the surge characteristics of the surge experienced in a coastal region (Zang and Tooley, 2003).

Where strong winds blowing over a long fetch are present, large waves can be created, increasing the likelihood of flooding at the coasts (Zang and Tooley, 2003; Hunt, 2005). Waves not only increase the local sea surface height but are also the primary suppliers of energy to the coast (Battjes, 2006). The energy contained within a wave breaking upon the coast is substantial, increasing the risk of flooding through the destruction of coastal defences, especially where sea levels are high enough to enable the waves to overtop defences, thereby attacking the rear face and increasing the likelihood of failure (Wolf and Flather, 2005).

The extreme risk posed to many regions, such as the Bay of Bengal, is generally not found in the UK, however, coastal inundation still poses a very serious threat to many coastal populations. For instance, it is estimated that in the UK, 5 million people and 1.85 million homes are at risk from coastal flooding (Penning-Rowsell *et al.*, 2006); while over 60% of grade I agricultural lands in the South lie below +5m Ordnance Datum (OD), yet the mean high water level in many areas is +5 m OD. In England and Wales, the expected annual damage due to coastal flooding is expected to increase to between £1.0 and £13.5 billion by 2100 (Hall *et al.*, 2010). Although rare, significant loss of life has occurred, most notably during the storm surge event of 1953 in which 307 and 1836 people died in the UK and Netherlands, respectively (Gerritsen, 2005; Wolf and Flather, 2005). Exceptionally strong winds over the North Sea created the surge which funnelled down into the southern North Sea, impacting much of eastern UK, raising sea levels more than 2.5 m (Gerritsen, 2005), in addition to the 3 m increase caused by the presence of spring tides. 150 defences were broken and over 100,000 people needed to be evacuated. Zang and Tooley (2003) suggest 24,000 homes and 200,000 acres of farmland were destroyed causing an equivalent of £5billion in damages (today's equivalent).

Due to the high value of assets at risk and the large scale disruption caused by coastal floods, the government invests a large amount of money in coastal management. Between 2001 and 2006, investment into flood defences rose from £303million to £550million (House of Commons, 2007), with a further £5billion allocated for investment over the subsequent 15 years (DEFRA, 2004). In their most recent report (Environment Agency, 2009a) the Environment Agency suggested that investment will need to increase to more than £1 billion per year by 2035 for building and maintaining new and existing flood and coastal risk management assets.

1.1.2. Reducing vulnerability: Forecasting

Due to the risks posed by coastal inundation, many regions throughout the world have attempted to increase their resilience through the implementation of warning systems. The ability to prepare for a severe flooding event can be vital in the prevention of loss of life and reduction to property damage. Forecasting systems often contain a suite of coupled models, linking predictions of atmospheric, hydrodynamic and wave conditions, for example, see Allard *et al*. (2008). Typically, the models used in ocean forecasts are of two varieties, empirical or physically-based numerical models, while some forecasting systems may contain components of both.

Physically-based modelling strategies have become widely utilised in operational forecasting systems. As the name suggests, these models aim to model explicitly the physics of the natural processes of interest, commonly over a computational mesh. Flather (2000) provides an assessment of the operational forecasting systems across Europe, all of which are based predominantly on the use of distributed physically-based models in which atmospheric predictions drive hydrodynamic and spectral wave model components. Numerous physically-based modelling software packages are available. Wavewatch III (Tolman, 2009) and Simulating WAves Nearshore (SWAN, Booij *et al*., 1999) for instance, are commonly utilised spectral wave models, while MIKE-21 (Warren and Bach, 1992) and ADCIRC (Luettich and Westerink, 2004) are two of the most well-known hydrodynamic model packages. Although some formulation differences will be present between the various models, most are based upon the same fundamental principles. Most commonly used wave models attempt to propagate wave energy across the computational domain in the form of an energy spectrum, which grows and decays in response to changes in the wind field (Liu *et al*., 2002). Similarly, two-dimensional (2D) hydrodynamic models attempt to propagate a boundary elevation fluctuation through the computational domain using vertically integrated, fully dynamic equations of continuity and conservation of momentum, based upon the numerical solution of the two-dimensional incompressible Reynolds averaged Navier-Stokes equations (Cañizares *et al*., 2001).

The use of physically-based numerical models has become extremely popular in recent years due to advances in computational resources and the ability to provide forecasts over large domains. This is particularly important in many nearshore regions as the variables of interest (e.g. currents, wave fields) often contain a high degree of variability (Bolanos and Sanchez-Arcilla, 2006). Furthermore, once constructed, the model can be utilised to provide 'what-if' assessments. However, large costs in terms of input datasets (e.g. high resolution bathymetric maps) and computational resources, often not widely available, are required where such models need to be utilised (Logemann *et al*., 2004).

Empirical models (sometimes referred to as statistical models) do not attempt to model real world processes. Instead, a relationship between a dependent variable and a set of independent variables is established. When producing the empirical model, the dependent variable usually represents the process one wishes to model (for instance, the wave height at a given location) and is represented by a measured dataset. Alternatively, the independent variable(s) represent the input datasets (for example, the forecasted local wind velocity will often be influential to the wave conditions experienced in a region). A variety of empirically-based forecasting tools have been developed, for instance see Deo and Naidu (1999); Cox *et al*. (2002); Sfetsos (2002); Bazartseren *et al*. (2003); Huang *et al*. (2003); Steidley *et al*. (2003); Kobayashi and Yasuda (2004); and Prouty (2007). Although the way in which the models map the transition from the independent variables to the dependent variable may vary between methods, for example Prouty (2007) utilised an artificial neural network approach (ANN), while Kobayashi and Yasuda (2004) used multiple regression, the underlying basis remains the same.

The relative simplicity of empirical approaches provides some potential benefits, relative to physical-based numerical models. Most notably, the computational demands from empirical models, typically, are significantly lower, as are the requirements for extensive amounts of data. This may be an important factor in resource-poor areas as, often, it is the regions where large computational and data resources are not available that are most in need of forecasting tools (Tilberg and Garvine, 2004). Kobayashi and Yasuda (2004) suggest that in some instances, such as when modelling very uncertain regions, empirical-based approaches may provide more accurate predictions due to their ability to create a direct cause – effect relationship between the independent and dependent variables, whereas a physical-based numerical model may use formulations or parameters that are not certain for those conditions. However, many empirical methods, typically, are designed to provide a forecast at a given location, where dependent variable measurements can be obtained. Therefore, uncertainty may arise when forecasts are required at un-gauged locations, given the complexity of many nearshore regions. Furthermore, empirical model quality is conditioned upon the quality and length of the datasets used to define them. Therefore, considerable time-series of measurements, including periods of particular interest (e.g. extreme events) are essential in creating a useful forecasting tool.

All model predictions will contain inherent uncertainty as no model of the real world is perfect (Maybeck, 1979). Model processes and structures are simplifications of an unknown reality, which has only been partially sampled by measured data, which themselves contain errors (Neal, 2007) and, therefore, can only be regarded as approximations of the truth (Kantha and Clayson, 2000). Errors may be introduced into most model predictions through a variety of sources, such as inaccurate estimations of

initial conditions, inaccurate forcing datasets (Kantha and Clayson, 2000), and a lack of complete knowledge of the system, leading to uncertainty in the ability to describe fully its physical properties (Madsen and Canizares, 1999). For instance, it is recognised widely that the prediction of tidal elevations from physically-based numerical models become increasingly uncertain in complex nearshore regions, leading to the use of harmonic analysis-based predictions in their place (Flowerdew *et al.*, 2007; Bocquet *et al.*, 2009; Hawkes *et al.*, 2009). Similarly, various authors have reported that commonly used spectral wave models tend to over-predict wave heights, while under-predicting periods, due to an over-prediction of the high frequency energy, particularly in shallow, short fetch areas (Ris *et al.*, 1999; Rogers *et al.*, 2002). Uncertainty in one component of a forecasting system can propagate through the model chain, reducing the reliability of a given prediction. For this reason, acknowledging uncertainty, and quantifying it, is an essential component of any prediction system.

1.1.3. Uncertainty: Probabilistic modelling and data assimilation

Uncertainty is a crucial factor in the provision of forecasts for coastal flooding. In order for coastal managers to make informed decisions they require information pertaining to the likelihood of a given event occurring, within a time frame that allows for action to be taken. The presence of uncertainty clearly inhibits this goal from being reached. It is for this reason that recent research has highlighted a desire to quantify and constrain uncertainty in model forecasts (Bocquet *et al.*, 2009).

The movement from deterministic to probabilistic forecasts is a key way in which one can attempt to quantify the uncertainty within a model forecast. A probabilistic forecast provides an ensemble of predictions, by sampling from an estimated uncertainty distribution for a given variable (most commonly given as the uncertainty within the input variables such as wind velocity), often using a Monte Carlo approach (Hammersley and Handscomb, 1964). Providing the uncertainty distributions are representative of the errors influential to the forecast, the resulting ensemble mean can be given as the 'best guess', while the ensemble spread can be used to provide valuable information, such as the magnitude of variance and the uncertainty in the forecast. This can also be essential in predicting low likelihood events that a deterministic approach might miss.

Data assimilation techniques, commonly used in atmospheric predictions, have recently been introduced into oceanographic systems in an attempt to increase the accuracy and reduce the uncertainty in forecasts (Kantha and Clayson, 2000). Data assimilation is a technique in which modelled and observed data are integrated in an optimal way taking into account uncertainty in both (Prandle, 2000) such as to reduce forecast error (de las Heras *et al.*, 1995). In the context of surge and wave forecasting,

a 'filtering' assimilation approach is most commonly used, in which an update is applied to the independent variable estimates to increase the accuracy of the datasets used to force the model (Mclaughlin, 2002). Alternatively, the prediction of the dependent variable can be updated to provide more accurate initial conditions for subsequent forecasts. A variety of data assimilation approaches have been utilised, for instance Miller (1985), Voorrips (1999) and Greenslade (2001) outline the use of optimal interpolation techniques which employ a relatively straightforward sequential methodology, while de las Heras *et al*. (1995) used an adjoint method. Siddons *et al*. (2008) provides a useful comparison between a variety of assimilation techniques used to integrate real-time radar based wave measurements into the SWAN nearshore wave model. The Kalman filter (Kalman, 1960), and more recent extensions of it (such as the ensemble Kalman filter, Evensen, 2003), is a particularly well established approach to data assimilation (Madsen and Canizares, 1999). It enables the optimal estimation of the state of a system that has a minimum error variance, considering both a predicted and measured value, and their respective uncertainties (Kantha and Clayson, 2000).

1.1.4. The Solent-Southampton Water estuarine system

The Solent lies between the south coast of England and the Isle of Wight, in the UK. It includes 12 separately defined estuaries and harbours, a high degree of spatial variability in water depths, ranging from artificially deepened channels for shipping, to inter-tidal mudflats, and contains a wide range of coastal habitats (Fletcher *et al.*, 2007). The region has various stakeholders, including protected habitats, a dense coastal population and two of the largest shipping ports in the UK.

The tidal hydrodynamics in the region are unique. The irregular geometrical shape, narrow channel configuration and shallow depth of the estuary results in an amplification of the shallow water tidal constituents, M_4 and M_6 ,creating a tidal elevation with a double high water and young flood stand, most prominent in the Southampton Water region (Rantzen, 1969; Levasseur, 2008).

Storm surges in this region most frequently occur due to low pressure systems from the Atlantic propagating eastwards, or as a result of surges propagating south from the North Sea (Law, 1975; Haigh *et al*., 2004). The region is prone to coastal flooding, with 2 particularly large events occurring between the 14th and 18th of December 1989 (Wells *et al*., 2001; Ruocco *et al*., 2011) and on the 10th March 2008 (Haigh *et al*., 2010).On average the region is flooded (defined as requiring significant pumping and affecting more than 15 properties) approximately every 2 years, for instance, between 1935 and 2005 34 events were recorded at Portsmouth (Ruocco *et al*., 2011).

A high degree of spatial variability exists in the region's exposure to storm waves. Much of the Solent, particularly the west and Southampton Water regions, are

protected from extreme wave events by the Isle of Wight and Hurst Spit. The greatest risk is found in the eastern Solent, which can be affected by large swells propagating through the English Channel. The Channel Coastal Observatory (CCO, http://www.channelcoast.org/) considers the region to have low-to-medium exposure to waves.

Due to the variety of nearshore conditions, the spatial variability in the exposure to extreme wave events, and the complexity of the tidal hydrodynamics, the Solent provides an interesting setting in which to investigate the accuracy of model predictions and model sensitivity to data uncertainty. Furthermore, the dense distribution of *in-situ* measurements enables the accuracy of predictions to be assessed throughout the region, while also providing measurements for updating using data assimilation.

1.2. Aims and objectives of this research

The wider contextual aim of this research was to provide a regional tide-surge-wave model for the provision of real-time probabilistic forecasts through the transformation of Mid-Channel forecasts to the nearshore regions of the Solent.

The more specific research objectives were to:

1. Assess the accuracy of a regional model for the prediction of tide, surge and wave states in the Solent-Southampton Water estuarine system, examining the spatial variability in accuracy across the domain.
2. Quantify the uncertainty in the wind field and boundary condition input datasets used to force the regional model, and assess the sensitivity of the model predictions to them.
3. Examine the influence of tide-surge-wave interactions upon the model predictions, particularly during storm conditions, examining the conditions under which the interactions are likely to be of greatest significance.
4. Develop a computationally efficient approach to the transformation of mid-channel ocean states to the Solent coastline, contrasting predictions accuracies and computational demands with those associated with the regional model developed using the MIKE-21 software.
5. Investigate the degree to which uncertainty in the model predictions can be quantified and reduced through the use of a Monte Carlo-based approach to probabilistic modelling, and the assimilation of *in-situ* measurements using the Kalman filter.

The aims and objectives presented coincide with current research interests in operational forecasting, particularly, the importance of signal interactions in complex

estuarine environments where model predictions are inherently uncertain, and the desire to move towards probabilistic modelling strategies in an attempt to quantify uncertainty in forecasts.

1.3. Chapter Overview

Chapter two reviews the relevant literature relating to the prediction of ocean states, expanding upon the concepts highlighted in the introduction. The important physical processes of wave, tide and surge generation, propagation and dissipation are discussed. The forecasting of the ocean using physical and empirical techniques are highlighted with particular detail given to MIKE-21, regression based modelling and the Kalman filter.

Chapter three provides an assessment of the spatial variability in the sensitivity of the wave and surge predictions to the local wind stress and boundary condition datasets provided by the Previmer system, a pre-operational hydrodynamic and spectral wave modelling system, currently under development, which aims to provide users with short-term forecasts of ocean state through the English Channel (http://www.previmer.org/en.). The Previmer datasets are contrasted with those from another operational system and the influence of the divergence within the datasets, upon the regional model predictions, is examined.

Chapter four assesses accuracy of the regional model predictions of tide and surge elevations in the Solent, contrasting its accuracies with those from operational forecasts. The tide-surge interactions are examined and the uncertainty in the surge prediction due to the errors in the modelled tidal amplitudes is quantified.

Chapter five assesses the accuracy of the regional model wave predictions throughout the domain. The accuracy of the predictions is contrasted with those expected from other systems. The sensitivity of the predictions to uncertainty in the modelled water levels, and the sensitivity of the surge prediction to the inclusion of the waves during storm events are examined. The spatial variability in prediction accuracy and the significance of wave-water level coupling is quantified.

Chapter six contrasts predictions from the MIKE-21-bassed regional model described in the previous chapters with those obtained using a computationally efficient empirical model, considering the prediction accuracy and computational demands. The empirical model is used to demonstrate how a probabilistic prediction and data assimilation scheme can be used to quantify and reduce uncertainty in the model predictions, providing valuable information to coastal managers interested in real-time forecasting.

Chapter seven provides a discussion of the research findings and highlights future research that could be conducted to extend the work in the thesis.

Chapter eight highlights the main conclusions that can be drawn from the research conducted.

Chapter 2: Literature review

2.1. Ocean waves

Waves are the most recognisable features in the ocean. They are the undulatory motion of the water surface, transporting energy over large distances without significant movement to the water particles themselves, which move in circular orbits. A wave form propagates after an initial energy source displaces water particles from their equilibrium position providing a source of potential energy. A restoring force (gravity) then returns the particle to its original position, producing kinetic energy (Knauss, 1996). The kinetic energy of the returning particle provides the displacement energy acting on the next water particle, therefore, producing a means of energy propagation without significant water movement.

Ocean waves are most commonly described using the idealised progressive sinusoidal wave form given in Fig. 2.1.

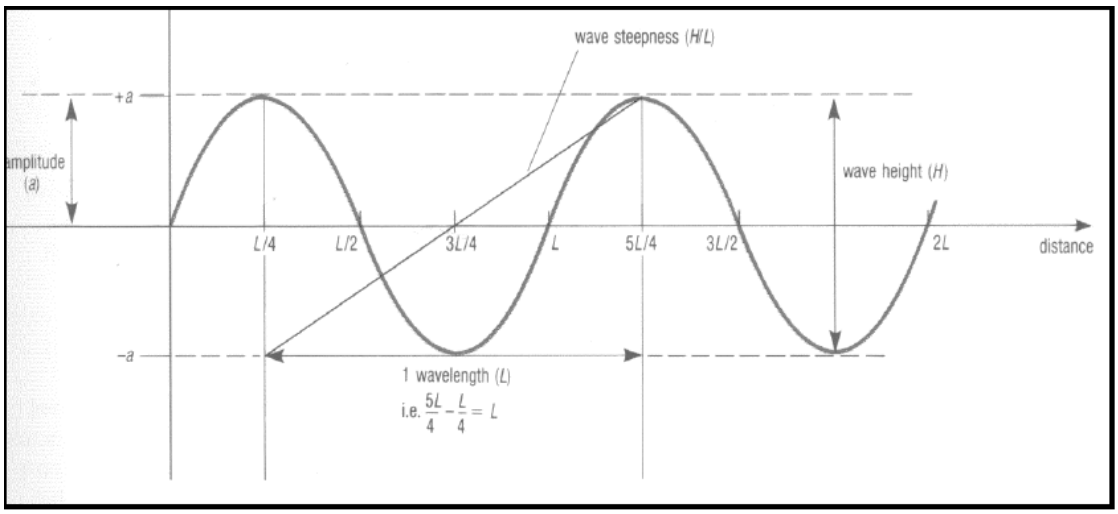

Fig. 2.1. Wave characteristics. Open University (1989). Where wave height (*H*) is the overall vertical change in height between crest and trough. This is twice the amplitude (*a*). Wavelength (*L*) is the distance between successive peaks, and steepness is defined as the height divided by wavelength. Frequency (*f*) is the number of peaks passing a fixed point per second.

Ocean waves can display a wide range of sizes and speeds. For instance, capillary waves usually contain periods (the time taken to be moved through one wavelength) of less and half a second and amplitudes of less than 1 cm, while tidal waves have periods of several hours and amplitudes can be more than 10 m. Waves can be

categorized broadly by the generating force acting upon them and their magnitudes. Wind waves (described in more detail in Section 2.1.1) are those obtaining energy from the wind blowing over the ocean surface, while tides (Section 2.1.2) contain an astronomical forcing from the moon and the sun, and surges (Section 2.1.3) are casued by the combination of local atmospheric pressure changes and wind stress.

2.1.1. Wind generated waves

Wind generated surface waves can contribute significantly to the risk of coastal inundation as they can overtop and weaken defensive structures, and contribute to the alteration of local sea levels, particularly during storm events. Surface waves occur at the air-ocean interface due to the influence of wind moving over the ocean at a differing speed to that of the water, thus creating a frictional stress as well as the direct push upon an existing wave moving at a slower speed to that of the wind (Kinsman, 1965). This results in the displacement of a water particle from its equilibrium position (providing it with potential energy required for the generation of wave motion). Typical wind waves can vary in size drastically from location to location depending upon the wind speed, the length of time the wind has been blowing and the distance of unobstructed sea available for build-up (Open University, 1989). At the Channel Lightvessel, situated in the central English Channel, wind wave periods typically less than a few minutes while wave heights can be exceed 10 m. The ocean surface consists of a vast array of waves, each with characteristics shaped by the winds from which they derived their energy.

2.1.1.1. Wave growth and propagation

Wave growth from initial surface ripples is complex and numerous mechanisms have been proposed to describe it (WISE group, 2007). A commonly used mechanism is the ‘resonance mechanism’ of Phillips (1957) and the ‘feedback mechanism’ of Miles (1957) which together highlight that growth occurs in both linear and exponential forms (Rogers *et al.*, 2002). The resonance mechanism states that wind blowing over the sea produces harmonic pressure waves that propagate at wind speed (WISE group, 2007). Where this pressure wave remains in phase with a surface wave then energy can be transferred to the surface wave and growth continues. The minimum wind speed required to promote resonance waves is 23 cm s^{-1} (Kinsman, 1965). The feedback mechanism acknowledges that surface waves will influence the water-air interface thus impacting the wind profile over the sea surface (Bolanos and Sanchez-Arcilla, 2006). This mechanism complements Phillips resonance model. As waves grow they will induce corresponding waves in air flow over the surface (Kinsman, 1965). This creates ‘over pressure’ on the wind ward side of the wave crest and ‘under pressure’ on the lee side which in turn results in pressure energy being transferred to the wave (Delft

University, 2008). An assumption made is that air and water motion is inviscid and incompressible, and that wave speed is unaltered by the influence of the wind (Kinsman, 1965). Unlike in the resonance mechanism, the energy transfer is proportional to the energy in the wave itself and therefore the higher the wave grows the larger the energy transfer becomes. This mechanism therefore is an exponential effect (Delft University, 2008).

The model of Phillips is most applicable during initial stages of the wave field generation, whereas the work of Miles explains the wind-wave interaction process (Jones and Toba, 2001). Commonly both processes are combined to estimate the energy available for wave growth; for instance, see SWAN (Booij *et al.*, 1999) and MIKE-21 SW (DHI, 2009c). Snyder *et al.* (1981) suggest that the overall work done on waves by wind at a wave number is given by:

$$W(k) = \frac{\partial E(k)}{\partial t} = 0.2\frac{\rho_a}{\rho}\left\{\frac{u_w}{c}\cos\theta_a\text{-}1\right\}\omega E(k) \begin{matrix} \text{for } u_w \cos\theta_a > c \\ = 0 \text{ for } u_w \cos\theta_a > c \end{matrix} \quad (2.1)$$

Where: *W(k)* is the rate of energy input per unit area per unit range of *k*, *E(k)* is the spectral density of the waves in terms of energy per unit area per unit range of *k*, u_w is wind speed (given here at a height of 5m), θ_a is the angle between wind direction and wave travel direction, p_a is the air density, p is the water density, *c* is the phase speed of the waves, ω is the absolute angular frequency ($2\pi/T$), and *k* is the wave number ($2\pi/L$)

The energy within a wave can be estimated by (Lamb, 1932):

$$E = \frac{1}{2}\rho g a^2 \quad (2.2)$$

Where: *E* is the energy per unit area of sea surface and *g* is the acceleration due to gravity.

Waves propagate following the direction of the wind that formed them. When discussing the speed at which a wave propagates, it is common to use the concept of the phase speed which is defined as the velocity at which the phase of a given frequency component of the wave travels. Commonly one might use the crest of a wave as the reference phase. This speed is influenced by the water depth: wavelength ratio (Knauss, 1966). In the open ocean waves are normally considered deep water waves, and become shallow waves as they approach coastlines. Deep water waves occur where water depth is deeper than half the wavelength, while waves are considered to be shallow when found in water depths of less than 1/20 of their wavelength. Deep water wave phase speed (c_{deep}) can be given by Eq. 2.3 whereas shallow water wave phase speed ($c_{shallow}$) is given by Eq. 2.4.

$$c_{deep} = \sqrt{gL/2\pi} \quad (2.3)$$

$$c_{shallow} = \sqrt{gd} \quad (2.4)$$

where *d* is the still water depth.

The sea surface is a confusing mixture of waves with varying heights and velocities. The waves found in a given location will often consist of waves generated from local wind conditions (local wind sea) as well as those propagating in from other regions, independent of local wind conditions (swells). Waves propagating through a given section of the ocean will gradually separate based upon their relative wavelengths and speeds; a process known as dispersion. Although the motion of one wave is considered to be independent of another, where two waves pass through one another, and the difference in wavelengths is small, they can combine to create a single resultant set of waves (a 'wave group'). This superposition of waves can result in an increase in the wave amplitude (constructive interference) where the respective wave crests fall in phase with each other, while a reduction in amplitude (destructive interference) occurs where the crests fall out of phase. The result is that the sea appears to consist of groups of waves separated by areas of calm water. Wave groups propagate more slowly than the individual wave components. The envelope which carries the energy of the wave group travels at group velocity (Tucker, 1991). The group speed (*C*) can be estimated by Eq. 2.5 (Janssen, 2004):

$$C = \frac{\partial \omega}{\partial k} = \frac{1}{2}\frac{g}{\omega} \quad (2.5)$$

Wave group speed and individual component speeds are identical in shallow water regions and therefore dispersion ceases to occur (Janssen, 2004).

A sea state that consists of a confusing mixture of continually varying wave heights and speeds is commonly defined as a function of time (*t*) by the summation of a number of harmonic wave forms (Delft University, 2008; Young, 1999) by:

$$\eta(t) = \sum_i a_i cos\left(\sigma_i\, t + c_{rand_i}\right) \quad (2.6)$$

Where : η is the surface elevation, σ is the relative angular frequency of the i^{th} wave component, and c_{rand} is the random phase of the i^{th} wave component.

Amplitude components defined from a Fourier transform can be related to the energy contained within a wave profile to give a wave energy density spectrum (Fig. 2.2) which describes the sea surface elevation as a function of wave energy distributed over a range of frequencies, $E(f)$ or frequencies and directions, $E(f, \Theta)$ (Delft University, 2008; Tucker, 1991):

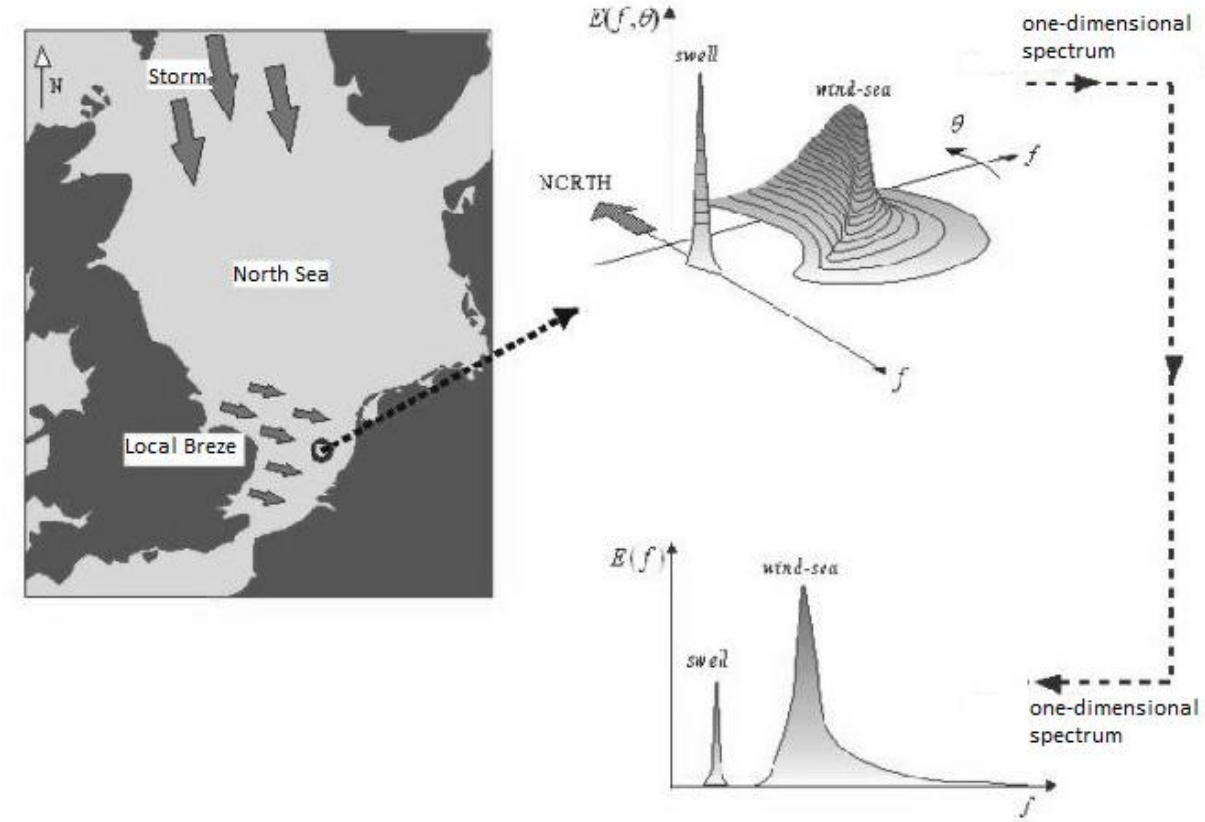

Fig 2.2. 1D and 2D wave spectrums. Delft University (2008).

It is also common to use averaged parameters such as the significant wave height (H_s) when describing the wave spectrum at a given time and place. This is usually considered as four times the square root of the zeroth-order moment of the wave spectrum (Tucker, 1991). The most commonly used term for describing the wave period is the mean wave period (or zero-crossing wave period) (T_z) (Palmer, 2011).

During propagation, waves will be influenced by a variety of processes which can reduce the total energy within a wave (dissipation), affect the distribution of energy over the spectrum (nonlinear interactions), and alter the shape and direction of the wave (refraction, diffraction, and reflection).

2.1.1.2. Dissipation of wave energy

Dissipation is the loss of energy from a wave and can occur due to a number of processes. Whitecapping is the partial breaking of the wave crest due to the wind accelerating it forward at a faster rate than the rest of the wave, occurring in deep water. The result is a loss of energy from the wave system, some of which is transferred into turbulent energy for ocean currents (WISE group, 2007). Whitecapping is not easily measured, which has made it hard to produce models and formulas with which to describe it. Theoretical understanding of the problem remains uncertain. Attempts to describe the dissipation by whitecapping have often utilised the theory of

a limiting wave. This is a theoretical wave height past which waves are assumed to become unstable and break, until stability in the wave profile is re-established (Young 1999; WISE group, 2007). Tucker (1999) quotes a crest-to-trough height: wavelength ratio of 1:7 as the limiting value for progressive waves in deep water. Kinsman (1965) suggests that a breaking angle is also important in determining the point at which whitecapping is induced, stating that at an angle of 120° breaking begins, as at this point crest particle motion is accelerated at the rate of gravity, making it accelerate faster than the wave profile. As the wave breaks it exerts a downward pressure on the upcoming particle motion of the moving water, thereby conducting negative work. This results in a linear dissipation function with the wave spectrum energy (WISE group, 2007). Whitecapping in deep waters only affects the upper part of the wave profile, with the main body left to roll on (Kinsman, 1965). Palmer (2011) suggests that there are a number of approaches that have been put forward to quantify dissipation by whitecapping, the most frequently utilised being the linear term proposed by Hasselmann (1974) which assumes that dissipation will occur once a significant steepness value, S_s (Eq. 2.7) is exceeded

$$S_s^2 = 2\pi H_s / gT_z^2 \tag{2.7}$$

In shallow water conditions waves start to contact the bottom and dissipate energy by various mechanisms (Luo and Monbaliu, 1994), such as percolation, bottom friction, and bottom motion (Padilla-Hernández and Monbaliu, 2001; Wolf, 2009), all of which transfer momentum form the orbital motion of the water particles just above the boundary layer into the turbulent motion in the boundary layer (Palmer, 2011). The relative strength of the mechanisms will vary from place to place, depending upon the conditions of the bottom that are present.

Bottom friction is caused by the drag upon the flow of the water particles as they propagate over the ocean bottom and can be seen to relate to shear stress and orbital velocity of the wave component. DHI (2009c) represent the process of bottom friction using the formulation of Weber (1991) while Booij *et al*. (1999) state that many models have been proposed and, therefore, offer three different options in the SWAN model defined by Hasselmann *et al*. (1973), Collins (1972) and Madsen *et al*. (1988). Cooper (2005) suggest that the influences upon the rates of dissipation due to bottom friction include water depth, incident wave conditions, the orbital velocity at the bottom and a friction factor which is commonly based upon the bed roughness.

Damping due to percolation in a permeable bed layer (e.g. sands), can lead to dissipation through the creation of a wave-induced pressure field at the bottom which will induce flow in the permeable sediment layer. The wave energy lost is proportional to the permeability of the sediment layer. Where a mud bottom dominates a surface wave can induce a wave at the mud-water interface which in turn causes flow in the

mud layer. The viscosity of the mud results in the rapid dissipation of wave energy to a greater extent than sand bottoms (WISE group, 2007). Möller *et al*. (1999) utilised the formulation defined by Sleath (1984) to represent the dissipation due to percolation which was a function of the wave period, wavelength, water depth, thickness of the soil layer, and the permeability of the sediment (Cooper, 2005).

Bottom motion refers to the physical movement of material to and from the sea bed by the wave, utilising a portion of the energy contained within the water body (Open University, 1989). Battjes (2006) suggests that wind generated waves are the primary drivers of sediment movement in coastal areas making them responsible for shaping the coasts. Hsiao and Shemdin (1978) discuss previous experiments which show attenuation characteristics that could not be explained by refraction, shoaling, bottom friction or bottom percolation, which was instead attributed to bottom motion. They conclude that dissipation due to bottom motion as great as that from either percolation or bottom friction in shallow water conditions flowing over a mud bottom.

Perhaps the most recognizable feature of wave dissipation is that of breaking waves in coastal zones. As waves propagate into shallow, coastal regions, they become classified as shallow water waves (Knauss, 1996). In these conditions the rate of wave propagation is no longer characterised by wavelength but purely by water depth, represented by Eq. 2.4. Under these circumstances, the shallower the water becomes, the slower the wave propagates, and therefore, the greater the energy density becomes, often termed shoaling (Jones and Toba, 2001). This results in an increase in the height and angle of the wave, leading to instability and collapse, causing complete scrambling and loss of form (Open University, 1989; Kinsman, 1965). This process is often referred to as depth induced breaking (Booij *et al*., 1999) as the instability is caused by a reduction to water depth. Knauss (1996) suggests that a wavelength: depth ratio between 0.7–0.8 causes instability leading to breaking. The formulation provided by Battjes and Janssen (1978), commonly used to represent depth-induced breaking in spectral wave models such as MIKE-21 SW and SWAN, is given as a function of the ratio of the root mean squared wave height to the maximum wave height a given water depth can sustain.

A variety of formulations have been developed to model the process of dissipation in coastal regions. For instance, Padilla-Hernández and Monbaliu (2001), and Luo and Monbaliu (1994) both compare a variety of commonly used formulations for bottom friction in the North Sea, which vary significantly in terms of complexity and processing time.

2.1.1.3. Non-linear interactions

In deep water situations, the wave spectrum can be influenced by non-linear interactions, called quadruplet interactions, which occur between waves which have similar frequencies, speeds and directions (Booij *et al*., 1999; Rogers *et al*., 2002;

Palmer, 2011). Where the resonance conditions between the wave sets are close an exchange of energy can occur which will result in the transfer of energy from the spectral peak to higher and lower frequencies, without any overall loss or addition of energy (Delft University, 2008). These interactions are described by the WISE group (2007) as being dominant in the evolution of wave spectrums in deep water as well as playing a major role in the occurrence of unusually large waves. A full expression has been given by Hasselmann (1962); however, an approximation by Hasselmann *et al*. (1985a, 1985b) is commonly used in modelling systems due to computational constraints (Palmer, 2011).

Quadruplet wave-wave interactions are important in the dissipation process in deep water waves as they cause a shift in energy to higher frequencies. This is caused as waves can be non-linear, and when certain resonance conditions are met, can create instability and therefore modulation in the wave train (Janssen, 2008). Quadruplet non-linear interactions don't directly dissipate energy but energy will gradually be reduced as the shift to higher frequency waves will result in greater levels of whitecapping.

In shallow water, non-linear triad interactions can develop. In much the same way as quadruplet interactions, triads transfer energy from incident wave components away from the spectral peak to higher and lower frequency components. These transfers can occur over very short periods and dramatically change single peaked spectra into multiple peaked spectra (Delft University, 2008). In addition to broadening of the spectra, transfers of energy result in higher levels of phase coupling of waves, leading to the steepening and pitching forward of crests (WISE group, 2007) which can increase dissipation of the wave energy. The approximation developed by Eldeberky and Battjes (1995) is commonly used to represent triad approximations in wave models.

2.1.1.4. Refraction, Diffraction and reflection

Abrupt changes in water depths in nearshore regions can alter the form of the wave as it propagates towards the coast without altering the energy contained within it (WISE group, 2007). Diffraction of waves is caused by the scattering of wave energy due to interaction of waves with objects in their path (Palmer, 2011), and can be particularly important in nearshore areas containing headlands, bays and man-made structures, around which the waves will bend, spreading energy laterally, perpendicular to the principle direction of propagation (Kinsman, 1965; Young, 1999).

Reflection of waves can occur where the wave propagates into an obstacle such as a sea wall, thus preventing the forward propagation (WISE group, 2007). Waves will rebound off the obstruction in a new direction. Depending upon the nature of the obstacle (i.e. whether its surface is rough or smooth), the reflected wave field can be more or less scattered than that originally approaching the obstacle (Delft University, 2008).

Refraction also results in the alteration of crest direction. Where wave speed is controlled by water depth, a variable bathymetry may cause refraction (Kinsman, 1965). As shown in Fig. 2.3 (top), the section of the wave that enters shallower waters becomes slower moving than those in the deeper water, thus resulting in a realignment of the crest with contours of water depths. Refraction can lead to defocusing or focussing of waves (Fig 2.3, bottom). Refraction does not alter the energy contained in a wave crest; therefore, a change in crest length will result in a change in wave height. Where focussing occurs, the wave height will increase. Defocusing, alternatively, will reduce wave height. These processes are vital to consider when predicting incoming wave profiles as they will modify the amount of energy that will be found at any particular location, especially within harbours (Kinsman, 1965).

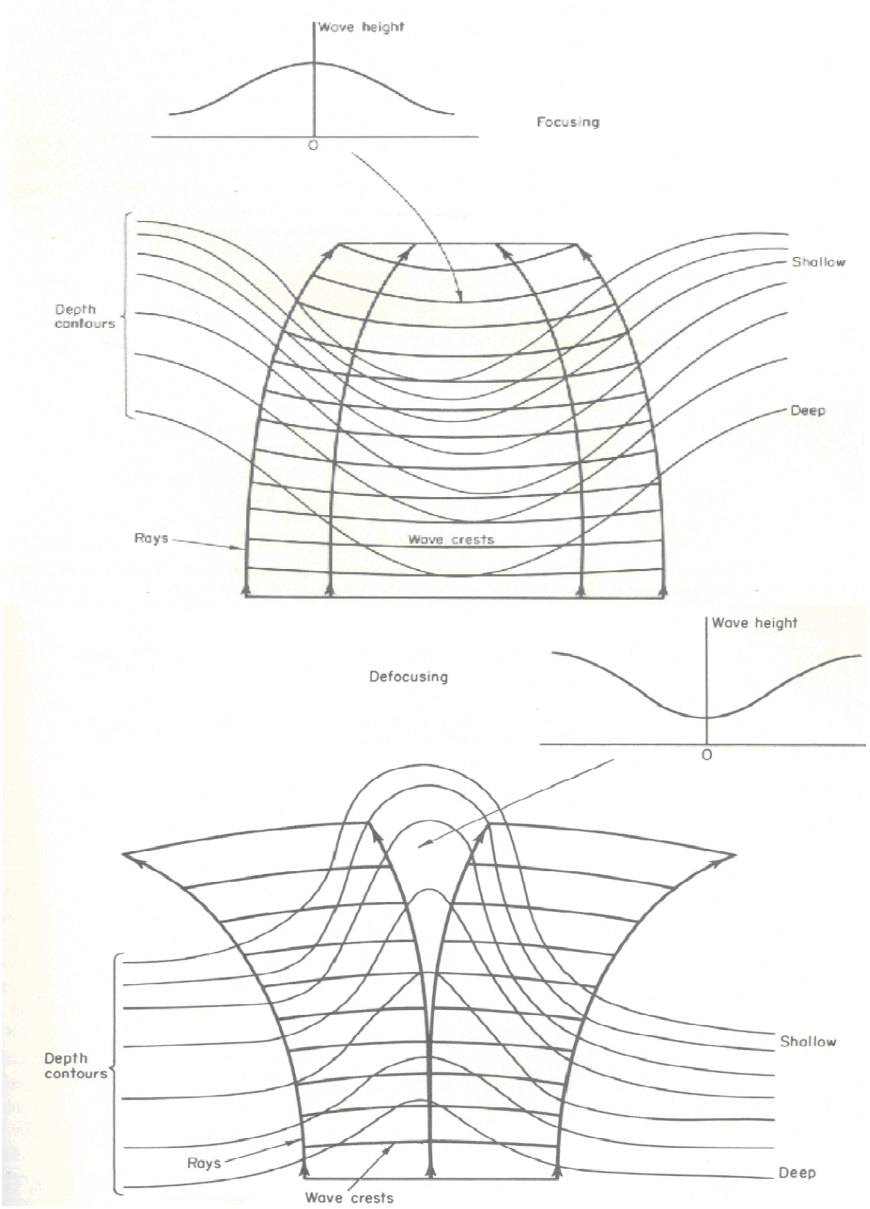

Fig. 2.3. Refraction leading to defocussing (top) and focussing (bottom). Kinsman (1965).

2.1.2. Tides

Tides can be described as long oceanic waves characterising the rhythmic increase and decrease in sea level about the mean (which is assumed static at a specific location), and a resulting horizontal current generation (Dyke, 1996; Pugh, 2006). Tides are driven by astronomical forcing, rather than atmospheric conditions, generated from the gravitational forces exerted on the Earth's oceans by the Moon and the Sun. Tide wavelengths exceed thousands of kilometres and heights can reach to more than 15 m globally. Unlike surface wind waves, they can affect every particle of water in the ocean basin. Due to their large wavelengths, tides are always considered as shallow water waves (Thurman, 1988).

2.1.2.1. Tide generating forces: The Earth-Moon-Sun system

It has long been known that there has been a strong connection between the tides, Sun and the Moon (Rantzen, 1969; Flather, 2000). Tidal elevations, for example, are shown to be highest when the Moon is full or new. Marchuk and Kagan (1984) highlight that the key theory underlying this relationship is that of Newton's Law of gravitational attraction; which states that two bodies attract each other with a force that is proportional to the product of their masses and inversely proportional to the square of the distance between them. This can be represented by:

$$F = g\left(\frac{O_1 O_2}{R^2}\right) \tag{2.8}$$

Where: F is the attractive force between two bodies, O_1 and O_2 are the two bodies in question, R is the distance between the bodies.

The primary driver of the common semi-diurnal tides is the gravitational forces exerted by the Moon upon the Earth. The Earth and the Moon rotate around a common centre of mass, situated within the Earth's radius, with a periodicity of 27.3 days. The centre of mass of the Earth describes a very small ellipse around this common centre of mass while the centre of mass of the Moon describes a much larger ellipse about this point.

The tide-generating force (TGF) experienced on the Earth's tides is caused by the differential force of the spatially variable gravitational attraction of the astronomical body (i.e. the Moon) over the Earth and the inertia forces acting upon the Earth, which are assumed to be spatially constant and equal (Pugh, 2006). This TGF (rather than simply the gravitational attraction given in Eq. 2.8) is inversely proportional to the cube of the distance between the two bodies; therefore, the force will vary spatially over the Earth. Assuming a uniform layer of water, the resulting TGF (i.e. the differential force) can be seen in Fig. 2.4.

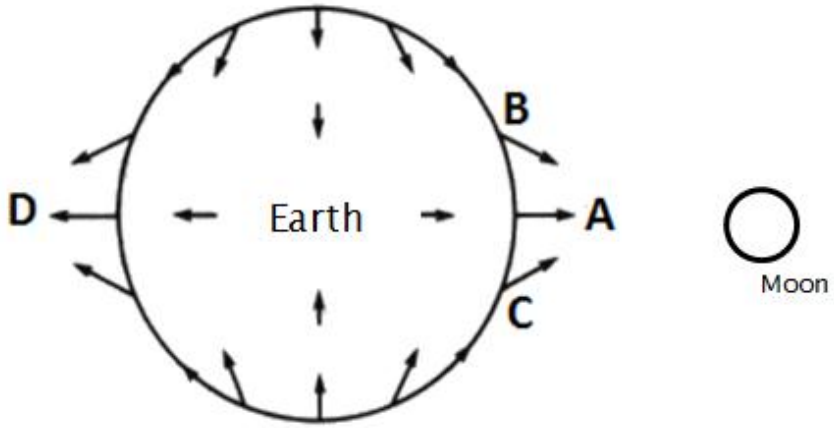

Fig.2.4. Resulting TGF on the Earth due to the gravitational attraction of the Moon.

The simplified example presented in Fig. 2.4 demonstrates that the TGF perpendicular to the line joining the Earth and Moon centres do not contribute to the tidal effect which, instead, is generated by the horizontal components which move water towards point A and point D. These horizontal components are called the tractive forces and are at a maximum along the line running 45° from the line connecting the Earth and Moon centres (Boon, 2004). For this reason, Bowden (1983) includes the angle of the force when defining the horizontal component of the differential force. An approximation of its magnitude at point P is given in Fig. 2.5 and Eq. 2.9.

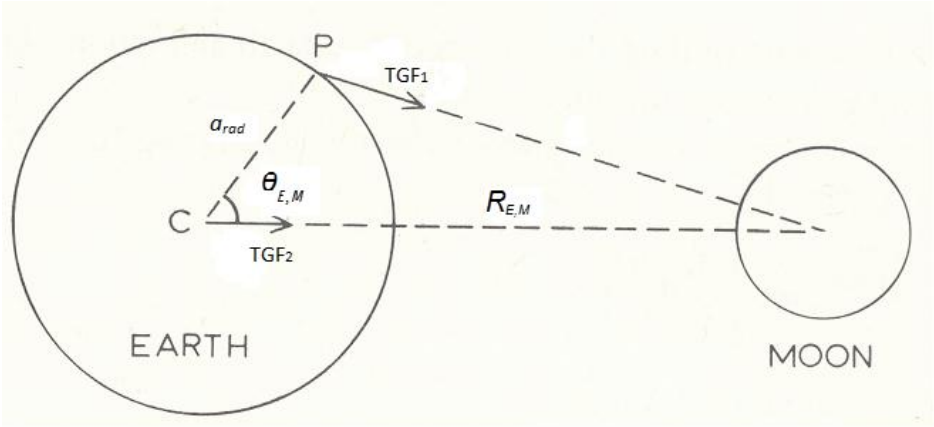

Fig. 2.5. The horizontal component of the tractive force. Bowden (1983)

$$Tractive\ force = \frac{3}{2}\frac{O_m^M}{O_m^E}\left(\frac{O_r^E}{R}\right)^3 g sin\ 2\theta_{E,M} \quad (2.9)$$

Where O_m^M is the Moon's mass, O_m^E is the Earth's mass, O_r^E is the Earth's radius, R is the distance between the centres of the Moon and the Earth, and $\theta_{E,M}$ is the angle between the line joining the centre of the Earth and the Moon and the radius vector from Earth's centre to the point on the surface.

Were the Earth composed only of infinitely deep water, and the response of the ocean to tidal forces was instantaneous, these tractive forces would result in the movement of water directly towards and away from the Moon (points A and D in Fig. 2.4) producing an ellipsoid with two bulges. As the Earth requires 24 hours to complete one roatation, point A (Fig. 2.4) would encounter each of the tides with each full rotation. However, as the Earth and Moon are rotating around a common centre of mass, while the Earth rotates on its own axis, a lunar day (the time taken for the Moon to make successive passages across point A on the Earth) is actually 24 hours and 50 minutes (Boon, 2004).

The Moon is not the only astronomical body imposing a force upon the Earth. The Sun too creates a gravitational pull upon the Earth's oceans. As with the Moon, the Earth's rotation around the Sun and the gravitational attraction between the two bodies results in the production of tractive forces which create two tides. Their calculation is carried out in the same manner as for the Moon (Open University, 1989). This produces a semi-diurnal tidal cycle of 24 hours, with a high tide every 12 hours. Although the Sun is very large, due to the distance from the Earth (and recalling that the TGF produced is inversely proportional to the cube of the distance between two bodies), its relative impact upon the tides is only 0.46 the magnitude of the Moon (Thurman, 1988; Boon, 2004).

The interaction of the Earth, Sun and Moon orbits produces a semi-diurnal tide with a fortnightly modulation termed the spring neap cycle. Where the Sun and the Moon act in the same direction then a large tidal range is created termed a spring tide. This can be where the Sun and Moon are in conjunction or opposition (collectively termed in syzygy). Alternatively where the Sun and the Moon are at right angles then the Sun acts against the force of the Moon and a small tidal range is produced. In this instance the Moon is said to be in quadrature and the resulting tides are termed neap tides (Open University, 1989).

The relationship between the Earth, Sun, and Moon is more complicated than the outline given above which assumes that the astronomical bodies remain at the same distance from one another, and that the Sun and Moon remained above the Earth's equator.

Declination is a term used to describe the angular distance of the Sun or the Moon above or below the equatorial plan of the Earth. As the Earth roates around the Sun, its axis is tilted 23.5° from vertical relative to the ecliptic, causing us to experience the seasons each year. At the same time the plane of the Moon's orbit is at an angle of 5° to the ecliptic. This plane rotates over an 18.61 year period in which the amplitude of the lunar declination increases and decreases steadily (Boon, 2004; Thurman, 1988), with a maximum value of 28.5°. As a result of declination, it can be seen that the tidal bulge would not be expected to be consistently aligned with the equator, rather an 18.51 year cycle in which they lie between 28.5° north and south of

the equator would emerge. The impact of this cycle on lunar semi-diurnal tides is a modulation of approximately 3.7%.

The Moon's orbit of the Earth-Moon common centre of mass is elliptical and therefore its distance from the Earth varies, which in turn, will produce variations in the TGF exeperienced. When the Moon is at its closest position to the Earth this is termed perigee. Apogee is used to describe the period where the Moon is furthest away. The interval between two successive perigee periods is 27.5 days and can create a variance in tide producing force up to 20% of the average. Like the Moon, the Earth's orbit of the Sun is also elliptical which creates a similar modulation. Perihelion describes the period where the Earth is furthest away from the Sun and Aphelion where it is closest. The effect is usually to create a 4% difference between the two extremes. Because of these movements, spring tides have greater ranges during the Northern Hemisphere winters then in summer (Thurman, 1988).

2.1.2.2. Dynamic tides

The description thus far has been based on the use of an 'equilibrium tide' which is a theoretical tide that would be expected to occur were the ocean of uniform depth and no friction occurred at the ocean floor (Pugh, 2006). However, in reality this model would not work for a number of reasons, for instance, in order for the equilibrium tides to remain in the same position relative to the Moon they would need to travel at the same rate at which the Earth rotates with respect to the Moon. As shallow water wave propagation velocity is proportional to the square root of the water depth, the depth of the idealised ocean would need to be 22 km, far deeper than the average depth found on Earth. Furthermore, real world oceans are enclosed by continents, creating seven major basins. As tidal waves approach coastal regions they will be shaped by the same shallow water processes as those influencing shallow water surface wind waves, as discussed in Section 2.1.1.

Within the enclosed basins on Earth, the tidal movements act as Kelvin waves in which oscillations occur in two horizontal directions rather than one, such as seen when one swirls liquid in a glass (Flather 2000; Boon, 2004). Within an enclosed basin, based on the theory of superposition, it can be seen that the pull of the tractive forces on a water body which then reflects back off an obstacle will create a section of water in which no waves appear (where the return waves amplitude cancels out the amplitude of the wave following it if they are out of phase) creating a 'standing wave' called an amphidromic point. As the Earth spins the water within a basin builds up against the west side of the basin and then sloshes back towards the centre of the ocean as the continent spins under the Moon. The movement of the water from west to east is also impacted by the Coriolis effect which in the Northern hemisphere induces an acceleration force causing the wave to bend to the right, creating a counter clockwise circulation, which is opposed to the tidal current which propagates in a clockwise

direction in the Northern hemisphere. The opposite is found in the southern hemisphere (Open University, 1989; Dyke 1996). Nodal lines are created in which no vertical motion occurs but their positions constantly rotate around the amphidromic point (where water level doesn't change). The range of the tide will increase with radial distance outwards from such a point so that lines of equal range (co-range lines) encircle it (Fig. 2.6).

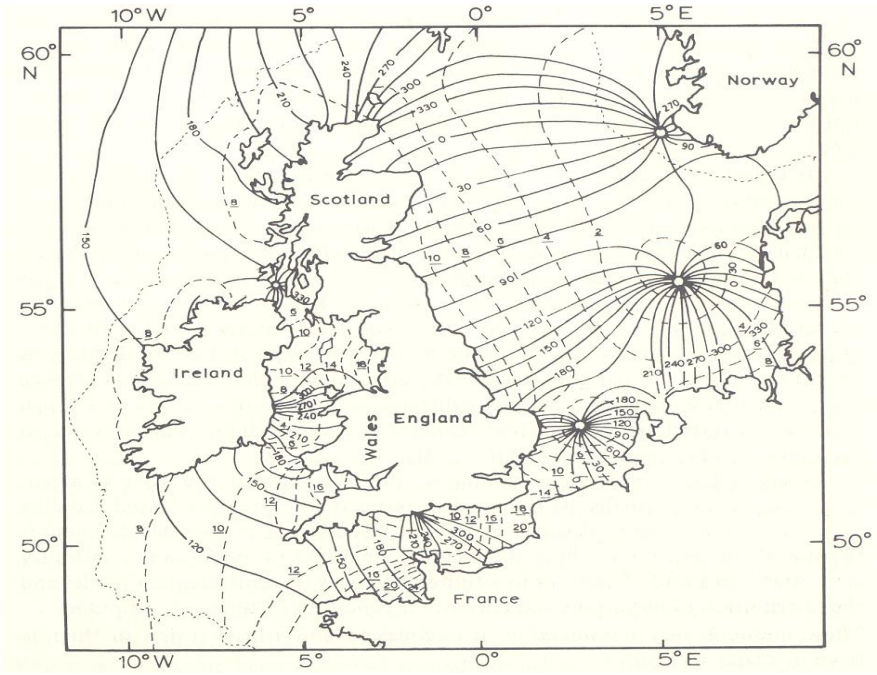

Fig. 2.6. The development of M_2 co-range and co-tidal lines around the UK. Bowden (1983).

2.1.2.3. Harmonic analysis

The unchanging nature of the astronomical forces acting to create a tide allows for high prediction accuracies when one considers the tide as a summation of harmonic constituents, each with a particular amplitude and phase at a given location (phase in this sense is often given relative to lunar transit of the equilibrium tide). Harmonic analysis has become the most widely utilised method with which to do this (Bowden, 1983; Boon, 2004; Pugh, 2006). Harmonic analysis represents the tidal elevation at a given place and time by the summation of *n* constituents, each with a regular oscillating wave with an amplitude and frequency (Eq. 2.10)

$$\zeta = Z_0 + \sum a_n cos(\omega_n t - \phi_n - \phi_n^L) \qquad (2.10)$$

where ζ is the tidal elevation, Z_0 is the reference water level, often given as the difference between mean sea level and chart datum, ϕ is the constituent phase relative to lunar transit of the equilibrium tide, and ϕ^L is the phase lag of the real tide to the equilibrium tide, often taken as the phase lag on the equilibrium tide phase at the Greenwich Meridian.

All frequencies and constants relating to the equilibrium tide are known, therefore, tidal predictions can be made once the values of a, φ^{L}, and Z_0 are established for a given location. To do this a least squares fitting procedure can be used to obtain the set of constituent amplitude and phases (and reference water level) which return the lowest sum of squared errors relative to an elevation time series. Eq. 2.10 can be used to give a combined surface elevation represented by any number of constituents, each representing a particular astronomical influence. For example, a primary harmonic would describe the Moon revolving around the Earth, creating a tidal oscillation with a 12 hour 25 minute periodicity. Each cycle will be identical to the last. This constituent is termed the M_2 tide. Solar tides also produce a known cycle (12 hours period). This constituent will be termed S_2.The recognition that differing constituents have different speeds is central to understanding that during summation of their curves, constituent amplitudes will fall in and out of phase (Fig. 2.7). For example, summation of the M_2 and S_2 tides (with their individual amplitude and phases) will create a new combined tidal cycle which would be representative of the spring-neap cycle (Fig. 2.7).

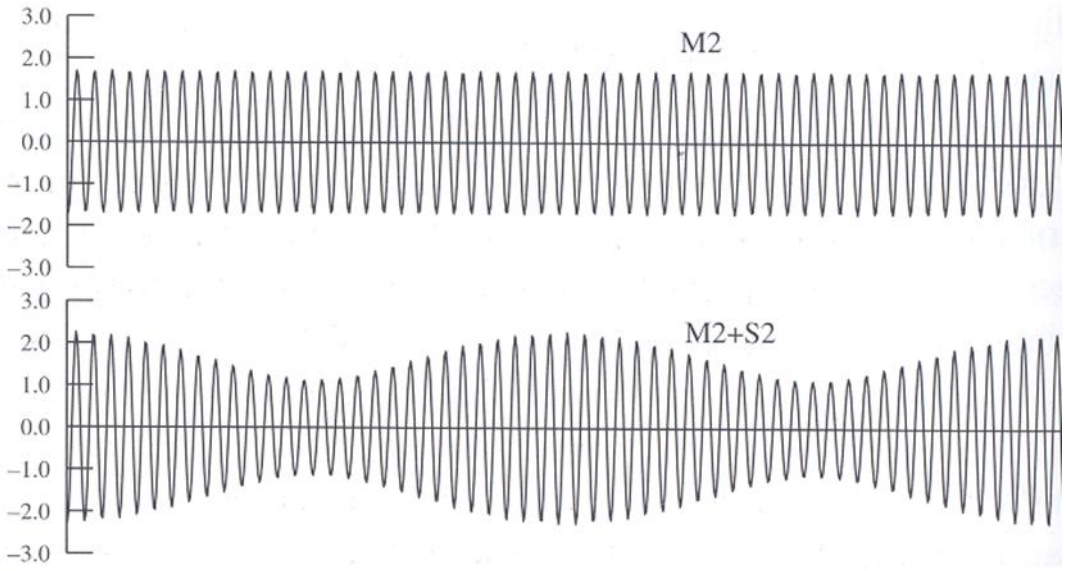

Fig. 2.7. The superposition of constituents, Pugh (2006). Note in particular the output tidal range where the two constituents fall in and out of phase.

As previously discussed, numerous factors will lead to modulations of the tidal cycle in a given region, including declination, elliptical orbits, and the propagation of tides in shallow water depths within enclosed basins with irregular coastlines. To represent such variability 'phantom satellites' are used (Pugh, 2006). Each will produce its own tide with a respective amplitude and phase. These can then be combined with other constituents to bring the overall tidal oscillation in line with observed data.

Examples of such constituents used to replicate modulations caused by the Moon's elliptical orbit around the Earth are the N_2 and L_2 constituents (Boon, 2004). Ducarne *et al*. (2006) found that terms were also required to account for tide modulations in shallow water regions in which non-linear behaviour occurred. Potentially there are several hundred constituents that make up a tidal signal (Doodsen, 1922). Mattocks and Forbes (2008) suggested that just eight were required to represent 90% of the tidal signal in their model for the North Carolina region, while Bowden (1983) lists ten constituents deemed as the most influential (Table 2.1). Proudman Oceanographic Laboratory (POL) defines 25 key constituents with which they define their operational model boundaries for a forecasting model of the UK.

Table 2.1. The most influential tidal constituents. Bowden (1983)

Species	Constituent	Symbol	Period
Semidiurnal	Principal Lunar	M_2	12.42 hrs
	Principal Solar	S_2	12.00 hrs
	Larger lunar Elliptic	N_2	12.66 hrs
	Luni-solar	K_2	11.97 hrs
Diurnal	Luni-solar	K_1	23.93 hrs
	Principal Lunar	O_1	26.87 hrs
	Principal Solar	P_1	24.07 hrs
Long Period	Lunar fortnightly	M_f	13.66 days
	Lunar monthly	M_m	27.55 days
	Solar semi-annual	S_{sa}	182.70 days

The accuracy of the tidal harmonic technique has been shown to be very robust and has been used for over 70 years. Boon (2004) for example demonstrated that using just nine constituents, a 29 day sea level sample and the SIMPLY TIDES software, that 99% of the total variance could be accounted for in the River Mersey. Operationally within the UK, forecasts of sea levels still use harmonic based predictions of tidal surface elevations from long standing gauges, which are then interpolated through a region (Flowerdew *et al*., 2007). However, it is an approximation and depending on the length of sample data used and the number of constituents included, one will find that the 'constants' produced will vary slightly, as will the accuracy of the tidal predictions. Boon (2004) for instance, found residual peaks in predictions relative to observed records at cycles of two, three, four and six a day. These periodicities related to

shallow water constituents not used in the original analysis representing short-term modulations produced by L_2, MK_3 and $2MS_6$ constituents.

2.1.3. Surge

The water surface elevation at a given point is not only influenced by tides and surface wind waves. Atmospheric forcing and wind stress can lead to an additional 'surge' elevation, which is a meteorological induced long wave motion capable of increasing or decreasing the sea level at a given location by several meters.

Large surges superimposed onto the tide are usually the result of wind stress and pressure variations on coastal shelf region associated with unusual storm weather conditions (Flather, 2000; Cañizares *et al*., 2001). Where the wave moves at a similar speed to the meteorological system resonance can occur resulting in the continual build-up of the surge wave (Bowden, 1983).

An alteration in air pressure induced by the storm event can create a dome shaped depression in the sea surface which, when combined with strong onshore winds, can be pushed towards the coastline adding to the water height. The inverted barometer effect is fundamental in describing the raising or lowering of the sea surface due to atmospheric pressure variation. It states that the addition of a local variance in atmospheric pressure (Δp_a) about the ocean mean will cause the level of the sea surface to change relative to the mean sea level (Pugh, 2006) by

$$\Delta d = -\frac{\Delta p_a}{\rho g} \tag{2.11}$$

Where ρ_a is the atmospheric pressure.

Assuming typical values of 1026 kgm^{-3} for seawater density and 9.80 ms^{-2} for gravity this equates to approximately one millibar increase in local pressure causing sea level to decrease by one centimetre under steady forcing conditions.

Accompanying winds can create a drag on the sea surface, thereby creating heightened sea levels at the downwind and 'push' existing surge waves towards the coast (Smith and Ward, 1998). This effect increases inversely with water depth so will be most important when winds blow over extensive regions of shallow water. The influence of winds upon the water surface is termed the wind stress. Moon *et al*. (2009) suggest that the wind stress is a key energy source to the storm surge and that it is dependent upon the wind speed, sea state and atmospheric stability. The drag coefficient of the air is a key term in defining the wind stress. An empirical formula by Wu (1980, 1994) is commonly used (e.g. in MIKE-21) in which a linear relationship is defined between the drag coefficient and wind speed, however, Moon *et al*. (2009) highlight that a variety of formula exist to estimate the drag coefficient, the selection of which can lead to significant changes to the model prediction of surge.

The surge moves as a wave and therefore is influenced by depth limited processes and friction terms, in the same way as the tides and surface wind waves, leading to changes in local height and direction. For this reason, the local bathymetry and coastal configuration can be influential upon the resulting surge elevations experienced at a section of coast from a given storm event. For instance, the National Hurricane Centre (http://www.nhc.noaa.gov/surge/) suggest that a category 4 storm occurring along the Lousiana coastline in the USA could produce a surge of approximately 6 m due to its wide, shallow continental shelf, wherease the same storm approaching a continental shelf with a rapid change in depth, such as Miami Beach in Florida, would be expected to produce a surge roughly half the size.

Although the surge elevation outlined above, induced by pressure variations and strong winds, can be considered as being independent of surface wind waves and tidal fluctuations, the term surge is commonly used to describe the difference between the predicted tide (based on harmonic analysis) and the measured water level. In this instance what is actually being referred to is the change to the expected tidal forced water levels (the residual) due to the presence of surge and waves, as well as the interaction of all three signals (discussed further in Section 2.1.4). The National Hurricane Center (http://www.nhc.noaa.gov) defines two commonly used terms; the storm surge (the non-tidal change in elevation) and the storm tide (the total surface elevation experienced due to all influences). Where peak water levels are of most interest, the skew-surge is often used (Fig. 2.8). This is defined as the difference between the observed peak water level in a given tidal cycle and the corresponding peak tidal elevation (Brown and Wolf, 2009; Royston *et al.*, 2012).

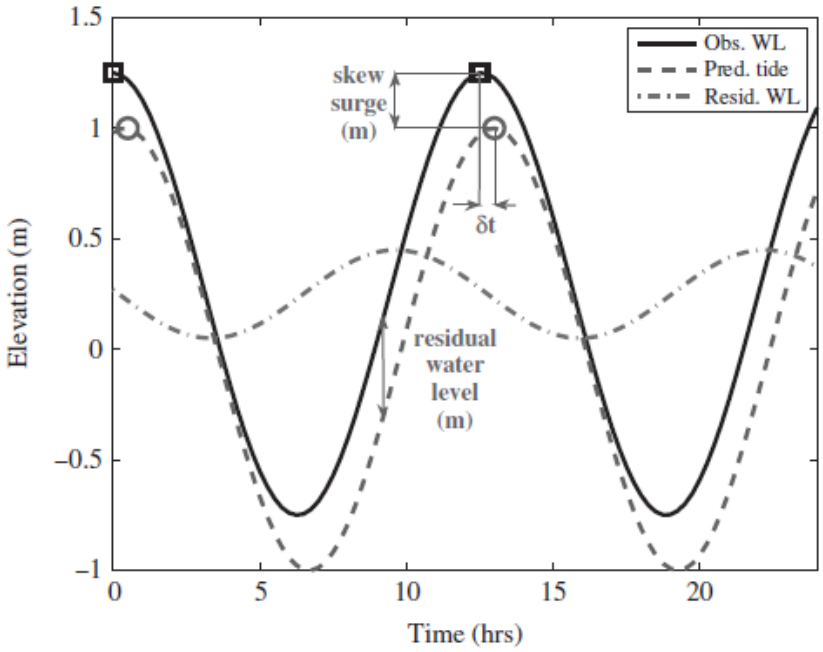

Fig. 2.8. Schematic of the components of the total water level in a tide gauge record (Royston *et al.*, 2012).

2.1.4. Tide-surge-wave interactions

Astronomical tides, meteorologically induced surge, and wind waves all contribute to the timing and amplitude of the water levels experienced during high tide, known as the storm tide (Graber *et al.*, 2006). These components are not independent; rather they have been shown to interact with one another.

The importance of the tidal elevations upon the predictions of wave states, most importantly relating to rates of dissipation and the speed at which the waves propagate, due to the alteration of water depth (Wolf, 2009), has been described in Section 2.1.3. Furthermore, water over which the waves propagate, is itself in motion (a current), and acts upon the wave form. Where there is a strong opposing current to the waves, then wave steepness and height can be increased rapidly (Delft University, 2008). The increase in wave height is a response to the reduction in wave speed imposed by the counter current (WISE group, 2007) and from direct energy transfer from the current to the wave. Alternatively, where a current is moving in the same direction as the waves, then wavelength can be increased, with a resultant decrease in height. As the strength of a current increases, so too does its impact upon the waves, however, a larger effect occurs where currents move against wave propagation (Kinsman, 1965). Current-wave interactions often occur along a limited section of the wave crest, resulting in a local change to crest speed, which results in refraction and alteration to wave direction (WISE group, 2007; Wolf, 2009).

Brown *et al.* (2011) found that offshore waves in their model responded solely to the local wind field, whereas those in the nearshore regions responded both to the winds and to tidal oscillations. Tolman (1990) investigated the influence of the tide and surge upon wave conditions in the North Sea. He demonstrated that the presence of tides and surges created an unsteady medium within which waves propagate, with tides resulting in oscillations of mean wave parameters, and surges resulting in systematic ones. In general he suggested that the interactions are small, leading to modulation in mean wave parameters such as H_s and T_z by 5 to 10 %. Funakoshi *et al.* (1994) also found that the influence of the long-wave motion of the tide upon the short-wave dynamics was relatively weak, and for this reason, suggest that a one-way coupling between hydrodynamic and spectral wave models is often sufficient.

Alternatively, the importance of the waves upon the surge component of the water level elevations has also been highlighted by a variety of studies. Their influence upon the surge is via two mechanisms. First, in nearshore regions, particularly on coastlines parallel to the direction at which the waves travel, when a wave breaks, the water particles can have momentum enough to transport a significant distance up the beach. This may result in movement above the tide only water level. This is often termed 'wave run-up'. In addition, the influence of wave-induced radiation stresses (the additional forcing due to the presence of the waves which changes the horizontal

momentum in the fluid layer) can lead to an increase in the water levels experienced in the surf zone relative to those experienced offshore. This is referred to as 'wave set-up'. Kim *et al*. (2010) demonstrated that measured typhoon-induced peak sea levels could not be modelled without the inclusion of radiation stresses. The influence upon sea levels was shown to be comparable with that due to wind stress and pressure changes. Funakoshi *et al*. (2008) found that the influence of coupling wave and hydrodynamic models could lead to an increase in surge heights of up to 15 %, due primarily to the transfer of momentum from the dissipation of short waves to the long wave motion of the storm surge. Wolf (2008) found that wave set-up accounted for up to 10% of the maximum surge magnitude in Liverpool Bay. Similarly, Mastenbroek *et al*. (1993), Davies and Lawrence (1994), Brown and Wolf (2009), and Wolf (2009) have all suggested that the inclusion of surface waves plays an important role in defining the surface drag, which is influential upon surge predictions. By coupling wave and hydrodynamic models, a variable Charnock parameter can be obtained which has been shown to provide a more accurate prediction of storm surge elevations.

The tide and surge can also be viewed as two separate, yet interacting signals (Wolf, 2009). Recent research in the North Sea and English Channel has been fundamental in describing this interaction. Horsburgh and Wilson (2007) provide a particularly detailed assessment of water level elevations at a variety of tide gauges in the North Sea, establishing mathematical explanations for the surge clustering presented. Their results demonstrated that phase shifts were created in both the surge and the tide signals due to their interactions, the result of which was that large surge events would generally avoid the high tide period by three to five hours, with secondary clustering within one to two hours. This is thought to be because both signals are shallow water waves whose phase speed is given as a function of depth. Therefore, negative surges have been shown to slow tidal progression while a positive surge can advance it (Rossiter, 1961; Wolf, 1981). Prandle and Wolf (1978), and Wells *et al*. (2001) have both reported tide-surge interactions resulting in a decrease of the peak surge elevations and that the effect can be localised, increasing in direct proportion to surge height and tidal range (Horsburgh and Wilson, 2007). Brown *et al*. (2010) found that the interaction could increase or decrease the surge significantly, altering peak levels by more than a metre. The processes leading to the alteration of water levels, due to tide-surge interactions, can be classified into three non-linear effects: non-linear advective effects, non-linear bottom stress effects, and non-linear shallow water effects (Bernier and Thompson, 2007; Zhang *et al*., 2010).

The understanding of the interactions between the tide, surge and wave processes is important in order to enable coastal modellers to provide better estimates of storm conditions that may lead to inundation.

2.2. Forecasting ocean states

Forecasting systems have been developed to aid coastal managers in increasing the resilience of coastal populations to flooding. After the flooding in the east of the UK in 1953, operational forecasting and warning systems were introduced. The ability to prepare for an ensuing flood event is vital in reducing the costs both financially and to loss of life. It is for this reason that many countries invest heavily in such systems, in addition to development of defences.

Forecasts can be made using a variety of different approaches, although generally the models can be divided into empirical (data driven) modelling approaches and those utilising physically-based distributed models. Often forecasts combine physically-based numerical models for some processes with empirically derived estimates for others.

2.2.1. Physically-based modelling approaches

Physically-based numerical models have become the most commonly utilised tools in coastal flood forecasting. This has been due to advances in computational resources and the ability to provide forecasts over large domains (Hsu *et al.*, 2005). This is particularly important in nearshore regions as the variables of interest (e.g. currents, wave fields) often contain a high degree of spatial variability (Bolanos and Sanchez-Arcilla, 2006).

Various ocean prediction systems based on differing ocean models and data analysis schemes have been developed (Ko *et al.*, 2008). Many operational systems share a common form. Nearly all include spectral wave models coupled with hydrodynamic models (e.g. Chueng *et al.*, 2003; Allard *et al.*, 2008).

Spectral wave models such as the Wave Action Model (WAM; Hasselmann *et al.*, 1988) or Wavewatch III (Tolman, 2009), which propagate wave energy across the computational domain in the form of an energy spectrum, which grows and decays in response to changes in the wind field (Liu *et al.*, 2002). Commonly a wave action density spectrum $N(\sigma,\theta)$ is related to the energy density spectrum $E(\sigma,\theta)$ by Eq.2.12 (DHI, 2009c).

$$N = \frac{E}{\sigma} \tag{2.12}$$

Where θ is the direction

The energy within the waves is increased or decreased during propagation over the computation domain due to the influence of a variety of source terms. Common source terms represented in many of the most widely used spectral wind wave models

include: wind energy input, nonlinear wave-wave interactions, depth-induced breaking, whitecapping, and bottom friction. In WAM, for example, this is done using Eq. 2.13 (Hasselmann *et al.*, 1988),

$$\frac{\partial N}{\partial t} + (cos\varphi)^{-1}\frac{\partial}{\partial \varphi}(\dot{\varphi} cos\varphi N) + \frac{\partial}{\partial \lambda}(\dot{\lambda} N) + \frac{\partial}{\partial \theta}(\dot{\theta} N) = S \qquad (2.13)$$

where N is the action density ocean wave spectrum with respect to wave frequency and direction as a function of latitude φ and longitude λ. The dotted variables represent the rate of change of the positions, the dispersion relation and propagating direction of waves travelling globally, while S represents the sum of various energy sources and sink terms.

Hydrodynamic models such as ADCIRC (Luettich and Westerink, 2004) and MIKE-21 HD (DHI, 2009b) are used to make predictions of tide and surge surface elevations by propagating boundary water level elevations (derived as a summation of harmonic constituents and the addition of atmospheric effects) throughout the computational domain, under the influence of air pressure, wind, and wave stresses (DHI, 2009b). Commonly, hydrodynamic models solve Navier-Stokes equations which describe the motion of fluids based on Newton's laws of motion, maintaining conservation of momentum, mass and energy (Cañizares *et al.*, 2001). Six dependant variables (pressure, temperature, density, and three velocity vectors (in *x*, *y*, *z* directions)), and four independent variables (the *x*, *y*, *z* spatial coordinates in a domain, and time) are central to the Navier-Stokes equations. The dependant variables are functions of each of the four independent variables, therefore, the equations are considered as partial differential equations. Hydrodynamic models also commonly account for external forcing (e.g. wind stresses or bottom friction). A useful overview is given by Knauss (1996).

In many systems, only two dimensions (*x*, *y*) are used in an effort to reduce computational demands. In such instances it is assumed that the vertical variation of the current can be simplified into a depth-averaged value without significant impacts upon model accuracy where surface elevation is of primary interest. However, with increasing computational resources, 3D models are now being used in numerous systems.

In order to implement the hydrodynamic and spectral wave equations in a computer model, only capable of performing discrete calculations, the flows occurring in the real world are required to be broken down into specified 'parcels' of time and space that can be solved by a computer. This is referred to as spatial and temporal discretization (DHI, 2009b,c). To do this, a region of interest is represented by the construction of a computational domain. Two approaches are commonly used, defined by the way in which the computational domain is discretized into a number of units;

structured or unstructured grids. Structured grids (using finite difference algorithms) have been the traditional approach to defining a computational domain. This method divides the domain into a set of equal sized cells. Unstructured grids (using finite element or finite volume methods) employ a variable mesh, often using triangular elements that can be of varying sizes in order to increase spatial resolution in nearshore environments without a corresponding increase in offshore regions. Recently, the use of unstructured approaches has become popular due to the ability to more accurately represent complex coastal processes and the removal of a need to provide nested model domains, through the ability to locally increase model grid resolution.

In either approach, the spatial and temporal parcel sizes are related by the Courant-Friedrichs-Lewy condition (CFL) which ensures convergence when solving the partial differential equations used in such models. The condition states that the selected time step must be large enough to allow for the propagation of the modelled wave from one grid point to the next during each set of calculations. In this way, the greater the spatial resolution of the model domain, the shorter the required time step will be.

For a fuller description of the forces acting upon hydrological models and their numerical implementations the reader is referred to Knauss (1996), Dyke (1996), and Kantha and Clayson (2000), while a detailed description of the formulations in the MIKE-21 software used in this research is provided in Section 2.4.3.2.

Table 2.2 provides a summary of a variety of hydrodynamic and spectral wave software packages currently available, while Flather (2000) provides an overview of the operational forecasting systems used throughout Europe.

Table 2.2. A selection of commonly utilised hydrodynamic and spectral wave models.

Name	Type	Reference
WAM	3rd generation waves	Hasselmann *et al.* (1988)
Wavewatch III	3rd generation waves	Tolman (2009)
SWAN	3rd generation waves	Booij *et al.* (1999)
MIKE-21 (SW)	3rd generation waves	Warren and Bach (1992)
ADCIRC	Hydrodynamics	Luettich and Westerink (2004)
MECO	Hydrodynamics	Herzfeld *et al.* (2002)
MIKE-21 (HD)	Hydrodynamics	Warren and Bach (1992)
POLCOMS	Hydrodynamics	Holt and James (2001)
TELEMAC	Hydrodynamics	Moulinec *et al.* (2011)

Currently, most operational forecasting systems employ physically-based numerical models in which the hydrodynamic and spectral-wave models use outputs from (and are often coupled with) atmospheric models which provide mean sea level pressures, wind speeds and directions. For instance, the Coupled Ocean / Atmospheric Mesoscale Prediction System (COAMPS; Hodur, 1997) model produces forecasts of winds at a 0.2° spatial resolution for the Distributed Integrated Ocean Prediction system (DIOPS, Allard *et al.*, 2008, Fig. 2.9). Battjes and Gerritsen (2002), and Vatvoni *et al.* (2002) provide descriptions of linked model systems in the Netherlands and India, respectively, while Williams and Horsburgh (2006), Flowerdew *et al.* (2007), and Bocquet *et al.*, (2009) describe the operational systems currently used in the UK.

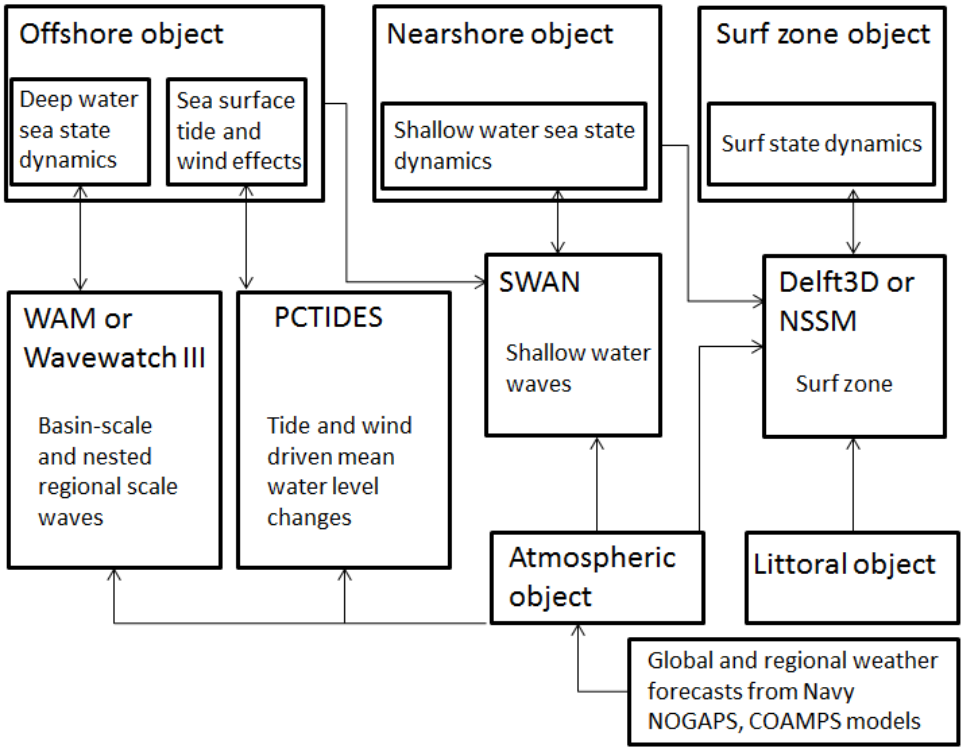

Fig. 2.9. Overview of the DIOPS nearshore wave and current forecasting system. Adapted from Allard *et al.* (2008).

2.2.2. Empirical modelling approaches

The use of physically-based numerical models, such as MIKE-21, WAM and SWAN has become very common in operational forecasting in many regions of the world. In the UK, for example, the current operational forecast couples numerous models, of varying resolutions, to model tide, surge, wave and atmospheric conditions over a variety of scales, including global and continental shelf domains. Such systems have been shown to provide forecasts which have significantly reduced risk from coastal flooding, through the provision of advanced warnings to coastal managers. However, such systems are computationally demanding and require large amounts of data in order to

model the processes contained within their code (Logemann *et al.*, 2004). To run these systems very large clusters of computers are often required. For such reasons, the use of empirical modelling approaches can be preferable, particularly where exhaustive computer resources may not be available. Empirical methods do not attempt to explicitly model the real world processes as the physically-based numerical models do. Instead, a series of independent variables are used to define a function that estimates a dependent variable. Once the function is produced, the model can normally provide a prediction of the dependent variable, given an input of independent variables, at a fraction of the computational processing time as physical-based numerical models. The near instantaneous nature of such techniques makes them especially useful in dealing with probabilistic approaches to modelling as very large ensembles can be simulated in a short period of time. Another potential benefit of using such an approach is found in complex regions. Where a model operating in a region is very uncertain, due to uncertainty in the parameter values or in the model's ability to fully describe the processes occurring, a data driven approach may provide more accurate predictions, due to the ability to ignore explicit modelling of real world processes and instead define an input – output relationship (Kobayashi and Yasuda, 2004).

Regression analysis is a commonly used empirical approach for making predictions. It aims to define a relationship between a dependent variable and one or more independent variables, in order to enable a prediction of the dependent variable, given a set of independent variable inputs. An example in ocean forecasting may use wave measurements at a coastal point as the dependent variable; while offshore wave predictions are used as independent variables (for instance see Kobayashi and Yasuda, 2004). Alternatively, where one wishes to provide an approximation of a complex model itself, the dependant variable will be the complex model predicted wave state in the nearshore region (O'Hagan, 2006; Conti *et al.*, 2009). Both approaches have benefits and drawbacks. The benefit to utilising *in-situ* data sources as the dependent variable is that the meta-model is being created towards a known, correct value (although in reality even measured variables have some uncertainty). When utilising a model output as the dependent variable on the other hand, another uncertainty source is included, as the model output which one is trying to recreate will have error relative to the real variable output (usually derived by measurements *in-situ*) as well as error between the meta-model prediction and the source code-based prediction (code uncertainty). However, observation-based regressions rely completely on the quality and length of the historical record with which they are trained, whereas a regression of a model output would not normally face this problem as the source model could be used to generate an extensive training dataset. A training set which does not include many extreme events for example, may find it hard to produce a model that is capable of forecasting such events. In addition, it is likely that the parameter space used to condition the model will be very densely represented in 'average' conditions. By

definition, the number of training points representing extreme conditions will be relatively low. In a study aiming to provide forecasts of extreme flooding events, this could be problematic

The basic linear regression model can be regarded as a function of a vector of inputs representing an independent variable (Y_i) and a set of unknown parameters which are used to estimate a dependent variable (Y) (Bates and Watts, 1988). The unknown parameters can be represented by two terms representing the slope of the independent variable (β_s) and a constant (β_0) so that the dependant variable is estimated as,

$$Y = \beta_0 + \beta_s * Y_i \tag{2.44}$$

The regression analysis aims to find the solution for *the* unknown parameters that will minimise the distance (error) between the predicted value and the dependant variable observed value. Fig. 2.10 provides a typical example of a linear regression in which a relationship is defined which provides the best fit between the observed and predicted values for the dependent variable as a function of the independent variable. Using this function, future predictions of the state of the dependent variable can be given based on the state of the independent variable.

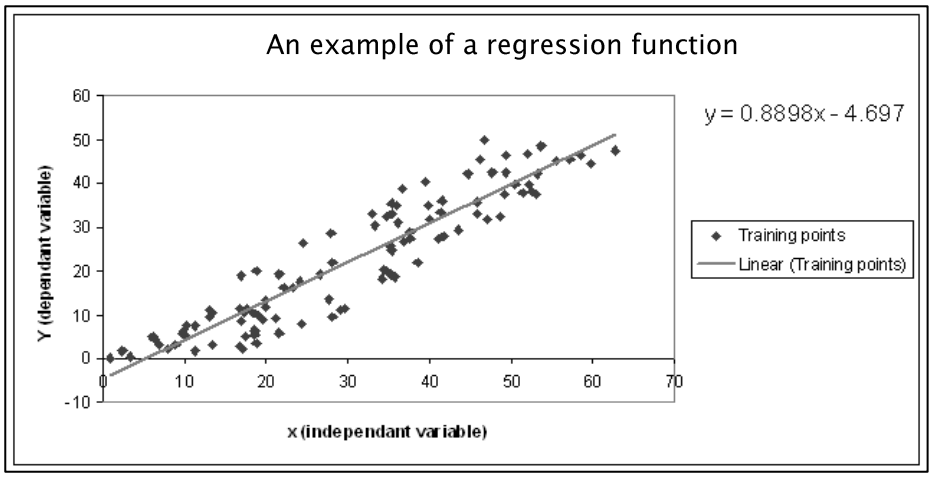

Fig. 2.10. An example of a linear regression function.

In reality, a regression model will often require many independent variables to accurately represent the complexity of a physical system. In this case, the dependent variable becomes a linear combination of the independent variables, each associated with individual unknown parameters (O'Hagan, 2006). This can be represented by extending Eq. 2.14 to give

$$Y = \beta_0 + \beta_{s_1} * Y_{i_1} + \beta_{s_2} * Y_{i_2} + \cdots + \beta_{s_n} * Y_{i_n} \tag{2.14}$$

Where n = 1 to the number of independent variables.

The estimate of the unknown parameters is provided through a least squares estimator, which aims to provide the best estimate, in terms of minimising the root mean squared distance between the observed and predicted dependent variable.

Various adaptations have been made to this function. Deo and Naidu (1999) for example, highlight the use of historical states of the variable when using the auto regressive function to predict wave heights. In this instance the wave height was the dependent variable in the regression, and the independent variable was the preceding wave height, consisting of a product of the states over the past *n* time steps, each with a weight. In this way, the regression function was based upon the historical change in the variable of interest, rather than using variables at a given time step to predict the dependent variable at the same time.

When defining a regression, Wu and Hamada (2002) highlight that the selection of variables to include is crucial. The goal is to identify the smallest subset of covariates that explains the data well. Those covariates whose regression coefficients are not significant should be removed. To achieve this, three strategies are commonly available (Wu and Hamada, 2002):

- Backwards elimination – The process starts with the full model, containing all covariates. Using a predefined threshold value, gradually covariates are dropped if their influence is too small. In this way only the most important covariates remain.
- Forward selection – The process starts with a model containing an intercept and then one covariate is added at a time. At each step the covariate with the largest influence is added to the model. Again, a predefined threshold should be employed to define when a covariates influence is too small to add to the model.
- Stepwise selection – This process combines both backwards and forwards elimination methods but using a two-backward step, followed by a single forward step routine, again utilising some predetermined threshold of influence.

Regression modelling contains important assumptions. The sample with which one trains the function should be representative of the population one wishes to predict. In addition, the variables are assumed to be error free and the relationship between them is predominantly linear. Where a large degree of curvature is found within the relationships, linear transformations may be required. Finally, all residuals are assumed to be normally distributed with a mean of zero (Mason *et al.*, 2003).

Various empirically based approaches exist, of which regression is one option, all of which aim to build a relationship with a dependent variable that is conditioned on a set of training data. A vast array of literature surrounding a variety of empirical-based approaches to modelling physical processes can be found. See, for example, Deo and

Naidu (1999), Cox *et al*. (2002), Sfetsos (2002), Bazartseren *et al*. (2003), Huang *et al*. (2003), Steidley *et al*. (2003) Kobayashi and Yasuda (2004), and Prouty (2007). For more information on Bayesian analysis and the use of emulators (models of complex source codes), O'Hagan (2006), Conti and O'Hagan (2010), Conti *et al* (2009), Kennedy and O'Hagan (2000), Logemann *et al* (2004) and Oakley and O'Hagan (2004) is recommended.

2.3. Uncertainty

No numerical model of the real world is perfect (Maybeck, 1979). Model processes and structures are simplifications of an unknown reality that has only been partially sampled by measured data, which itself contains errors (Neal, 2007), and therefore, can only be regarded as approximations of the truth (Kantha and Clayson, 2000). Errors may be introduced into model predictions through a variety of sources including; inaccurate estimations of initial conditions, inaccurate forcing, and lack of complete knowledge of the system, leading to uncertainty in the ability to fully describe its physical properties (Madsen and Canizares, 1999; Kantha and Clayson, 2000). The result will be a divergence from reality in model predictions.

Tremendous progress has been made in storm-tide prediction, however, substantial prediction errors still exist (Peng *et al*., 2007). For example, prediction of tidal elevations from operational forecasts is considered to become increasingly uncertain in complex nearshore regions. For this reason, harmonic predictions of the tides are substituted in the place of outputs from physically-based numerical models in many operational systems due, to their greater accuracy (Flowerdew *et al*., 2007; Bocquet *et al*., 2009; Hawkes *et al*., 2009). Recent research has shown that the tide and surge signals are not independent, rather, they influence upon one another, often with significant effects (Prandle and Wolf, 1978; Wells *et al*., 2001; Horsburgh and Wilson, 2007). Where the modelled tides are very uncertain, this uncertainty may propagate through the system via the influence of tidal errors upon the prediction of the surge.

Spectral wave models also contain known uncertainties, in addition to unknown errors that may be induced from the error in the input datasets. For example, all waves are assumed to follow linear wave theory. However, often waves can be regarded as weakly non-linear, and focussing of wave energy in space and time can occur (Janssen, 2008). The interactions between wave trains that are non-linear (termed quadruplet and triad interactions) are highly complex and are not feasible to compute in a forecasting system. To include such interactions into the model, approximations are used to reduce the computational demand (Hunt, 2005). Of the methods produced, the

Discrete Interaction Approximation (DIA) of Hasselman *et al*. (1985) has become one of the most widely used.

The uncertainty in spectral wave models is thought to increase in complex nearshore regions. Palmer (2011) highlights that there is uncertainty in how well current spectral wave models predict bimodal spectra resulting from the interaction of swell and local wind-sea due to a poor understanding of the physical processes relating to swell transformation in shallow tidal areas such as the English Channel. Furthermore, previous research has described a tendency of such models to over-predict H_s, while under-predicting T_z, due to an over-prediction of the high frequency energy, particularly in shallow, short fetch areas (Ris *et al*., 1999; Rogers *et al*., 2002). An assessment by Moeini and Etemad-Shahidi (2007) found Scatter Index (SI) errors of up to 20% in both H_s and T_z when hindcasting with SWAN and MIKE-21 SW models in an enclosed basin, despite using measured wind conditions.

The spatial and temporal variability in accuracy, and the variety of sources from which errors may emerge, make uncertainty a difficult issue to address. However, in order for coastal managers to make informed decisions, a measure of the accuracy of forecasts is required. A vital component of this is the ability to understand the uncertainty in a given prediction. Recent research has tended towards addressing uncertainty in predictions through two means; quantifying it through the sampling of uncertainty in probabilistic predictions, and reducing it, with the application of data assimilation strategies.

2.3.1. Quantifying uncertainty: probabilistic predictions

The use of an ensemble-based approach enables a probabilistic output based on several forecasts (rather than one), each with slightly different initial conditions, boundary conditions, and/or model physics, with the aim of sampling the range of forecast results consistent with the uncertainty in the observations and the modelling system itself (Bocquet *et al*., 2009). Each forecast is driven using datasets that are perturbed to sample from defined uncertainty distributions, often using a Monte Carlo approach (Hammersley and Handscomb, 1964). In this way one can attempt to account for, rather than ignore, uncertainty in the forecast. The use of ensemble-based probabilistic approaches is of interest operationally. For example, it has recently been considered for forecasts within the UK (Flowerdew *et al*., 2007). Bocquet *et al*. (2009) provide a useful overview of the intended Met Office probabilistic forecasting set-up (Fig. 2.11) in which each of the input variables can be considered as uncertain, and therefore, represented by a probability distribution. Using a large number of simulations, where each input variable value is drawn from its respective distribution, a large ensemble of possible outcomes can be generated, from which a mean and range is normally used to define the hazard. The application of probabilistic forecasting

approaches has become popular due to the potential benefits they offer to coastal managers, for instance, the 'best guess' magnitude of a given event (given as the mean of the ensemble) and the likelihood of the event in question exceeding magnitudes of varying degrees. This can be particularly useful in aiding in the preparation for extreme events that may be not have been predicted where a single deterministic approach was used.

Given a set of error distributions, representing the uncertainty in each parameter that is considered to provide a source of error to a model output, one would ideally provide an ensemble of outputs, sampling every point in the multi-parameter space. However, particularly when running complex, computationally expensive models, this cannot be the case. Consider a model that contains ten parameters, each with some degree of uncertainty which the modeller wished to represent in an ensemble. Where just three levels were used in representing the potential range in the variable, the number of simulations required to represent the parameter space would be an ensemble of 3^{10} (over 59,000). Even using just two levels, perhaps representing upper and lower bounds of the potential variable value, would require an ensemble of over 1000 simulations. Clearly, where the model simulation takes hours to run, it becomes infeasible to generate so many simulations in a forecasting setting (Conti *et al.*, 2009). With their vast computational resources, the Met Office operational oceanographic forecast currently aims to provide a 25 member ensemble (Bocquet *et al.*, 2009) while the European Centre for Medium-Range Weather Forecasts (ECWMF) forecast contains 50 (Persson and Grazzini., 2007). A trade-off clearly exists between the size of the ensemble desired, the complexity of the modelling approach, and the computational resources available. When considered in a real-time forecasting situation, the additional requirement to provide simulations within reasonable output time frames is an important consideration, particularly where data assimilation strategies wish to be used to provide real-time updates as often as possible.

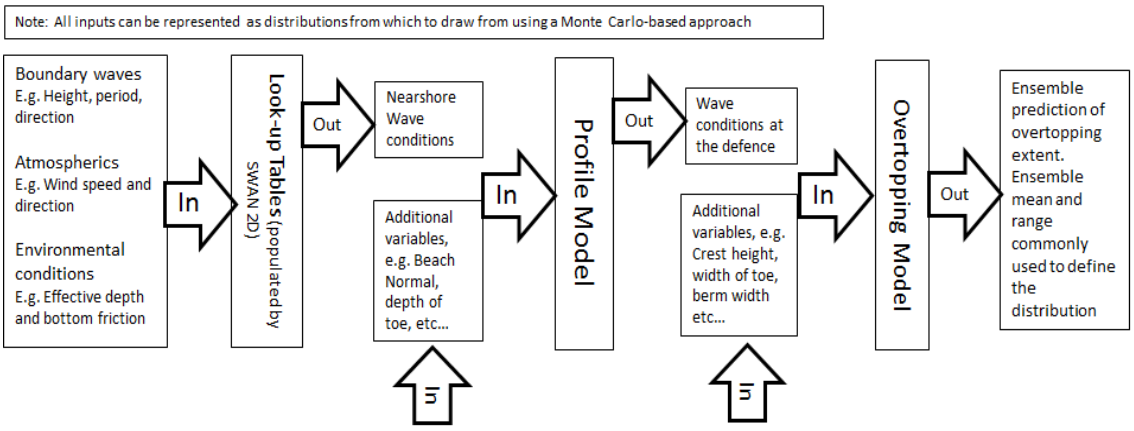

Fig. 2.11. Met Office probabilistic forecast pilot scheme, adapted from Bocquet *et al.* (2009).

2.3.2. Reducing uncertainty: data assimilation and the Kalman filter

Many forecasting systems implement data assimilation schemes to increase forecast accuracies (Kantha and Clayson, 2000). Data assimilation is a technique in which modelled and measured data are integrated in an optimal way, taking into account uncertainty in both (Prandle, 2000) in order to reduce forecast error. Mclaughlin (2002) highlights that there are three categories of assimilation; interpolation (a time invariant system at a single measurement time), smoothing (a time dependent system through a time interval), and filtering (a time dependent system at the most recent measurement time). In most systems aspects of each will often be used, for example, interpolation of a bathymetry layer from point measurements is common in order to provide a full grid that a numerical model can use (for more information refer to Longley *et al.*, 2005 and Lam, 1983). In terms of short-term ocean forecasting, focus often lies on filtering, in order to update model predicted states. Neal (2007) highlights four categories of filtering applications commonly used: input updating, parameter updating, error prediction, and state updating. Prandle (2000) suggests that within operational storm surge forecasting, such assimilation techniques are commonplace, usually utilising tide gauge measurements. Flather (2000) emphasises this, suggesting that the use of real-time assimilation of measurements is vital for accurate predictions, in a review of European operational oceanographic forecasting systems. In weather centres, forecasts are commonly updated in a similar way (Kantha and Clayson, 2000). The techniques used in filtering of states for update all aim to include state measurements with modelled outputs, in order to improve the prediction. They can range from very simple insertion techniques (i.e. replacing the predicted value with the observed value) to complex techniques that include model dynamics.

In an oceanographic modelling perspective, the majority of assimilation uses two measured data sources; *in-situ* and satellite or ground-based remote sensing measurements. Satellite sensor-based data over the oceans have become widely available. Numerous satellite sensors offer altimeter and Synthetic Aperture Radar (SAR) data, which estimate ocean surface state due to the impact that surface roughness (waves) has on the backscatter coefficient of the sensor signal (Krogstad and Barstow, 1999; Campbell, 2002). The accuracy of such measurements has been found to compare well with *in-situ* buoy measurements (Steabs and Bauer, 1998). The global coverage of various ocean viewing satellites, such as TOPEX/POSEIDON (Fu *et al.*, 1994), ERS-2 (Crapolicchio *et al.*, 2012) and Seasat (Evans *et al.*, 2005) have become appealing options for providing data sources with which to update ocean state predictions. Numerous studies have assessed the potential to reduce error in predicted ocean states, most commonly wave fields, using satellite sensor-based remote sensing data, assimilated into model predictions.

Foreman *et al*. (1994), Lionello *et al*. (1995) and Dunlop *et al*. (1998) provide examples in which satellite sensor-based altimeter data have been assimilated with WAM ocean wave predictions. These, and many other studies, including operational systems such as those used by the Met Office (Krogstad and Barstow, 1999) tend to agree that the impacts are positive in terms of reduction of bias and scatter, but the reductions tend to be small when assessing impacts upon commonly used wave statistics such as H_s and T_z. Where the swell component of the wave field was large, the level of error reduction in the predicted wave fields was greater due to the under-prediction of swell by the model. Siddons *et al*. (2008) provides a comparison between various assimilation techniques used to integrate real-time radar-based oceanographic measurements into the SWAN nearshore wave model.

The use of satellite sensor-based data suffers from coarse spatial and temporal resolution, inhibiting greater use in many operational forecasting models. The return period of many ocean based satellites is often in the region of 10 days (e.g. TOPEX). This allows for only infrequent updates of a wave field forecast, rather than the near-continuous update available from a fixed buoy. Furthermore, the standard altimeter data capture period is one second. This relates to approximately 7 km spatial resolution over which the wave measurement is averaged (Krogstad and Barstow, 1999). It is for these reasons that such data assimilation strategies have been used only in deep water ocean models, where spatial variability is significantly lower than in shallow, coastal regions. Siddons *et al*. (2008) assimilated radar-based data into the nearshore model SWAN at Holderness. They were able to do so using two stationary HF radars, enabling a continuous 1 km spatial resolution output of wave height and currents. Until satellite sensor spatial resolutions increase and techniques to account for the impact of landforms upon the altimeter waveform are improved, the use of such data sources for updating in coastal shallow water regions will be restrained. Recent research, however, has indicated that altimeter data previously flagged as 'bad' due to the complexities of data capture in coastal zones (due to uncertainty in the interpretation of land effects upon altimeter waveforms) may be recoverable using new techniques, thereby expanding the use of satellite sensor-based data into the coastal zone for assimilation purposes (see the COASTALT project which aimed to address these issues, http://www.coastalt.eu/).

In areas where buoys are abundant, such as the English Channel and the Solent, assimilation of *in-situ* wave and water level measurements may prove useful. Buoys are considered to give very accurate observations. In Greenslade's (2001) study in Australia, buoy estimates were assumed to have errors no larger than 2% for H_s. The high accuracies and stationary nature (allowing for many more measurements compared to satellite sensor data) makes the assimilation of buoy data appealing to modellers. An additional benefit found from the assimilation of buoys, in terms of

wave field updating, is that many buoys can provide measurements in terms of a directional spectrum. Where such information is available, spectral partitioning can be used to gain a greater understanding of the model prediction accuracies. For example, many studies using such techniques have found that wave models, such as SWAN, tend to under-predict low frequency energy and over-predict high frequency energy (Rogers *et al.*, 2002). Voorrips (1999) presented an insightful account of wave buoy assimilation in the North Sea. In this study, data from seven wave buoys were used to update predictions from the WAM model. Spectral partitioning was used to allow the update of multiple portions of the energy spectrum independently from another. Over one year, tests were conducted comparing accuracies with and without assimilation. The data demonstrated that assimilation reduced the error in mean wave height and period. The increase in accuracy was significantly higher where wave propagation was more important than wave generation. Swell dominated seas experienced error reductions of up to 20% in mean wave height predictions.

A variety of different approaches to assimilating buoy measurements for storm-surge updating have been used ranging from simple updating of boundary conditions (Williams *et al.*, 2008) to more complex domain state updating procedures (Canizares *et al.*, 1998; Siek and Solomatine, 2011; Butler *et al.*, 2012).

Sequential techniques have gained significant popularity in oceanographic applications, of which the Kalman filter has become the standard approach (Madsen and Canizares, 1999; Sørensen *et al.*, 2006). The Kalman filter (Kalman, 1960) provides an unbiased estimate for current state of a system that has a minimum error variance (Kantha and Clayson, 2000). It is described as an optimal linear predictor, accounting for the state of the predicted variable of interest, the measurement of it, and the uncertainty in both (Maybeck, 1979). The model error covariance statistics are calculated dynamically at each time step replacing the single fixed value utilised in more basic sequential methods (Miller, 1985; Voorrips, 1999).

The Kalman filter works in a two-step feedback system (Neal, 2007). The 'predictor' stage includes the simulation of a state vector (and its uncertainty) at a future point in time, based upon the system state (and its uncertainty) at a previous time step, by advancing a deterministic estimate of the system state and adding noise to the estimate of uncertainty. The next stage, the 'analysis' aims to increase the accuracy of this prediction by assimilating measured data (which are also uncertain) using a 'Kalman Gain', which weights the observed and predicted values based upon their relative uncertainties. In this way the Kalman filter can provide a best estimate of the current state of a system as well as providing a prediction at a future point based on the dynamics of the model. The following section outlines the Kalman filter in more detail.

Let X_f and X_o refer to the forecasted value and observed value of a state, respectively, and the best estimate of the true value of the state (X_t) is given as X_a. Both X_f and X_o will have an error from the true state value. The errors are represented by

$$e_f = X_t - X_f \quad \text{and} \quad e_o = X_t - X_o \tag{2.15}$$

where e_f and e_o refer to the error in the forecast and observation, respectively.

Alternatively this can be described in terms of variance (denoted here by V) by

$$V_f = (X_f - X_t)^2 \text{ and } \quad V_o = (X_o - X_t)^2 \tag{2.16}$$

Finally, covariance can be established as

$$P_f = \overline{e_f e_f} \qquad \text{and} \quad P_o = \overline{e_o e_o} \tag{2.17}$$

where P_f is the forecast error covariance and P_o is the observed error covariance.

The best guess of the value of X is given combining the forecasted and observed estimates, including their relative uncertainties using a weighting factor, referred to as the Kalman gain (K) by

$$X_a = X_f + K(X_o X_f) \tag{2.18}$$

The Kalman gain is a relative weighting given after considering the accuracy of both X_o and X_f. The addition of both weights will equate to 1. Therefore, the weight associated with X_o can be rewritten as K by

$$K = \frac{1}{V_o}\left(\frac{1}{V_f} + \frac{1}{V_o}\right) = \frac{A_2}{A_1 + A_2} \tag{2.19}$$

Where A is the accuracy (given as the inverse to the variance).

The error associated with this new analysed value can be given by

$$K(e_o + e_f) - e_f \tag{2.20}$$

and the error covariance of it (P_a) will equate to

$$P_a = (1 - K)P_f \tag{2.21}$$

This demonstrates the ability of the Kalman filter to update a single point in which no time element has been included. A relatively straightforward example can be viewed in the Appendix. The representation of the Kalman filter prediction and update

sequence in a matrix based multi-state variable situation is presented by Neal (2007) in Fig. 2.12.

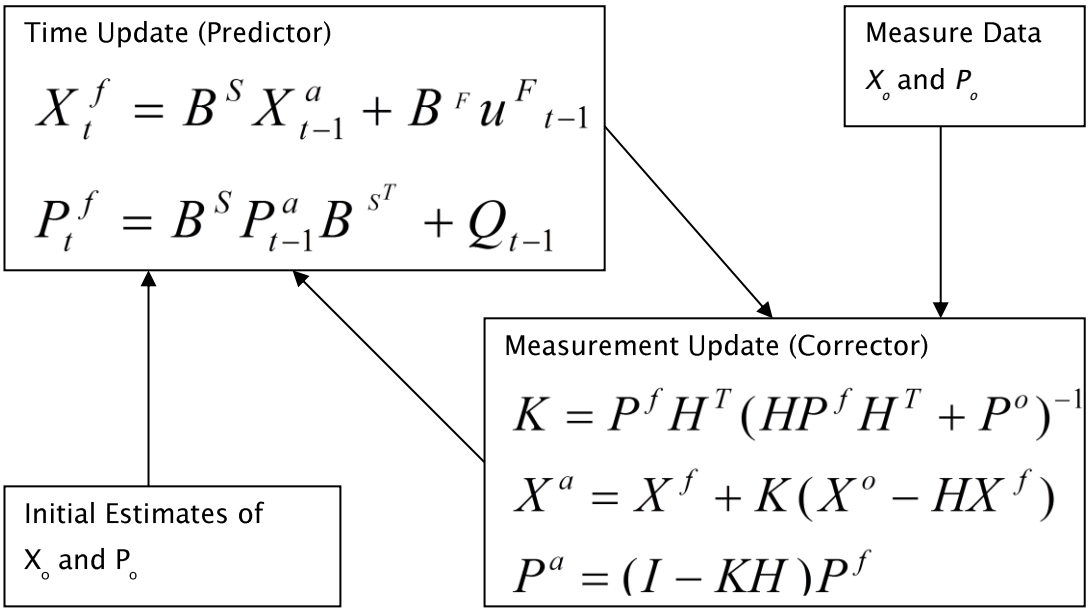

Fig. 2.12. The Kalman filter. Neal (2007).

Where, I is an n by n identity matrix, H is the m by n measurement operator, X^f_t is the forecasted state vector at time (t), P^f_t is the error covariance matrix associated with the forecasted state vector, B_S is an n by n state transition matrix describing the state of system changing from the previous time step, ^{T} is a transpose of a matrix, Q_{t-1} is an n by n process noise covariance matrix describing system state errors at t_{-1}, X^a_{t-1} is the state vector of the previous period, P^a_{t-1} is the error covariance matrix associated with the previous state vector, u_F is a forcing term, B_F is a n by 1 matrix relating the forcing term to the state vector, K is the Kalman gain matrix, P^o_t is an m by m measurement noise covariance matrix describing covariance of the measurement errors at time step t, and X_o is a m by 1 vector of measurement values.

The Kalman filter has been shown to be effective when used to describe systems based on linear dynamics (Evensen, 2002). In practice, however, various difficulties face a modeller, most importantly, the estimation of the modelled and measured error covariance, which are essential elements in the updating methodology. Sørensen *et al*. (2006) discuss this and other important data assimilation parameters, concluding that the better the observation network used, the less influence poorly represented assimilation parameters have.

In recent years extensions of the Kalman filter have been designed to address limitation within the original. The Ensemble Kalman filter is such an example (Evensen, 1994), which utilises a Monte Carlo prediction of the modelled state. Statistical

properties of the system state vectors are represented by an ensemble of possible state vectors, providing the basis for estimating both the forecasted state vector and its error covariance (Madsen and Canizares, 1999, Sørensen *et al.*, 2006). For instance, the forecasted state can be given as the mean of the ensemble, while the variance associated with it can be time varying as it is estimated from the ensemble spread. The Kalman filter and the Ensemble Kalman filter have been immensely popular due to their simple conceptual frameworks and relative ease of implementation. An exhaustive review of studies that have used it can be found in Evensen (2003).

2.4. Study site, data and software selection

2.4.1. The Solent – Southampton water estuarine system

The Solent lies between the south coast of England and the Isle of Wight, in the UK (Fig. 2.13). It includes 12 separately defined estuaries and harbours and contains a wide range of coastal habitats and inter-tidal zones (Fletcher *et al.*, 2007). The region has various stakeholders, including conservation organisations for protected habitats, a dense coastal population and two of the largest shipping ports in the UK.

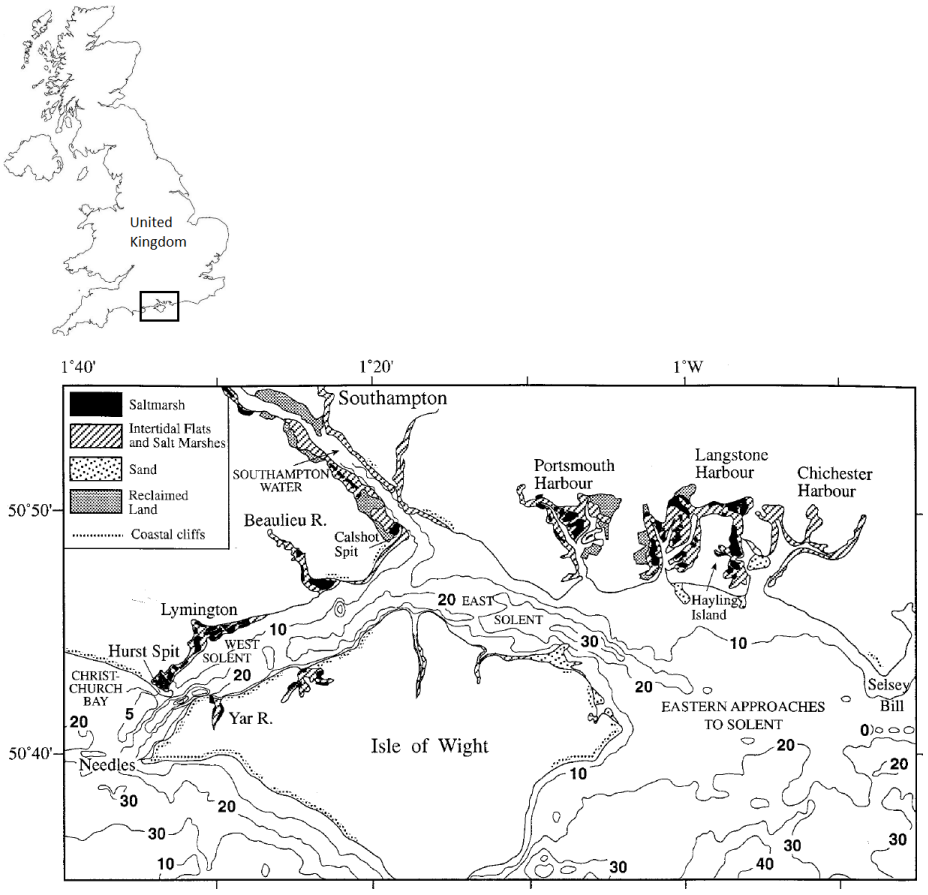

Fig. 2.13. The location of the Solent–Southampton Water estuarine system (Levasseur, 2008)

The region lies in the English Channel, in which the M_2 tide is the dominant tidal component and tidal ranges typical are in the order of 6 to 10 m. The M_2 is also the dominant forcing within the Solent. However, the irregular geometrical shape, narrow channel configuration and shallow depth of the estuary results in an amplification of the shallow water tidal constituents, M_4 and M_6 (Levasseur, 2008). For example, at the Southampton tide gauge the M_2, M_4 and M_6 tidal constituent amplitudes are approximately 1.34, 0.24 and 0.17 m, respectively. At Newhaven, further east, in a more exposed coastal location in the English Channel, the constituent amplitudes are approximately 2.19, 0.08 and 0.02 m, respectively. Within the Solent these amplifications create a tidal elevation with a double high water and young flood stand, most prominent in the Southampton Water region (Rantzen, 1969; Levasseur, 2008).

Storm surges in this region most frequently occur due to low pressure systems from the Atlantic, propagating eastwards, or as a result of surges propagating south from the North Sea (Law, 1975; Haigh *et al.*, 2004). Large storm surge events have influenced the English coast in the past, the most notable occurring in 1953, which resulted in significant loss of life (Gerritsen, 2005; Wolf and Flather, 2005). During this event the surge propagated from the North Sea increasing in intensity as it moved south into shallow waters. Other notable events to have caused flooding, within the Solent region specifically, include those occurring on 14th to 18th December 1989 (Wells *et al.*, 2001; Ruocco *et al.*, 2011) and 10th March 2008 (Haigh *et al.*, 2010). A review of flood events within the Solent since 1935 can be found in Ruocco *et al.* (2011). Generally, coastal flooding within the Solent is considered frequent, occurring once every two years on average, but with no recorded loss of human life (Wadey *et al.*, 2012). Previous attempts at modelling the hydrodynamics have shown significant errors in the western Solent and Southampton Water regions. Levasseur (2008), for instance, quote errors in the mean spring range (MSR) and mean neap range (MNR) at Southampton, of 0.44 m and 0.39 m, respectively. This uncertainty is exacerbated by a limited amount of information available on the major sediment depositional areas of the system, such as the tidal deltas and offshore banks (Velegrakis, 2000).

The English Channel is fairly sheltered from extreme waves, with a long-term average H_s of 1.5 m (Inter-Agency Committee on Marine Science and Technology, 2004) and T_z of typically 6 -10 s. The largest waves that occur usually arrive from either 240 ° due to storm waves and swells from the Atlantic (Dix *et al.*, 2007), or occasionally, storm waves propagating from 40-50 °. The Solent and Hampshire coastline is protected from extreme wave events by the Isle of Wight and Hurst Spit. The CCO (http://www.channelcoast.org/) considers the region to have low-to-medium exposure to waves due to the sheltering influences and the fetch-limited conditions. At Lymington and Sandown Pier, for example, the average 5% exceedence height for H_s in 2003 and 2008 was 0.8 m and 0.5 m, respectively. However, the eastern region,

particularly Hayling Island, is less sheltered and can be affected by storm waves propagating through the English Channel. For example, over the same period, the average 5% exceedence value for H_s was 1.59 m, while events greater than 3.8 m were recorded. Recent research by Palmer (2011) has examined the propagation of waves through the English Channel, revealing that refraction of waves due the Channel's topography, leads to a focussing of wave energy in the eastern Solent.

The coastal population has increased steadily, reaching 835,731 in 2001 with nearly 4000 ha of land, supporting 17,000 dwellings and a population of 37,600 considered at risk from coastal flooding (Hampshire County Council, 2006). The southern coast of the UK is expected to experience some of the largest increases in flood risk during the 21st century in the country (Evans, 2004). This is likely to be due to a variety of reasons including an increase in the number of assets at risk in coastal zones (Zang and Tooley, 2003), subsidence of the southern English coast by approximately 0.3 mm a^{-1} over the last 1ka in the Hampshire region (Shennan *et al.*, 2012), and the alteration of the land height itself. Evidence suggests that sea levels will rise in the future as a result of thermal expansion and the melting of land-based ice, caused by warming over the last century and expected to continue in the future (Houghton, 2005; Hall *et al.*, 2006; Haigh *et al.*, 2009). Even relatively small changes in mean sea level, due to changes in the land and sea heights are predicted to increase the likelihood of extreme sea level events. Haigh *et al.* (2011) for instance, estimated potential future extreme high sea levels throughout the English Channel during the 21st century based on expected sea level increases of 12, 40 and 81 cm. They reported that the exceedence frequency of extreme high sea levels in the region would, on average, increase by a factor of 10, 100 and 1800, respectively, due only to mean sea level changes.

Moreover, intensification of wave conditions within the North Atlantic-North Sea shelf has been linked to an increase in storminess and mean wind speeds over the last 30 years (Bacon and Carter, 1991; Zang and Tooley, 2003; Inter Agency Committee on Marine Science and Technology, 2004), although research by Wolf and Woolf (2006) indicates that the latter is likely to be the most significant factor contributing to an increase in wave heights. Changes in global mean sea levels have been found to further intensify wave conditions. Chini *et al.* (2010) highlighted that an increase in water levels, due to surge or an increase in mean sea level, results in waves breaking later and, therefore, more energy reaching the coast. They suggest that within the south east of the UK, an increase in sea level of 7 mm $year^{-1}$ could result in a 4% increase in height of a 100 year event by 2090.

As a result, funding into flood defence within the UK has increased from £303 million to £550 million between 2002 and 2006, and continues to increase each year to cope with heightened risks (Environment Agency, 2007). Due to the complexity of the region, and the large errors found in previous research, there is a strong desire for

the establishment of a regional model for the Solent region, capable of transforming offshore predictions of wave and water levels from the English Channel to the coast. Quantifying the most significant sources of uncertainty in the system, and developing ways to reduce it, is an important consideration when attempting to improve the quality of forecasts in the region.

2.4.2. Boundary forcing and *in-situ* measurements

The central English Channel, in particular the Solent, contains numerous *in-situ* gauges measuring water levels, atmospheric conditions and wave states, both in offshore and nearshore conditions; vital in the calibration of a regional tide-surge-wave model. Datasets can be obtained free of charge from the National Tidal and Sea Level Facility (NTSLF, at http://pol.ac.uk/ntslf/), the Centre for Environment, Fisheries and Aquaculture Science (CEFAS, www.cefas.defra.giv.co.uk) and the CCO. Furthermore, three temporary wave buoys provisioned from EMU (http://www.emulimited.com/) for a three month period from October to December 2009 provided data for this research.

A new forecasting system (Previmer) is currently under development in the English Channel region which could provide boundary forcing datasets to a regional model of the Solent. Previmer is a pre-operational hydrodynamic and spectral wave modelling system, currently under development, which aims to provide users with short-term forecasts of ocean state over a variety of model domains, including global and North East Atlantic models, with smaller nearshore nests at selected regions along the French coast (http://www.previmer.org/en.). The North East Atlantic model generates forecasted water level elevations and wave states throughout the English Channel, with higher spatial resolutions (under 6km) than are currently available from the present shelf scale operational forecasting in the UK. Tide and surge components are modelled using the Model for Application at Regional Scale (MARS 2D) system (Lazure and Dumas, 2008) while wave conditions a predicted using the the Wavewatch III model (Tolman, 2009). More information regarding the partners involved in the development of Previmer, and its current operational status can be found at http://www.previmer.org/en.

2.4.3. Software selection: MIKE-21

2.4.3.1. Justification

The MIKE-21 hydrodynamic and spectral wave modelling software has been used in this research to model the Solent- Southampton Water region. The MIKE-21 software is a comprehensive modelling system, developed by the Danish Hydraulic Institute (DHI),

applicable to oceanographic, coastal and estuarine environments. It includes a wide variety of modules ranging from the core hydrodynamic module (used to simulate water level variations and flows) to more specialist modules such as the oil spill module and the sediment transport module. This research utilised the hydrodynamic (HD) and spectral wave (SW) modules. This software was selected for a variety of reasons. First, the software provides a user friendly GUI feature, particularly useful during domain mesh generation and optimisation. Furthermore, at the University of Southampton there is a history of MIKE-21 use, providing a useful support structure. Both these factors were important in enabling the software to be used to model the region of interest. In addition, MIKE-21 has been designed to be applicable to both offshore and nearshore regions, while also allowing for both 1-way and 2-way coupling between the HD and SW modules. The applicability to both deep and shallow water regions is of importance when modelling through the English Channel where depths range from approximately 100 m to less than 10 m, while the ability to couple the models is essential in the examination of the tide-surge-wave interactions.

In addition to the applicability and ease of use, the MIKE-21 software was also considered to be acceptable as the fundamental equations used in both the HD and SW modules are common among other widely used software. MIKE-21 HD is based on the numerical solution of the Navier Stokes equations and consists of continuity, momentum, temperature, salinity and density equations. Such equations are standard among other widely utilised hydrodynamic models, for instance, TELEMAC (Moulinec et al., 2011; http://www.opentelemac.org/) and ADCIRC (Luettich and Westerink (2004); http://www.adcirc.org/document). Similarly, MIKE-21 SW was developed from the WAM 3rd generation wave model (Hasselmann *et al.*, 1988) which is widely regarded as the state of the art wave model (Wolf, 2009). MIKE-21 SW propagates the wave spectrum using the action balance equation in a similar manner to SWAN (Booij *et al.*, 1999) and is applicable in both deep and shallow water applications by incorporating shallow water source terms into the model equations. Both employ explicit Euler schemes and utilise finite volume approaches in their numerical implementations.

The common usage of the fundamental equations found in the MIKE-21 software implies that the model approach and formulations should be robust. This is further suggested by its wide application in research and industry, including the Federal Emergency Management Agency (FEMA, 2001) and many others, such as Johnson and Kofoed-Hansen (2000), Cañizares *et al.* (2001), Madsen and Jakobsen (2004), Sørensen *et al.*, (2004), Sørensen *et al.*, (2006), and Dix *et al.* (2007). Such research has validated MIKE-21's modelling capabilities. For instance, Cañizares *et al.* (2001) used MIKE-21 HD to model tidal elevations through the North Sea and Baltic Sea regions, reporting root mean squared errors (RMSE) in predicted peak tidal amplitudes of between 0.07 m to 0.97 m. At 4 class A coastal tide gauges along the Eastern coast of the UK, the model predicted the tidal amplitudes with a normalised RMSE of between

8 – 13 %. Within the English Channel, Dix *et al.*, (2007) were able to accurately recreate the tidal currents in order to force a sediment mobility model using the HD module. Sørensen *et al.*, (2004b) and Rugbjerg *et al.*, (2006) used coupled HD and SW modules to forecast wave conditions in the German Blight and the eastern North Sea respectively. Both report very good correlations with *in-situ* measurements in depths between 15 m and 10 m. Rugbjerg *et al.*, (2006), for instance, report SI values of 20 % and 12 % in the H_s and T_z respectively, which are reasonable relative to other currently operational forecast accuracies (Bradbury *et al.*, 2004; Bidlot *et al.*, 2007) . Furthermore, Sørensen *et al.*, (2006) have demonstrated that the ability to vary the degree of coupling between the MIKE-21 HD and SW modules can be used to examine the wave-tide interactions in their study of the Bristol Channel, crucial to the proposed research contained in this thesis. These studies indicate that the MIKE-21 HD and SW module should be suitable to meet the aims of this thesis.

2.4.3.2. Model formulations

The follow section provides an overview of the fundamental default terms used in the HD and SW modules in the MIKE-21 software. Further details relating to the formulation descriptions, numerical implementations, and the vast array of user options can be found in the DHI scientific documentation (DHI, 2009a, 2009b, 2009c) from which the following summary was provided.

MIKE-21 HD is central within the system as it drives all the other models within the MIKE package (such as the transport and wave models). The HD model solves vertically integrated, fully dynamic equations of continuity and conservation of momentum in two horizontal directions, using an explicit scheme, in either Cartesian or Spherical coordinate systems (Cañizares *et al.*, 2001). The system is based on the numerical solution of the two-dimensional incompressible Reynolds averaged Navier-Stokes equations (DHI, 2009a). The spatial discretization is performed using a cell-centred finite volume method. The governing equations for the two-dimensional model in shallow water conditions are given by integrating the horizontal momentum equations and continuity equation over the depth (in Cartesian coordinates) using Eq. 2.22 (DHI 2009b), where *x, y* are Cartesian co-ordinates; $h=\eta+d$ is the total water depth; *u, v* are the velocity components in the *x, y* direction; s_{xx}, s_{xy}, s_{yx}, s_{yy} are components of the radiation stress tensor; ρ_o is the reference density of water; f_{cor} is the Coriolis parameter; and $(\tau_{sx,} \tau_{sy})$, (τ_{bx}, τ_{by}) are the *x* and *y* components of the surface wind and bottom stress. S_m is the magnitude of the discharge due to point sources and (u_s, v_s) is the velocity by which the water is discharged into the ambient water.

$$\frac{\partial h}{\partial t}+\frac{\partial h\bar{u}}{\partial x}+\frac{\partial h\bar{v}}{\partial y}=hS_m$$

$$\frac{\partial h\bar{u}}{\partial t}+\frac{\partial h\bar{u}^2}{\partial x}+\frac{\partial h\bar{v}\bar{u}}{\partial y}=f_{cor}\bar{v}h-gh\frac{\partial \eta}{\partial x}-\frac{h}{\rho_o}\frac{\partial p_a}{\partial x}-$$
$$\frac{gh^2}{2\rho_o}\frac{\partial \rho}{\partial x}+\frac{\tau_{sx}}{\rho_o}-\frac{\tau_{bx}}{\rho_o}-\frac{1}{\rho_o}\left(\frac{\partial s_{xx}}{\partial x}+\frac{\partial s_{xy}}{\partial y}\right)+$$
$$\frac{\partial}{\partial x}\left(hT_{xx}\right)+\frac{\partial}{\partial y}\left(hT_{xy}\right)+hu_sS_m$$

$$\frac{\partial h\bar{v}}{\partial t}+\frac{\partial h\bar{u}\bar{v}}{\partial x}+\frac{\partial h\bar{v}^2}{\partial y}=-f_{cor}\bar{u}h-gh\frac{\partial \eta}{\partial y}-\frac{h}{\rho_o}\frac{\partial p_a}{\partial y}-$$
$$\frac{gh^2}{2\rho_o}\frac{\partial \rho}{\partial y}+\frac{\tau_{sy}}{\rho_o}-\frac{\tau_{by}}{\rho_o}-\frac{1}{\rho_o}\left(\frac{\partial s_{yx}}{\partial x}+\frac{\partial s_{yy}}{\partial y}\right)+ \qquad (2.22)$$
$$\frac{\partial}{\partial x}\left(hT_{xy}\right)+\frac{\partial}{\partial y}\left(hT_{yy}\right)+hv_sS_m$$

The overbar indicates a depth average value. The $\bar{u}$ and $\bar{v}$ depth averaged velocities are defined by

$$h\bar{u}=\int_{-d}^{\eta}udz \quad \text{and} \quad h\bar{v}=\int_{-d}^{\eta}vdz \qquad (2.23)$$

Lateral stresses (T_{Lij}) include viscous friction, turbulent friction and differential advection. They are estimated using an eddy viscosity formulation based on the depth averaged velocity gradients

$$T_{xx}=2A_{ev}\frac{\partial \bar{u}}{\partial x}$$
$$T_{xy}=A_{ev}\left(\frac{\partial \bar{u}}{\partial y}+\frac{\partial \bar{v}}{\partial x}\right) \qquad (2.24)$$
$$T_{yy}=2A_{ev}\frac{\partial \bar{v}}{\partial y}$$

where A_{ev} is the sub-grid scale horizontal eddy viscosity (after Smagorinsky, 1963) given by

$$A_{ev}=c_s^2l^2\sqrt{2S_{d\,ij}S_{d\,ij}} \qquad (2.25)$$

where c_s is a constant, l is a characteristic length and the deformation rate is given by

$$S_{dij} = \frac{1}{2}\left(\frac{\partial u_i}{\partial x_j} + \frac{\partial u_j}{\partial x_i}\right)(i, j - 1,2)) \tag{2.26}$$

Bottom stress is determined by a quadratic friction law (Eq. 2.26) in which c_f is the drag coefficient and $\vec{u}_b = (u_b, v_b)$ is the flow velocity above the bottom.

$$\frac{\vec{\tau}_b}{\rho_o} = c_f \vec{u}_b |\vec{u}_b| \tag{2.26}$$

The friction velocity associated with the bottom stress is given by

$$U_{\tau b} = \sqrt{c_f |\overrightarrow{u_b}|^2} \tag{2.27}$$

For 2D calculations $\vec{u}_b$ is the depth averaged velocity and c_f can be determined from the Manning number, *M*

$$c_f = \frac{g}{(Mh^{1/6})^2} \tag{2.28}$$

In areas not covered by ice the surface stress is determined by the winds above the ocean surface. This wind stress ($\bar{\tau}_s$) is given by the empirical relation

$$\bar{\tau}_s = \rho_a c_d |u_w| \left(u_{w_x}, u_{w_y}\right) \tag{2.29}$$

where c_d is the wind drag coefficient, and u_{wx} and u_{wy} are wind speed components along *x* and *y* axes.

The friction velocity associated with the surface stress is given by

$$U_{\tau s} = \sqrt{\frac{\rho_a c_d |\overline{u}_w|^2}{\rho_o}} \tag{2.30}$$

and drag coefficient is parameterised using the empirical formula proposed by Wu (1980; 1994),

$$C_d = \begin{cases} C_a & u_w < W_a \\ C_a + \frac{C_b - C_a}{W_b - W_a}(u_w - W_a) & W_a \le u_w < W_b \\ C_b & u_w \le W_b \end{cases} \tag{2.31}$$

where c_a, c_b, w_a and w_b are empirical factors and u_w is the wind speed (given here at 10 m above the sea surface). The empirical factors are given as $c_a = 1.255 \cdot 10^{-3}$, $c_b = 2.425 \cdot 10^{-3}$, $w_a = 7 ms^1$ and $w_b = 25\ ms^1$ as default and are suggested to provide good results for open sea conditions.

The time integration of the shallow water equations utilises an explicit scheme. In order to retain stability, a restriction is used in the implemented numerical scheme so that the time step used ensures the CFL number is below a value of 1. Within MIKE-21 HD a variable time step interval is used. The CFL number is defined by

$$CFL_{HD} = \left(\sqrt{gh} + |u|\right)\frac{\Delta t}{\Delta x} + \left(\sqrt{gh} + |v|\right)\frac{\Delta t}{\Delta y} \tag{2.32}$$

where Δx and Δy are a characteristic length scale in the *x*- and *y*- direction for an element, Δt is the time step interval, *u* and *v* are velocity components in the *x*- and *y*- direction.

It can be shown that as grid points become closer (i.e. grid spatial resolution increases) then the upper limit for acceptable time steps decreases for stability of the explicit numerical solution.

MIKE-21 SW is a third generation spectral wind-wave model that simulated the growth, decay and transformation of wind-generated waves and swells in offshore and coastal areas, based upon the wave action density spectrum, which varies in time and space as a function of wave direction and frequency (DHI, 2009c). The governing equation is the wave action balance equation, formulated in Cartesian co-ordinates, and given, after Komen *et al.*, (1994) and Young (1999), as

$$\frac{\partial N}{\partial t} + \nabla \cdot \left(\vec{v} N\right) = \frac{S}{\sigma} \tag{2.33}$$

Where $N(\vec{x}, f, \theta, t)$ is the action density, $\vec{x} = (x,y)$ is the Cartesian co-ordinates, $\vec{v} = (c_x, c_y, c_\sigma, c_\theta)$ is the propagation velocity of a wave group in the four dimensional phase space $\vec{x}$, σ and θ. ∇ is a four dimensional differential operator in the $\vec{x}$, f, θ -space.

The model is applicable for propagation of the wave field from deep to shallow-water regions by incorporating shallow water terms into the energy source term,

$$S = S_{in} + S_{nl} + S_{ds} + S_{bot} + S_{surf} \tag{2.34}$$

where S_{in} is the generation of energy by wind, S_{nl} is wave energy transfer due to non-linear wave-wave interactions, S_{ds} is the dissipation of wave energy due to whitecapping, S_{bot} is the dissipation due to bottom friction and S_{surf} is the dissipations of wave energy due to depth induced breaking.

The wind input, S_{in}, is given by

$$S_{in}(f,\theta) = \alpha + \gamma E(f,\theta) \tag{2.35}$$

where S_{in} is the energy input from the wind, α (linear wave growth) and γ (nonlinear wave growth) factors depend on wave frequency and direction and wind speed and direction.

The non-linear growth is defined after Janssen (1991) who suggests that

$$\gamma = \varepsilon\beta\sigma {x_{nl}}^2 \tag{2.36}$$

where ε is the ratio of density of air to water and x_{nl} is given by Eq. 2.37 in which u_* is the wind friction velocity and θ and θ_w are the wave and wind directions, respectively.

$$x_{nl} = \frac{u_*}{c}\, cos(\theta - \theta_w) \tag{2.37}$$

Finally, β is given by

$$\beta = \frac{1.2}{\kappa^2}\mu 1\mathrm{n}^4\mu \quad \mu \leq 1 \tag{2.38}$$

$$\beta = 0 \quad \mu > 1 \tag{2.39}$$

where κ is von Karman's constant (0.41) and μ is the dimensionless critical height given by

$$\mu = kz_c \tag{2.40}$$

where z_c is the critical height defined as the elevation above sea level where wind speed is exactly equal to phase speed.

The linear growth, α, is given after Ris (1997) as

$$\alpha = \begin{cases} \frac{c_{lg}}{g^2 2\pi}\left(-\left(u_* cos(\theta - \theta_w)\right)^4\right) exp\left(-\left(\frac{\sigma}{\sigma_{PM}}\right)^{-4}\right) & cos(\theta - \theta_w) > 0 \\ 0 & cos(\theta - \theta_w) \leq 0 \end{cases} \tag{2.41}$$

where $c_{lg} = 1.5{\cdot}10^{-3}$ and σ_{PM} is the Pierson-Moskowitz frequency, defined by

$$\sigma_{PM} = \frac{0.13g}{28u_*} \tag{2.42}$$

The friction velocity is given using Eq. 2.43 and the drag coefficients are defined after Wu (1982)

$$u_*^2 = c_d \cdot u_w^2, c_d = \alpha_{drag} + \beta_{drag} \cdot u_w \tag{2.43}$$

where u_w is the wind speed and α_{drag} and β_{drag} are two constants.

The non-linear interactions, S_{nl}, include quadruplet-wave interactions and triad interactions. The quadruplet-wave interactions are not computed in an exact manner due to computational time constraints. Instead, an approximate of the DIA is used (developed by Hasselmann *et al.*, 1985a, 1985b) after Komen *et al.* (1994), who found

that an exact estimation of the non-linear interactions could be simulated by one mirror-image pair of intermediate range interaction configurations (Eq. 2.44)

$$\frac{\partial}{\partial t}\begin{pmatrix} N \\ N_+ \\ N_- \end{pmatrix} = \begin{pmatrix} -2 \\ +1 \\ +1 \end{pmatrix} C_{nl} g^{-8} f^{-19} [N^2(N_+ + N_-) - 2NN_+N_-]\Delta k, \tag{2.44}$$

Where $\partial N/\partial t, \partial N_+/\partial t, \partial N_-/\partial t$ are the rates of change in action at wave numbers k, k_+, k_- within the interaction phase-space element Δk, and C_{nl} is a constant. Summation of Eq. 2.44 over all wave numbers, directions and interaction configurations provides the net source function, S_{nl}. For a detailed examination of quadruplet interactions see DHI (2009 c).

The shallow water triad-interactions are modelled using the simplified approach proposed by Eldeberky and Battjes (1995, 1996),

$$S_{nl}(\sigma,\theta) = S_{nl+}(\sigma,\theta) + S_{nl-}(\sigma,\theta) \tag{2.45}$$

where

$$S_{nl+}(\sigma,\theta) = max\begin{pmatrix} 0, \alpha_{EB} 2\pi c_g J^2 |sin(\beta_{tri})| (cE^2(\sigma_-,\theta) -) \\ 2c_- E(\sigma_-,\theta)E(\sigma,\theta) \end{pmatrix} \tag{2.46}$$

$$S_{nl-}(\sigma,\theta) = -2S_{nl+}(\sigma_+,\theta) \tag{2.47}$$

Here $\sigma_- = \sigma/2$, $\sigma_+ = 2\sigma$, and $c_- = \sigma_-/k_-$ is the phase velocity, where k_- is the wave number corresponding to σ_-. α_{EB} is a tuning parameter, β_{tri} is a parameter relating to the biphase and J is an interaction coefficient, given by

$$J = \frac{k_-^2(gd+2c_-^2)}{-kd\left(gd+2Bgd^3k^2-\left(B+\frac{1}{3}\right)\sigma^2d^2\right)} \tag{2.48}$$

where B=1/15.

The dissipation due to whitecapping, S_{ds}, based on the theory of Hasselmann (1974), and adapted after Janssen (1989)

$$S_{ds}(f,\theta) = -C_{ds}\left(\frac{\hat{\alpha}}{\hat{\alpha}_{PM}}\right)^m \left\{(1-\delta)\frac{k}{\bar{k}} + \delta\left(\frac{k}{\bar{k}}\right)^2\right\}\bar{\sigma}E(f,\theta) \tag{2.49}$$

where C_{ds}, δ and m are constants, of which C_{ds}, and δ are tuneable, and $\hat{\alpha}$ is the overall wave steepness

The rate of dissipation due to bottom friction is given after Weber (1991) by

$$S_{bot}(f,\theta) = -\left(C_f + f_c\left(\bar{u}\cdot\bar{k}\right)/k\right)\frac{k}{sinh2kd}E(f,\theta) \tag{2.50}$$

where C_f is a friction coefficient, u is the current velocity and f_c is the friction coefficient for the current which can be calculated based upon a constant geometric roughness size (k_N) by

$$C_f = f_w u_{wb} \tag{2.51}$$

where u_{wb} is the rms wave orbital velocity at the bottom and the friction factor (f_w) is calculated after Jonsson and Carlsen (1976)

$$\begin{aligned} f_w &= e^{-5.977+5.213(a_b/k_N)^{-0.194}} \quad a_b/\, k_N \geq\ 2.016389 \\ f_w &= 0.24 \qquad\qquad\qquad\qquad\quad a_b/\, k_N <\ 2.016389 \end{aligned} \tag{2.52}$$

where a_b is the orbital displacement at the bottom.

Depth-induced breaking is calculated using the formulation of Battjes and Janssen (1978), written in MIKE-21 as

$$S_{surf}(f,\theta) = -\frac{2\alpha_{BJ} Q_b \bar{f}}{X} E(f,\theta) \tag{2.53}$$

where α_{BJ} is a constant ≈1, Q_b is the fraction of breaking waves, $\bar{f}$ is the mean frequency, and x_r is the ratio of the total energy in the random wave train to the energy in a wave train with the maximum possible wave height, given by

$$X = \frac{E_{tot}}{(H_m^2/8)} = \left(\frac{H_{rms}}{H_m}\right)^2 \tag{2.54}$$

where E_{tot} is the total wave energy, H_m is the maximum wave, and $H_{rms} = \sqrt{8E_{tot}}$. In shallow water the maximum wave height can be given as $H_m = \gamma_{di} d$, where γ_{di} is the breaking parameter.

Within MIKE-21 SW, the numerical propagation step is carried out by an explicit Euler scheme. In order to overcome the CFL stability restrictions a multi sequence integration scheme is employed (based on the work of Vilsmeier and Hänel, 1995), in which the maximum time step can be altered locally by employing a series of integration steps, where the number of steps may vary element to element (DHI, 2009c). Using this method the CFL criteria differs from that given in the HD module and is represented by

$$Cr_{i,l,m} = \left| c_x \frac{\Delta t}{\Delta x_i} \right| + \left| c_y \frac{\Delta t}{\Delta y_i} \right| + \left| c_\sigma \frac{\Delta t}{\Delta f_l} \right| + \left| c_\theta \frac{\Delta t}{\Delta \theta_m} \right| < 1 \tag{2.55}$$

where $Cr_{i,l,m}$ is the Courant number and Δx_i and Δy_i are characteristic length scales in the x and y- directions for the i^{th} element. C_x, C_y, C_σ, C_θ are propagation velocities of a wave group in four dimensional space.

Chapter 3: Modelling waves and water levels in the Solent and surrounding waters: sensitivity to local wind stress and boundary conditions

Abstract

The sensitivity of a regional wave and surge model to local wind stress and boundary condition input datasets is examined in the Solent, a complex nearshore region containing an array of water depths, wave conditions, and unique tidal hydrodynamics. The prediction of the surge was most sensitive to the boundary surge elevations, with the local wind stress accounting for less than 10% of the magnitude of the surge during the largest events. Predictions of the wave state, on the other hand, demonstrated that despite the limited domain extent, the local winds contributed a significant amount of energy to the waves, accounting for 60.6% of the H_s during two storm events in November 2009. Spatial variability in the model sensitivity was high, particularly when predicting wave conditions, due to the sheltering effect provided to the western Solent by the Isle of Wight and Hurst Spit.

The Previmer wind and boundary condition datasets, used to force the regional model, were contrasted with those from another, currently operational system, during a three month period from October to December 2009. The datasets from both systems were broadly similar on average, with the substitution of one not resulting in a significant change to the accuracy of the three month predictions of surge and wave states. However, short-term divergence in the datasets was high, particularly during an event on the 14th November 2009, leading to divergence in the two predictions of surge and wave peak magnitudes by up to 10%.

The findings presented in this research provide information, relating to the sensitivity of nested regional coastal models to dataset uncertainty, which will be of interest to coastal managers working in the Solent and other, similar, environments. Furthermore, the assessment of the Previmer datasets during the three month period, and the corresponding sensitivity of the predictions to divergence from other systems, provides valuable information to those interested in the Previmer products.

3.1. Introduction

Coastal flooding is a threat to many regions around the world, responsible for the deaths of thousands, and millions of dollars' worth of damages each year. For

instance, two flooding events in the Bay of Bengal, occurring in 1970 and 1991, resulted in the deaths of 440,000 people (Flather, 1994). To protect against the threat of coastal flooding, numerical models have been utilised in many regions around the world to provide forecasts of ocean water levels and wave states. Ocean forecasting systems usually involve a suite of models, often coupling tide, surge, and wave predictions with atmospheric models that provide forecasts of wind and air pressures through the region of interest (e.g., Allard *et al.*, 2008). Flather, (2000) provides a summary of a variety of operational systems that have been utilised throughout Europe. Such systems commonly provide forecasts over global and continental-shelf scale domains (e.g. Williams and Horsburgh, 2006). To reduce computational demands, relatively coarse spatial resolutions are often used in deep water regions where spatial variability in the ocean state is limited, while nearshore nests are utilised in specific nearshore regions where finer spatial discretization is required.

Where a nested modelling approach is used, the predictions made will often be influenced significantly by the state of the ocean entering the domain, due to the limited size of the regional model. For instance, it has been shown that for extreme wave conditions to develop, a sufficiently long fetch is often required (Knauss, 1966). Many small-scale, regional nests will not be sufficiently large to enable realistic representations of the wave field to develop. For this reason regional nests require boundary conditions to be specified, representing the state of a system outside the immediate model domain. Depending on the size of the domain, the additional influence of the local atmospheric conditions may also strongly modulate the incoming boundary conditions. As both the boundary conditions and the internal atmospheric conditions are usually outputs from larger scale modelling applications, the quality of these datasets will be an important influence upon the accuracy of the solutions obtained from the regional model to which they are applied. Quantifying data quality and the sensitivity of the model to errors in the datasets can provide end users with greater understanding of model predictions and their inherent uncertainty, while also highlighting in which datasets uncertainties can be of greatest significance to the model predictions.

Previmer is a pre-operational ocean modelling system, currently under development, which aims to provide users with short-term forecasts of ocean state over a variety of model domains, including global and North East Atlantic models, with smaller nearshore nests at selected regions along the French coast (http://www.previmer.org/en). The North East Atlantic model generates forecasted wave states and water level elevations throughout the English Channel, providing a potential source for boundary driving conditions for a regional model of the Solent and Hampshire coastline, on the south coast of the UK, an area thought likely to be affected by increased flood risk in the future (Evans, 2004).

This region provides a unique setting in which to examine the sensitivity of regional surge and wave models to boundary conditions and local wind stresses. It is a complex region, containing a large range of environments within which to examine model sensitivity, ranging from artificially deepened channels for shipping, to inter-tidal mudflats (Levasseur, 2008). Furthermore, it is a region that can be susceptible to large storm surge and wave events, most commonly propagating west from the North East Atlantic. The protection offered to the western Solent from large swells by the Isle of Wight provides an interesting mixture of regions exposed to large swells and those experiencing only local, fetch-limited, wave action. Due to the complexity of the coastal environment, this region requires a relatively fine spatial resolution model domain to accurately recreate the variability in the coastal ocean state. The assessment of the prediction sensitivity in the variety of conditions found within the region, to uncertainty in the boundary and local wind forcing, therefore, could provide information of value to the understanding of regional models in the Solent, while also being applicable to nested models in other coastal environments.

This research aimed to assess the sensitivity of the regional wave and surge predictions to the local wind and boundary condition input datasets. By meeting this aim, this research highlighted the temporal and spatial variability in model sensitivity, in order to provide coastal managers with an indication of the datasets in which high accuracy is of greatest importance in estuarine environments, such as those contained in the Solent. Furthermore, the research also aimed to quantify the errors within the datasets provided by Previmer (relative to another operational system) and assess the influence of the 'dataset selection uncertainty' upon the prediction of the surge and wave states in the Solent region. This aimed to provide coastal modellers with a case study with which to assess the quality of the wind, wave and surge data products currently available from the Previmer system in the English Channel.

The datasets, model set up, and analysis used are described in Sections 3.2, 3.3, and 3.4, respectively. The results are given in Section 3.5. A discussion is provided in Section 3.6 and the conclusions are drawn in Section 3.7.

3.2. Study Site and Data

3.2.1. The Solent

The Solent is a body of water that lies between the south coast of England and the Isle of Wight in the UK (Fig. 3.1). It includes 12 separately defined estuaries and harbours and contains a range of coastal habitats and inter-tidal zones (Fletcher *et al.*, 2007). The region has various stakeholders, protected habitats, a dense coastal population and two of the largest shipping ports in the UK.

The irregular geometrical shape, narrow channel configuration and shallow depths, results in the amplification of shallow water tidal constituents, M_4 and M_6 (Levasseur, 2008). These amplifications create a tidal elevation with a double high water and young flood stand, most prominent in the Southampton Water region (Rantzen, 1969; Levasseur, 2008). Previous attempts at modelling the tidal hydrodynamics within the region have shown relatively large errors in the western Solent and Southampton Water regions (Levasseur, 2008).

Storm surges in this region most frequently occur due to low pressure systems from the Atlantic propagating eastwards, or as a result of storm surges propagating south from the North Sea (Law, 1975; Haigh *et al.*, 2004). Notable events have caused flooding within the region include those occurring on 14th – 18th December 1989 (Wells *et al.*, 2001) and 10th March 2008 (Haigh *et al.*, 2010).

The region is generally considered to be sheltered from extreme waves, with long-term average H_s of 1.5 m or less (Inter-Agency Committee on Marine Science and Technology, 2004) and T_z of typically 6 -10 seconds. The largest waves that occur usually arrive from either 240° due to storm waves and swells from the Atlantic (Dix *et al.*, 2007) or occasionally 40-50° (storm waves from the eastern English Channel). The eastern Solent regions, particularly Hayling Island, and Milford to the west of the Solent, are the most exposed areas to significant wave energy within the region of interest (Palmer, 2011). A review of flood events in the Solent since 1935 can be found in Ruocco *et al.* (2011).

3.2.2. Data

Tidal elevations, surge elevations, wave and wind conditions, derived from the Previmer group (http://www.previmer.org/en) were used in this research to force the regional models. These datasets were outputs from a pre-operational system, currently under development, which aims to provide users with short-term forecasts of the state of the ocean along French coastlines bordering the English Channel, the Atlantic Ocean, and the Mediterranean Sea. Tide and surge components of the water surface elevation (velocities were not specified) were provided at 5.5 km spatial resolution, and 1 hour temporal resolution throughout the English Channel. These data were model outputs created using the Model for Application at Regional Scale (MARS 2D) system (Lazure and Dumas, 2008). Wave conditions (H_s, T_z, direction and spreading) were provided at 3.5 km spatial and 3 hour temporal resolution from forecasts made using the Wavewatch III model (Tolman, 2009). The Previmer models utilise modelled wind fields at 3 hour temporal and 4 km spatial resolution provided by the European Centre for Medium Range Weather Forecasts (ECMWF, www.ecmwf.int/about). These wind field datasets were supplied via the Previmer group for this research. Atmospheric pressure fields were interpolated from measurements

provided by the Channel Coastal Observatory (CCO). Measurements at seven sites located along the south coast of England, between longitudes of -3.48° and -0.48° were used; Teignmouth, West bay Harbour, Portland Harbour, Swanage, Lymington, Sandown and Arun Platform. Data were available at 10 minute intervals at each site and interpolation was used to provide estimates over the computational domain.

In-situ measurements of water level, wave and wind conditions were given at the sites in Fig. 3.1, provided online by the NTSLF (at http://pol.ac.uk/ntslf/), CEFAS (www.cefas.defra.giv.co.uk) and the CCO. Further measurements were provided by three temporary buoys provided for this research by EMU (http://www.emulimited.com).

Further modelled wind fields, boundary wave conditions, and boundary surge elevations from the Met Office operational Wavewatch III model (Bradbury *et al*. 2004; Tolman, 2009) and storm surge model (Flather, 2000; Williams and Horsburgh, 2006), respectively, were obtained to enable comparisons with the Previmer datasets to ascertain the suitability of the Previmer data for use in the regional model. Data were supplied at 12 km spatial and 1 hour temporal resolutions through the English Channel.

When utilised in the MIKE-21 model, all datasets were interpolated to provide temporal resolutions matching the simulation time step of the model.

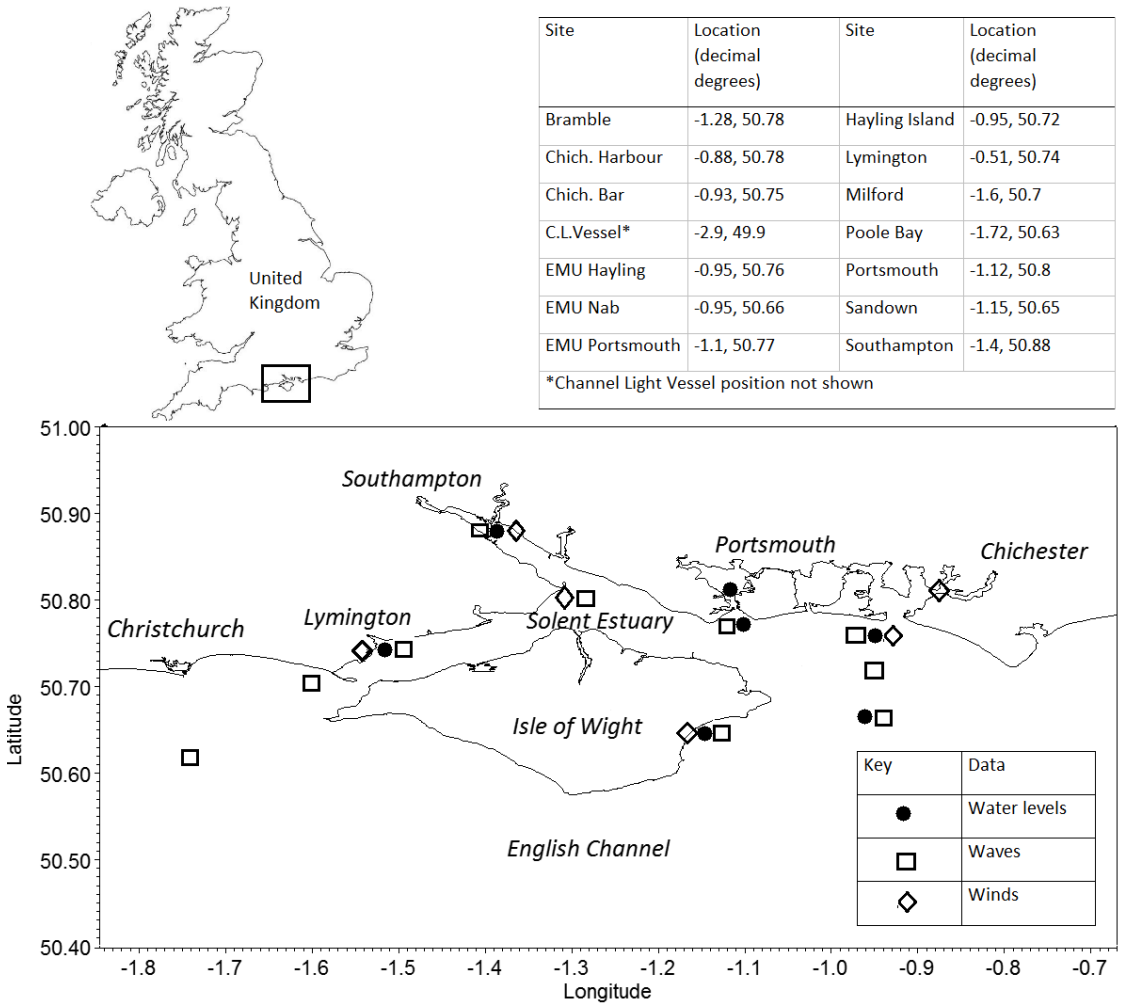

Site	Location (decimal degrees)	Site	Location (decimal degrees)
Bramble	-1.28, 50.78	Hayling Island	-0.95, 50.72
Chich. Harbour	-0.88, 50.78	Lymington	-0.51, 50.74
Chich. Bar	-0.93, 50.75	Milford	-1.6, 50.7
C.L.Vessel*	-2.9, 49.9	Poole Bay	-1.72, 50.63
EMU Hayling	-0.95, 50.76	Portsmouth	-1.12, 50.8
EMU Nab	-0.95, 50.66	Sandown	-1.15, 50.65
EMU Portsmouth	-1.1, 50.77	Southampton	-1.4, 50.88
*Channel Light Vessel position not shown			

Fig. 3.1. The location of the Solent and *in-situ* measurements.

3.3. Model set-up

The MIKE-21 software was used to model the domain of interest. MIKE-21 is a widely used 2D modelling package designed by the DHI group. MIKE-21 has a history of use in research and industry, including FEMA (FEMA, 2001) and many others, such as Johnson and Kofoed-Hansen (2000), Cañizares *et al.* (2001), Madsen and Jakobsen (2004), Sørensen *et al.* (2004), Sørensen *et al.* (2006), and Dix *et al.* (2007), who have used the software in both offshore and coastal environments.

The hydrodynamic (HD) module used in this research is central within MIKE-21. It solves a full set of vertically integrated, equations of continuity and conservation of momentum in two horizontal directions using an explicit scheme in either a Cartesian or Spherical coordinate system (Cañizares *et al.*, 2001). The system is based on the numerical solution of the two-dimensional incompressible Reynolds averaged Navier-Stokes equations. The horizontal eddy viscosity is given after Smagorinsky (1963).

Bottom stress is estimated using a quadratic friction law, in which the drag coefficient can be determined from the Manning number (given in MIKE-21 as the reciprocal of the value used in many textbooks). Wind stress is given as a function of the air density, the wind speed 10m above the sea surface, and a drag coefficient, parameterised after Wu (1980; 1994).

MIKE-21 SW is a third generation spectral wind-wave model that simulated the growth, decay and transformation of wind-generated waves and swells in offshore and coastal areas, derived from the WAM formulation (Hasselmann *et al.*, 1988). The governing equation is the wave action balance equation, formulated in Cartesian co-ordinates, is given, after Komen *et al.* (1994) and Young (1999). The model is applicable to offshore and coastal environments as it includes shallow water sources terms for wave generation by the wind (after Janssen, 1991), quadruplet nonlinear interations (after Komen *et al.*, 1994), triad nonlinear interactions (after Eldeberky and Battjes., 1995; 1996), as well as dissipation due to whitecapping (Hasselmann, 1974), bottom friction (Weber, 1991) and depth-induced breaking (Battjes and Janssen, 1978). Further information regarding the MIKE-21 HD and SW models can be found in DHI (2009b) and DHI (2009c).

Fig. 3.2 demonstrates the model domain mesh and bathymetry. Bathymetry data of 100 m resolution provided by the National Oceanographic Centre (NOC), Southampton (http://www.noc.soton.ac.uk) were interpolated to the domain mesh. Boundary tide, surge and wave time-series provided by Previmer, were given at the two domain boundaries, located along the -3.5° and -0.1° lines of longitude.

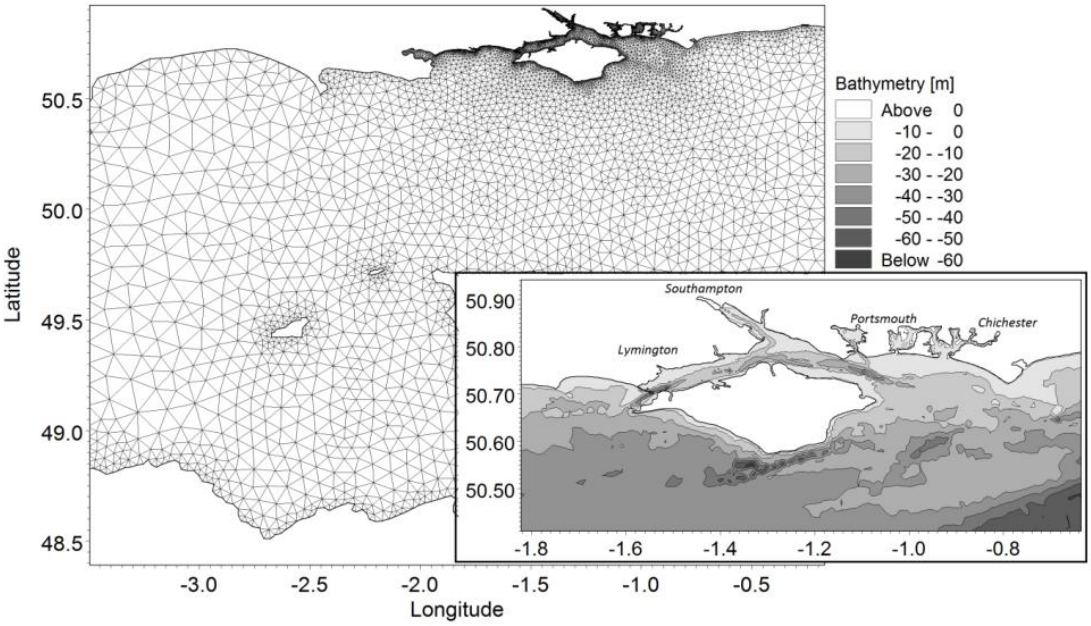

Fig. 3.2. Model domain mesh and bathymetry.

Sensitivity of the model to the domain mesh resolution was examined over a series of tide and wave predictions, utilising model mesh designs with increasing spatial resolution in the nearshore regions. Mesh resolution was limited through the use of maximum element area constraints, ranging from 1e-3°^{2} to 5e-6°^{2}, representing approximate element centre distances of between 1500 – 1800 m and 50 – 100 m, respectively. The upper limit of 5e-6°^{2} was used due to computational demands. The predictions from October to December 2009 obtained using the different mesh designs were compared. The results indicated that the mesh resolution required to recreate the model predictions given using the highest mesh resolution was dependent upon the location and output parameter of interest. Table 3.1 provides examples from a selection of the assessed sites, indicating the error (%) in a variety of model outputs relative to those given using the highest mesh resolution.

The results indicated that the surface elevation was relatively insensitive to the mesh resolution relative to the other model outputs considered. When considering the impact upon modelled currents, $H_{s,}$ and T_z, many of the sites were shown to provide model outputs within 2 % of those obtained from the 5e-6°^{2} mesh when using mesh designs with maximum element sizes of 1e-5°^{2} and 2.5e-5°^{2} (corresponding to approximately 150-200 m and 225 – 300 m resolution). Three sites (Portsmouth, Lymington, Sandown) in particular demonstrated more significant deviations from the 5e-6°^{2} simulation, of as much as 12 %, even when using the next highest resolution mesh (1e-5°^{2}) were found. These findings indicated that in particular regions, for instance, the entrance into harbours such as Portsmouth, or shallow bathymetries such as those found near the Lymington gauge, the use of a high resolution mesh would be required, while in deeper offshore areas such as the EMU Nab site a lower resolution would suffice. For this reason, the domain was divided into 'nearshore' and 'offshore' regions, with a maximum element size of 5e-6°^{2} restriction applied to the former only. Further analysis examined the relaxation of mesh resolution constraint that could be applied to the 'offshore' areas (containing the deeper mid-Solent areas and the English Channel), while retaining convergence (given as 2 % deviation from the 5e-6°^{2} mesh outputs). Final mesh resolution was approximately 2 km, 150 – 200 m and 50 – 100 m in the English Channel, mid-Solent, and harbours and coastal regions, respectively.

Within the MIKE-21 HD model, the user is able to make decisions relating to three formulations of particular interest to this research; the eddy viscosity, the bed roughness, and the wind drag.

The default wind stress empirical coefficients of $c_a = 1.255 \cdot 10^{-3}$, $c_b = 2.425 \cdot 10^{-3}$, $w_a = 7 ms^{-1}$ and $w_b = 25\ ms^{-1}$ provided by DHI were used in this research as they are considered to be robust when modelling in most open sea conditions (DHI, 2009b), which is representative of the majority of the domain of interest.

Table. 3.1. Errors (%) in model outputs at a selection of measurement sites relative to those obtained using a mesh with a maximum element area of 5e-6°².

Mesh area constraint (degrees^2)		1e-3	5e-4	2.5e-4	1e-4	7.5e-5	5e-5	2.5e-5	1e-5
Surface Elevation (m)									
	Poole Bay	0.89	0.89	0.77	0.45	0.42	0.35	0.23	0.07
	Sandown	0.20	0.00	0.02	-0.13	0.19	0.12	0.00	0.00
	EMU Nab	-0.02	-0.23	-0.36	-0.46	-0.12	-0.08	-0.16	-0.05
	Lymington	-0.41	-1.09	-1.39	-2.72	-0.10	-1.00	-0.84	-0.26
	Portsmouth	-0.50	-0.82	-0.99	-2.69	-1.99	-0.39	0.22	0.07
Current Speed (ms^{-1})									
	Poole Bay	23.02	20.91	20.72	20.05	16.47	12.03	1.93	0.61
	Sandown	-40.04	-44.14	-45.69	-49.78	-36.53	-48.78	-36.94	-11.64
	EMU Nab	-0.12	-4.15	-10.06	-6.55	-6.84	-2.85	-1.01	-0.32
	Lymington	-12.08	-12.10	-11.61	-67.84	-54.68	-33.90	-24.55	-7.74
	Portsmouth	12.94	11.09	11.48	4.31	6.51	17.11	1.92	0.61
H_s (m)									
	Poole Bay	9.32	7.19	5.67	5.47	4.91	4.84	3.49	1.10
	Sandown	-41.38	-40.21	-37.74	-26.20	-31.42	-38.35	-22.87	-7.20
	EMU Nab	-2.91	-1.68	-1.96	-0.39	-0.04	0.39	0.35	0.11
	Lymington	-9.28	-10.30	-6.50	-9.65	-4.96	-4.66	-3.46	-1.09
	Portsmouth	-32.58	-29.14	-28.35	-25.02	-25.56	-22.17	-15.84	-4.99
T_z (s)									
	Poole Bay	2.18	0.86	0.85	-0.54	-0.42	0.37	0.06	0.02
	Sandown	-10.10	-9.11	-6.56	-3.72	-8.18	-8.06	-2.31	-0.73
	EMU Nab	-4.59	-4.39	-4.21	-1.19	-1.52	-1.41	-0.69	-0.22
	Lymington	-59.45	-59.62	-53.49	-33.76	-19.61	-29.35	-22.00	-6.93
	Portsmouth	-38.61	-21.35	-39.74	-28.54	-25.13	-26.12	6.44	2.03

Previous research by Dix *et al*. (2007), which utilised MIKE-21 HD to model tidal elevations and current velocities in the English Channel, demonstrated that an accurate representation of the hydrodynamics in the region could be obtained through the alteration of the Mannings coefficient. They found that the most accurate model outputs were obtained when the default value of 32 was increased to 39, while the alteration of the Smagorinski coefficient from the default of 0.28 did not result in any increase in model accuracy. Based on these findings, the calibration of the HD model in this research focussed on the optimisation of the Mannings coefficient. To do this, a series of tidal simulations were conducted over the period between 1st November and 30th November 2009, in each case altering the Mannings coefficient value. A range of values between 29 and 59 were used. The model outputs were compared to tidal elevations obtained from the *in-situ* measurements in the Solent region. The RMSE of the model outputs, relative to the tidal elevations extracted from the tide gauges, was used to define the best fit. Fig. 3.3, for instance, provides an example of the sensitivity to the Mannings coefficient at the Portsmouth and Lymington gauge sites. The results

indicated that the best results, on average, were obtained given a Mannings coefficient of 42.

Subsequent assessment of the impact of the Smagorinsky coefficient was also conducted. Recommended values from DHI range from 0.25 to 1, with a default setting of 0.28. Tidal simulations were conducted with the coefficient values of 0.25 to 0.75. The results indicated that the coefficient had relatively little impact upon the model outputs. For instance, at Portsmouth, Lymington and Southampton the maximum change in tidal elevation (at any point in the predicted time series) was less than 6 cm, while changes to the high tide elevations were consistently less than 2 cm.

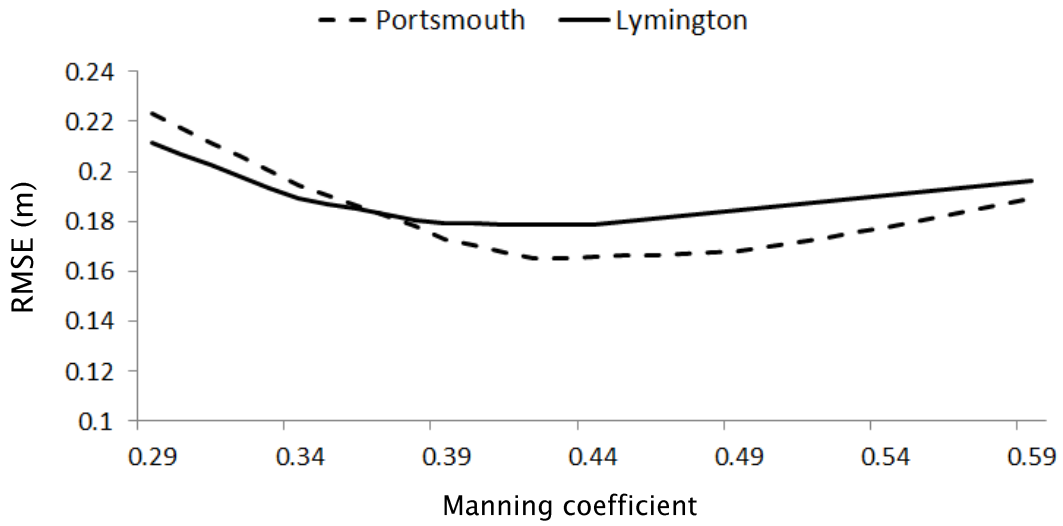

Fig. 3.3. Tidal accuracy plotted against Mannings coefficient value at the Portsmouth and Lymington tide gauges during a one month simulation of November 2009.

Within the SW model, numerous processes were considered. Diffraction was included as it was expected to be of significance due to the variability in the Solent coastline, and in particular, when modelling wave propagation into the various harbours found in the region. Similarly, non-linear interactions were included in order to properly represent both the quadruplet and triad interactions that can form between waves in both offshore and nearshore regions. In order to estimate the remaining parameters, primarily relating to the wave breaking, bottom friction, and whitecapping, a previously calibrated model of the Severn estuary, provided by DHI, was referred to (Sørensen *et al.*, 2006), the parameters for which are available with the download of the software from http://www.dhisoftware.com/Download/MIKEByDHI2012.aspx. The Severn model was used as a starting point due to the perceived similarities between the Severn model domain and that used in this research. Both models, for instance, aimed to propagate offshore waves, most commonly southwesterlies from the north east Atlantic, from depths of approximately 100 m into complerx nearshore estuarine environments which included a variety of nearshore conditions. From this starting

point, the bottom friction coefficient was used as the initial calibration parameter (Table 3.2). The November 2009 period was simulated using a variety of bottom friction coefficient values ranging from 0.1 to 0.001. The accuracy of the model predictions of peak H_s and average T_z were examined relative to *in-situ* measurements. The results indicated that the optimal value was dependent upon location and model output parameter of interest. However, when considering both model outputs, on average, throughout the domain, the most accurate predictions were obtained when using a constant value of 0.06.

Table 3.2. Model accuracies relative to *in-situ* wave measurements for a selection of Nikuradse constant values. H_s and T_z values relate to the average accuracies across all measurement sites. The 'average' row refers to the average of the H_s and T_z rows. All accuracies are given in terms of % error.

Nikuradse constant	0.01	0.02	0.03	0.04	0.05	0.06	0.07	0.08
H_s peak	21.39	19.70	18.58	16.75	15.53	14.35	14.68	14.79
T_z mean	17.87	15.52	13.17	10.82	11.32	11.82	12.32	12.99
Average	19.63	17.61	15.87	13.78	13.43	13.09	13.50	13.89

Further sensitivity tests examined the supplementary influence of the whitecapping delta (influential in determining the weighting of dissipation across the range of frequencies in the wave spectra) and wave breaking gamma (influential to the depth-induced dissipation to waves) coefficients to the model predictions. Both parameters can be influential to wave heights and periods as they propagate into shallow coastal waters. A range of simulations considered values of these coefficients within a range of 0.1 to 0.9, and 0.1 to 1.5 for the whitecapping and wave breaking coefficients respectively. These simulations were particularly interested in addressing large predictions errors found in some very shallow (less than approximately 5 m water depth) sites, such as EMU Portsmouth and Lymington, relative to the accuracies obtained elsewhere (discussed in more detail in Chapter 5). The results indicated that alteration to either coefficient was not able to provide a solution to such errors. The wave breaking coefficient was the most influential upon the model predictions, particularly H_s. Reducing the coefficient value resulted in a decrease in the predicted peak H_s, improving the model accuracy at sites such as Lymington. However, the decrease to peak H_s occurred throughout the domain, resulting in a reduction in prediction accuracies in many of the other sites. As alteration to either coefficient was not able to increase the average accuracy of the model outputs considered, nor address the relatively large errors found in the shallowest gauge sites, the model set-up retained the values specified in the Severn model (representing default MIKE-21 estimates for both coefficients).

The final formulations and parameter value choices used in the regional model are given in Table 3.3. Using the model set-up and data sources described, the regional model was capable of providing predictions of the tide-surge-wave conditions with accuracies broadly consistent with those expected from other model accuracy assessments in similar conditions (as discussed in more detail in subsequent chapters). For instance, tidal errors were significant, but closely resembled those from a 3d hydrodynamic model of the Solent presented by Levesseurr (2008), while surge residuals contained an average RMSE of 0.1 m which is broadly consistent with accuracies obtained from the operational storm surge model (http://www.pol.ac.uk/ntslf/model.html) at the Portsmouth gauge (Chapter 4). Similarly, waves, particularly in depths greater than approximately 10 m, performed within the common accuracy levels of assessments of operational systems (e.g. Bradbury *et al.*, 2004; Bidlot *et al.*, 2007), while larger relative errors have been reported in a variety of other systems (e.g. Moeini and Etemad-Shahidi, 2007; Brown *et al.*, 2011) in shallow (< 5 m) depths when using spectral wave models (Chapter 5).

Due to computational resource constraints, the calibration procedure used was not able to sample a vast proportion of the parameter space associated with the coupled HD-SW model. Given greater resources, it may be that a more exhaustive examination of the parameter space, for instance, through the use of a Generalised Likelihood Uncertainty Estimation (GLUE) approach (Beven and Binley, 1992), could enable more accurate model predictions to be made. However, given the constraints present in the research, and the findings that the model predictions compared broadly with those expected from other systems in similar locations, it is proposed that the current model adequately represents the tide-surge-wave conditions in the region, and therefore, provides a suitable tool with which to meet the aims of the thesis.

Table 3.3. Key formulation and parameter values for the coupled MIKE-21 HD and SW model

Parameter	Value
MIKE-21 HD	
Bathymetric resolution	100 m
Mesh resolution	2000 m in the central Channel, refined to approximately 100 -200m through most of the Solent, and 50 – 100 m in the harbour entrances
Flood and dry	On.
Drying depth, flooding depth, and wetting depth respectively	0.005 m, 0.05 m, 0.1 m,
Eddy viscosity formulation	Smagorinkski
Eddy viscosity coefficient	0.28
Bed roughness formulation	Mannings
Bed roughness coefficient	42
Coriolis forcing	Varying in domain
Wind forcing	Varying in time and across the domain. Wind speed, direction and atmospheric pressures.
Wind drag coefficients: c_a, c_b,w_a and w_b respectively	0.001255, 0.002425, 7, 25, After Wu (1980; 1994)
Precipitation and evaporation	No. No.
Wave radiation from SW model	Yes.
Boundary conditions	Varying along boundaries and through time. Tide and surge water level elevations.
MIKE-21 SW	
Spectral formulation	Fully spectral
Time formulation	Instationary
Frequency discretization (number of frequencies)	25
Directional Discretization (number of directions)	16
Water level conditions from HD model	Yes
Current conditions from HD model	Yes
Wind forcing formulation	Janssen (1991)
Wind forcing air-sea interaction	Coupled
Wind forcing Charnock parameter	0.01
Diffraction	Yes.
Quadruplet interactions formulation / inclusion	Komen *et al.* (1994) / Yes
Triad interactions formulation / inclusion	Eldeberky and Battjes (1995, 1996) / Yes
Wave breaking formulation	Battjes and Janssen (1978)
Wave breaking coefficients: α_{BJ} and γ_{di}	1, 0.8
Bottom friction formulation	Weber (1991)
Bottom friction Nikuradse roughness coefficient	0.06
White capping formulation	Janssen (1989)
White capping coefficients: C_{ds}, and δ	4.5, 0.5
Boundary conditions	Varying along boundaries and through time. H_s, T_p, mean wave direction, and directional spreading

3.4. Analysis

To meet the objectives of the research, three sets of experiments were undertaken. The first experiment examined the uncertainty in the wind, boundary wave, and boundary surge datasets. The wind predictions were contrasted with *in-situ* measurements and predictions provided by the Met Office, while the boundary surge and wave uncertainty was considered relative to the datasets provided by the Met Office. Comparisons were made for the three month period from October to December 2009.

The second set of experiments examined the sensitivity of the model-based surge and wave predictions to wind and boundary conditions (specifically boundary surge and boundary waves). Three simulations were conducted in each case, for the October to December 2009 period, as well as an event on the 10th March 2008.

The first simulation predicted the surge elevations obtained when both the wind and boundary surge conditions were included, while in simulations ii and iii the winds and boundary surge conditions were removed, respectively.

i. Tidal elevations + Previmer winds + Previmer boundary surge

ii. Tidal elevations + **no winds** + Previmer boundary surge

iii. Tidal elevations + Previmer winds + **no boundary surge**

The sensitivity of the surge predictions to winds and boundary surge was explored by calculating the difference between the model predictions obtained from simulation I, from those obtained from ii and iii.

Simulation iv predicted the state of the waves when both the wind and boundary wave conditions were included, while in simulations v and vi the winds and boundary wave conditions were removed, respectively.

iv. Water level elevations + Previmer winds + Previmer boundary waves

v. Water level elevations + **no winds** + Previmer boundary waves

vi. Water level elevations + Previmer winds + **no boundary waves**

The sensitivity of the wave predictions to winds and boundary waves was explored by calculating the difference between the model predictions obtained from simulation iv from those obtained from v and vi.

The third set of experiments assessed the uncertainty in the surge and wave predictions, given the selection of the Previmer datasets over those provided by the Met Office. Two simulations were conducted in each case, for the October to December 2009 period, as well as the 10th March 2008 event.

Simulations vii and viii predicted the surge elevations where the Met Office winds and boundary surge elevations, respectively, were utilised in place of those provided by the Previmer system.

vii. Tidal elevations + **Met Office winds** + Previmer boundary surge

viii. Tidal elevations + Previmer winds + **Met Office boundary surge**

The sensitivity of the surge predictions to the input datasets was calculated as the difference between the model predictions obtained from simulation i and those obtained from simulations vii and viii.

Simulations ix and x predicted the state of the waves where Met Office winds and boundary waves, respectively, were utilised in place of those provided by the Previmer system.

ix. Water level elevations + **Met Office winds** + Previmer boundary waves

x. Water level elevations + Previmer winds + **Met Office boundary waves**

The sensitivity of the wave predictions to the input datasets was calculated as the difference between the model predictions obtained from simulation iv and those obtained from simulations ix and x.

Clearly, the above sets of experiments represent a large number of comparisons. Therefore, to increase clarity over which datasets are being contrasted, the subscripts $_i$, $_h$, and $_m$ are used to represent input data, hindcast predictions and *in-situ* measured data, respectively. For example, the RMSE describing the error between a model hindcast and *in-situ* measurements is given as $RMSE_{h,m}$.

3.5. Results

3.5.1. Model sensitivity to the winds

3.5.1.1. Uncertainty in the wind fields

The uncertainty in the Previmer wind forcing data was assessed by comparing model outputs with wind gauge measurements and with a second predicted dataset provided by the Met Office (Table 3.4). The results indicate the error in the Previmer wind field relative to *in-situ* measurements and the Met Office dataset. Relative to the measured data, the Previmer wind speed resulted in an average $RMSE_{i,m}$ of 3.42 ms^{-1}, while wind direction contained a $RMSE_{i,m}$ of 54.29°. At each location the wind speed was over-estimated in the Previmer dataset on average. The errors were smaller when the Previmer and Met Office data were contrasted, with an average $RMSE_{i,i}$ of 1.55 ms^{-1} and 22.51° for wind speed and directions, respectively, with the Met Office speeds shown to be greater on average, during the period considered. Local variation was shown to be small. For example, the Met Office – Previmer $RMSEs_{i,i}$ in wind speeds, at each location, were within 0.2 ms^{-1} of the domain average. During the event on 14th November 2009, the timing of the wind speed peak occurred approximately three hours later in the Met Office-based wind field, relative to that in the Previmer dataset. Relative to the *in-situ* measurements, the Met Office-based wind field, particularly the timing of the peak, was the more accurate of the two input datasets.

Table 3.4. Comparison of wind fields modelled using Previmer inputs with those utilising Met Office inputs (bottom) and measured (top)

Previmer v. Measured				
Location	Wind Speed (ms^{-1}) RMSE	Wind Direction (degrees) RMSE	U Stress (Nm^{-2}) RMSE	V Stress (Nm^{-2}) RMSE
Bramble Bank	2.78	41.25	0.122	0.08
Chichester bar	2.55	37.9	0.22	0.18
Chich. Harbour	3.37	46.3	0.29	0.2
Lymington	2.76	–	–	–
Sandown Pier	4.19	80	0.29	0.18
Southampton	4.85	66	0.32	0.23
Average	3.42	54.29	0.25	0.17
Previmer v. Met Office				
Location	Wind Speed (ms^{-1}) RMSE	Wind Direction (degrees) RMSE	U Stress (Nm^{-2}) RMSE	V Stress (Nm^{-2}) RMSE
Bramble Bank	1.5	21.9	0.07	0.09
Chichester bar	1.58	22.9	0.14	0.18
Chich. Harbour	1.5	21.9	0.16	0.2
Emu Hay Buoy	1.58	22.9	0.13	0.16
Emu Nab Buoy	1.71	24.5	0.07	0.08
Emu Ports Buoy	1.55	22.5	0.09	0.11
Lymington	1.47	21.7	0.12	0.15
Portsmouth	1.55	22.4	0.08	0.01
Sandown Pier	1.56	22.3	0.1	0.12
Southampton	1.47	22.1	0.12	0.15
Average	1.55	22.5	0.11	0.13

The wind stresses, revealed that, on average, the largest errors were contained within the U component of the wind stress, when contrasting the Previmer and measured datasets, while the opposite was shown when comparing the Previmer and Met Office data. In both comparisons, differences of up to 1.5 Nm^{-2} were revealed at times. The errors in both the Met Office and Previmer datasets, relative to the *in-situ* measurements, were shown to be similar, suggesting that both datasets were able to recreate the measured wind fields with comparable accuracies.

3.5.1.2. Influence upon model predictions

3.5.1.2.1. Removal of the wind fields

The exclusion of wind stress input data (Table. 3.5) led to a domain average $RMSE_{h,h}$ and $Pbias_{h,h}$ of 0.03 m and 6.5%, respectively, (i.e., contrasting surge predictions with and without the inclusion of wind stresses).

Some spatial variability was present, with the largest changes shown to occur at Southampton. The exclusion of wind forcing data during the event on March 10th 2008 resulted in the smallest change in terms of $RMSE_{h,h}$ at the Nab Buoy site during the three month winter simulation and the event on the 10th March 2008. During this event, the change to peak surge magnitudes at Southampton was 13.9%, approximately 8% greater than that found at the Nab Buoy. The exclusion of the wind data resulted in a decrease to peak water levels of up to 0.2 m, while the skew-surge was decreased by up to 15.6%.

The wave model prediction was heavily modified by the local wind data. Domain average $RMSEs_{h,h}$ between model predictions without local wind data and those forced with Previmer wind fields were 0.69 m and 2.66 s for H_s and T_z, respectively, while $Pbias_{h,h}$, in both cases, was greater than 60%. The regions most sheltered from swell propagation contained larger $Pbias_{h,h}$ than others, due to the proportion of the wave field generated by the local winds. For example, at Southampton, Bramble and Lymington, the reduction in the H_s event peak was up to 91% of the incident height. Similar results were found when the wind field was removed from the prediction of the event on 10th March 2008, with reductions to peak wave heights greater than 90% at Southampton and Bramble, while the changes were reduced to 43% and 57.9% at the Poole Bay and Hayling Island sites, respectively.

Table 3.5. Change in model predictions due to the exclusion of wind stress, October to December 2009.

Location	Surge			H_s			T_z	
	RMSE (m)	PBIAS (%)	Peak Error (m)	RMSE (m)	PBIAS (%)	Peak Error (m)	RMSE (s)	PBIAS (%)
Bramble Bank	0.03	7.3	0.02(2.7)	0.44	96.14	0.94(90.3)	1.36	-37.4
Channel vessel	-	-	-	0.77	21.5	1.52(21.4)	2.9	-44.7
Chichester Bar	0.03	5.1	0.03(4.9)	-	-	-	-	-
Emu Hay Buoy	0.02	2.5	0.04(5.1)	0.71	55.07	1.39(56.7)	2.5	-57.6
Emu Nab Buoy	0.02	4.2	0.02(2.3)	1.10	53.7	2.2(53.4)	2.65	-53.6
Emu Ports Buoy	0.03	10.6	0.02(2.9)	0.5	76.2	0.84(63.6)	2.43	-83
Hayling Island	-	-	-	0.95	56.1	1.8(54.3)	2.9	-64.9
Lymington	0.03	8.14	0.03(4.6)	0.33	74.8	0.78(78.8)	4.16	-160.8
Milford	-	-	-	0.88	46.2	1.7(51.5)	2.05	-43.4
Poole Bay	-	-	-	1.15	47.11	2.51(52.7)	2.88	-54.16
Portsmouth	0.03	5.5	0.02(3.5)	-	-	-	-	-
Sandown Pier	0.03	4.5	0.03(3.9)	0.58	59.4	1.08(52.5)	2.66	-64.4
Southampton	0.04	10.7	0.03(3.9)	0.17	98.9	0.51(91.1)	-	-
Average	0.03	6.5	0.03(3.8)	0.69	62.28	1.39(60.6)	2.66	-68

3.5.1.2.2. Sensitivity to dataset selection

Table 3.6 indicates that the difference between the Met Office and Previmer forced prediction of the surge contained a $RMSE_{h,h}$ of 0.02 m on average, while the average change to peak surge elevations was 0.04 m. The $Pbias_{h,h}$ indicated that the surge was

larger, on average, when using the Met Office data. However, $Pbias_{h,h}$ between the two simulations was less than 3.5% at each location. The largest changes were shown to occur at Southampton, although, local variability was small generally, (for example, all locations contained a $RMSE_{h,h}$ within 0.01 m of the domain average).

Fig. 3.4 plots the change in wind conditions in the Previmer and Met Office simulations, and the corresponding change in the predicted surge, during the event on the 14th November 2009. During this event, the Previmer dataset did not reproduce a peak in the wind stresses that was present in both the Met Office and measured records, resulting in an under-estimation of the wind stress. The peak in the Met Office V component of the wind stress (of 0.7 Nm^{-2}) corresponded with an increase in peak surge elevation not contained in the Previmer-based prediction.

Table 3.6. Change in model predictions due to the differences in the wind stress datasets provided by Previmer and the Met Office, October to December 2009.

Location	Surge			H_s			T_z	
	RMSE (m)	PBIAS (%)	Peak Error (m)	RMSE (m)	PBIAS (%)	Peak Error (m)	RMSE (m)	PBIAS (%)
Bramble Bank	0.02	-3.4	0.04(6.1)	0.10	-4.30	0.05 (4.8)	0.25	-5.60
Channel vessel	-	-	-	0.23	1.40	0.44 (6.2)	0.20	0.44
Chichester Bar	0.02	-3.1	0.03(4.4)	-	-	-	-	-
Emu Hay Buoy	0.02	-3.8	0.03(4.3)	0.15	-0.90	0.05 (2)	0.58	-5.27
Emu Nab Buoy	0.02	-4.1	0.02(2.5)	0.24	1.25	0.32 (7.76)	0.59	-4.80
Emu Ports Buoy	0.02	-3.3	0.03(4.8)	0.14	-8.40	0.13 (9.8)	0.42	-6.37
Hayling Island	-	-	-	0.21	-0.16	0.18 (5.43)	0.57	-5.10
Lymington	0.02	-4.4	0.05(7.7)	0.08	-3.20	0.05 (5.05)	0.32	-0.60
Milford	-	-	-	0.16	0.48	0.11 (3.3)	0.28	-0.97
Poole Bay	-	-	-	0.29	-1.38	0.03 (0.63)	0.40	-0.84
Portsmouth	0.02	-3.3	0.04(6.1)	-	-	-	-	-
Sandown Pier	0.02	-3.1	0.04(5.8)	0.19	-8.80	0.20 (9.7)	0.53	-5.40
Southampton	0.03	-2.8	0.07(9.4)	0.10	-45.60	0.14 (25)	-	-
Average	0.02	-3.5	0.04(5.6)	0.17	-6.33	0.15(7.2)	0.41	-3.45

The differences in the wind stresses resulted in an increase to the accuracy of the event peak when using the Met Office dataset, the largest of which occurred at Southampton, where peak error was reduced by an average of 0.06 m over the two events in November 2009. The analysis also helps explain the relatively small changes shown between the surge predictions when comparing the Previmer wind and wind excluded simulations, during the event on the 14th November 2009. Due to the missing peak within the Previmer dataset, the change between the Previmer and Met Office stresses was approximately equal to the stress found within the Previmer data at this time. A more useful estimate of the influence of wind stress upon the model solution

during the events is, therefore, given by contrasting the Met Office–based solution and that using no wind stress. In this instance, over the two events, the domain average change over the two events was 0.07 m, with the largest single change of 0.16 m (over 20%) observed at Southampton, during the event on 14th November 2009.

Based upon the three month comparison of wind conditions (Table 3.4), it was found that the average error between the Previmer and Met Office wind stresses was 14%. This uncertainty, when applied to the event on the 10th March 2008, resulted in a normalised change to peak surge magnitudes at the Southampton gauge of 6.3%, while the smallest change was at the Nab Buoy (2.4%).

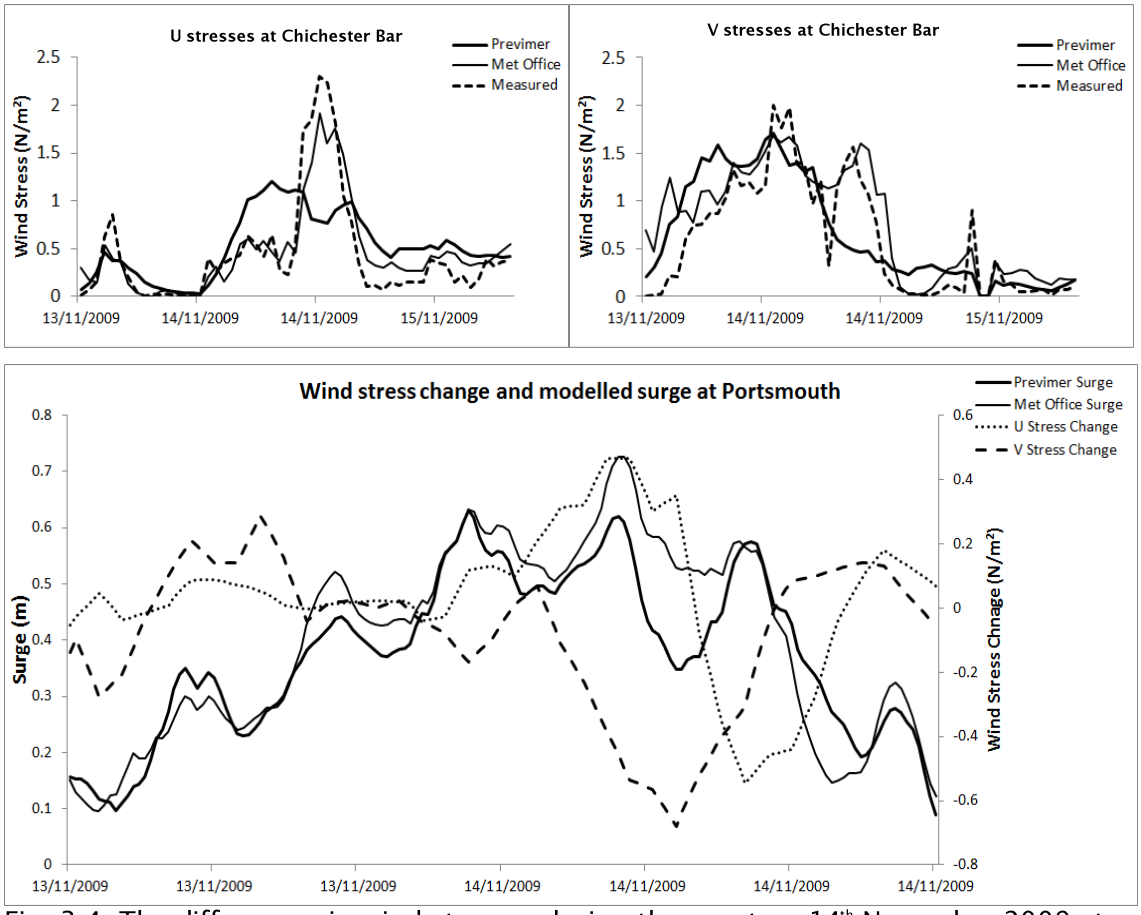

Fig. 3.4. The differences in wind stresses during the event on 14th November 2009 at Chichester Bar (top). The differences in wind stress and modelled surge during the event on 14th November 2009 at Portsmouth (bottom). A negative value in the stress change refers to a period in which the Met Office value was larger than that of Previmer, and *vice versa*.

During the October to December 2009 period, the substitution of the Met Office dataset did not provide an improvement in $RMSE_{h,m}$ accuracy, relative to the measured record, of more than 0.01 m on average. Domain average absolute $Pbias_{h,m}$ was shown to reduce by 3% using the Met Office winds, with local variance present. The larger

wind stresses found in the Met Office forcing increased accuracies relative to the Previmer-based predictions at Sandown (9% reduction in $Pbias_{h,m}$), while at Portsmouth the Pbias was increased.

The relative influence of the local wind stress and local pressure variation upon the surge was also examined. A simulation in which no winds or atmospheric pressure variation was included was considered. The results indicated that the average $RMSE_{h,h}$ across the domain increased to 0.13 m, while $Pbias_{h,h}$ increased to 20.5%. During the two larger events in November 2009, considerable changes were shown, with peak heights being reduced, on average, by 0.26 m. The results indicated that the wind stress contribution to the internal surge was smaller than that of the atmospheric pressure.

The domain averaged $RMSE_{h,h}$ between the Previmer and Met Office-based wave predictions was 0.17 m and 0.41 s, for H_s and T_z, respectively. Local variability within the H_s $RMSE_{h,h}$ ranged from 0.1 m to 0.29 m, while T_z at each location lay between 0.2 and 0.59 s. All $Pbias_{h,h}$ errors were less than 10% with the exception of the H_s at Southampton, where a value of 45.6% resulted despite a $RMSE_{h,h}$ of only 0.1 m, due to the relatively small predicted H_s compared to other regions.

Domain averaged change to the H_s event peak was 0.15 m, with no change greater than 0.44 m. The largest change, normalised to the size of the event, occurred at Southampton, where a 0.14 m (25%) increase in the H_s peak resulted from the use of Met Office winds, rather than those from Previmer, on the 14th November 2009. In addition to a change in peak height, a timing shift was demonstrated, in which the Met Office-based H_s peak occurred later than that of the Previmer record. This helped to correct a timing error, relative to the measured data, found in the Previmer-based prediction of the event. An example of the change in the wind speed and H_s at Poole Bay is given in Fig. 3.5. During the March 10th 2008 event, winds were perturbed based on the averaged errors between the Met Office and Previmer datasets. The uncertainty applied to the winds resulted in an average H_s peak change of 10.7%, with the largest normalised changes occurring at the Southampton site.

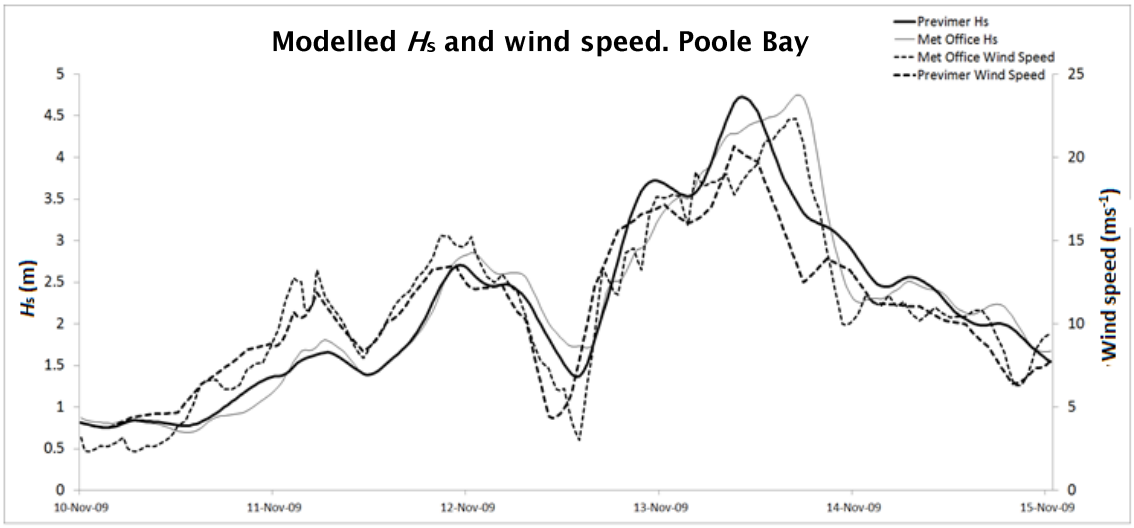

Fig. 3.5. Modelled wind speed and H_s using Previmer and Met Office data products at Poole Bay. See also Fig. 3.4 for a comparison of the wind stresses during this event.

3.5.2. Model sensitivity to boundary conditions

3.5.2.1. Uncertainty in the boundary conditions

The uncertainty in the boundary surge elevations was represented as the difference between the Met Office and Previmer datasets. Comparisons were made along a series of mid-channel locations at each boundary. Fig. 3.6 plots the surge elevations at a central point on both boundaries and gives the boundary average $RMSE_{i,i}$ and $Pbias_{i,i}$.

The Previmer surge elevations were larger on average than those provided by the Met Office, with a $Pbias_{i,i}$ of 22.65%. Both boundaries contained similar $RMSE_{i,i}$ and $Pbias_{i,i}$ values. The largest divergence occurred during the event on the 14th November 2009, during which the Met Office predicted elevations were significantly larger and contained a double high feature. The average difference in the peak surge elevation during the two event peaks, along both boundaries, was 0.13 m. However, the majority of this divergence was contained within the first event.

Boundary wave datasets (H_s and T_z) were also contrasted. Time-series plots are given in Fig. 3.7 for the western boundary from which the majority of the external energy originates. Fig. 3.7 indicates that the Previmer and Met Office datasets were similar, particularly at the western boundary from which the majority of wave energy originated within the English Channel. H_s and T_z $Pbias_{i,i}$ were below 3% and the $RMSEs_{i,i}$ were 0.49 m and 0.77 s, respectively. During the event on 14th November the H_s event peak contained a 3 hour and 1.3 m shift between the two datasets at the Western boundary.

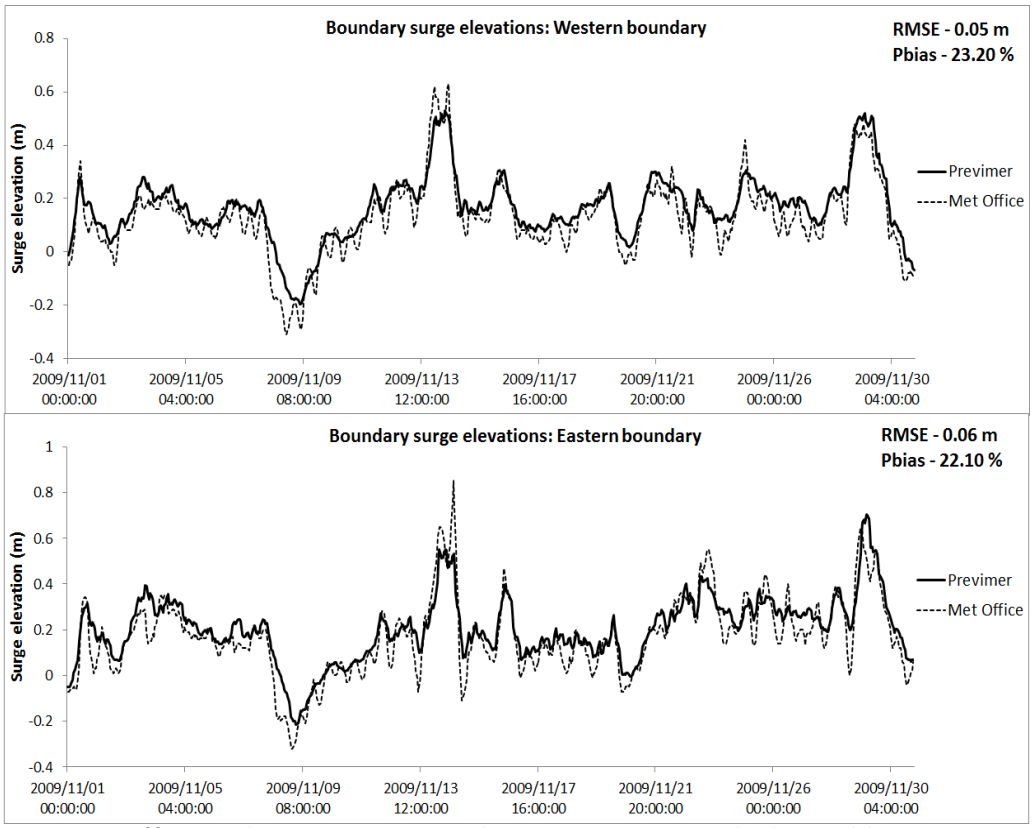

Fig. 3.6. Met Office and Previmer surge elevations at two mid-channel locations on the western boundary (top) and eastern boundary (bottom) during November 2009.

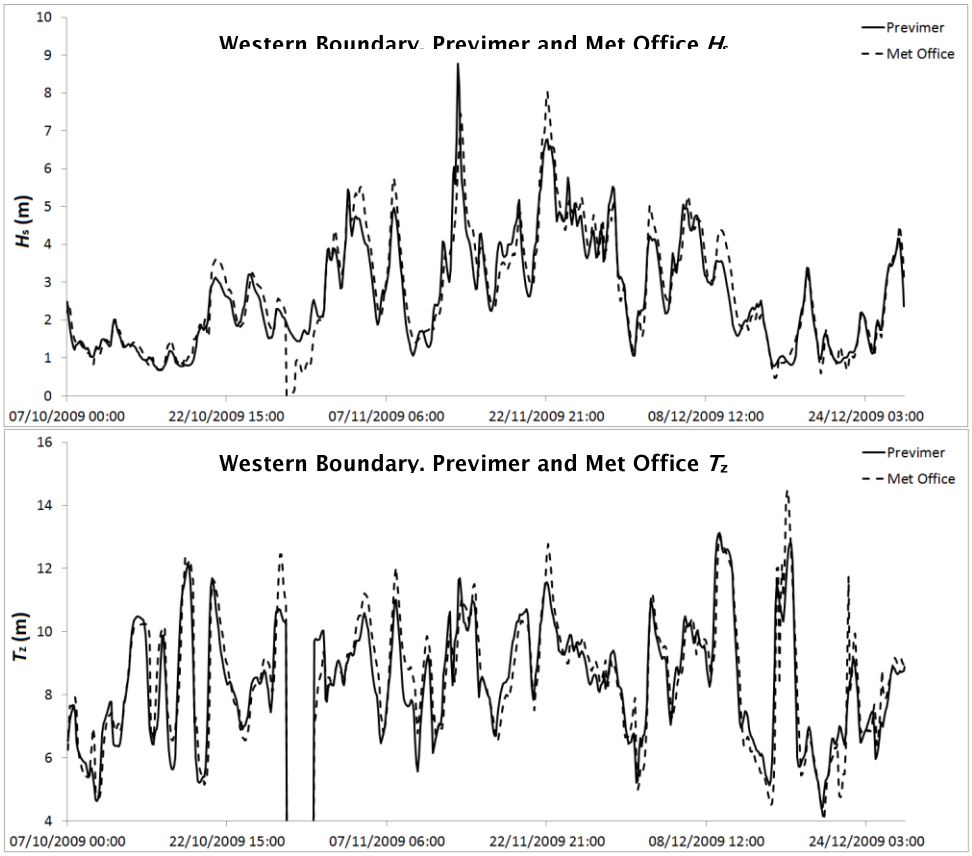

Fig. 3.7. Western boundary wave conditions from the Met Office and Previmer datasets.

3.5.2.2. Influence upon model predictions

3.5.2.2.1. Removal of the boundary conditions

The sensitivity of the model outputs to the exclusion of the boundary condition datasets is provided in Table 3.7.

As might be expected, the influence of the external surge on the nearshore surge predictions was high. Over the October to December 2009 period the change to the surge prediction, in terms of $RMSE_{h,h}$, was 0.18 m on average across the domain, while the $Pbias_{h,h}$ indicated a reduction in the surge of 30.93%. During the two largest peaks in November 2009, the exclusion of the boundary surge resulted in a decrease in peak heights of 87.8%.

Table 3.7. The impact of the removal of boundary surge and boundary wave datasets, on the predicted surge and wave states, respectively, October to December 2009.

Location	Surge			H_s			T_z	
	RMSE (m)	PBIAS (%)	Peak Error (m)	RMSE (m)	PBIAS (%)	Peak Error (m)	RMSE (m)	PBIAS (%)
Bramble Bank	0.19	32.17	0.57(84.2)	0.03	4.73	0.06(5.8)	0.01	5.37
Channel vessel	-	-	-	1.78	50.57	3.8(53.4)	2.68	37.32
Chichester Bar	0.19	27.96	0.60(88.9)	-	-	-	-	-
Emu Hay Buoy	0.18	26.68	0.59(85.3)	0.02	14.39	0.15(6.12)	0.11	19.02
Emu Nab Buoy	0.19	28.15	0.62(94.9)	0.31	20.60	0.61(14.8)	0.06	16.60
Emu Ports Buoy	0.19	29.07	0.59(86.8)	0.03	8.40	0.11(8.3)	0.62	10.42
Hayling Island	-	-	-	0.23	17.94	0.46(13.9)	0.97	15.60
Lymington	0.14	41.11	0.54(88.4)	0.02	4.30	0.02(2.02)	0.46	9.78
Milford	-	-	-	0.38	21.30	0.48(14.5)	0.82	11.30
Poole Bay	-	-	-	0.55	25.09	1(21)	1.02	18.06
Portsmouth	0.19	28.61	0.58(84.8)	-	-	-	-	-
Sandown Pier	0.19	32.00	0.59(94.3)	0.14	14.20	0.2(9.7)	0.81	13.36
Southampton	0.17	32.64	0.57(82.5)	0.01	0.95	0.1(1.78)	-	-
Average	0.18	30.93	0.58(87.8)	0.32	16.59	0.63(13.8)	0.76	15.68

During the event on the 10th March 2008, the predicted surge peaks were reduced by 58.5% on average, during the storm events considered. Spatial variability was small, for instance, a decrease in peak surge elevations of between 56.5% and 61.2% occurred at all gauged sites during the event. At Portsmouth, the exclusion of the boundary surge dataset resulted in a decrease in peak water levels of 0.6 m, while the skew-surge was decreased by 47%.

Domain averaged $RMSEs_{h,h,}$ between wave predictions with no boundary wave input and those utilising Previmer boundary datasets were 0.32 m and 0.76 s for H_s and T_z, respectively. $Pbias_{h,h}$ was approximately 16% in both cases. On average, the removal of boundary wave inputs reduced the height of the H_s event peak by 0.63 m. Model sensitivity was spatially variable. Regions largely protected from swells, such as Southampton, Lymington and Bramble, were relatively insensitive to the removal of the

boundary wave data. At other sites, for instance Poole Bay and EMU Nab Buoy, the sensitivity was high, resulting in a reduction to the H_s event peak$_{h,h}$ of more than 0.5 m.

During the event on 10th of March 2008, the same trends were shown, with domain average changes in the peak H_s of 16.4%, while alterations in the nearshore areas of the western Solent and Southampton Water regions did not exceed 5%.

3.5.2.2.2. Sensitivity to dataset selection

The changes to the model predictions due to the use of the Met Office derived boundary datasets are presented in Table 3.8.

Table 3.8. The impact of the substitution of Met Office-derived boundary surge and boundary wave datasets, on the predicted surge and wave states, respectively, October to December 2009.

Location	Surge			H_s			T_z	
	RMSE (m)	PBIAS (%)	Peak Error (m)	RMSE (m)	PBIAS (%)	Peak Error (m)	RMSE (m)	PBIAS (%)
Bramble Bank	0.07	12.34	0.11(16.7)	0.01	0.10	0.00 (0)	0.00	-0.11
Channel vessel	-	-	-	0.43	2.07	1.10 (15.5)	0.65	-1.05
Chichester Bar	0.07	10.54	0.14(21.3)	-	-	-	-	-
Emu Hay Buoy	0.07	9.86	0.15(21.7)	0.00	0.08	0.06 (2.44)	0.02	-1.09
Emu Nab Buoy	0.07	10.70	0.15(22.9)	0.08	1.06	0.17 (4.12)	0.01	-0.12
Emu Ports Buoy	0.07	11.08	0.13(19.2)	0.02	0.26	0.07 (5.3)	0.10	-0.40
Hayling Island	-	-	-	0.06	0.68	0.10 (3.02)	0.17	-0.55
Lymington	0.06	15.88	0.09(14.5)	0.01	0.15	0.00 (0)	0.20	-1.70
Milford	-	-	-	0.07	0.46	0.14 (4.24)	0.28	-1.3
Poole Bay	-	-	-	0.12	1.12	0.30 (6.3)	0.34	-1.1
Portsmouth	0.07	10.92	0.11(16)	-	-	-	-	-
Sandown Pier	0.07	12.17	0.15(24.2)	0.05	-0.85	0.05 (2.43)	0.20	0.70
Southampton	0.07	11.99	0.16(22.6)	0.00	-0.28	0.00 (0)	0.00	-0.23
Average	0.07	11.72	0.13(19.9)	0.08	0.44	0.17 (3.94)	0.18	-0.64

Variation between surge predictions, due to the differences between the Previmer and Met Office boundary surge input datasets, resulted in an average RMSE$_{h,h}$ of 0.07 m and Pbias$_{h,h}$ of 11.72% within the regional model. Local variability was shown to be small, with RMSE$_{h,h}$ and Pbias$_{h,h}$ at all locations falling within 0.01 m and 5% of the domain averages, respectively.

During the two surge events in November 2009 the average change to peak surge height was 0.13 m. The largest change was shown to occur at Southampton (0.16 m) while the smallest occurred at Lymington (0.09 m). Relative to the size of the average incident height, all locations resulted in an average change of between 14% and 25%. The change in the modelled surge, occurring on 14th November 2009, utilising the two different boundary conditions, is presented in Fig. 3.8. It indicates that the Met Office dataset provided a more accurate representation of the peak

measured surge elevation. This was demonstrated at each location and corresponds to the differences in boundary conditions given in Fig. 3.6.

Using the average uncertainty in the boundary surge input (as represented by the difference between the two datasets), the March 10th 2008 event was simulated with increased boundary elevations of 22%. The results revealed that the average change to the peak surge elevation was 9% across the gauge sites. Spatial variability was small, with all site values falling within 1% of this mean.

Relative to the measured observations, the inclusion of the Met Office boundary surge resulted in a domain averaged increase in peak surge elevation accuracy of 0.05 m during the two November 2009 events. Over the October to December 2009 period the average $RMSE_{h,m}$ accuracy was not changed by more than 0.01 m relative to the Previmer-forced prediction accuracy. $Pbias_{h,m}$ increased by 12% on average where Met Office data were used. This indicated that the inclusion of the Met Office boundary conditions resulted in an increase in the under-estimation of the surge elevations on average. However, during the larger events, particularly that occurring on the 14th November 2009, the Met Office boundaries provided a more accurate representation of both the size and shape of the measured surge.

A further simulation was conducted for the October to December 2009 period, using both Met Office boundary surge and wind datasets, and the predictions were contrasted with the Previmer-forced simulation. The results indicated that the predictions diverged less than when only the Met Office boundary was substituted in, for instance, domain average $Pbias_{h,h}$ between the Previmer and Met Office-forced predictions was less than 5% when both boundary and wind Met Office data were used. Peak surge elevations were shown to diverge by 14.3% on average across the domain. The largest change was shown to occur at the Portsmouth gauge during the event on the 14th November 2009 with a change of 19%.

The domain averaged $RMSE_{h,h}$ between the wave predictions using the Previmer and Met Office wave boundary datasets was 0.08 m and 0.18 s for H_s and T_z, respectively, while $Pbias_{h,h}$ remained below 2% in each case. The largest alteration to the H_s event peak (excluding the Channel Light Vessel) occurred at Poole Bay (0.3 m) equating to 6.3% of the incident height. No change greater than 0.17 m was found elsewhere in the region. Similarly, during the March 10th 2008 event, the 'expected' error, due to input dataset selection, resulted in an average change in peak H_s of 4.2%, while no change exceeding 0.25 m was found at any gauged site, with the exception of the Channel Light Vessel.

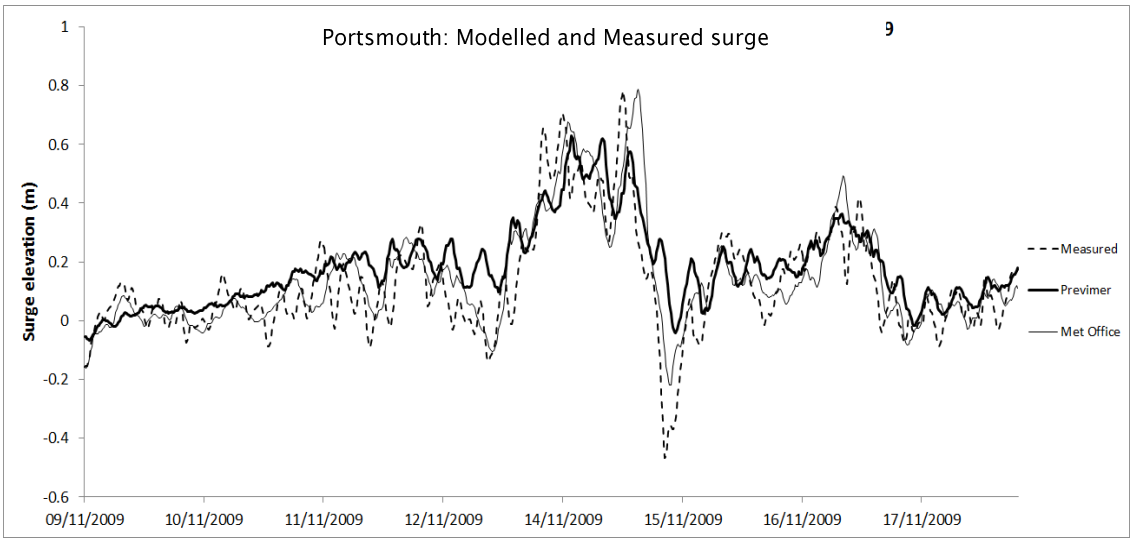

Fig. 3.8. Modelled and measured surge elevations during the event occurring on 14th November 2009 at Portsmouth

The sensitivity of the model to external and internal forcing upon the wave field during the 14th November 2009 event was demonstrated. During the event local winds had the greatest influence on the model prediction. This was shown most clearly in the alteration of the wave H_s between the Channel Light Vessel and the nearshore regions (Fig. 3.9). Despite considerable deviation of the H_s between the three simulations at the Channel Light Vessel, the predictions closely converged by the time the waves propagated to sites outside of the Solent (e.g., Poole Bay and EMU Nab Buoy). Where no external component was included, upon reaching the EMU Nab Buoy the H_s event peak was within 0.6 m of the predictions including boundary wave inputs, despite a 3.8 m difference between the predictions at the Channel Light Vessel, indicating that the main component shaping the H_s time-series was the local wind field rather than the waves propagating in from the domain boundaries.

Where the Met Office-based boundary wave datasets were used in conjunction with the Met Office winds, the results indicated a high degree of similarity with those obtained using the Previmer datasets, in terms of errors relative to *in-situ* measurements. The domain averaged prediction H_s and T_z $RMSEs_{h,m}$, when forcing the model with Met Office data products, were 0.34 m and 0.88 s, respectively. These errors were similar to the $RMSEs_{h,m}$ of 0.32 m and 0.81 s contained within the predictions forced with Previmer datasets. Domain averaged changes to peak H_s between the two predictions was less than 10%.

Relative to *in-situ* measurements both predictions over-predicted H_s and under-predicted T_z in the shallow, nearshore regions. The largest deviation between the predictions was observed during the event on 14th November 2009. Throughout the domain the H_s event peak occurred approximately three hours later in the Met Office-

based prediction than in the Previmer-based prediction. The later timing more closely corresponded with the timing shown within the wind field comparisons and the *in-situ* measurements of H_s. However, the size of the event peak was under-predicted in the Met Office-based prediction, while the larger H_s within the Previmer-based prediction more accurately recreated the measured heights.

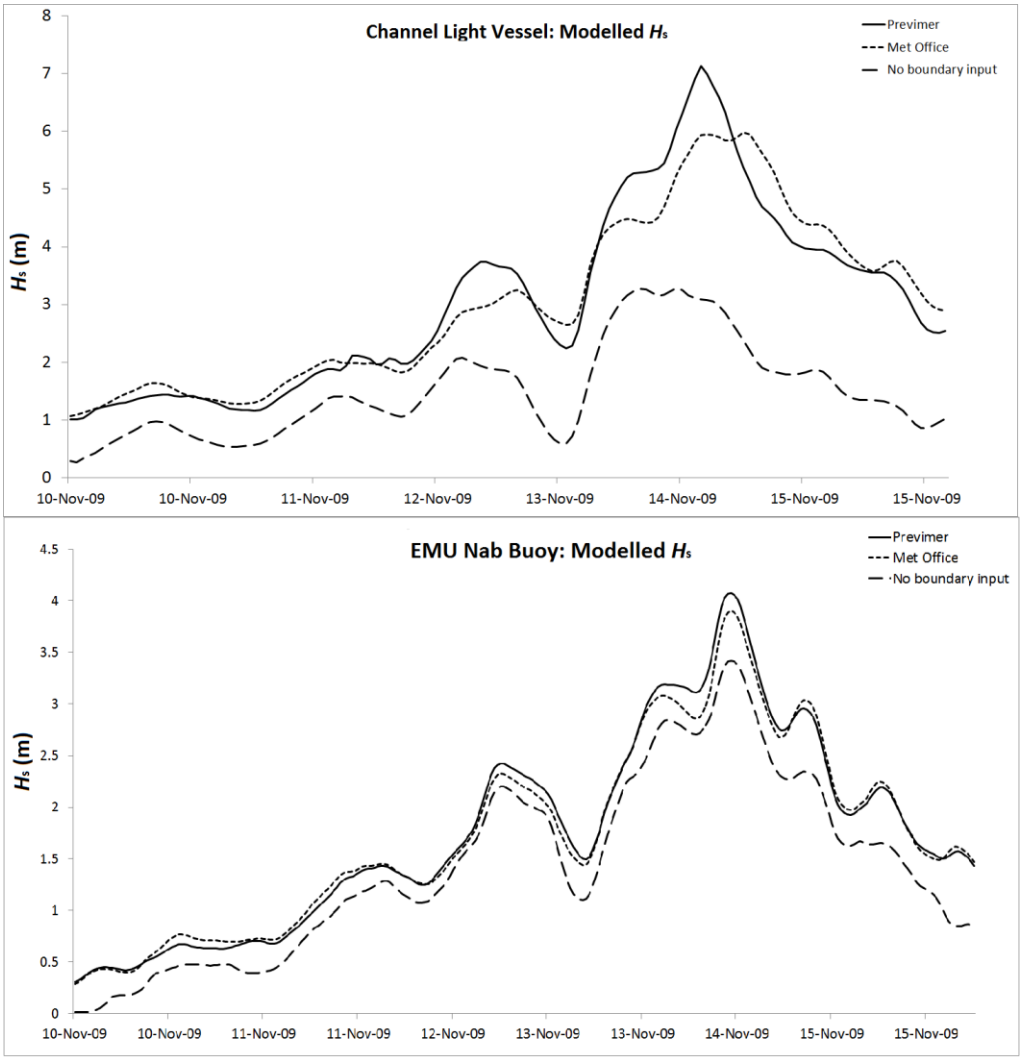

Fig. 3.9. Modelled H_s at the Channel Light Vessel (top) and EMU Nab Buoy (bottom) using the three wave boundary data options.

3.6. Discussion

The sensitivity of regional hydrodynamic and spectral wave models of the Solent to uncertainty in the wind and boundary condition input datasets was examined. The wind fields and the boundary conditions from the Previmer system were contrasted with those derived from the current Met Office operational system in the UK for the

period from October to December 2009. In addition, the accuracy of the winds was also compared to *in-situ* measurements.

Previmer and Met office wind stresses were shown to be well correlated on average over the three months, with little local variation present in the differences between them. On average, the Previmer dataset predicted smaller wind speeds than the Met Office data. Both datasets produced similar errors when compared to *in-situ* measurements, with $RMSE_{i,m}$ in the stress components lying within 0.1 Nm^{-2} of each other throughout the domain, indicating that neither dataset was significantly more accurate than the other over the three month period. The size of the errors in the wind speed predictions, relative to *in-situ* measurements, were larger than expected based upon previous accuracy assessments of operational systems. Bidlot *et al*. (2007), for example, found that the RMSE from the ECMWF, SHOM and Met Office global systems was approximately 1.5 ms^{-1} at offshore locations; roughly half the average error found here. The larger errors in both datasets given in this research may relate to the proximity to the coast relative to the results given by Bidlot *et al*. (2007), while Bradbury *et al*. (2004) also suggest that the English Channel itself is problematic for wind modelling due to a possible misrepresentation of a funnelling effect of shore parallel winds. In addition, the relatively coarse temporal resolution of the input datasets (three hours and one hour in the Previmer and Met Office datasets, respectively) may have contributed to this error, particularly during peak events. For instance, the smoothing that would be contained in datasets of such resolutions would be expected to reduce peaks in the time-series. Contrasting the Previmer, Met Office and measured time-series provided evidence of this, with the Met Office record more accurately recreating the peak wind speeds.

The role of wind stress upon the surge was particularly relevant during the event on 14th November 2009, where short-term deviations between the two wind fields resulted in a change to peak surge heights of more than 0.9 m (14.4%) at Southampton, while a 6.3% change was shown during the 10th March 2008 event where the 'expected error due to dataset selection' (i.e. 14% in terms of wind stress) was applied. These results indicated that on average the sensitivity of the surge to wind dataset selection was relatively low (e.g. an average $Pbias_{h,h}$ of less than 5% was realised between October and December 2009) across the gauged sites, but periodic shifts in storm timing and intensity created larger discrepancies in peak surge magnitudes of up to 6% at Southampton.

Previous research has reported a significant influence of the wind field on the predicted surge. For instance, Davis *et al*. (2010) suggested that the wind field is one of the most important factors in an accurate prediction of surge, while Wells *et al*. (2001) stated that the local wind stress resulted in a significant contribution to the model solution during an extreme surge in the English Channel. Furthermore, Wortley

et al. (2007) stated that a 10% change to the wind field could lead to a change in surge magnitudes of 0.5 m. This estimate was considerably larger than the changes presented in this research. However, it was related to extreme surges, under the influence of very strong winds, which are generally larger than those considered in this research, such as those that affected the English south coast in 1989, where the surge exceeded 1.32 m at Dover.

The influence of the wind stress upon the regional model solution was shown to be smaller than the atmospheric pressure, which when removed, increased average $Pbias_{h,h}$ across the gauges from 4% to over 20%. The results demonstrated that although the local wind stress was an influential additive source to the surge magnitudes within the region, the accurate representation of the atmospheric pressure is likely to be of more importance to modellers in similar environments.

$RMSE_{i,i}$ between the two boundary surge input datasets was, on average 0.06 m, with significant divergence during the event on the 14th November 2009. Despite the $RMSE_{h,h}$ between the two surge predictions of 0.07 m, their accuracies relative to the measured data were similar, with the Previmer predictions more accurately reproducing the measured surge elevations, on average, by only 0.01 m. However, $Pbias_{h,m}$ was increased by 12% when utilising Met Office datasets, due to an overall reduction in surge size. Despite this, during the event on the 14th November 2009, the use of the Met Office data resulted in both an increase to the size of the surge peak and an increase in the accuracy of its shape, resulting in a reduction in error of over 0.15 m at Southampton. This indicated that although, on average, both forecasting systems provided similar estimates of the external surge, divergence, if during storm surge conditions, could result in significant changes to the model predictions, during the periods of greatest relevance to flood risk.

The boundary surge elevations provided a considerable contribution to the model prediction. The removal of the boundary surge input data resulted in an average $RMSE_{h,h}$ of 0.18 m between the two predictions (with and without boundary surge input datasets), while during the two events in November, the peak surge heights were reduced by 87.8% on average, and 58.5% during the March 10th 2008 event. These findings demonstrated the importance of the accurate representation of the surge entering the computational domain, particularly during large storm events. This is particularly important in the Solent as the movement of the surge through a narrowing passage such as the English Channel, combined with a long fetch, enables the continual build-up of the surge as it propagates through to the regional model domain boundaries. Smith and Ward (1998) highlighted that the funnel shape and extended fetch conditions within the North Sea were key factors in the occurrence of seven 'disastrous' floods in the region, including the 1953 event.

Contrasting the wave model sensitivity to the wind field and boundary wave datasets revealed that, despite the local extent of the model domain, the local wind

was the most influential force upon the wave predictions. This was most clearly demonstrated when the boundary wave dataset was removed. During the event on 14th November 2009, despite the removal of the boundary wave input, the predicted H_s peak at the EMU Nab site was within 15% of that predicted with the boundary waves included (Fig. 3.9). The boundary wave dataset was most influential in the less sheltered regions (e.g. the EMU Nab Buoy and Poole Bay) which were more exposed to large waves developing over relatively large fetch conditions. At the sheltered sites, changes to the peak H_s was up to 1 m while the T_z $RMSE_{h,h}$ was 1.02 s during the event on the 14th of November 2009. Domain averaged $Pbias_{h,h}$ between model predictions of H_s and T_z with and without local winds was greater than 60% in both instances. The H_s event peak decreased by 60% on average, while in the most sheltered regions, such as Southampton, this value rose to 90% during the events on November 14th 2009 and March 10th 2008. These findings indicated that the model prediction was highly sensitive to the local wind field which, despite the regional extent of the domain, was able to contribute a significant amount of energy for wave growth (after Miles, 1957; Phillips, 1957; Janssen, 2008).

Where both the boundary wave and wind field datasets supplied by the Met Office were used, in place of those from Previmer, the resulting model predictions contained a high degree of similarity to those given by the Previmer-forced model in terms of error relative to *in-situ* measurements. Domain average predicted H_s and T_z $RMSEs_{h,m}$, when forcing the model with Met Office data products, were 0.34 m and 0.88 s, respectively. These errors were similar to the $RMSEs_{h,m}$ of 0.32 m and 0.81 s contained within the predictions forced with Previmer datasets. Over the October to December 2009 period both simulations over-predicted H_s throughout the region, while the opposite was shown for T_z. This may have been due to the over-prediction of the wind speeds from both sources used within the model. For instance, domain average $Pbias_{i,m}$ in the Previmer-based wind speeds was 30%, while the domain average H_s $Pbias_{h,m}$ was 28.4%. Furthermore, Met Office-based winds speeds were larger than those from Previmer (containing a $Pbias_{i,l}$ of 5%) while the domain average $Pbias_{h,h}$ between the two wave predictions of H_s was 6.9%.

The largest divergence in the wind and boundary wave datasets occurred during the event on 14th of November 2009. During this event the Met Office-derived peak wind speed and boundary H_s occurred three hours later than in the Previmer data. This resulted in the predicted H_s peak occurring later in the regional model, increasing the accuracy, relative to *in-situ* measurements, compared to the predictions derived from the model when forced with Previmer datasets. Although the accuracy of the timing of the peak H_s was increased, the magnitude was under-predicted when compared with *in-situ* measurements in the exposed regions (e.g. Hayling Island) to a greater degree than for the Previmer-forced model prediction due to smaller H_s in the Met Office

boundary wave dataset. Bradbury *et al*. (2004) also found that the Met Office model under-predicted H_s when modelling conditions above 2.5 m at Hayling Island.

The relatively large divergence between the input datasets during the largest storm event on the 14th November 2009 is of particular interest as the greatest risk of flooding occurs during storm events, and therefore, where the highest prediction accuracies are required. Further research should build upon the findings presented in this research, by extending the length of time over which comparisons are made, in order to more robustly assess the degree to which the datasets diverge during large storm events.

The findings presented in this research quantified the sensitivity of the regional model to input datasets provided by the Previmer system. The findings will be of interest to those working in the Solent specifically, but are also capable of providing general indications related to prediction uncertainty in nested regional models. Furthermore, the assessment of the Previmer datasets, relative to another operational system, and the quantification of the uncertainty in model predictions due to dataset selection will provide valuable information to coastal managers interested in the Previmer system.

3.7. Conclusion

This research utilised regional hydrodynamic and spectral wave models of the Solent region to investigate the uncertainty within the wind, boundary surge, and boundary wave forcing datasets provided by the Previmer system, and examined the influence such uncertainties have upon the model predictions. The results indicated that:

- The Previmer input datasets examined were broadly consistent with those provided by the Met Office, resulting in similar RMS errors when contrasting modelled surge and wave outputs, forced by the respective datasets, with *in-situ* measurements. However, during the largest event, divergence was greatest and the Met Office predictions more accurately resembled the measured event magnitude, likely due to the coarser temporal resolution (and resultant smoothing) of the Previmer datasets.
- The boundary surge characteristics were found to be the dominant influence upon the modelled surge conditions throughout the region, accouting for more than 80% of the modelled surge elevation during storm events.
- Modelled wave conditions were most sensitive to alteration to the local wind fields (increasing peak H_s by more than 60% on average throughout the domain). However, a high degree of spatial variability was demonstrated in the additional influence of boundary wave conditions, with the eastern Solent

region, less sheltered by the Isle of Wight from swells, found to be most sensitive to the boundary wave input datasets.

The complexity of the Solent region provided a useful case study with which to assess the spatial variability in model prediction sensitivity to input data uncertainty. The research highlighted the importance of accurate boundary forcing and local winds upon model predictions of waves and surge that will be of interest to coastal managers interested in sources of prediction uncertainty in nested coastal models, applicable to a variety of environments, while the comparison of the Previmer and Met Office data products will be of interest to those wishing to use similar products to force other coastal models. Furthermore, the research provided a greater understanding of the processes occurring in the region, upon which subsequent research could be based.

Chapter 4: Modelling Tide and Surge Elevations in the Solent and Surrounding Waters: Importance of Tide-Surge Interactions

Quinn,N., Atkinson, P., Wells, N., 2012. Modelling of tide and surge elevation in the Solent and surrounding waters: The importance of tide-surge interactions. *Estuarine, Coastal and Shelf Science*, http://dx.doi.org/10.1016/j.ecss.2012.07.011

Abstract

A regional 2D hydrodynamic model using the MIKE-21 software and data from a pre-operational forecasting system of the English Channel is described and applied to the Solent-Southampton Water estuarine system. The regional model was able to predict surge heights with a RMSE accuracy of 0.09 m during a three month hindcast in the winter of 2009, comparing closely with accuracy assessments from other independent systems. However, consistent under-prediction of tidal harmonic constituent amplitudes was present throughout the region leading to errors in the prediction of the total water level elevations. Despite the complex nature of the Solent tidal regime, interpolation of tidal elevations from harmonic analysis at fixed tide gauge locations was shown to be effective in reducing this uncertainty at gauged and un-gauged sites. The degree to which tide-surge interactions were taking place was examined. Of particular interest was the quantification of the sensitivity of the predicted surge to the levels of uncertainty expected in the prediction of the tide within a complex nearshore region such as the Solent. The tide-surge interaction during three surge events was shown to be greatest in the Western Solent and Southampton Waters regions, where the tidal uncertainty was greatest. Interaction between the tide and surge resulted in a change of up to 0.3 m (11%) in the predicted total peak water level when the surge was added to the harmonic analysis-based tidal prediction. Despite the significant effect of removing the tide-surge interactions, tests indicated that the error in tidal range expected in the regional models tidal prediction altered the prediction of the surge only enough to induce changes in peak total water elevations by up to 0.03 m during an event on 10th March 2008. The findings suggest that the current tidal predictions in complex estuarine systems, such as the Solent, are of high enough quality to reproduce the majority of the tide-surge interactions taking place and that the error in the surge due to uncertainties in the predicted tide are expected to be relatively small.

4.1. Introduction

In the UK, it is estimated that 5 million people and 1.85 million homes are at risk from coastal flooding (Penning-Rowsell *et al.*, 2006). Although rare, significant loss of life has occurred, most notably in 1953 in which 307 and 1836 people died in the UK and Netherlands, respectively (Gerritsen, 2005; Wolf and Flather, 2005). Such events usually occur when the local sea surface is elevated above the predicted tidal levels due to large atmospheric induced surges (Bowden, 1983; Boon, 2004).

To protect against the threat of coastal flooding numerical models of the shelf seas have been utilised in many regions around the world to provide forecasts of ocean surface elevations. A change in surface elevation is usually referred to as the change in height from the mean sea level at a given location and is composed of two influences, the astronomical tidal elevation and the non-tidal residual (often termed 'storm surge'). Tides are the change in sea levels resulting from the combined impact of gravitational forces from astronomical bodies and the rotation of the Earth. An estimation of tidal elevations can be achieved through the summation of a series of harmonic terms, using Eq. 4.1 (Boon, 2004).

$$\zeta = Z_0 + \sum a_n cos(\omega_n t - \phi_n - \phi_n^L) \qquad (4.1)$$

where ζ is the tidal elevation, Z_0 is the reference water level, often given as the difference between mean sea level and chart datum, ω is the angular frequency, ϕ is the constituent phase relative to lunar transit of the equilibrium tide, and ϕ^L is the phase lag of the real tide to the equilibrium tide, often taken as the phase lag on the equilibrium tide phase at the Greenwich Meridian.

The additional non-tidal residual, or surge, can be defined as a meteorological long wave motion, which produces an elevation of the water surface above (or below) the level caused by astronomical forcing alone. It is the result of the influence of wind stress, atmospheric pressure, and waves on the shallow coastal shelf regions (Smith and Ward, 1998; Cañizares *et al.*, 2001; Kim *et al.*, 2010).

Systems for storm surge prediction usually involve a suite of models, often coupling atmospheric models that provide forecasts of wind forcing and air pressures to hydrodynamic models for a region of interest (e.g., Allard *et al.*, 2008; Wolf, 2009). Flather (2000) provides a summary of a variety of operational systems that have been utilised throughout Europe. Such models are based on the solution of the two or three-dimensional incompressible Reynolds averaged Navier-Stokes equations, subject to the assumptions of Boussinesq and of hydrostatic pressure.

Operational storm surge forecasts have been used in the UK since 1953 (Wolf, 2009). Present accuracy assessments are available from

http://www.pol.ac.uk/ntslf/model.html. Forecasting systems are continually being improved to provide more accurate warnings and greater information content to coastal managers and decision makers. For example, recent research has investigated the progression from deterministic to probabilistic modelling (Flowerdew *et al.*, 2007; Bocquet *et al.*, 2009; Davis *et al.*, 2010) and the use of data assimilation techniques (Prandle, 2000; Mclaughlin, 2002).

The degree to which uncertainty in the predicted tidal elevations may influence the prediction of surge through tide-surge interactions is of interest, and recent research in the English Channel has demonstrated the existence of an interaction between the two signals. Prandle and Wolf (1978), and Wells *et al.* (2001) have both reported tide-surge interactions resulting in a decrease of the peak surge elevations and that the effect can be localised, increasing in direct proportion to surge height and tidal range (Horsburgh and Wilson, 2007). Brown *et al.* (2010) found that the interaction could increase or decrease the surge significantly, altering peak levels by more than a metre. The timing of the surge has also been shown to be influenced by the tide. Horsburgh and Wilson (2007) demonstrated that due to the interaction of the two signals, the peak of large surge events would typically avoid the high tide period by 3 to 5 hours, with a secondary clustering within 1 to 2 hours. Phase shifts occur in both the tide and the surge signals due to tide-surge interactions. This is because both signals are shallow water waves whose phase speed is given as a function of the water depth. Therefore, negative surges have been shown to slow tidal progression while a positive surge can advance it (Rossiter, 1961; Wolf, 1981; Horsburgh and Wilson, 2007). The processes leading to the alteration of water levels due to tide-surge interactions can be classified into three nonlinear effects: nonlinear advective effects, nonlinear bottom stress effects, and nonlinear shallow water effects (Bernier and Thompson, 2007; Zhang *et al.*, 2010).

Predicting tidal elevations from operational forecasts is considered to become increasingly uncertain in complex nearshore regions. For this reason, harmonic predictions of the tides are substituted in the place of outputs from physically-based numerical models in many operational systems due to their greater accuracy (Flowerdew *et al.*, 2007; Bocquet *et al.*, 2009; Hawkes *et al.*, 2009). In regions where the tidal elevations are the main component of the combined water level elevations it is often best practice to use this substitution. However, particularly in complex nearshore regions, a high degree of uncertainty in the predicted tides may induce uncertainty in the surge if tide-surge interactions are significant. This error will still then be propagated through to the combined water level elevation predictions when the surge is added to the harmonic-based estimate of the tides. Horsburgh and Wilson (2007) commented on this issue, suggesting that due to the difficulty in separating the tide and surge signals, forecasting systems would benefit from increasing the accuracy of

the predicted water level elevations, avoiding the need to separate the two signals. For this reason, even where substitution is used, quantification of the uncertainty in the modelled tide-surge interaction due to error in the prediction of the tide can be useful in evaluating the confidence in the model forecast, particularly in complex tidal regions.

Previmer is a pre-operational hydrodynamic modelling system currently under development which aims to provide users with short-term forecasts of ocean state over a variety of model domains, including global and North East Atlantic models, with smaller nearshore nests at selected regions along the French coast (http://www.previmer.org/en.). The North East Atlantic model generates forecasted water level elevations throughout the English Channel, providing a potential source for boundary driving conditions for a regional model of the Solent and Hampshire coastline, on the south coast of the UK, an area thought likely to be affected by increased flood risk in the future (Evans, 2004).

This region is important to numerous stakeholders, including a variety of protected habitats, a dense coastal population and two of the largest shipping ports in the UK. The coastal population has increased steadily reaching 835,731 in 2001 with nearly 4000 ha of land, supporting 17,000 dwellings and a population of 37,600 considered at risk from coastal flooding (Hampshire County Council, 2006). The southern coast of the UK is expected to experience some of the largest increases in flood risk during the 21st century in the country (Evans, 2004). This is likely to be due to a variety of reasons including an increase in the number of assets at risk in coastal zones (Zang and Tooley, 2003), changes of wave conditions (increasing frequency and intensity of large wave events) in the North Atlantic and North Sea shelf in recent decades (Bacon and Carter, 1991; Zang and Tooley, 2003; Inter Agency Committee on Marine Science and Technology, 2004;) and subsidence of the southern English coast by approximately 0.3 mm a^{-1} over the last 1ka in the Hampshire region (Shennan *et al.*, 2012). In addition to the alteration of the land height itself, evidence suggests that sea levels will rise in the future as a result of thermal expansion and the melting of land-based ice, caused by warming over the last century (Houghton, 2005; Hall *et al.*, 2006; Haigh *et al.*, 2009). Even relatively small changes in mean sea level due to changes in the land and sea heights are predicted to increase significantly the likelihood of extreme sea level events. Haigh *et al.* (2011) for instance, estimated potential future extreme high sea levels throughout the English Channel during the 21st century based on expected sea level increases of 12, 40 and 81 cm. They reported that the exceedence frequency of extreme high sea levels in the region would on average increase by a factor of 10, 100 and 1800, respectively, due only to mean sea level changes. As a result of the above, funding into flood defence within the UK has increased from £303 million to £550 million between 2002 and 2006 and is likely to increase in the future to cope with heightened risk (Environment Agency, 2007).

There is a strong desire for a regional real-time flood forecasting system for the Solent and Hampshire coastline. Thus, this research contained two primary aims. The first was to assess the accuracy of a regional hydrodynamic modelling system for predicting water level elevation within the Solent region utilising boundary datasets from the Previmer forecasting system. The second aim was to assess the influence of the local tide-surge interaction upon the predicted surge and, therefore, the water level elevations propagating between the domain boundaries and the nearshore region. Furthermore, the degree to which uncertainties in current tidal predictions might induce uncertainties in the final predicted water level elevations was investigated. The study site and datasets are described in Section 2, followed by a description of the model set up and analysis structure in Sections 3 and 4, respectively. Section 5 presents the results which are discussed in Section 6. The main conclusions are drawn in Section 7.

4.2. Study Site and Data

4.2.1. The Solent

The Solent lies between the south coast of England and the Isle of Wight, in the UK (Fig. 4.1). It includes 12 separately defined estuaries and harbours and contains a wide range of coastal habitats (Fletcher *et al.*, 2007). The region has various stakeholders, including protected habitats, a dense coastal population and two of the largest shipping ports in the UK. The region lies in the English Channel, in which the M_2 tide is the dominant tidal component and tidal ranges typical are in the order of 6 to 10 m. The M_2 is also the dominant forcing within the Solent. However, the irregular geometrical shape, narrow channel configuration and shallow depth of the estuary results in an amplification of the shallow water tidal constituents M_4 and M_6 (Levasseur, 2008). For example, at the Southampton tide gauge the M_2, M_4 and M_6 tidal constituent amplitudes are approximately 1.34, 0.24 and 0.17 m, respectively. At Newhaven, further east, in a more exposed coastal location within the English Channel, the constituent amplitudes are approximately 2.19, 0.08 and 0.02 m, respectively. Previous studies have also noted that within the central English Channel the M_4 and M_6 over-tides become increasingly important (Pugh, 1987; Wells *et al.*, 2001). Within the Solent these amplifications create a tidal elevation with a double high water and young flood stand, most prominent in the Southampton Water region (Rantzen, 1969; Levasseur, 2008). Previous attempts at modelling the hydrodynamics within the region have shown increasing uncertainty in the western Solent and Southampton Water regions (Levasseur, 2008).

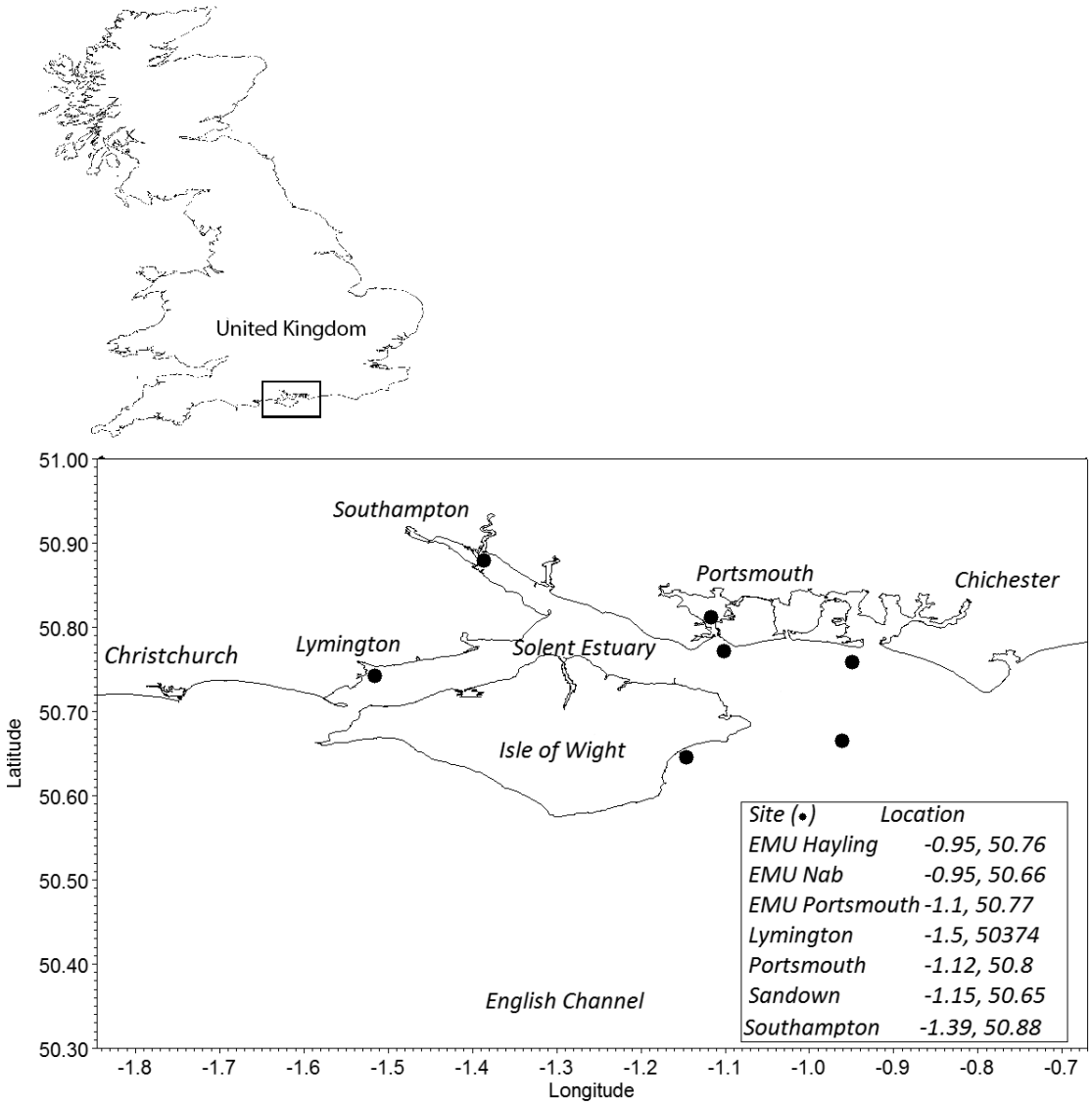

Fig. 4.1. The location of the Solent and *in-situ* measurements

Storm surges in this region most frequently occur due to low pressure systems from the Atlantic propagating eastwards or as a result of storm surges propagating south from the North Sea (Law, 1975; Haigh *et al.*, 2004). Large storm surge events have influenced the south coast in the past, the most notable occurring in 1953, which resulted in significant loss of life (Gerritsen, 2005; Wolf and Flather, 2005). During this event the surge propagated south from the North Sea increasing in intensity as it moved south into shallow waters. Other notable events to have caused flooding within the region include those occurring on 14th to 18th December 1989 (Wells *et al.*, 2001; Ruocco *et al.*, 2011) and 10th March 2008 (Haigh *et al.*, 2010). A review of flood events within the Solent since 1935 can be found in Ruocco *et al.* (2011). Generally, coastal flooding within the Solent is considered frequent, but usually involving small water depths, and with no recorded loss of human life (Wadey *et al.*, 2012).

4.2.2. Data

Tidal elevations, surge elevations and wind conditions derived from the Previmer group (http://www.previmer.org/en) were used in this research. These datasets were outputs from a pre-operational system currently under development which aims to provide users with short-term forecasts of the state of the ocean along French coastlines bordering the English Channel, the Atlantic Ocean, and the Mediterranean Sea. Tide and surge components of the water surface elevation (velocities were not specified) were provided at 5.5 km spatial resolution, and 1 hour temporal resolution throughout the English Channel. These data were model outputs created using the Model for Application at Regional Scale (MARS 2D) system (Lazure and Dumas 2008). The Previmer models utilise modelled wind fields at 3 hour temporal and 4 km spatial resolution provided by the European Centre for Medium Range Weather Forecasts (ECMWF, www.ecmwf.int/about). These wind field datasets were supplied via the Previmer group for this research. Atmospheric pressures fields were interpolated from measurements provided by the Channel Coastal Observatory (http://www.channelcoast.org/) which is the data management and regional coordination centre for the Regional Coastal Monitoring Programmes (see Isle of Wight Council (2005) for a useful overview). Measurements at seven sites located along the south coast of England, between longitudes of -3.48° and -0.48° were used; Teignmouth, West bay Harbour, Portland Harbour, Swanage, Lymington, Sandown and Arun Platform. Data were available at 10 minute intervals at each site and interpolation was used to provide estimates over the computational domain.

In-situ measurements of water surface elevations (supplied as separated tide and surge components where the surge was defined as the residual between the harmonic prediction of the tide and the measured water levels) throughout the Solent were used to assess the accuracy of the model predictions (Fig. 4.1). Data were available at a variety of tide gauge and buoy sites provided online by the CCO, the National Tidal and Sea Level Facility (NTSLF, at http://pol.ac.uk/ntslf/) and three temporary buoys provided for this research by EMU (http://www.emulimited.com/). The temporal resolution of the datasets was greater than 15 minutes at all sites.

Data for the periods from 7th October to 30th December 2009 and 5th March to 12th March 2008 were used. The autumn 2009 period coincided with the deployment of three buoys measuring the water level, while the 10th March 2008 event was also considered as it was the most extreme event in recent years and led to coastal inundation. All data were quality checked prior to use.

4.3. Model Set-up

The MIKE-21 software package was used to model the domain of interest. MIKE-21 is a widely used 2D modelling package designed by the Danish Hydraulic Institute (DHI) group. Among its many users is the FEMA National Flood Insurance Programme using both the hydrodynamic and wave modules (FEMA, 2001).
The hydrodynamic (HD) module solves a full set of vertically integrated equations of continuity and conservation of momentum in two horizontal directions using an explicit scheme in either a Cartesian or Spherical coordinate system (Cañizares *et al.*, 2001). The system is based on the numerical solution of the two-dimensional incompressible Reynolds averaged Navier-Stokes equations subject to the Boussinesq and hydrostatic assumptions.

The MIKE-21 software has been used to model coastal hydrodynamics for numerous conditions, for example, see Cañizares *et al.* (2001), Madsen and Jakobsen (2004), and Dix *et al.* (2007). Further information regarding the MIKE-21 modules can be found on the download section of the DHI website at http://www.mikebydhi.com/Download/DocumentsAndTools/ShortDescriptions.aspx.
An unstructured mesh was used to avoid the problem of 'staircase' coasts (Jones and Davies, 2007a, 2007b). Bathymetry data of 100 m resolution, provided by the National Oceanography Centre, Southampton (http://www.noc.soton.ac.uk) was interpolated to the domain mesh (Fig. 4.2.). Boundary tide and surge time-series provided by Previmer, were given at the two domain boundaries, located along the -3.5° and -0.1° lines of longitude.

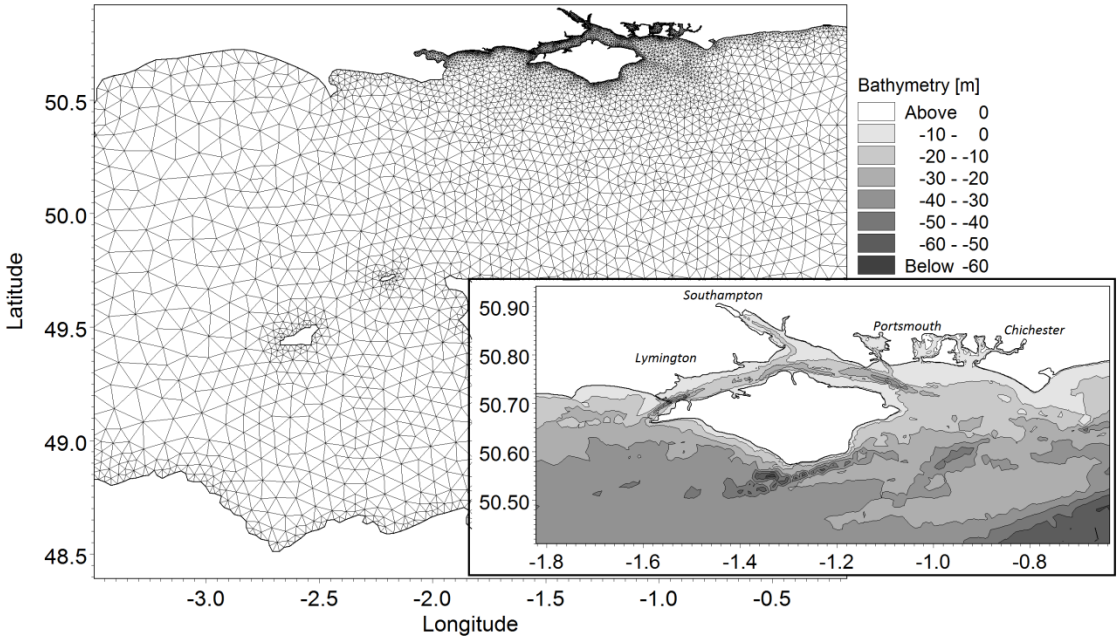

Fig. 4.2. The model domain and Solent bathymetry.

Sensitivity of the model to the domain mesh resolution was examined over a series of predictions, forced with only the boundary tidal elevation datasets, utilising model mesh designs with increasing spatial resolutions in the nearshore regions. The tidal elevation time-series predicted from October to December 2009 obtained using the different mesh designs were contrasted. Convergence was reached when increases in resolution no longer resulted in a significant root mean squared error (RMSE) between the tidal predictions at the locations given in Fig. 4.1. Final mesh resolution was approximately 2 km, 200 m and 100 m in the English Channel, Solent and harbours, respectively. The Mannings coefficient, defining the resistance of the bed of a channel to the flow of water in it, was shown to be highly influential upon the tidal solution. Calibration of this parameter based on the RMSE of the tidal solution relative to the tidal elevations extracted from the *in-situ* measurements of water levels was used to estimate the optimal value. An inverse Mannings coefficient of $42 m^{1/3} s^{-1}$ and a Smagorinsky coefficient (related to the eddy viscosity) of $0.28 m^2 s^{-1}$ was used.

4.4. Analysis

Two sets of tests were used to meet the aims given in the introduction. The first assessed the regional models ability to recreate water levels in the Solent region. A three month hindcast of tide, surge and combined water levels was conducted between October and December 2009. The accuracy of the tidal predictions at three tide gauges located in the East Solent (Portsmouth), West Solent (Lymington) and Southampton Waters (Southampton) regions was assessed using harmonic analysis. The predicted amplitudes and phases for eleven of the most significant constituents (after Levasseur, 2008) and the errors relative to those obtained from measured water level elevations were examined. The T-TIDE tidal package (Pawlowicz *et al.*, 2002) was used to extract the constituents from the predicted tide and the tidal elevations derived from the measured time-series. Modelled surge elevations (defined as the total water level elevations minus the astronomical tidal elevations) and combined water levels were contrasted with those from *in-situ* measurements at the sites given in Fig. 4.1. The RMSE was used as a measure of overall accuracy while the percentage bias (Pbias) indicated the bias relative to the average size of the factor considered (Brown *et al.*, 2010).

The second set of experiments was used to assess the degree to which tide-surge interaction influenced the surge throughout the region. The regional model was used to hindcast three events occurring on 14th November 2009, 29th November 2009 and 10th March 2008. For each event the model was used to predict the surge with and without the inclusion of the tide. The difference between the predictions indicated the influence of the tide-surge interactions upon the predicted surge. The sensitivity of the

surge predictions to uncertainty within the modelled tide was also examined. Using the event on 10th March 2008, the tidal range was reduced at 10% intervals for a set of simulations. The changes to the predicted surge elevations as a result of the alterations to the tidal elevation were assessed. Particular focus was placed on the 10th March 2008 event as it was the most extreme in recent years and led to significant coastal inundation.

The simulations used in the two experiments reported in this paper included the following datasets:

A) Tidal boundaries only

B) Tidal boundaries + Surge boundaries + Atmospheric forcing

C) No tidal boundaries + Surge boundaries + Atmospheric forcing

D) Tidal boundaries (of decreasing range from 100% to 0% at 10% intervals) + Surge boundaries + Atmospheric forcing

Simulations A and B were run for the 10th March 2008 event and for the October to December 2009 period. Simulations in group C were conducted for the three events occurring on 14th November 2009, 29th November 2009 and 10th March 2008, while simulations in group D were conducted for the event on 10th March 2008 only.

4.5. Results

4.5.1. The regional model hindcast

4.5.1.1. The tide

The harmonic constituent phases and amplitudes extracted from the modelled tides, and their errors relative to those from the measurement-based time-series are presented in Table 4.1. Relative to the size of the harmonic amplitudes extracted from the measured water levels, the predicted semi-diurnal components N_2, M_2, S_2 and most shallow water components contained errors less than 15% at Portsmouth and Lymington, and 18% at Southampton. Exceptions were found in the M_6 and $2MS_6$ constituents with errors being between 30 and 40% at all tide gauges. Larger discrepancies, ranging from 45 to 55% in amplitude between the model and measurements were obtained for constituent K_1. Constituent phase errors were consistently less than 20° at all three tide gauges in the semi-diurnal, quarter-diurnal and sixth-diurnal constituents, resulting in relatively little phase error in the tidal elevations relative to those derived from measurements. However, the error for the K_1 constituent was up to 25°, while the O_1 constituent contained errors as large as 55°. Constituent amplitudes were underestimated in most instances by the model. This resulted in Mean Spring Range (given as $2(M_2 + S_2)$) errors of 0.34, 0.15, and 0.48 m at

Portsmouth, Lymington and Southampton tide gauges, respectively. Mean Neap Range (given as $2(M_2 - S_2)$) errors were 0.21, 0.16 and 0.44 m.
Tidal elevations, on average, were underestimated by 19%. At Lymington the error was notably higher, with errors up to 29%.

Table 4.1. Harmonic constituents extracted from predicted tidal elevations. Errors are given relative to harmonics extracted from POL and CCO tidal elevations at the tide gauges.

Portsmouth	Amplitude Modelled (m)	Error (m)	Phase Modelled (°)	Error (°)
O_1	0.06	0.02	53.53	39.75
K_1	0.03	-0.04	254.12	24.93
N_2	0.20	-0.04	56.5	11.46
M_2	1.22	-0.14	90.81	9.38
S_2	0.53	-0.04	33	14.27
MN_4	0.06	0	253.45	0.9
M_4	0.16	-0.01	295.79	14.73
MS_4	0.14	-0.02	243.15	8.62
$2MN_6$	0.04	0	157.46	6.9
M_6	0.06	-0.04	176.46	13.19
$2MS_6$	0.09	-0.05	131.27	2.98
Lymington				
O_1	0.06	0.01	225.87	25.61
K_1	0.04	-0.03	58.72	25.36
N_2	0.14	-0.01	29.74	16.46
M_2	0.72	-0.08	63.31	11.65
S_2	0.33	0	342.92	17.08
MN_4	0.06	-0.01	230.04	3.71
M_4	0.16	-0.02	262.39	9.49
MS_4	0.13	-0.03	194.49	2.29
$2MN_6$	0.04	0	109.96	20.09
M_6	0.05	-0.04	122.11	5.77
$2MS_6$	0.08	-0.04	57.59	5.83
Southampton				
O_1	0.05	0.02	330.71	55.51
K_1	0.05	-0.05	143.36	9.4
N_2	0.19	-0.04	355.77	14.23
M_2	1.15	-0.2	281.18	12.95
S_2	0.36	-0.02	342.71	14.89
MN_4	0.07	-0.02	30.81	13.1
M_4	0.22	-0.03	321.87	12.37
MS_4	0.16	0.02	43.67	12.41
$2MN_6$	0.07	-0.01	116.44	4.58
M_6	0.10	-0.07	31.19	9.49
$2MS_6$	0.10	-0.07	109.1	9.87

4.5.1.2. The surge

Table 4.2 gives the RMSE and Pbias statistics between the predicted surge and those obtained from the measured time-series. The surge elevation accuracy on average contained a RMSE of 0.09 m. RMSE ranged from 0.08 m to 0.12 m, while the absolute

Pbias lay between 10.1 and 23.2% at all locations. The bias was positive at all sites with the exception of Lymington, where the predicted surge was smaller than that estimated by the CCO. Fig. 4.3 is a time-series of surge elevations extracted from predicted and measured water levels at Portsmouth. The figure indicates that the pattern of the surge, including two main peaks was reproduced by the model. However, the predicted surge was generally smoother than that in the measured time-series, consistently underestimating the positive and negative peaks, accounting for much of the RMSE given in Table 4.2. These findings were consistent throughout the domain. Despite this, across all tide gauges, the predictions of the two highest peak surge elevations lay within 15% of those from the measured record on average. Similar accuracy was found when considering the skew-surge, for instance, at Lymington the error in the skew-surge (the difference between the observed peak water level in a given tidal cycle and the corresponding peak tidal elevation) was 0.9 m (17.2%) on average during the two events.

Table 4.2. RMSE and absolute Pbias accuracy of the predicted surge during the October – December 2009 simulation period.

	EMU Hayling	EMU Nab	EMU Portsmouth	Lymington	Portsmouth	Sandown	Southampton	Average
RMSE (m)	0.1	0.09	0.12	0.11	0.09	0.08	0.08	0.09
Pbias (%)	13.1	11.6	17.1	23.2	18.4	10.1	13.1	15.2

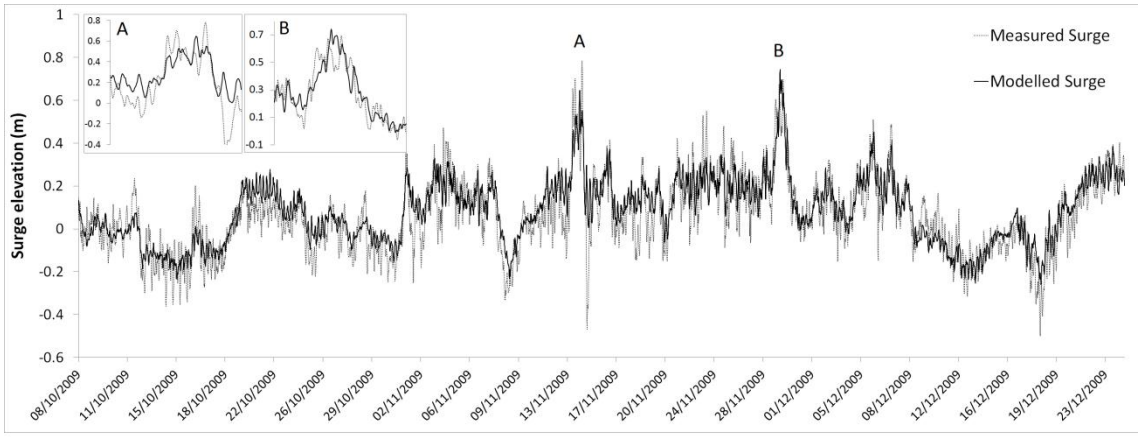

Fig. 4.3. Surge elevations extracted from modelled and measured water levels at Portsmouth, October to December 2009.

4.5.1.3. The combined surface elevation

The combination of the tide and surge elevations predicts the total surface elevation at a given location. Table 4.3 provides an assessment of the accuracy of the combined water level elevations from the model at the *in-situ* measurement sites. The average RMSE at the seven tide gauges was 0.25 m, with errors ranging from 0.31 m at Southampton to 0.2 m at Sandown. The averaged absolute Pbias over all of the tide gauges was 6% during all measured time steps, and 13.4% at the high tide points. Pbias was negative at every measurement site when considering the high tide periods. The largest Pbias was at Lymington (-17.7%). Under-prediction of the tidal ranges, outlined in Section 4.5.1.1 contributed significantly to the errors, particularly during the high tide periods. However, it has been reported that model-based tidal predictions, particularly in complex nearshore regions, can contain a high degree of uncertainty. Therefore, tidal predictions from harmonic analysis at tide gauge sites are utilised and the predicted surge added in operational systems. Interpolation or regression can then be used to estimate the tide at un-gauged sites. This approach was tested in this study, the results of which are given in the bracketed values in Table 4.3. At the permanent tide gauge locations, harmonic analysis was used to predict the tidal elevations. The temporary EMU buoys were used to demonstrate the suitability of predicting tidal elevations from those based on harmonic analysis at the permanent tide gauges.

Table 4.3. RMSE and absolute Pbias accuracy of the combined water levels. Values in brackets represent the accuracies where tidal substitution was utilised.

	EMU Hayling	EMU Nab	EMU Portsmouth	Lymington	Portsmouth	Sandown	Southampton	Average
Accuracy over full time-series								
RMSE (m)	0.28 (0.14)	0.22 (0.12)	0.26 (0.14)	0.23 (0.14)	0.25 (0.12)	0.2 (0.12)	0.31 (0.11)	0.25 (0.13)
Pbias (%)	9.7 (3.4)	5.2 (2.1)	2.5 (1.2)	13.5 (7)	1.4 (2.7)	5 (1.8)	4.8 (2.6)	6 (2.9)
Accuracy at high tides								
RMSE (m)	0.23 (0.16)	0.22 (0.12)	0.27 (0.14)	0.26 (0.15)	0.30 (0.12)	0.22 (0.12)	0.3 (0.12)	0.26 (0.13)
Pbias (%)	12.5 (5.3)	9.8 (2.6)	13.1 (3)	17.7 (8)	14.6 (1)	11.4 (2.2)	15.3 (1.2)	13.4 (3.3)

The results indicate that the substitution of the tide removed much of the tidal uncertainty in the signal, reducing the averaged RMSE error in the water levels by half in both the full time-series analysis and when considering only the high tide points at all of the tide gauges. These findings were consistent at both the stationary tide gauge sites and the EMU buoys where tides were predicted using regression from the values at the permanent tide gauges.

4.5.2. Tide-surge interaction

4.5.2.1. Removal of the tide

Across the seven tide gauges, the averaged RMSE between the surge predictions with and without the tidal signal was 0.07 m during the three events. The spatial variability in the tide-surge interaction was similar across all of the events. The influence of the tide-surge interaction was greatest at the Southampton site, resulting in an averaged RMSE of 0.11 m and change of surge peak heights of 0.07 m. Relative to the size of the surge events, the change of surge peak heights at Southampton ranged from 7 to 11% during the three events. The smallest influence occurred at the EMU Nab Buoy and Sandown sites with RMSEs of 0.05 m and changes of surge peak heights of 0.02 m at both sites. The changes were no larger than 5% of the surge elevation at either site during the three events.

Fig. 4.4 a, b and c, demonstrate the effect of the tide-surge interaction on the maximum predicted surge height, the RMSE between the two predicted surge elevations, and the change in the peak total water level elevations when the two surge predictions were added to the tidal elevations on March 10th 2008, respectively. Although the change to the predicted surge peak height was relatively small (e.g. never larger than 0.11 m or 11% of the surge magnitude, Fig. 4.4a), the combination of the shift in timing and magnitude led to significantly larger absolute alterations (up to 0.3 m) to the combined peak water levels predicted (Fig. 4.4c). In this instance, the inclusion of the tide caused the peak of the predicted surge to arrive later, occurring very near the high tide, particularly further into the Solent region. This created differences in the two predicted water level elevation peaks of up to 0.3 m at the Southampton tide gauge (Fig. 4.5). Relative to the size of the “normal” peak water levels at Southampton, this represented a 10% change in magnitude. This change in the peak water levels can also be considered in terms of the change to the skew-surge, which is often of great interest to coastal managers. Relative to the “normal” skew-surge, the exclusion of the tide-surge interaction component of the surge resulted in changes of up to 32% in the predicted skew-surge, with the greatest change occurring at the Southampton tide gauge. Considering all seven tide gauges, the averaged

change of the peak water level elevation was 0.15 m during this event, while the smallest change occurred at Sandown (0.1 m, or 4% of the peak water level).

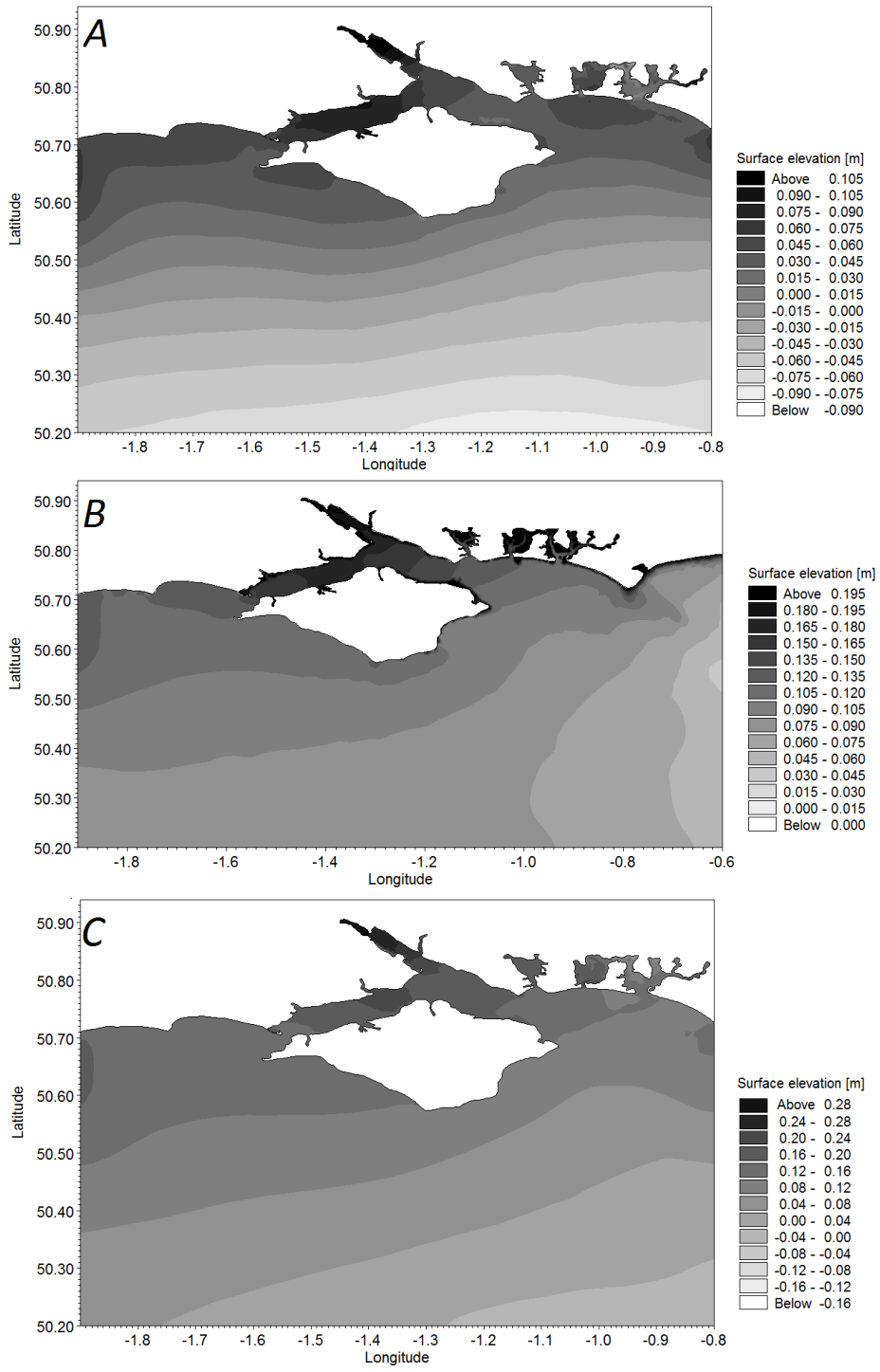

Fig. 4.4. The effect of the tide on the predicted surge. (A) Difference in peak surge height between the predicted surge with and without the tide. (B) The RMSE between the predicted surge with and without the tide. (C) Difference in peak combined water levels when the predicted surge with and without the tide was added to the "normal" tide and contrasted.

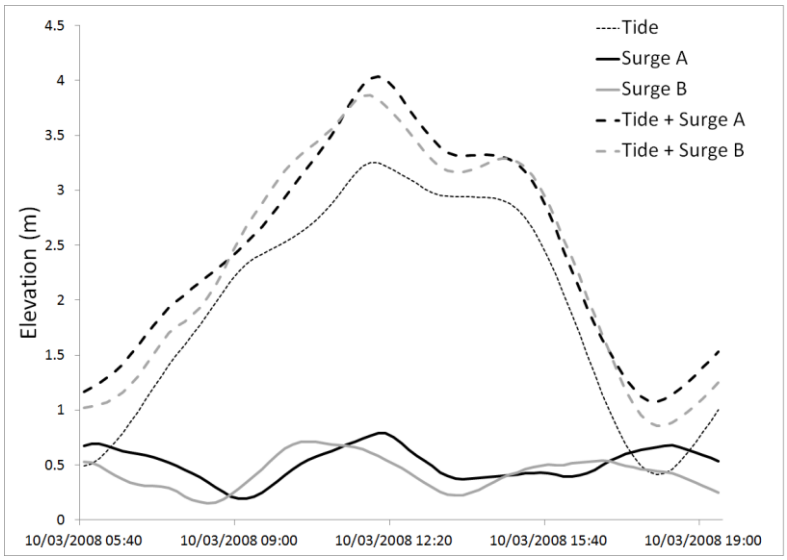

Fig. 4.5. Predicted surge and water levels at Lymington during the event on 10th March 2008. (Surge A) The surge predicted with the influence of the tide. (Surge B) The surge predicted without the influence of the tide. The difference between the two surge peaks was 0.07 m. However, due to the difference in timing, the resulting change in the peak water levels was 0.18 m.

During the November events the inclusion of the tide resulted in the surge moving away from the high tide slightly, occurring very near the end of the flood tide, while the surge predicted without the inclusion of the tide usually occurred during the high tide period. There was not a considerable difference between the size of the change in the peak surge height and the size of the change in the peak water levels. This appeared to be due to the shift away from the high tide in the "with tide" surge taking the surge peak only just off the high tide, therefore, the difference between the tidal elevations between the two surge peaks remained small. The resulting change in the skew-surge (and peak water levels), therefore, broadly resembled the difference in the peak surge heights. For instance, during the 29th November 2009 event the largest change to the total water elevation was at Southampton (0.08 m, 4.1%) while the corresponding change to the peak surge elevations was 0.07 m (8.5%). Relative to the "normal" skew-surge, this equated to less than a 10% change in magnitude. This contrasts with the 10th March 2008 event where the larger "with tide" surge lay very near the high tide, while the "without tide" surge fell earlier on the flood tide resulting in an alteration to the skew-surge and peak water levels due to both a direct change in surge height and a change in the position of the surge peak relative to the high tide. In this instance, the change in the skew-surge was as large as 20%.

4.5.2.2. Sensitivity of the model to uncertainty in the predicted tide

Across the domain, the largest RMSE between the "normal" surge prediction and that in the presence of 30% smaller tidal ranges was 0.03 m, while the largest change to the peak surge heights under the same conditions was less than 3%. The largest shift in the timing of the peak surge elevation was no greater than 20 minutes. The resulting influence upon the skew-surge or the total combined water level elevations was never greater than 0.03 m (or 3% of the skew-surge magnitude) during the high tide on 10th March 2008.

Fig. 4.6 plots the RMSE between the "normal" surge prediction and those given with alterations in the tidal range (hashed line) at Southampton during the event on 10th March 2008. The surge predictions, forced with the reduced tidal ranges, were added to the "normal" tidal elevations to give the combined water levels (solid line). The change in the peak water levels, relative to the "normal" water level prediction, is given by the solid line. The RMSE appears to increase linearly with a reduction in the tidal range, whereas the influence upon the maximum combined water level elevation does not. This was due to the effect of the tide-surge interaction has upon the timing of the surge. When tidal ranges were decreased by 30%, the timing of the surge peak occurred earlier, by approximately 20 minutes. The relatively short time shift meant that the peak of the surge was still located near to the high tide point. As the tidal range was further reduced, the surge peak moved further away from the high tide point. With no tide included, the surge peak occurred approximately 1 ½ hours earlier than the "normal" surge peak, and lay on the flood tide (as demonstrated in Fig. 4.5).

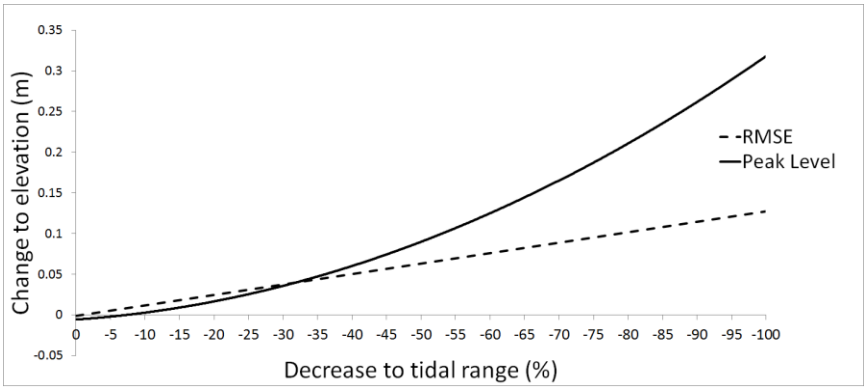

Fig. 4.6. The influence of the alteration to the tidal range at Southampton during the event on 10th March 2008. The RMSE given contrasts the predicted surge with each tidal dataset with the "normal" surge predicted using the unaltered tides. The peak level error is the change in peak combined water levels during the event relative to the level given where the "normal" surge prediction was used.

4.6. Discussion

A regional 2D hydrodynamic model using the MIKE-21 software and data from the Previmer system has been described and applied to the Solent – Southampton Water estuarine system. To assess the accuracy of the tide, surge, and combined water level elevation predictions, a three month hindcast was undertaken using operational data outputs from Previmer. Model predictions were contrasted with tide and surge elevations extracted from *in-situ* water level measurements.

The model consistently underestimated the amplitude of the tide throughout the region, with errors in the semi-diurnal constituents of up to 18% at the Southampton tide gauge. However, the predictions of the tidal constituents were broadly consistent with previous attempts at modelling through the region. Levasseur (2008) utilising a 3D modelling package also reported errors of up to 15% in the semi-diurnal amplitudes, while K_1 and some shallow water constituents (particularly $2MS_6$ and $2MN_6$) contained errors greater than 40%. Furthermore, Levasseur (2008) quotes errors in the MSR and MNR at Southampton, of 0.44 m and 0.39 m, respectively. These errors are very similar to the 0.48 m and 0.44 m errors found in this research. The uncertainty in the predicted tides was shown not to be due to the spatial resolution of the mesh or the simulation time step as increasing the resolution of both did not alter the model predictions at the *in-situ* measurement sites. The similarities in the tidal errors and the convergence of the model set-up, implies that the use of the 2D rather than 3D model was reasonable. The uncertainty in the predicted tide may, therefore, have been due to uncertainty in the datasets used to force the model, such as the tidal predictions at the domain boundaries. Levasseur (2008) also suggested that most of the error associated with diurnal and semi-diurnal constituents could be attributed to tidal inputs at the boundaries. Furthermore, issues relating to the accuracy of predicted tides from numerical models within complex nearshore regions have been noted in previous research and for this reason, in operational forecasting systems, predicted tides are replaced with those defined from harmonic analysis at class A tide gauges (Flowerdew *et al.*, 2007; Hawkes *et al.*, 2009).

The substitution of the modelled tide with those estimated from harmonic analysis was tested at the permanent tide gauges (Portsmouth, Southampton, Lymington and Sandown). At the temporary EMU buoys, tidal elevations were predicted from the values at the permanent tide gauges using regression. The addition of the modelled surge to the substituted tide resulted in considerable reductions in the error of the predicted combined water level elevations, reducing the RMSE compared to the "normal" predicted water levels by around half. The distribution of the EMU buoys, lying in water depths ranging from 5 m to 15 m, indicated that predictions at un-gauged sites, based on tides at the permanent tide gauges, were suitable in both very

nearshore and more offshore areas. However, the EMU buoys were located within the Eastern Solent, and yet tidal complexities (such as the development of double high waters and young flood stands) were more pronounced within the West and Southampton Water regions. For this reason the prediction of tidal elevations may not spread as well in these regions, particularly where only class A gauges are used (i.e. Portsmouth and Bournemouth in the West). The inclusion of the Lymington and Southampton tide gauges may be useful in the prediction of tidal elevations within these regions. When tidal substitution was utilised, the predictions of total water level elevations produced a RMSE of 0.13 m on average throughout the region during the October to December 2009 period.

The predicted surge elevation was given as the difference between the tidal elevations and the combined tide and surge elevations. During the three month assessment from October to December 2009, the averaged RMSE of the seven tide gauges was 0.09 m while absolute Pbias was 15.2%. RMSE and absolute Pbias accuracies at each site lay within 0.03 m and 8% of the averages obtained from all of the tide gauges, respectively. Time-series plots indicated that much of the error was related to the smooth nature of the predicted surge relative to that extracted from the measured record. Previous research by Horsburgh and Wilson (2007) found that due to small errors in harmonically predicted tides, the surge elevations given at tide gauges could often contain tidal patterning. Bocquet *et al*. (2009) found similar discrepancies in the surge smoothness between predicted and measured surges. They suggested that the harmonic estimation of tidal elevations can contain a RMSE of up to 0.1 m and suggest accuracy assessments of surge predictions are likely to be penalised due to such uncertainty in the measured record. For this reason, alternative statistics, such as the accuracy during specific event peaks, were also considered.

Predicted surge accuracies from the regional model were comparable with those obtained from the operational storm surge model developed by Proudman Oceanographic Laboratory (archives of accuracy assessments are available to download from http://www.pol.ac.uk/ntslf/model.html). Over the period between October 2009 and December 2009, the accuracy of the operational storm surge model at Portsmouth was an average RMSE of 0.07 m. Data from the operational model was not available at other locations used in this research. The regional model was able to reproduce two peak surge heights in November 2009 and the event on 10th March 2008 with an accuracy of 0.12 m (15%) on average across the domain. Although the operational model accuracy over the same events is not known, previous technical reports, such as Wortley *et al*. (2007) have stated that average accuracy over 25 'alert' events at Portsmouth was a RMSE of 0.11 m.

Using the regional model, the influence of the local tide-surge interaction on the predicted surge was assessed during the surge events from 10th March 2008, 14th November 2009, and 29th November 2009. Contrasting the predicted surge elevations

with and without tidal influence, the tide-surge interaction was shown to be greatest in the Western Solent and Southampton Water regions. The largest uncertainty in the tidal predictions was also found in these regions. Over the three events the largest average RMSE between the two time-series was 0.11 m, occurring at Southampton. The predicted surge amplitude and timing was influenced by the tide-surge interaction. The largest alteration of the peak surge elevations and timing were found to occur at the Lymington and Southampton tide gauges during the event on 10th March 2008. Predicted peak surge elevations were reduced by 9.9% and 11%, respectively, at the two tide gauges.

Previous research has reported tide-surge interactions. Wells *et al*. (2001) demonstrated that during an extreme surge event, the tide-surge interaction resulted in a reduction of the peak surge elevations predicted within the English Channel. Prandle and Wolf (1978) also noted that the tide-surge interaction routinely led to the reduction of the surge magnitude. In addition, they also stated that the spatial distribution of the magnitude of the interaction could be highly localised. The results presented in this research concur with previous research indicating that the tide-surge interaction can alter the surge magnitude and timing (Horsburgh and Wilson, 2007; Wolf, 2008; Wolf, 2009), and that the magnitude of the influence can vary spatially. However, during the event on 10th March 2008 in particular, the results indicate that the tide-surge interaction increased the size of the surge peak rather than reducing it. Similar results were found by Brown *et al*. (2010) who stated that the tide could significantly enhance or reduce the surge.

The importance of the tide-surge interaction upon the combined water level elevations varied between the events considered. The most important factor was not just the change in the peak surge magnitude but also the alteration to the timing of the surge relative to the timing of the high tide as demonstrated in Fig. 4.5. Where the surge peak fell on or very near to the high tide, the tide-surge interaction was most important as shifts of more than an hour were capable of moving the surge peak away from high tide resulting in alteration to the skew-surge and peak water level elevations by up to 30% and 10%, respectively, at Southampton. Therefore, it is apparent that accurate representation of the local tide-surge interaction can be essential in the provision of high quality flood warnings, particularly when the surge occurs on or near to the high tide. Brown and Wolf (2009) discussed the tide-surge interaction and its implications for coastal managers. They too acknowledged that the change to the overall water level elevations was due to a combination of both magnitude and timing changes, and suggested that an important factor for coastal managers was the skew-surge.

Using the event on 10th March 2008, the uncertainty in the predicted surge as a result of the uncertainty in the predicted tidal range was investigated. This event was used as it: was the largest in recent years; led to coastal inundation; and was the most

sensitive to alteration in the timing of the surge peak of the three events considered. Reductions to the tidal range at 10% intervals were considered. Alteration of the tidal range by 30% (the largest uncertainty found in the predicted tides) did not alter the timing of the surge peak closest to the high tide by more than 20 minutes at any of the measurement sites. As a result, the impact upon the combined predicted water levels never exceeded 0.03 m (and less than 4% of the skew-surge magnitude). These results suggest that the uncertainties expected in predicting tidal ranges within the Solent using current hydrodynamic models should not result in significant errors in the predictions of peak surge elevations relative to the 0.1 m uncertainty attributed to tidal predictions from harmonic analysis in previous research.

This research utilised a regional case study to assess the levels of uncertainty in predicted surge elevations that might arise from errors in tidal predictions. Quantifying uncertainty is important in any modelling system. The present results indicate that expected tidal uncertainty in the Solent is unlikely to lead to significant uncertainty in the prediction of surge elevations. This indicates that the accuracy of current tidal predictions from numerical models is not expected to be a significant limiting factor to the provision of accurate surge forecasts in operational systems. Although the research is based within the Solent, the results will be of interest to modellers in other regions. The magnitude of the influence of the tide-surge interaction and the spatial variability demonstrated that it could be used as a useful first indication of the type and size of interactions one might expect to see in other regions, particularly those experiencing similar typical surge conditions.

Further research could validate the findings within the region and provide more widely applicable results. This research considered tide-surge interactions over only three events, one of which resulted in significant inundation, and only the tidal range uncertainty was examined. To extend this research, the influence of both the tidal range and phase errors, upon events of a variety of sizes, could be considered. By doing so one could validate the findings from the events already considered, or find instances where the influences revealed in this research are not representative. Furthermore, by perturbing both tidal range and phases, a more holistic assessment of tidal uncertainty upon surge predictions could be obtained. This could be particularly useful in predicting tide-surge interactions in other regions, such as those in which tidal phases contain the most significant errors. Similarly, using methodologies presented in previous research, for instance Bernier and Thompson (2007) or Zang *et al*. (2010), a detailed assessment of the factors contributing to tide-surge interactions could be made to foster the understanding of the nonlinear processes taking place in complex estuarine systems.

4.7. Conclusion

A regional hydrodynamic model of the Solent-Southampton Water estuarine system, forced with data from the pre-operational Previmer system, was used to examine the tide-surge interactions and the influence of data uncertainty to model predictions in the region. The research conducted indicated:

- The regional model was capable of predicting surge elevations with accuracies similar to those derived from alternative operational forecasting systems, indicating that the model and forcing datasets were suitable for representing the processes occurring in the region.
- Under-prediction of the tidal range throughout the region, consistent with previous research, was significantly reduced through the replacement of the modelled tide with those derived from harmonic analysis at permanent tide gauges and interpolated to un-gauged sites.
- Tide-surge interactions in the region were shown to be influential upon both the height and timing of the surge peak and resultant peak water levels, accounting for up to 10 % of the total water elevation during an event on the 10th March 2008. However, the expected errors in the tidal predictions were found to lead to an insignificant (0.03 m maximum) change to the modelled peak water levels throughout the region.

These findings indicate that current hydrodynamic models commonly utilised in coastal regions, such as the one described in this research, are unlikely to contain errors in the predictions of tidal elevations that will induce significant uncertainty in surge predictions even in a complex estuarine environment. Furthermore, the use of tidal substitution should still be considered 'best practice' even in complex estuarine environments such as the Solent where tidal prediction uncertainty is expected to be greatest; a finding that will of value to coastal modellers working in a wide variety of regions.

Chapter 5: Modelling wave and water levels in the Solent and surrounding waters: importance of wave-surge interaction and tidal uncertainty

Abstract

A regional 3rd generation spectral wave model, using the MIKE-21 software and data from a pre-operational forecasting system of the English Channel, is described and applied to the Solent-Southampton Water estuarine system. This region was used as a case study to highlight the accuracy of the wave model and the importance of tide-wave interactions in a complex region which contains a wide range of water depths, irregular tidal regimes, and high degree of spatial variability in the exposure to waves. The regional model was able to predict H_s and T_z conditions with an average root mean square error (RMSE) accuracy of 0.32 m and 0.81 s, respectively, during a three month hindcast in the winter of 2009. Model accuracies in depths greater than 10 m contrasted well with accuracy assessments from other systems, while larger errors were demonstrated in shallower nearshore areas. The significant uncertainty in the very shallowest regions has been attributed to uncertainty in the bathymetric and atmospheric datasets. The sensitivity of the wave model to uncertainty in the predicted water level elevations was assessed. The results indicated that the inclusion of accurate water level elevations was most important in the eastern Solent region, where the largest wave heights were found. Bathymetric depth also played an important role, with the greatest sensitivity found in the shallow, nearshore regions of the domain. The exclusion of the water level elevation datasets resulted in reductions to predicted H_s peaks by up to 16.3%, while alterations to the water level elevations of 30% induced change in the model predictions by up to 6%. The influence of the wave upon the surge was also examined. Sensitivity was greatest in nearshore regions exposed to relatively large wave conditions, for instance, the eastern Solent. The inclusion of the waves was shown to be a vital component in the prediction of peak surge elevations, resulting in an increase of up to 9% relative to those where waves were excluded.
Despite the local nature of the research, the variability in conditions found in the region provided a useful setting in which to assess the spatial variability in model accuracy and tide-wave coupling. The findings are expected to be of interest to coastal managers in the Solent, while also being applicable to other estuarine environments. The relatively large errors in shallow, nearshore regions, indicates a strong

requirement for high resolution bathymetric datasets, potentially indicating drawbacks in current wave model formulations when considered in the light of other research in similar conditions. This research quantified the interaction between the HD and SW model outputs, clearly indicating that the influences upon both signals can be significant, particularly during extreme events, often of most interest to coastal managers.

5.1. Introduction

Where strong winds blow over a long fetch, large waves can be created, increasing the likelihood of coastal flooding, particularly when coupled with high spring tides and storm surge events (Zang and Tooley, 2003; Hunt, 2005). Waves increase the local sea surface height, supplying vast amounts of energy to the coast (Battjes, 2006). The energy contained within a wave breaking upon the coast can destroy coastal defences, especially where sea levels are high enough to enable waves to overtop defences, thereby attacking the rear face and increasing the likelihood of failure (Wolf and Flather, 2005). Furthermore, the influence of wave-induced stresses can be influential upon storm surge water levels (Wolf, 2009). Kim *et al*. (2010), for example, demonstrated that measured typhoon-induced peak sea levels could not be modelled without the inclusion of wave-induced radiation stresses. The influence on sea level was shown to be comparable with that due to wind stress and pressure changes. Funakoshi *et al*. (2008) found that the coupling of wave and hydrodynamic models could lead to an increase in surge heights of up to 15%, due primarily to the transfer of momentum from the dissipation of short waves to the long wave motion of the storm surge. Similar findings have been reported by Mastenbroek *et a*l. (1993), Choi *et al*. (2003), Xie *et al*. (2008), and Wolf (2009). Therefore, the accurate prediction of wave states, and the quantification of their contribution to the predicted surge elevations, within coastal regions, can be a vital component of coastal flood forecasting systems.

Forecasting wave conditions has become commonplace in many areas of the world, usually as part of a multi-component system, coupling the outputs of atmospheric, hydrodynamic and wave models (e.g., Battjes and Gerritsen, 2002; Vatvani *et al*., 2002; Allard *et al*., 2008; Bocquet *et al*., 2009). Model accuracies vary between systems and the regions modelled. Bidlot *et al*. (2007) compared the accuracies of a variety of operational forecasting systems at numerous offshore sites and found that they routinely predicted significant wave heights (H_s) with a root mean squared error (RMSE) of between 0.25 and 0.4 m, relative to *in-situ* measurements. Scatter Index (SI) values (where the RMSE is normalised by the average size of the incident) of mean wave period (T_z) and H_s lay within 20% in the same study. National Oceanic and Atmospheric Administration (NOAA) online assessments of their system

(http://polar.ncep.noaa.gov/waves/valid_wna.html) demonstrated accuracies within a SI of 25%.

Validation accuracies presented in the literature generally refer to offshore sites as the model domains used in operational systems are often of too coarse a spatial resolution to accurately model the complexity found in coastal regions. For example, the Met Office provides operational shelf-scale forecasts of wave state at 12 km spatial resolution as outputs from their UK Waters Wave Model for the entire UK coastline. Where desired, for example, for flood forecasting warnings, projects have been undertaken to develop site-specific transforms of the offshore predictions to the nearshore. The TRITON system is an exemplar nearshore flood forecasting system in the NW region, in which, offshore wave conditions provided by the UK Waters Wave Model are transformed to the nearshore using pre-defined look up tables (Saulter, 2007; Tozer *et al.*, 2007; Environment Agency, 2009b). The tables were generated using a dedicated high resolution, nearshore spectral wave model; Simulation WAves Nearshore (SWAN; Booij *et al.*, 1999).

As operational systems routinely consist of coupled physically-based models, relatively large errors in the water level elevations, obtained from the hydrodynamic components (Flowerdew *et al.*, 2007), may lead to uncertainty in nearshore wave predictions. Waves in shallow waters are influenced by water depth and tidal oscillations (Knauss, 1996; Brown *et al.*, 2011), and so, significant errors in predicted water levels could lead to uncertainty in predictions of wave states in such regions. Quantifying such uncertainty is an important element when evaluating the confidence of a model forecast particularly in complex nearshore regions.

Previmer is a pre-operational hydrodynamic modelling system, currently under development, which aims to provide users with short-term forecasts of ocean state over a variety of model domains, including global and North East Atlantic models, with smaller nearshore nests at selected regions along the French coast (http://www.previmer.org/en.). The North East Atlantic model generates forecasted wave states and water level elevations throughout the English Channel, providing a potential source for boundary driving conditions for a regional model of the Solent and Hampshire coastline, on the south coast of the UK, an area thought likely to be affected by increased flood risk in the future (Evans, 2004).

This region is important to numerous stakeholders, including a variety of protected habitats, a dense coastal population and two of the largest shipping ports in the UK. The coastal population has increased steadily reaching 835,731 in 2001 with nearly 4000 ha of land, supporting 17,000 dwellings and a population of 37,600 considered at risk from coastal flooding (Hampshire County Council, 2006). Concerns exist over increased risk of coastal flooding in the future due to (i) a rise in the number of assets located in the coastal zones (Brown *et al.*, 2010) and (ii) sea level rise from eustatic and isostatic change (Inter Agency Committee on Marine Science and

Technology, 2004; Houghton, 2005; Hall *et al.*, 2006; Haigh *et al.*, 2009; Shennan *et al.*, 2012). Moreover, intensification of wave conditions within the North Atlantic-North Sea shelf has been linked to an increase in storminess and mean wind speeds over the last 30 years (Bacon and Carter, 1991; Zang and Tooley, 2003; Inter Agency Committee on Marine Science and Technology, 2004), although research by Wolf and Woolf (2006) indicates that the latter is likely to be the most significant factor contributing to an increase in wave heights. Changes in global mean sea levels have been found to further intensify wave conditions. Chini *et al.* (2010) highlighted that an increase in water levels, due to surge or an increase in mean sea level, may result in waves breaking later and, therefore, more energy reaching the coast. They suggest that within the South East of the UK, an increase in sea level of 7 mm $year^{-1}$ could result in a 4% increase in height of a 100 year event by 2090. Evans (2004) states that the southern coast of the UK is expected to experience some of the largest increases in flood risk during the 21st century in the country. There is, thus, a strong desire for a regional real-time flood forecasting system for the Solent and Hampshire coastline, while at the same time, there is a push for quantifying uncertainty in forecasting systems (Davis *et al.*, 2010).

This research had two aims. The first was to demonstrate the accuracy of a regional model for predicting wave states within the Solent region, utilising boundary datasets from the Previmer forecasting system. The second aim was to use the Solent region as a case study with which to assess the interactions between the hydrodynamic and spectral wave components of the regional model, quantifying both the influence of the water level elevations on the predictions of the wave states, and the sensitivity of the hydrodynamic model to the wave fields generated from the spectral wave model.

The study site and datasets are described in Section 5.2, followed by a description of the model set up and analysis structure in Sections 5.3 and 5.4, respectively. Section 5.5 presents the results which are discussed in Section 5.6. The main conclusions are drawn in Section 5.7.

5.2. Study Site and Data

5.2.1. The Solent

The Solent lies between the south coast of England and the Isle of Wight, in the UK (Fig. 5.1). It includes 12 separately defined estuaries and harbours and contains a wide range of coastal habitats (Fletcher *et al.*, 2007). The region has various stakeholders, including protected habitats, a dense coastal population and two of the largest shipping ports in the UK.

The region lies in the English Channel, in which the M_2 tide is the dominant tidal component and tidal ranges typical are in the order of 6 to 10 m. The M_2 is also the

dominant forcing within the Solent. However, the irregular geometrical shape, narrow channel configuration and shallow depth of the estuary results in amplification of the shallow water tidal constituents, M_4 and M_6 (Levasseur, 2008). Storm surges in this region most frequently occur due to low pressure systems from the Atlantic propagating eastwards, or as a result of storm surges propagating south from the North Sea (Law, 1975; Haigh *et al.*, 2004).

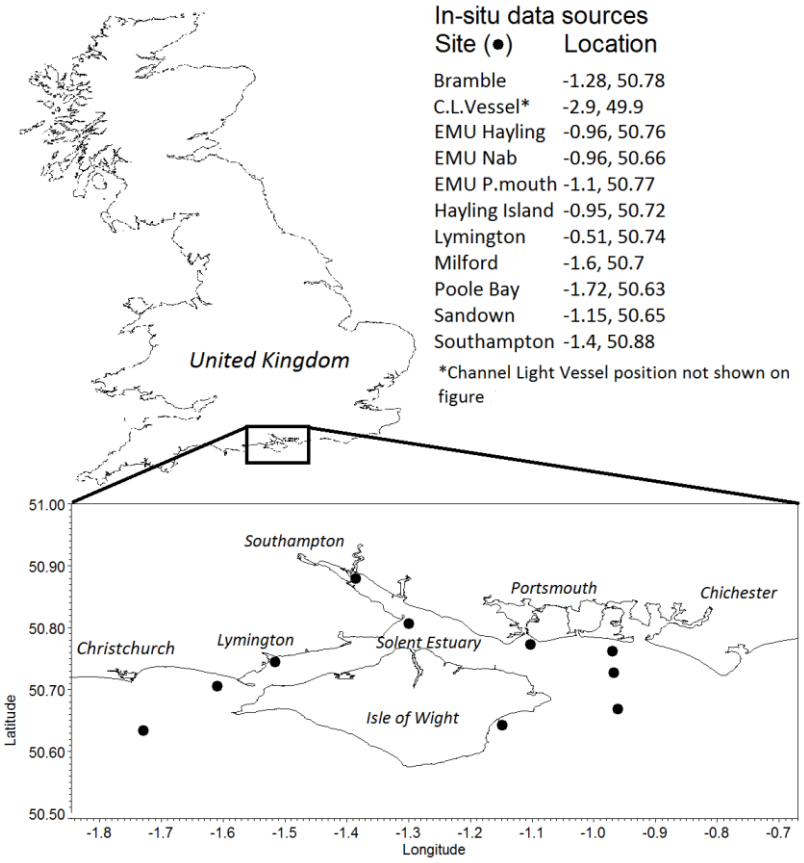

Fig. 5.1. The location of the Solent Estuary and *in-situ* data sources

The English Channel is fairly sheltered from extreme waves, with a long-term average H_s of 1.5 m (Inter-Agency Committee on Marine Science and Technology, 2004) and T_z of typically 6 -10 s. The largest waves that occur usually arrive from either 240° due to storm waves and swells from the Atlantic (Dix *et al.*, 2007) or occasionally 40-50° (storm waves from the North Sea). The Solent and Hampshire coastline is protected from extreme wave events by the Isle of Wight and Hurst Spit. The Channel Coastal Observatory (http://www.channelcoast.org/), the data management and regional coordination centre for the Regional Coastal Monitoring Programmes (see Isle of Wight Council (2005) for a useful overview), considers the region to have low-to-medium exposure to waves due to sheltering influences and the fetch-limited conditions. At Lymington and Sandown Pier, for example, the average 5% exceedence height for H_s between 2003 and 2008 were 0.8 m and 0.5 m, respectively.

However, sites in the eastern region (such as Hayling Island), are less sheltered and can be affected by large swells propagating through the English Channel. For example, over the same period the average 5% exceedence value for H_s was 1.59 m while events greater than 3.8 m were recorded. Recent research by Palmer (2011) has examined the propagation of waves through the English Channel, revealing that refraction of waves due the Channel's topography, leads to a focussing of wave energy in the eastern Solent.

A review of flood events within the Solent since 1935 can be found in Ruocco *et al*. (2011). Generally, coastal flooding within the Solent is considered frequent, but usually with no recorded loss of human life (Wadey *et al*., 2012).

5.2.2. Data

Tidal elevations, surge elevations, wave conditions and winds derived from the Previmer group (http://www.previmer.org/en) were used in this research. These datasets were outputs from a pre-operational system, currently under development, which aims to provide users with short-term forecasts of the state of the ocean along French coastlines bordering the English Channel, the Atlantic Ocean and the Mediterranean Sea. Tide and surge components of the water surface elevation (velocities were not specified) were provided at 5.5 km spatial resolution, and 1 hour temporal resolution, throughout the English Channel. These data were model outputs created using the Model for Application at Regional Scale (MARS 2D) system (Lazure and Dumas, 2008). Wave conditions (H_s, T_z, direction and spreading) were provided at 3.5 km spatial and 3 hour temporal resolution from forecasts made using the Wavewatch III model (Tolman, 2009). The Previmer models utilise modelled wind fields at 3 hour temporal and 4 km spatial resolution provided by the European Centre for Medium Range Weather Forecasts (ECMWF, www.ecmwf.int/about). These wind field datasets were supplied via the Previmer group for this research. Atmospheric pressure fields were interpolated from measurements provided by the Channel Coastal Observatory. Measurements at seven sites located along the south coast of England, between longitudes of -3.48° and -0.48° were used; Teignmouth, West bay Harbour, Portland Harbour, Swanage, Lymington, Sandown and Arun Platform. Data were available at 10 minute intervals at each site and interpolation was used to provide estimates over the computational domain.

In-situ water levels and wave conditions were given at a variety of tide gauge and buoy sites (Fig. 5.1) provided online by the National Tidal and Sea Level Facility (at http://pol.ac.uk/ntslf/), the Centre for Environment, Fisheries and Aquaculture Science (www.cefas.defra.giv.co.uk) and the CCO. Further measurements were provided by three temporary buoys provided for this research by EMU (http://www.emulimited.com).

Data for the periods from 7th October to 30th December 2009 and 5th March to 12th March 2008 were used. The autumn 2009 period coincided with the deployment of three buoys, while the 10th March 2008 event was included as it was the most extreme event in recent years and led to coastal inundation. All data were quality checked prior to use.

5.3. Model Set-up

The MIKE-21 software was used to model the domain of interest. MIKE-21 is a widely used 2D modelling package designed by the Danish Hydraulic Institute (DHI) group. Among its many users is the FEMA National Flood Insurance Programme which uses both the hydrodynamic and wave modules (FEMA, 2001; Cañizares *et al.*, 2001; Madsen and Jakobsen, 2004; Dix *et al.*, 2007). A coupled model, using both the hydrodynamic and spectral wave modules, was used in this research.

The hydrodynamic (HD) module is central within MIKE-21. It solves a full set of vertically integrated, equations of continuity and conservation of momentum in two horizontal directions using an explicit scheme in either a Cartesian or Spherical coordinate system (Cañizares *et al.*, 2001). The system is based on the numerical solution of the two-dimensional incompressible Reynolds averaged Navier-Stokes equations.

The MIKE-21 Spectral Wave (SW) module (Warren and Bach, 1992) is derived from the WAve prediction Model (WAM) formulation (Hasselmann *et al.*, 1988) and has been utilised in a variety of operational and research-based applications (e.g., Johnson and Kofoed-Hansen, 2000; Sørensen *et al.*, 2004; Sørensen *et al.*, 2006). MIKE-21 SW is a 3rd generation wind-wave model that simulates growth, decay and transformation of wind-generated waves and swells in offshore and coastal areas. The evolution of the wave spectrum in the position (x, y) and time (t) is propagated in horizontal Cartesian co-ordinates by:

$$\frac{\partial N}{\partial t} + \nabla \cdot \left(\vec{v} N\right) = \frac{S}{\sigma} \tag{5.1}$$

Where $N(\chi, \sigma, \theta, t)$ is the action density, t is the time, $\vec{v} = (cx, cy, c\sigma, c\theta)$ is the propagation velocity of a wave group in the four dimensional phase space x, y, σ and θ, and S is a source term for the energy balance equation. ∇ is a four dimensional differential operator in the x, y, σ, θ-space.

The model is applicable for propagation of the wave spectrum from deep to shallow water regions by incorporating shallow water source terms into the model equations by

$$S = S_{in} + S_{nl} + S_{ds} + S_{bot} + S_{surf} \quad (5.2)$$

Where S_{in} is the generation of energy by wind, S_{nl} is wave energy transfer due to non-linear wave-wave interactions, S_{ds} is the dissipation of wave energy due to whitecapping, S_{bot} is the dissipation due to bottom friction and S_{surf} is the dissipation of wave energy due to depth-induced breaking.

Further information regarding MIKE-21 modules can be found on the download section of the DHI website at http://www.mikebydhi.com/Download/DocumentsAndTools/ShortDescriptions.aspx.

Fig. 5.2 demonstrates the model domain mesh and bathymetry. Bathymetry data of 100 m resolution provided by the National Oceanographic Centre, Southampton (http://www.noc.soton.ac.uk) were interpolated to the domain mesh. Boundary tide, surge and wave time-series provided by Previmer, were given at the two domain boundaries, located along the -3.5° and -0.1° lines of longitude. Sensitivity of the model to the domain mesh resolution was examined over a series of tide and wave predictions, utilising model mesh designs with increasing spatial resolution in the nearshore regions. The predictions from October to December 2009 obtained using the different mesh designs were compared. Convergence was reached when increases in resolution no longer resulted in a significant RMSE between the tidal or wave predictions at the locations given in Fig. 5.1. Final mesh resolution was approximately 2 km, 150-200 m and 50-100 m in the English Channel, Solent and harbours, respectively.

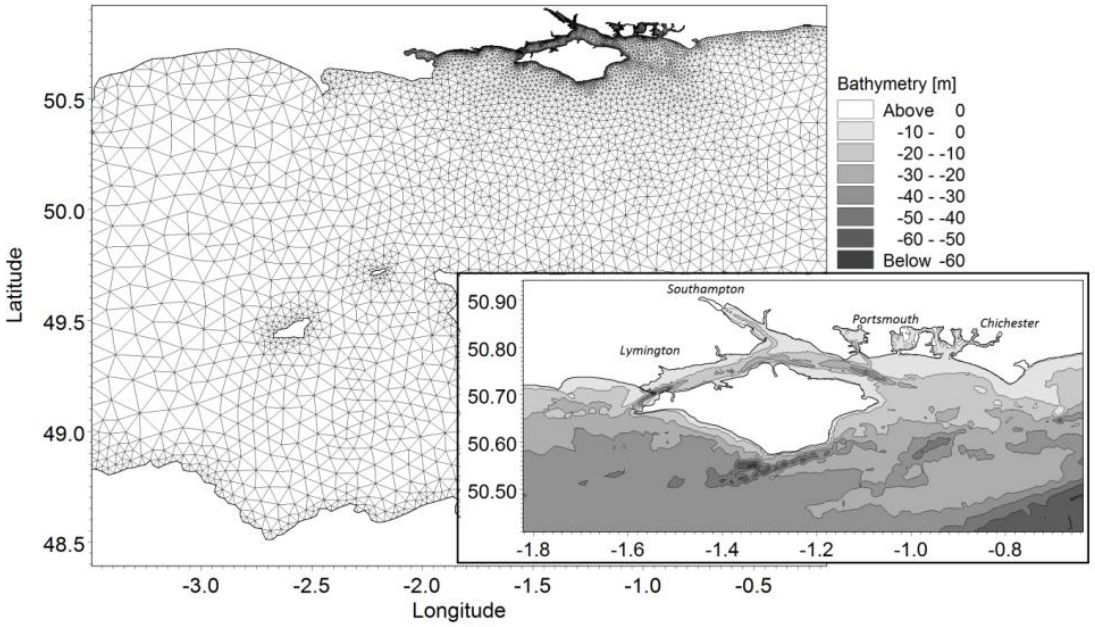

Fig. 5.2. Model domain mesh and bathymetry.

5.4. Analysis

Three sets of tests were used to meet the aims given in the introduction. The first assessed the regional models ability to recreate wave states (H_s and T_z) in the Solent region. A three month hindcast of the waves was conducted between October and December 2009 using the regional model. The accuracy of the wave predictions at the nine *in-situ* measurement sites (Fig. 5.1) was assessed against measured time-series. The RMSE was used as a measure of overall accuracy while the percentage bias (Pbias) indicated the bias relative to the average size of the factor considered (Brown *et al.*, 2010).

The second set of tests was used to assess the degree to which the water level elevations, defined from the HD module, influenced the predictions from the SW model. The regional model was used to hindcast two events, occurring on the 14th November 2009 and the 10th March 2008. For each event, the model was used to predict the wave state with and without the inclusion of the water level elevations from the HD module. The differences between the predictions indicated the degree to which the water level elevations influenced the wave predictions. The sensitivity of the wave predictions to 'expected' uncertainty in the water level predictions was also examined. The regional HD model was found to consistently under-predicted water levels by up to 30% in some regions. The impact of such errors upon the wave predictions were assessed by hindcasting the events with an increase of 30% to the modelled water levels and contrasting the outputs with those in the original hindcast.

The third set of tests examined the influence of the waves upon the surge prediction. The regional model was used to hindcast surge elevations during the two events occurring on the 14th November 2009 and the 10th March 2008. Surge elevation was defined as the total water level elevation minus the astronomical tidal elevation. In each event, the HD model was run with and without the coupling with the wave model and the differences were used to indicate the sensitivity of the surge predictions to the state of the waves.

A summary of the simulations used in the research is given as:

i. 'Normal' coupled model: HD module + SW module

ii. Exclusion of water level elevations: SW module only

iii. Increasing water level elevations: HD module (with 30% larger boundary elevations) + SW module

iv. Exclusion of the waves: HD module only

Simulation i was run for the October to December 2009 period and for the March 10th 2008 event, while simulations ii, iii and iv were run for the events from the 14th November 2009 and the 10th March 2008.

5.5. Results

5.5.1. The regional wave model hindcast

Model prediction accuracies, relative to *in-situ* measurements at the locations given in Fig. 5.1, are presented in Table 5.1 for the October to December 2009 period.

Table 5.1. Model errors utilising Previmer datasets relative to *in-situ* measurements.

Previmer / Measured				
	H_s (m)		T_z (s)	
Location	RMSE (m)	Pbias (%)	RMSE (s)	Pbias (%)
Channel Light Vessel	0.76	24.80	-	-
Hayling Island	0.25	7.50	0.72	-5.90
Poole Bay	0.27	1.50	0.61	-4.75
Sandown Pier	0.25	32.00	0.60	-0.03
EMU Hayling	0.25	22.20	0.80	-9.50
EMU Nab Tower	0.31	10.60	0.90	14.70
EMU Portsmouth	0.30	87.60	1.55	-36.00
Milford	0.36	22.90	0.69	-1.40
Lymington	0.15	49.50	0.57	-8.80
Average	0.32	28.40	0.81	-6.46

In the hindcast, the domain average RMSE was 0.32 m and 0.81 s for the H_s and T_z, respectively, while average absolute Pbias was 10% and 28.7%. An over-prediction of H_s at the Channel Light Vessel was reduced by more than 50% by the time the waves propagated to the Poole Bay and EMU Nab sites. Model error, relative to the size of the event, increased further into the Solent. The largest Pbias errors occurred in the shallow water regions, at sites where model bathymetry was less than 10 m. At the Lymington and EMU Portsmouth sites H_s Pbias was greater than 49%. H_s was over-predicted, while the T_z was under-predicted throughout most of the region.

Normalising the RMSE revealed a distinction between the nearshore and deeper regions (e.g. Fig. 5.3). In bathymetry depths greater than approximately 10 m, such as EMU Nab Tower, Poole Bay and Hayling Island, the average normalised RMSE was 20% and 21% for H_s and T_z, respectively. However, at sites such as Sandown, EMU Hayling,

EMU Portsmouth and Lymington, the average normalised RMSE increased to 67% and 33%, respectively.

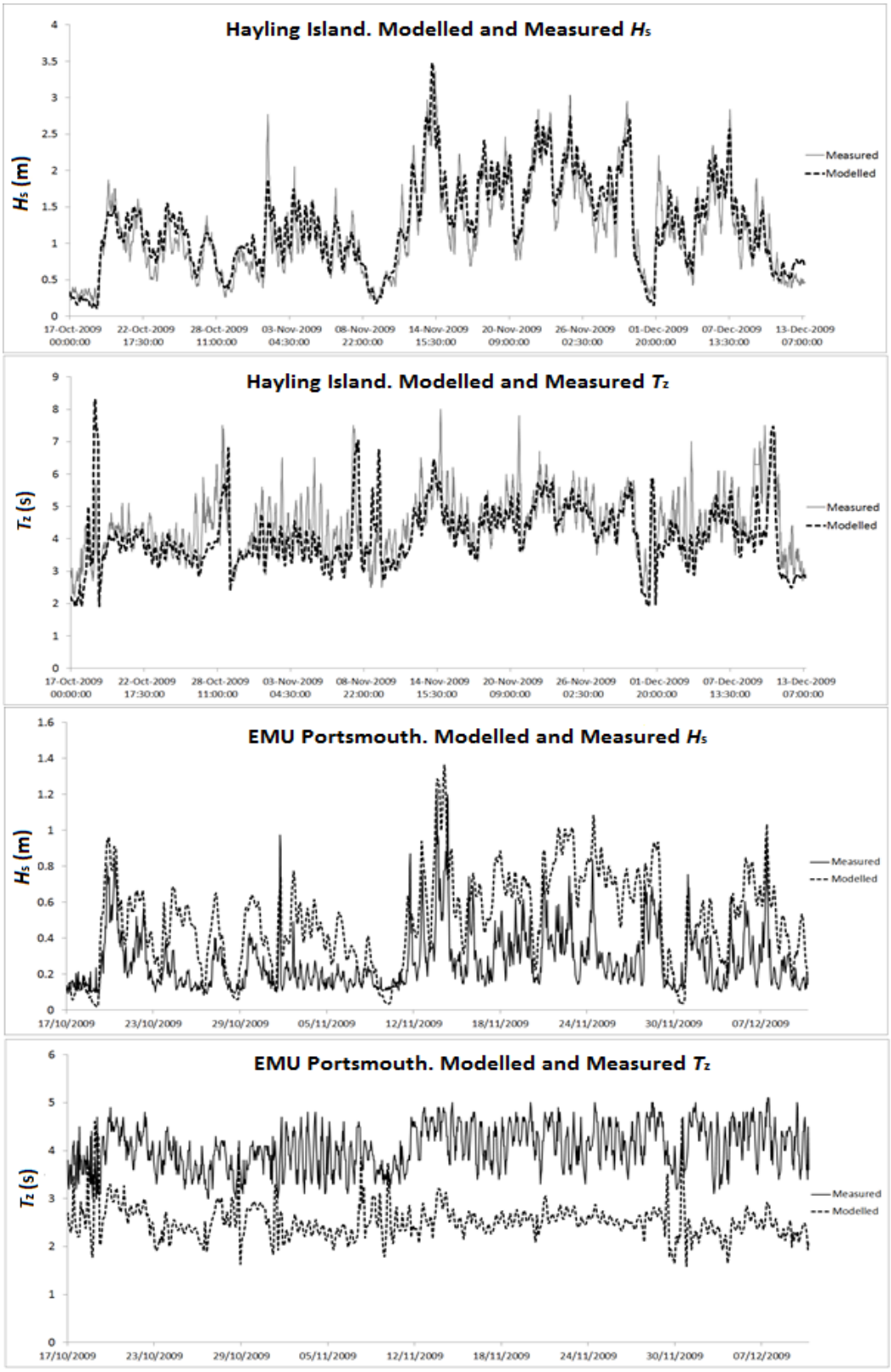

Fig. 5.3. Modelled and measured H_s and T_z at Hayling Island (top) and EMU Portsmouth (bottom).

5.5.2. The influence of the HD model upon the wave hindcast

5.5.2.1. The removal of the surface elevation data

The influence of the water level elevation upon the prediction from the SW model is given in Table 5.2.

Table 5.2. Differences in wave states between the normal hindcast and that without water level elevation datasets. Average values for both events are shown. '( )' indicate error as a percentage of the original prediction, while '| |' indicates the average absolute Pbias.

Previmer Water Levels / Water levels excluded					
	H_s (m)			T_z (s)	
Location	RMSE (m)	Pbias (%)	Change to H_s peak (m)	RMSE (s)	Pbias (%)
Bramble	0.08	4.95	0.12 (1.9)	0.14	<1
Channel Vessel	0.1	<1	0.1 (1.4)	0.1	<1
Emu Hayling	0.14	3.15	0.42 (16.3)	0.32	<1
Emu Nab	0.1	1.15	0.24 (5.53)	0.11	<1
Emu Portsmouth	0.07	1.38	0.17 (10.63)	0.3	-1.76
Hayling Island	0.12	1.62	0.35 (9.90)	0.39	<1
Lymington	0.12	8.15	0.12 (10.45)	0.65	1.14
Milford	0.14	1.55	0.24 (7.21)	0.5	3.67
Poole Bay	0.11	<1	0.12 (2.5)	0.24	<1
Sandown	0.08	<1	0.11 (3)	0.54	5.36
Southampton	0.04	<1	0.09 (13.8)	0.01	<1
Average	0.1	1.94 |2.15|	0.19 (7.51)	0.3	<1 |1.3|

Domain average RMSE was 0.1 m and 0.3 s for H_s and T_z, respectively, while average Pbias was less than 3% in both when contrasting model hindcasts without water level input against those obtained including water level elevation datasets. The largest average change to the H_s event peak (0.42 m) occurred at the EMU Hayling Buoy equating to 16.3% of the incident height. Local variability within the alteration to the H_s event peak ranged from 16.3% to 1.4%.

The relative contribution of the water level change and the inclusion of currents contained a high degree of local variability (Fig. 5.4). In the deepest regions (e.g., the Channel Light Vessel or EMU Nab) most of the change to the model hindcast was contributed by the removal of the currents. However, in the shallower, nearshore regions, the hindcast was also sensitive to water level fluctuations. The largest changes to H_s and T_z occurred within regions where sensitivity to water level fluctuations was

present. Sensitivity to the water level datasets was temporally variable. Alteration to the model hindcast was often largest when the H_s was at its peak.

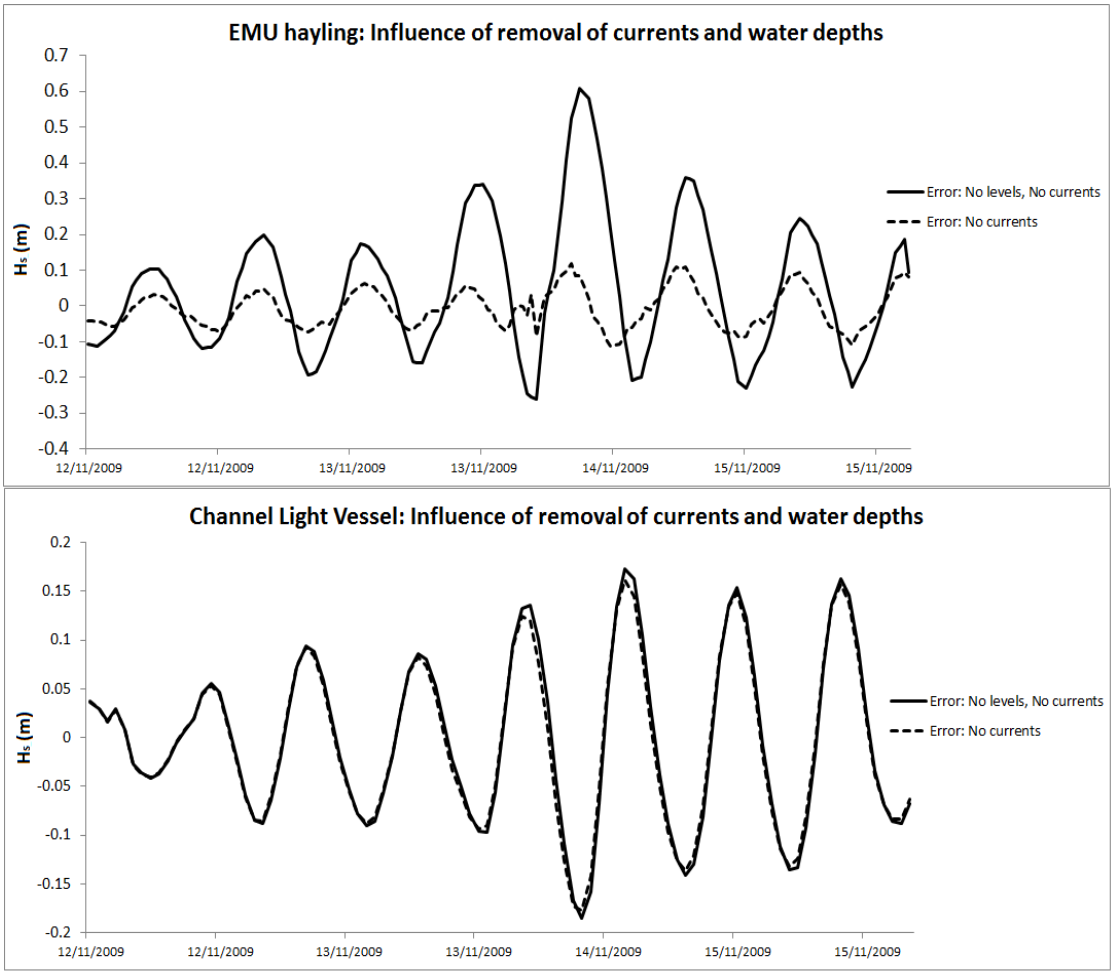

Fig. 5.4. Comparison of relative influence of current and water depths upon the H_s hindcast at EMU Hayling Island and Channel Light Vessel during the November 2009 event. "Error" refers to the change induced in the model hindcast by excluding a particular input variable (or variables) relative to that obtained when the variable was included.

5.5.2.2. Sensitivity of the model to uncertainty in the predicted tide

The effect of increasing water level elevation amplitudes by up to 30% during the wave hindcasts is given in Table 5.3.

The domain average RMSE for the two events was 0.02 m and 0.06 s when comparing the two predictions of H_s and T_z, respectively. Pbias never exceeded 2% in the predictions of either H_s or T_z. On average, the increase in water level elevations increased the peak wave height by 0.03 m. Spatial variability was observed in the results. For example, at Southampton the peak wave heights were increased by only 0.01 m, whereas at the EMU Hayling Buoy differences of 0.07 m were observed. The

domain average peak error (as a percentage of the 'normal' prediction) was 1.66%. The largest normalised difference to peak H_s was found at the Emu Hayling Buoy during the 14th November 2009 event, where the alteration in the surface elevation led to a 6% change in amplitude.

Table 5.3. Influence of increasing the water level elevation dataset upon the prediction of wave state. Errors refer to differences in the prediction from those given by the model hindcast in experiment A.

Previmer Water Levels / 30% increase to water level elevations					
	H_s (m)			T_z (s)	
Location	RMSE(m)	Pbias (%)	Change to H_s peak (m)	RMSE (s)	Pbias (%)
Bramble	0.01	<1	0.02 (<1)	0.03	<1
Channel Vessel	0.01	<1	0.01 (<1)	0.02	<1
Emu Hayling	0.03	<1	0.07 (2.6)	0.14	<1
Emu Nab	0.01	<1	0.03 (1.03)	0.03	<1
Emu Portsmouth	0.02	<1	0.03 (1.83)	0.04	<1
Hayling Island	0.02	<1	0.05 (1.61)	0.05	<1
Lymington	0.02	-1.28	0.04 (4.1)	0.13	<1
Milford	0.03	<1	0.06 (2.1)	0.05	-1.13
Poole Bay	0.02	<1	0.01 (<1)	0.04	<1
Sandown	0.02	<1	0.04 (<1)	0.13	<1
Southampton	0.01	<1	0.01 (1.51)	0	<1
Average	0.02	<1	0.03 (1.66)	0.06	<1

5.5.3. Contribution of the wave signal to the predicted surge

Table 5.4 gives the average peak difference between the prediction of the surge with and without the influence of the waves, during the two events.

The results indicate that the largest alterations to the predicted surge coincided with the period of greatest wave activity (the peak in the H_s conditions). The average maximum change upon the surge prediction during the two events, across the *in-situ* measurement sites was 0.03 m. Spatial variability was observed in the results, with the largest absolute differences and normalised differences, shown in the eastern Solent region. At the Emu Hayling Buoy the largest sensitivity was found, with an average peak difference of 0.05 m, corresponding to 6.9% of the 'without waves' peak surge. The influence of the waves upon the surge was largest during the 10th March 2008 event, during which the maximum change to the predicted surge height, of 9.2%,

occurred at the Emu Hayling Buoy. However, during both events, the change to the predicted skew-surge was smaller, with no change greater than 5% found at any of the gauged sites.

Table 5.4. Influence of the wave stresses upon the predicted surge. Differences relate to the average during the two events on the 14th November 2009 and the 10th March 2008 between the predictions of surge with and without the influence of the waves.

Surge with presence of waves / Surge where wave are excluded		
	RMSE (m)	Change (%)
Bramble	0.02	1.72
Emu Hayling	0.05	6.9
Emu Nab	0.01	2.08
Emu Portsmouth	0.03	3.3
Hayling Island	0.02	2.26
Lymington	0.02	2.65
Milford	0.02	1.79
Poole Bay	0.01	1.89
Sandown	0.04	6.3
Southampton	0.03	2.1
Average	0.03	3.88

Fig. 5.5 gives the maximum change to the predicted surge elevations throughout the model domain during the 14th November 2009 event. The greatest influence of the waves occurred along the south west coast of the Isle of Wight, where differences between the predicted surge elevations were as large as 0.11 m (17%).

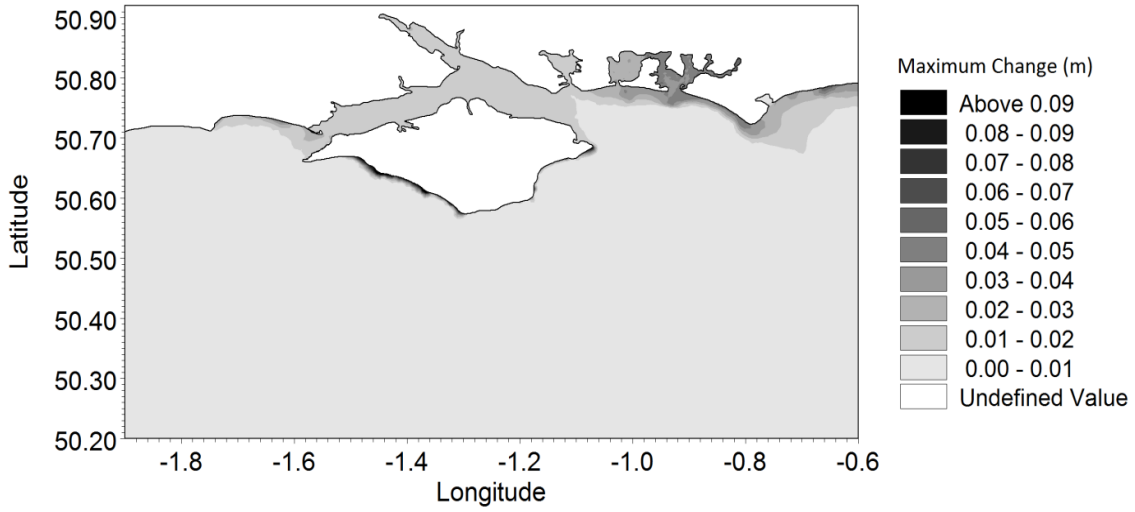

Fig. 5.5. Maximum change to predicted surge elevations during the November 2009 event between predictions made with and without the influence of the wave signal.

5.6. Discussion

A regional coupled spectral wave-hydrodynamic model, using the MIKE-21 software and data from the Previmer system, was described and applied to the Solent-Southampton Water estuarine system. To assess the accuracy of the wave predictions, a three month hindcast was undertaken using operational data outputs from Previmer. Model predictions were contrasted with wave states from *in-situ* measurements.

The regional model hindcasts were able to provide predictions of H_s and T_z with domain average RMSE of 0.32 m and 0.81 s, respectively. Pbias and normalised RMSE statistics indicated that the model performed more accurately at sites located in deeper waters (greater than 10 m). In the shallower, nearshore regions, particularly Lymington and the EMU Portsmouth buoys, H_s Pbias was greater than 50%. At all *in-situ* gauge sites considered, the Pbias indicated that the regional model over-predicted wave heights. As H_s over-prediction was present throughout the domain, it is likely to be due to uncertainty in the wind datasets used to force the model, which also consistently over-predicted wind speeds when contrasted with *in-situ* measurements in subsequent analysis. It has been well established that wind forcing is the most significant energy input into surface waves (Knauss 1996).

In depths greater than 10 m, such as EMU Nab Tower, Poole Bay and Hayling Island, the average normalised RMSE was 20% and 21% for H_s and T_z, respectively. These errors were comparable with those expected from operational systems. Bidlot *et al*. (2007) compared a variety of operational forecasting systems and found that the Met Office, Service Hydrographique et Océanographique de la Marine (SHOM) and ECMWF system predictions of H_s produced RMSEs of between 0.25 and 0.4 m. Where the RMSE was normalised by the average size of the incident, the H_s and T_z error was found to be approximately 20% within the systems. Similarly NOAA online assessments of their system (http://polar.ncep.noaa.gov/waves/valid_wna.html) demonstrate normalised RMSE errors of 25%, while Bradbury *et al*. (2004) analysed the Met Office UK Waters model through the English Channel and found normalised T_z and H_s RMSEs of 20%. Recent research by Palmer (2011) found that model predictions well represented buoy measurements of H_s (with an average RMSE of 0.3 m), while T_z predictions contained significant errors (e.g. more than 1 second at Hayling Island) when simulating through the English Channel during a 4 week period in November 2005. The larger errors found in the very nearshore sites are difficult to contrast with operational systems as many reports, for example, Bidlot *et al*. (2007) contrasted forecasting systems in deeper offshore sites only. Similarly, Bradbury *et al*. (2004) did not utilise *in-situ* measurements in nearshore areas, such as Lymington, due to the complex bathymetry and an insufficiently fine model spatial resolution to provide a reasonable comparison.

Previous research has described a tendency of wave models to over-predict H_s, while under-predicting T_z, due to an over-prediction of the high frequency energy, particularly in shallow, short fetch areas (Ris *et al.*, 1999; Rogers *et al.*, 2002). Brown and Wolf (2009) highlight that forecasts from a coupled tide-surge-wave model had lower accuracies in water depths of 5 m or less. An assessment by Moeini and Etemad-Shahidi (2007) found SI errors of up to 20%, in both H_s and T_z, when hindcasting with SWAN (Simulating WAves Nearshore) and MIKE-21 SW models in an enclosed basin, despite using measured wind conditions. Brown *et al.* (2011) contrasted the prediction accuracy of coupled hydrodynamic and wave models in the Irish Sea region, also finding that errors were greater in shallow regions (approximately 10 m in depth) relative to those obtained at offshore (between 20 and 30 m) sites. To reduce model H_s within such regions Wolf *et al.* (2002) altered local bottom friction coefficients while Lin *et al.* (2002) adjusted local surface drag coefficients. Research by Johnson and Kofoed-Hansen (2000) has also indicated that the formulations used in MIKE-21 SW in shallow water conditions may be innacurate due to an overestimation of the sea surface roughness where Jannsen's (1989, 1991) formulation is used (as in MIKE-21 SW).

Additional analysis, not presented, considered the wave model sensitivity to several model parameters with the aim of increasing the accuracy of H_s hindcasts in the shallow, nearshore regions. Alterations to the C_{dis} (linked to whitecapping) and γ (linked to wave breaking) parameters, as well as local bathymetry depths, were all capable of reducing model H_s in the nearshore regions. However, alteration to both C_{dis} and γ coefficients also significantly reduced H_s in deep regions, leading to increased errors. The influence of the alteration of the bathymetric dataset, however, was shown to be localised to the nearshore regions. This enabled H_s to be reduced in the nearshore without significant changes in the deeper water regions. At Lymington, alteration of the bathymetry reduced the H_s RMSE from 0.17 m to 0.09 m. Using the regional model, the influence of the modelled surface elevations upon the predicted wave state was assessed during the storm events from 10th March 2008 and 14th November 2009. Contrasting the predicted wave states, with and without the surface elevation influence, the sensitivity was shown to be greatest in the shallow, nearshore regions where both the currents and the change to water levels influenced the model hindcast. Where water levels increased, so too did the H_s and T_z. This corresponds with previous research by Chini *et al.* (2010) and Wolf (2009) who found that the inclusion of tide-surge data was important in the accurate prediction of H_s, as increased depths enabled waves to break later, resulting in larger wave heights in shallow regions. Alternatively, where water level fluctuations reduced depths, H_s and T_z were reduced. This corresponds with previous research concerning waves interacting with the sea bed. In such instances, linear and non-linear bottom dissipation mechanisms such as

percolation, bed motion, shear stress and scattering reduce the energy within the wave (Luo and Monbaliu, 1994; Padilla-Hernandez and Monbaliu, 2001; WISE group, 2002).

Sensitivity was also conditioned by the size of the incident waves, as both depth and wave heights determine the degree to which the wave interacts with the sea bed. This is particularly important within the context of coastal flooding as it indicates that the greatest sensitivity to uncertainty within the input data will occur during extreme events, which are the events one would wish to model with the highest degree of accuracy. Previous research within the Southern North Sea (Tolman, 1991), and the English Channel and Irish Sea regions (Wu *et al*. 1994), also found that the inclusion of tides and currents had a relatively small influence upon mean wave parameters. However, the effects were highly localised. The largest impacts were found in shallow regions, during storm peaks, in which changes of 10% were generally found. These findings correspond with the 9.17% average change to the H_s event peak at the Emu Hayling Buoy and the local variability demonstrated presented in this research. Palmer (2011) indicated that the influence of tidal fluctuations was of particular importance in the eastern Solent region where wave focussing due to refraction in the English Channel occurred.

Using the two events, the uncertainty in the predicted wave state, as a result of 'expected' uncertainty in the predicted surface elevations, was investigated. The hydrodynamic model was shown, in previous research, to contain errors in the predicted surface elevations by as much as 30%. Sensitivity of the regional wave model to these errors was relatively small, with domain average RMSEs in the H_s and T_z of only 0.02 m and 0.06 s, respectively, while Pbias errors were commonly less than 1% in both. The largest average change of peak H_s, during the two events, occurred at the Emu Hayling Buoy (0.07 m), while the largest normalised influence was shown to occur at Lymington (4.1%). Although variability between events was present, the largest normalised difference in peak H_s during either event did not exceed 6% at any of the gauged sites. The results indicate that across the gauges considered, the uncertainty in the water level predictions was not an important influence upon the wave predictions in general, except in the eastern Solent, where vulnerability to extreme wave conditions was greatest.

Quantifying the error in the hydrodynamic predictions, and the uncertainty these errors propagate to the wave model, has been shown to be particularly useful in identifying the regions where improved tidal predictions could increase wave prediction accuracies. The research presented here indicates that the importance of tidal uncertainty upon the predicted waves will be dependent upon the size of the waves and the water depth, with the greatest sensitivity found in nearshore regions, under the influence of large storm waves (when the greatest certainty is usually desired). In this research, the eastern Solent was found to be the most likely to benefit from increasing the accuracy of tidal predictions. As previous research has indicated

that tidal predictions from hydrodynamic models are generally considered to become increasingly uncertain in complex nearshore regions (Flowerdew *et al.*, 2007), these findings may be useful in such regions as an indication of the levels of uncertainty one might expect to find due to 'expected' tidal errors, particularly in shallow water regions experiencing relatively low wave energy events, such as the Solent. Depending on the vulnerability of a particular region, uncertainties on such scales may be an important consideration that would require more accurate HD model predictions.

The influence of the wave field on the prediction of the surge was also assessed by comparing surge predictions with and without the predicted wave field datasets. The results indicated that a high degree of spatial variability was present in the sensitivity of the hydrodynamic model to the influence of waves, with the largest changes to the surge peaks found at the gauges located in the eastern Solent and along the south west coast of the Isle of Wight, coinciding with the most extreme wave conditions. During the event on the 10th March 2008, the inclusion of the wave field led to an increase in predicted peak surge heights of up to 9.2% at the Emu Hayling Buoy.

Previous research has also indicated that coupling of wave and hydrodynamic models can significantly alter the height of modelled surge elevations and currents (Wolf, 2009). Kim *et al*. (2010) found that extreme typhoon-induced surge events could not be modelled without the inclusion of wave radiation stresses which accounted for up to 40% of the surge elevation. The conditions of this particular event were extreme, with wave heights exceeding 18 m. Choi *et al*. (2003), Funakoshi *et al*. (2008) Xie *et al*. (2008) reported changes to surge predictions of between 10 – 15% due to model coupling. In each case, the authors note that the influence of the waves upon the surge displayed high degrees of spatial variability. Mastenbroek *et al*. (1993) found both spatial and temporal variability in the change to the predicted surge, while Wolf (2008) found that wave set-up magnitude was dependent upon water depth and bottom slope. When considering three independent events, they found that in two of them the effect of the wave model was negligible, while in the third the increase to predicted surge heights was in the region of 5%. These results from previous studies fit well with the sensitivity of the Solent-Southampton Water regional model to wave-hydrodynamic coupling presented. The spatial variability in the model sensitivity, correlating to the magnitude of the waves, as well as the 9.2% – 17% increase of peak surge heights at the Emu Hayling Buoy and along the south west coast of the Isle of Wight, are particularly similar to those results given by Choi *et al*. (2003) under similar wave and surge conditions (e.g. H_s heights of 2.5–6 m and surge elevations of 1.5–2 m) and research by Wolf (2008) in Liverpool Bay. The results of this research, therefore, support previous studies, indicating that the inclusion of the wave field is an important component of a storm-surge prediction system, even in the Solent, where wave energy is relatively low due to the sheltering effects of the Isle of Wight. These findings will be

of interest to coastal managers, aiding in the quantification of the magnitude and spatial variability in the expected contribution of the inclusion of waves upon the prediction of large surge events, which are often of most interest.

Further research could validate the findings within the region and provide more widely applicable results. This research considered the coupling of the wave and hydrodynamic models during just two events. Tidal uncertainties were considered only in terms of 100% and 30% amplitude errors, while no assessment of the influence of phase shifts in the tidal signal were considered. Similarly, the influence of the waves upon the surge was considered only during the same two events. Although this analysis provided a useful assessment of the signal interactions and the conditions during which the coupling would be of greatest significance, during periods of particular interest to coastal managers, in both instances, future research could extend the analysis presented here to provide a more holistic assessment of the signal interactions. For instance, Monte Carlo techniques could be used to quantify the influence of one signal upon the other, given a distribution for each parameter (e.g. tidal uncertainty, wave height and period) given increased computational resources. By doing so one could validate the findings from the events already considered, or find instances where the influences revealed in this research are not representative. It might also be particularly useful in constructing relationships between the signals that can be applied easily to other regions, of a variety of conditions, such as those in which considerably larger wave conditions are found.

5.7. Conclusion

A regional model of the Solent-Southampton Water estuarine system was used to examine the importance of HD-SW coupling in a complex coastal region containing a variety of tidal characteristics, water depths, and wave conditions. The research revealed that:

- The wave model accuracies lay within the range reported for operational forecasting systems, in previous research, at most of the *in-situ* sites considered. Accuracy, relative to the size of the event, decreased in some of the shallowest regions, indicating a requirement for high resolution bathymetric and accurate local wind datasets, and may also indicate uncertainties in current wave model formulations, when considered in the light of other research using 3rd generation models in similar conditions.
- The influence of the HD-SW coupling to the model predictions was shown to be spatially variable, with the greatest influence found in the nearshore areas of the east Solent, where wave energy was greatest. The presence of the waves

increased surge peaks by up to 9.2 % while the variable water depths from the HD model resulted in an alteration to peak H_s by up to 16.3 %.

- The modelled wave field was insensitive to the expected errors in the tidal elevations throughout most of the region, with the maximum change to peak H_s (6 %) found in the eastern Solent.

These findings indicate that the coupling of HD and SW models can be essential, particularly during storm events where wave energy is greatest (often the most important in terms of flood forecasting) and in shallow water regions where wave energy is greatly influenced by changes in water depth. Despite the importance of model coupling, the uncertainty in the HD tidal predictions (Chapter 4) was not a significant constraint to the wave model accuracy throughout much of the region, indicating that the majority of the errors in the model predictions are likely to be attributed to uncertainties in other forcing datasets used or formulations in current 3rd generation wave models. These results provide a useful insight into the spatial variation in tide-wave interactions that can be expected in coastal environments, and demonstrate the suitability of commonly utilised models in such regions, which will be of interest to coastal managers in a variety of coastal regions.

Chapter 6: Modelling Waves and Water levels in the Solent and Surrounding Waters: Assessment of an Empirical-Based Approach

Abstract

A regional model, transforming mid-Channel wave and surge conditions through the Solent-Southampton Water estuarine system, using a multiple regression-based approach is described in this research. During a three month prediction from October to December 2009, the regression model was shown to provide similar accuracies to those obtained from a regional model defined using the physically-based numerical software MIKE-21. Both approaches provided an average RMSE of 0.1 m in the surge, while the RMSE in the H_s was 0.21 m and 0.25 m in the regression and MIKE-21 predictions, respectively. During extreme events the regression model tended to under-predict the magnitudes of both surge and wave peaks to a greater degree than the MIKE-21 model. Average error in the prediction of the surge peaks was 0.12 m and 0.14 m in the MIKE-21 and regression predictions, while errors of 0.19 m and 0.39 m were found in the wave predictions, respectively. Divergence between the model predictions of peak water levels was less than that shown between the peak surge elevations, due in part to the tendency for the surge to avoid the high tide periods. The regression model was highly computationally efficient relative to the MIKE-21 model, enabling the production of a 2000 member ensemble, at approximately 20,000 mesh points, for 280 time steps, in less than 40 minutes. A demonstration probabilistic model prediction, using a Monte Carlo approach was described, with data assimilation used to update independent variable states every hour, using a Kalman filter. The research clearly indicates the benefits to coastal managers of using a probabilistic approach for quantifying uncertainty and the Kalman filter for constraining it. The benefits of the data assimilation were most significant in short-term forecasts (up to six hours) after which the predictions demonstrated no significant benefits in terms of accuracy. Inaccuracies in the ensemble distributions were found due to the uncertainty in defining the error in the independent variables. It is thought that the use of ensemble forecasts provided by the Met Office could significantly increase the accuracy of the ensemble in the regional model. This research will be of interest to a wide range of modellers interested in the switch from deterministic to probabilistic forecasts, particularly those in regions where computational resources are low and suitable low-costs alternatives are sought.

6.1. Introduction

Coastal flooding is a serious threat to communities throughout the world. The risk of flooding increases where large surge and wave events coincide with a high spring tide, resulting in sea levels exceeding above coastal protection structures. It is well established that coastal flooding events result in financial loss and human fatalities. Globally, 200 million people live on floodplains, while two million km^2 and one trillion dollars' worth of assets lie less than 1 m elevation above the current sea level (Stern, 2007).

In the UK coastal flooding is estimated to put 5 million people and 1.85 million homes at risk (Penning – Rowsell *et al.*, 2006). Historically, there have been several disastrous events; in 1953 when a large surge coincided with high tides in the North S, the ensuing flood killed 307 and 1836 people in the UK and the Netherlands, respectively (Gerritsen, 2005; Wolf and Flather, 2005). Future flood risk will increase due to an increased number of assets in coastal zones (Brown *et al.*, 2010), increased mean sea levels (Hall *et al.*, 2006; Haigh *et al.*, 2009; Haigh *et al.*, 2010) and worsening wave conditions (Bacon and Carter, 1991; Zang and Tooley, 2003; Inter Agency Committee on Marine Science and Technology, 2004; Chini *et al.*, 2010).

To protect against the threat of coastal flooding, forecasting systems have been developed. Within the UK, operational forecasts have been in use since 1953. Present systems utilise complex numerical modelling packages, often combining a set of atmospheric, wave and hydrodynamic modelling systems (e.g. Allard *et al.*, 2008). Commonly used hydrodynamic and spectral wave models include MIKE-21 (Warren and Bach, 1992; www.mikebydhi.com), Wavewatch III (Tolman, 2009) and Simulating Waves Nearshore (SWAN) (Booij *et al.*, 1999). Flather (2000) provided a summary of a variety of operational systems used throughout Europe. Such systems provide forecasts of future ocean state, warning coastal managers when potential flood-causing conditions are likely to occur. These warnings enable coastal managers to prepare, reducing the risk of damage and disruption.

Most operational systems attempt to represent real world physical processes. To do so, sufficiently complex modelling packages must be developed. The operational storm surge model within the UK (Flather, 2000; Williams and Horsburgh, 2006) is required to make predictions of surface elevation across the North East Atlantic at grid resolutions ranging from 35 km to 1.8 km in selected regions. It considers not only calculations relating to the hydrodynamic model, but also the changing state of the wave and atmospheric systems, and their interactions. The number of calculations required within a modelling system can, therefore, be enormous. This presents difficulties when modelling nearshore regions as coarse spatial resolution grids, suitable for largely uniform conditions in the deep sea regions, cannot adequately

represent the highly variable conditions of coastal locations. Furthermore, data assimilation techniques, such as the Kalman filter (Kalman, 1960; Kantha and Clayson, 2000; Kobayashi and Yasuda, 2004; Neal, 2007) have become increasingly utilised (Prandle, 2000; Mclaughlin, 2002) to decrease uncertainty and increase accuracy of forecasts by providing an optimal estimate of the state of the system through the combination of a predicted and measured state, with recognition of the uncertainty in both. Applying a data assimilation scheme, and increasing the spatial resolution of a model domain, through an increase in the number of cells, can significantly increase the computational demand of the modelling system. To account for this, it is common practice for modelling systems to run relatively less demanding, coarse resolution model domains over the deep water regions that provide boundary conditions to high resolution nearshore nested grids. Due to the high spatial resolution and the introduction of numerous additional processes not relevant within deeper water areas (usually referred to as shallow water processes), the nested components can represent a significant proportion of the computational burden in the forecasting system. To enable such modelling systems to exist, extensive computational resources are required. Previmer for instance, utilises the IFREMER computing cluster (wwz.ifremer.fr) which contains 256 compute nodes, each containing two quad core processors, resulting in the availability of 2048 computing cores.

The application of complex numerical models is dependent upon the situation to which they are to be applied. For instance, where computer resources are limited, the computational run time to simulate complex model domains may inhibit its use as a forecasting tool, particularly where high spatial resolutions are required. This is likely to become increasingly important as current research trends in ocean forecasting have focused on the transfer from deterministic to probabilistic modelling strategies (Flowerdew *et al.*, 2007; Bocquet *et al.*, 2009; Davis *et al.*, 2010). To quantify the uncertainty in a forecast, numerous simulations (an ensemble) are required, increasing computational demands. Ironically, Tilburg and Garvine (2004) suggest that often the regions that lack the resources required for such forecasting systems are those that require them the most. Where exhaustive computer resources may not be available computationally inexpensive modelling approaches are preferable.

Empirical methods do not attempt to model any real world processes explicitly as physically-based numerical models do. Instead, a series of independent variables are used to define a function that estimates a dependent variable. Once the function is produced, the model aims to provide a prediction of the dependent variable using an input of independent variables. This uses a fraction of the computational processing time required by physically-based numerical models. In the light of the present desire to move from deterministic to probabilistic modelling, such methods may become increasingly appealing relative to the computationally demanding options used routinely at present.

Aside from the data and computational demand benefits, Kobayashi and Yasuda (2004) suggest that in some instances, such as when modelling very uncertain regions, statistical-based approaches may provide more accurate predictions. This is due to their ability to create a direct cause-effect relationship between the independent and dependent variables, whereas a physical-based numerical model may use formulations or parameters that are not sufficiently certain for those conditions.

A vast array of literature surrounds statistical-based approaches to modelling physical processes. See, for example, Cox *et al*. (2002), Huang *et al*. (2003), Steidley *et al*. (2003), and Prouty (2007) for work relating to artificial neural networks applied to water levels, while Deo and Naidu (1999), Sfetsos (2002), Bazartseren *et al*. (2003), and Kobayashi and Yasuda (2004) provide examples of the use of multiple regression strategies. Kennedy and O'Hagan (2000), Oakley and O'Hagan (2004), O'Hagan (2006), Conti *et al*. (2009), and Conti and O'Hagan (2010) provide examples of the use of emulators, and how they can be utilised in reduced cost sensitivity and uncertainty analysis of complex systems.

This research aimed to assess the accuracy of transforming offshore wave and surge conditions, provided by a shelf-scale, ocean forecasting system, to the nearshore regions of the Solent and Southampton-Water estuarine system using a regression-based modelling approach. The region was selected for a variety of reasons. First, it is a complex system with a highly variable nearshore bathymetry, where uncertainty in physically-based models is relatively high. Previous research by Levasseur (2008) and demonstrated in Chapter 3 for instance noted particularly large errors in predictions of tide, surge and waves in the shallow nearshore areas of the Western Solent where unique tidal patterns including double high water levels are found. There is also a requirement for very fine nearshore meshes, and the presence of a dense *in-situ* measurement system which provides a useful opportunity for the demonstration of the merits of the inclusion of a data assimilation strategy. Prediction accuracy was contrasted with model outputs derived using physically-based numerical modelling software and *in-situ* measurements throughout the region. In addition, the computational demands of the two approaches were contrasted. A simple Monte Carlo-based ensemble, with Kalman filter updating, was used to demonstrate how a computationally efficient approach could enable the generation of a vast ensemble of predictions in a suitable time for operational forecasts looking to develop probabilistic outputs

6.2. Study Site and Data

6.2.1. The Solent

The Solent is a body of water that lies between the south coast of England and the Isle of Wight in the UK (Fig. 6.1). It includes 12 separately defined estuaries and harbours and contains a range of coastal habitats and inter-tidal zones (Fletcher *et al.*, 2007). The region has various stakeholders, protected habitats, a dense coastal population and two of the largest shipping ports in the UK.

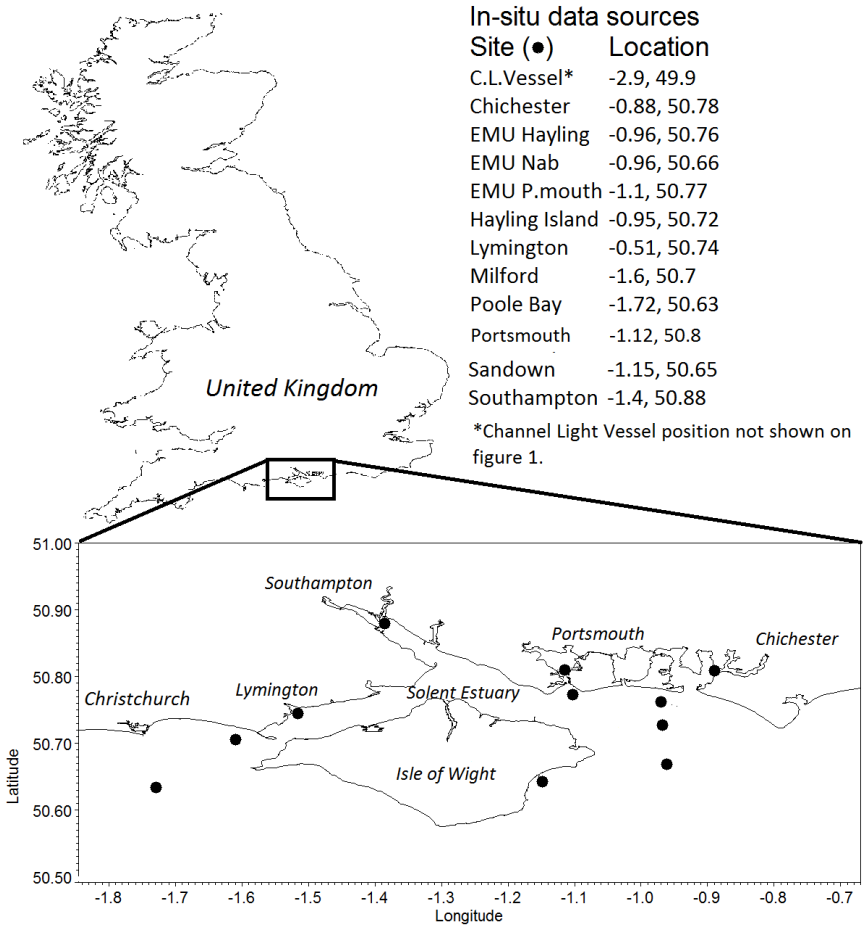

Fig. 6.1. The location of the Solent and *in-situ* data sources.

The Solent region lies in the English Channel, within which the M_2 tide is the dominant tidal component and ranges typical are in the order of 6-10 m. The irregular geometrical shape, narrow channel configuration and shallow depths of the Solent estuary, results in the amplification of shallow water tidal constituents M_4 and M_6 (Levasseur, 2008). Previous studies have also noted that within the central English Channel the M_4 and M_6 over-tides become increasingly important (Pugh, 1987; Wells *et al.*, 2001). Within the Solent these amplifications create a tidal elevation with a double

high water and young flood, most prominent in the Southampton Water region (Rantzen, 1969; Levasseur, 2008). Previous attempts at modelling the tidal hydrodynamics within the region have shown relatively large errors in the Western Solent and Southampton Water regions (Levasseur, 2008).

Storm surges in this region most frequently occur due to low pressure systems from the Atlantic propagating eastwards or as a result of storm surges propagating south from the North Sea (Law, 1975; Haigh *et al*., 2004). During the 1953 event, discussed previously, the surge propagated south from the North Sea increasing in intensity as it moved south into shallow waters of the North Sea. Other notable events to have caused flooding within the region specifically occurred on 14th – 18th December 1989 (Wells *et al*., 2001) and 10th March 2008 (Haigh *et al*., 2010).

The region is generally considered to be sheltered from extreme waves, with long-term average significant wave heights (H_s) of 1.5 m or less (Inter-Agency Committee on Marine Science and Technology, 2004) and mean wave periods (T_z) of typically 6 -10 seconds. The largest waves that occur usually arrive from either 240° due to storm waves and swells from the Atlantic (Dix *et al*., 2007) or occasionally 40-50° (storm waves from the English Channel). The Eastern Solent regions, particularly Hayling Island, and Milford to the West of the Solent, are the most exposed areas within the region of interest. The Channel Coastal Observatory (http://www.channelcoast.org/), the data management and regional coordination centre for the Regional Coastal Monitoring Programmes (see Isle of Wight Council (2005) for a useful overview), considers these regions to have medium exposure to wave influence as large swells and relatively large fetch distances increase the risk of extreme wave events. A review of flood events within the Solent since 1935 can be found in Ruocco *et al*. (2011).

6.2.2. Data

Tidal elevations, surge elevations, wave and wind conditions derived from the Previmer group (http://www.previmer.org/en) were used in this research to force the MIKE-21and regression models. These datasets were outputs from a pre-operational system currently under development which aims to provide users with short-term forecasts of the state of the ocean along French coastlines bordering the English Channel, the Atlantic Ocean, and the Mediterranean Sea. Tide and surge components of the water surface elevation (velocities were not specified) were provided at 5.5 km spatial resolution, and 1 hour temporal resolution throughout the English Channel. These data were model outputs created using the Model for Application at Regional Scale (MARS 2D) system (Lazure and Dumas, 2008). Wave conditions (H_s, T_z, direction and spreading) were provided at 3.5 km spatial and 3 hour temporal resolution from forecasts made using the Wavewatch III model (Tolman, 2009). The Previmer models

utilise modelled wind fields at 3 hour temporal and 4 km spatial resolution provided by the European Centre for Medium Range Weather Forecasts (ECMWF, www.ecmwf.int/about). These wind field datasets were supplied via the Previmer group for this research, while winds and atmospheric pressures from the Sandown CCO site and Channel Light Vessel were used to provide atmospheric conditions when atmospheric data were unavailable. Atmospheric pressure fields were interpolated from measurements provided by the Channel Coastal Observatory. Measurements at seven sites located along the south coast of England, between longitudes of -3.48° and -0.48° were used; Teignmouth, West bay Harbour, Portland Harbour, Swanage, Lymington, Sandown and Arun Platform. Data were available at 10 minute intervals at each site and interpolation was used to provide estimates over the computational domain.

In-situ measurements of water level, wave and wind conditions were given at the sites in Fig. 6.1. Additional data not shown in the figure included surge elevations from two gauges located at Newhaven (-0.05 W, 50.767 N) and Devonport (-4.18 W, 50.37 N), with 15 minute temporal resolutions. Water levels and wave conditions were given at a variety of tide gauge and buoy sites provided online by the National Tidal and Sea Level Facility (at http://pol.ac.uk/ntslf/), the Centre for Environment, Fisheries and Aquaculture Science (www.cefas.defra.giv.co.uk) and the CCO. Further measurements were provided by three temporary buoys provided for this research by EMU (http://www.emulimited.com).

6.3. Model Set Up

6.3.1. MIKE-21

A physically-based numerical model, MIKE-21, was used to hindcast the surge and wave states through the region to provide a baseline methodology against which to compare the regression approach. MIKE-21 is a widely used 2D modelling package designed by the Danish Hydraulic Institute (DHI) group. Among its many users is the FEMA National Flood Insurance Programme which uses both the hydrodynamic and wave modules (FEMA, 2001; Cañizares *et al.*, 2001; Madsen and Jakobsen, 2004; Dix *et al.*, 2007). Further information regarding MIKE-21 modules can be found on the download section of the DHI website at http://www.mikebydhi.com/Download/DocumentsAndTools/ShortDescriptions.aspx.

An unstructured mesh was created for the central English Channel, with boundaries located along the -3.5° and -0.1° lines of longitude, at which tide, surge and wave time-series, provided by Previmer, were applied. Bathymetry data of 100 m resolution, provided by the National Oceanographic Centre, Southampton (http://www.noc.soton.ac.uk), were interpolated to the domain mesh. Sensitivity of the

model to the domain mesh resolution was examined over a series of tide and wave predictions, utilising model mesh designs with increasing spatial resolution in the nearshore regions. Convergence was reached when increases in resolution no longer resulted in a significant RMSE between the tidal or wave predictions at the locations given in Fig. 6.1. Final mesh resolution was approximately 2 km, 150–200 m and 50–100 m in the English Channel, Solent and harbours, respectively.

6.3.2. The Regression model

The regression model was defined using the Matlab stepwise regression function. Regression modelling is one of the most widely used empirical modelling techniques for fitting a quantitative response variable (dependent variable) as a function of one or more predictor variables (independent variables) (Mason *et al.*, 2003). Previous research in which it has been utilised includes Deo and Naidu (1999), Sfetsos (2002), Wu and Hamada (2002), Bazartseren *et al.* (2003), and Kobayashi and Yasuda (2004). Where multiple independent variables are used to represent the system, the dependent variable becomes a linear combination of the independent variables, each associated with an individual unknown parameter β. This can be represented by

$$Y = \beta_0 + \beta_{s_1} * Y_{i_1} + \beta_{s_2} * Y_{i_2} + \cdots + \beta_{s_n} * Y_{i_n} \quad (6.1)$$

Where Y is the dependent variable, Y_i is an independent variable, β_0 is a constant, and β_s is a parameter termed the slope of variable Y_i, $n = 1$ to the number of independent variables.

Wu and Hamada (2002) highlight that the selection of relevant independent variables is a vital part of the regression model development process. To account for this the regression function within Matlab utilises a stepwise selection process to remove independent variables whose influence does not exceed a predefined threshold.

The regression function provided predictions of ocean states at the permanent gauge locations, using the *in-situ* measurements as the dependent variables. The independent variables consisted of atmospheric forcing (wind speed, direction and atmospheric pressures), tidal elevations at the point of interest (derived from harmonic analysis) and the state of the ocean (H_s, T_z and surge) at the open boundaries. The ocean can be viewed as a dynamic system. Therefore a regression function should acknowledge that the state of the dependent variable will be a function not only of the state of the independent variables at a specific given time, but also of the state of the system previously (Conti and O'Hagan, 2010). To help account for this, the dependent variables at a given time step were represented by the sum (or 'build up') of the previous five hours of data for that variable.

Data used for training the regression functions, consisting of time-series of 24 months in length, varied between the models. For the surge regression, data for the

independent and dependent variables was provided at four sites; Portsmouth, Southampton, Lymington and Sandown. Data were used for the wave regression from five locations; Lymington, Sandown, Milford Haven, Poole Bay and Hayling Island..

An advantage of mesh-based numerical models is the ability to make predictions over extensive domains. This can be particularly important when coupling ocean and inundation models, where predictions of ocean states are required at specified intervals along the coast. To provide a prediction surface, a 'secondary' regression was created to spread the hindcasts at gauged locations to un-gauged sites. As *in-situ* measurements cannot be available at all locations, the spread was defined by the MIKE-21 model. The MIKE-21 model was used to hindcast the October - December 2009 period. Time-series data were then extracted from the elements corresponding to the locations of the permanent gauges and each of the nodes in the domain mesh. The time-series from the permanent gauges were used as independent variables, while the data from the remaining mesh nodes represented the dependent variables, and a regression function for each of the un-gauged nodes was constructed.

6.3.3. The ensemble regression model

Regression functions defined in 6.3.2 were used to create probabilistic model outputs by generating large ensembles that sampled from pre-defined uncertainty distributions relating to the errors in the winds, tidal elevations and boundary input datasets, relative to *in-situ* measurements. When simulating the ensembles, each time step prediction used the original input data with a random perturbation to its value drawn from the relevant distribution. In the method used in this research, each time step was independent of all others, while the direction and size of the perturbations were also independent. In order to determine an optimum group size, ensembles of increasing sizes were generated. Each ensemble was run 10 times and the resulting means contrasted to define a convergence point. In addition, the time taken to complete the computations was recorded.

6.3.4. The Kalman filter

The Kalman filter (Kalman, 1960) provides an unbiased estimate of the current state of a system with minimum error variance (Kantha and Clayson, 2000). It is described as an optimal linear predictor, accounting for the state of the predicted variable of interest, the measurement of it, and the uncertainty in both (Maybeck, 1979). This research utilised the 'analysis' step of the Kalman filter to update the independent variables, using the Kalman Gain, which weights the observed and predicted values based on their relative uncertainties. In this way, the Kalman filter provides a best estimate of the current state of the system by

$$X_a = X_f + K\left(X_o X_f\right) \tag{6.2}$$

Where X_a is the analysed state, X_f is the forecasted state, K is the Kalman Gain, and X_o is the observed state. The Kalman Gain is given as

$$K = \frac{V_f}{V_f + V_o} \tag{6.3}$$

Where V_f is the variance in the forecast and V_o is the variance in the measurement. The variance of the analysed state can then be estimated by

$$V_a = V_f - KV_f \tag{6.4}$$

6.4. Analysis

Three groups of experiments were used to meet the aims given in the introduction. The first assessed the accuracy of the surge and wave regression model predictions. Each month of available data was removed systematically and used to validate the wave and surge regression models, defined using the remaining data points. Four sites were modelled for surge (Portsmouth, Sandown, Southampton and Lymington) while five locations were considered for waves (Lymington, Sandown, Milford Haven, Poole Bay and Hayling Island). The RMSE and Pbias (a measure of bias relative to the average size of the factor considered, after Brown *et al.*, 2010) were used to define the accuracy of the predictions.

The second set of experiments contrasted the regression and MIKE-21 hindcasts, during a three month period between October and December 2009, at the nine locations (four surge and five wave) given above, as well as at the three temporary EMU buoys. Further comparisons were made during a series of the largest events extracted from the available time-series. The comparisons of the surge predictions considered eight events exceeding 0.6 m at the Portsmouth tide gauge, with the errors given as the difference between the measured peak surge and the predicted peak surge. The surge from the MIKE-21 model was defined as the difference between two simulations; one forced with only tidal boundary elevation datasets, the second forced with tide and surge boundaries and atmospheric forcing datasets. The Hayling Island site was used to contrast the two models' abilities to recreate storm wave conditions during eight events in which H_s exceeded 2.6 m.

The third set of experiments attempted to provide a probabilistic model output whereby a distribution of predictions was provided at each time step that accounted for the uncertainty within the independent variables. First, the uncertainty distributions in the independent variables were examined. The upper and lower bounds of the distributions were given, based on the 95% error bounds between the Previmer

products and *in-situ* measurements, between October and December 2009, when considering wind conditions and boundary forcing. Boundary surge errors were derived from comparisons between Previmer model outputs and measurements at two tide gauges located near to the domain boundaries; Newhaven in the east and Devonport in the west. Wave H_s and T_z boundary errors were obtained by contrasting Previmer outputs with measurements at the Channel Light Vessel, while error in wind speed data was given as the average of the differences between the Previmer winds and those measured at Lymington, Chichester harbour and Sandown Pier. Tidal uncertainty was given as 0.1 m in line with previous literature discussing uncertainties in the separation of tide and surge from water level measurements (Horsburgh and Wilson, 2007; Bocquet *et al.*, 2009).

Using the designated distributions, the 2000 member ensemble was generated at the four surge and five wave gauged sites, as outlined in Section 5.3.3. The ensemble's prediction accuracy was assessed by considering the ensemble mean Pbias and RMSE (relative to the measured time-series), comparing the average RMSE in the prediction accuracy against the average RMSE in the ensemble spread (used as an indicator of the suitability of the size of the spread), and the proportion of the measured time-series contained within the ensemble boundaries. Rank histogram plots (Hamill, 2001) were also used to investigate the quality of the ensemble distributions, where a flat histogram indicates a correct average spread, a disproportionally high count at the extremes indicates an ensemble spread that is too small, and a disproportionally high count in the central bins indicates an ensemble spread that is too large.

An exemplar event was created, using the H_s ensemble regression function and implementing a Kalman filter update. A simulation of 20 hours was run, representing the 'measured' event. The independent variables were then perturbed using values extracted randomly from the negative half of the uncertainty distributions used to define the ensembles. A 12 hour ensemble forecast was conducted from each time step sequentially. For each forecast, it was assumed that measurements would be available at the given time and for all time steps leading up to it. The states of the independent variables at T_0 and earlier, therefore, were updated (along with their uncertainties) using the Kalman filter. The accuracies of the measurement devices were given by suppliers in terms of percentage of the measured values. Measured wave state and wind uncertainty was estimated as 0.5% and 1% of the variable value in each case, respectively. To provide a similar measure of uncertainty, the input data from Previmer for the wave states and wind conditions were contrasted with *in-situ* measurements to provide a RMSE, which was then given as a percentage of the average incident value. This percentage could then be used at each time step to estimate the uncertainty in the predicted independent variable. A diagram outlining the steps in the production of the ensemble prediction and the Kalman filter updating schemes is given in Fig. 5.2.

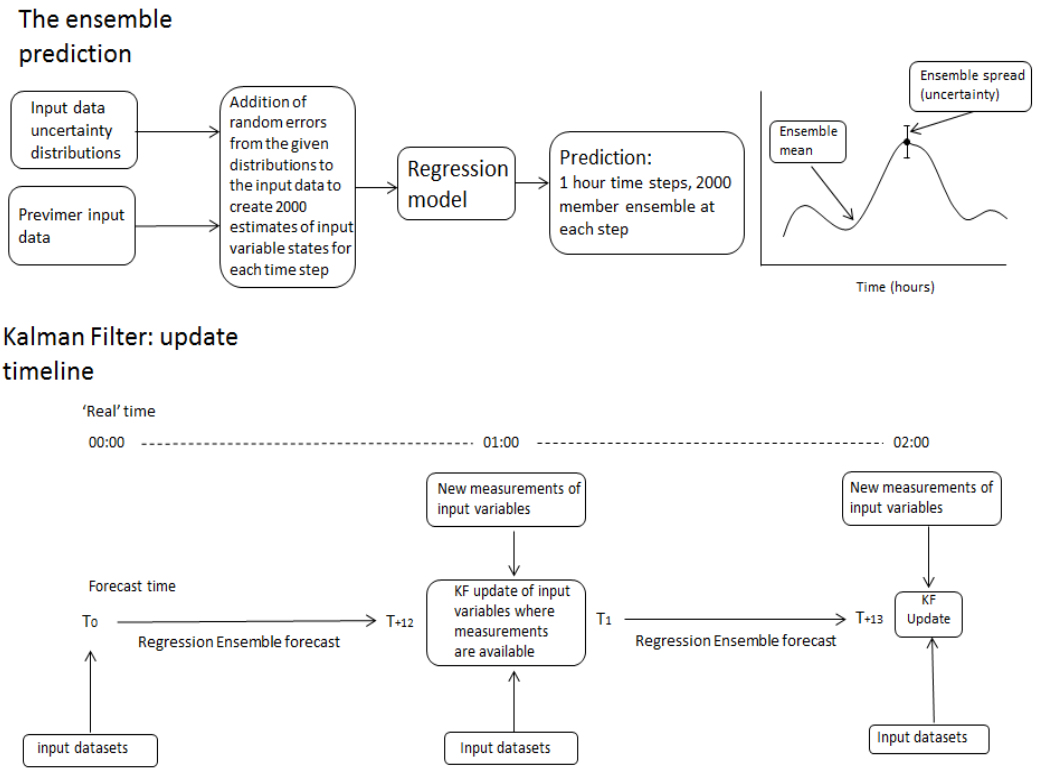

Fig. 6.2. Schemes for the ensemble predictions (top) and the addition of a data assimilation step (bottom).

6.5. Results

6.5.1. Accuracy of the regression predictions

The accuracy of the surge predictions at the four tide gauges and the wave predictions at five gauges are presented in Table 6.1.

6.5.1.1. Surge

Domain average RMSE over all months was 0.08 m. Variance throughout the domain was small, with the average RMSE across all sites lying within 0.01 m of the domain average. Normalising the RMSE by the average surge magnitude indicated that the average error for all sites lay within 10% of the domain average. No significant directional bias was found at any site, while, when direction was ignored, average Pbias was no greater than 17% at any site. Temporal variability was present, with the largest RMSE occurring during the winter periods at all sites. However, when the RMSE was normalised this trend was no longer present. At all sites the average deviation from the mean RMSE and the mean normalised RMSE over the two year period was no greater than 0.02 m and 15%, respectively.

6.5.1.2. Waves

Domain average RMSE for all months was 0.15 m and 0.61 s for H_s and T_z, respectively. Average Pbias at all sites was less than 10% in both. Spatial variability was relatively low when considering the normalised errors, with the average errors for all sites lying within 8% of the domain averages for both H_s and T_z. Winter months contained the largest RMSE in both instances. However, when normalised values were considered the variability between the months was reduced. On average, monthly normalised RMSE values lay within 6% and 5% of the two year mean RMSE for H_s and T_z, respectively.

Table 6.1. Surge and wave regression accuracies. Values represent average values from all predicted months. Brackets indicate the normalised RMSE relative to the average measured magnitude and '||' indicates the average absolute Pbias.

		Hayling	Lymington	Milford	Poole Bay	Portsmouth	Sandown	Southampton	Average
Surge	RMSE (m)	-	0.09	-	-	0.08	0.07	0.09	0.08 (73.8%)
	Pbias (%)	-	-0.35	-	-	-0.65	-1.16	-1.3	-0.86 |13.8|
H_s	RMSE (m)	0.17	0.04	0.16	0.22	-	0.15	-	0.15 (31.1%)
	Pbias (%)	0.68	0.07	0.85	0.72	-	0.95	-	0.65 |6|
T_z	RMSE (s)	0.7	0.56	0.82	0.68	-	0.31	-	0.61 (16.9%)
	Pbias (%)	0.4	0.16	0.6	0.12	-	0.8	-	0.1 |2.6|

6.5.2. Comparison with MIKE-21

The regression model hindcast of the surge and wave states during the period of October-December 2009 is compared with that from the MIKE-21 model in Table 6.2. Values in brackets present errors within the predictions from the MIKE-21 model while unbracketed values provide the accuracy of the regression model.

Table 6.2. October – December 2009 surge and wave prediction accuracies. Values in brackets present errors within the predictions from the MIKE-21 model for the same period.

	Surge		H_s		T_z	
	RMSE (m)	Pbias (%)	RMSE (m)	Pbias (%)	RMSE (m)	Pbias (%)
Permanent Gauges						
Portsmouth	0.09 (0.09)	11.4 (18.4)	-	-	-	-
Sandown	0.08 (0.09)	2.5 (10.1)	0.19 (0.25)	9.8 (32)	0.4 (0.6)	2.9 (0.03)
Southampton	0.11 (0.1)	10.6 (13.1)	-	-	-	-
Lymington	0.12 (0.11)	12.7 (23.2)	0.06 (0.15)	7 (49.5)	0.49 (0.57)	0.16 (8.8)
Poole Bay	-	-	0.31 (0.27)	8.9 (1.5)	0.71 (0.61)	1 (4.7)
Milford	-	-	0.25 (0.36)	8.12 (22.9)	0.87 (0.69)	1.26 (1.4)
Hayling	-	-	0.24 (0.25)	9.3 (7.5)	0.79 (0.72)	1.59 (5.9)
Average	0.1 (0.1)	9.3 (16.2)	0.21 (0.25)	8.6 (22.7)	0.65 (0.64)	1.4 (4.2)
Secondary Gauges						
EMU Nab	0.09 (0.09)	12.2 (5)	0.34 (0.33)	13.8 (10.5)	1.17 (1.01)	22 (13.5)
EMU Hayling	0.1 (0.11)	8.8 (11.1)	0.24 (0.25)	15.8 (18.7)	0.9 (1.5)	24.3 (36)
EMU Ports.	0.1 (0.11)	18.2 (14)	0.26 (0.29)	70.4 (85.4)	1.5 (1.64)	35.6 (38.4)

6.5.2.1. Surge

During the three month comparison, both models recreated surge magnitudes with the same RMSE accuracy, on average, across the domain, while average Pbias values lay within 7% of each other, when compared to *in-situ* measurements. Fig. 6.3 provides a comparison of the regression, MIKE-21 and measured time-series at Portsmouth. It demonstrates that both the MIKE-21 and regression-based approaches recreated the pattern of the measured surge, including two main peaks. However, both model outputs appeared to be smoother than the measured time-series, which was likely to contribute significantly to the RMSEs given in Table 6.2.

Using the secondary regression to provide a prediction surface (as outlined in sections 6.3.2.) the regression-based predictions of the surge at the three temporary EMU buoys were also examined. RMSE accuracies at all three buoys fell within 0.01 m of the domain average (the average of the 4 primary gauge points) and within 9% of the average Pbias. RMSE accuracies of the regression hindcasts were within 0.01 m of those obtained using the MIKE-21 model at each site.

The accuracy of both models in predicting the peaks of the eight storm events exhibited variability, both spatially and between events, with peak surge errors ranging from less than 0.05 m to more than 0.2 m. On average, over the eight events, the MIKE-21 model predictions were more accurate than those from the regression model, with average peak errors of 0.12 m (14%) and 0.14 m (17%), respectively.

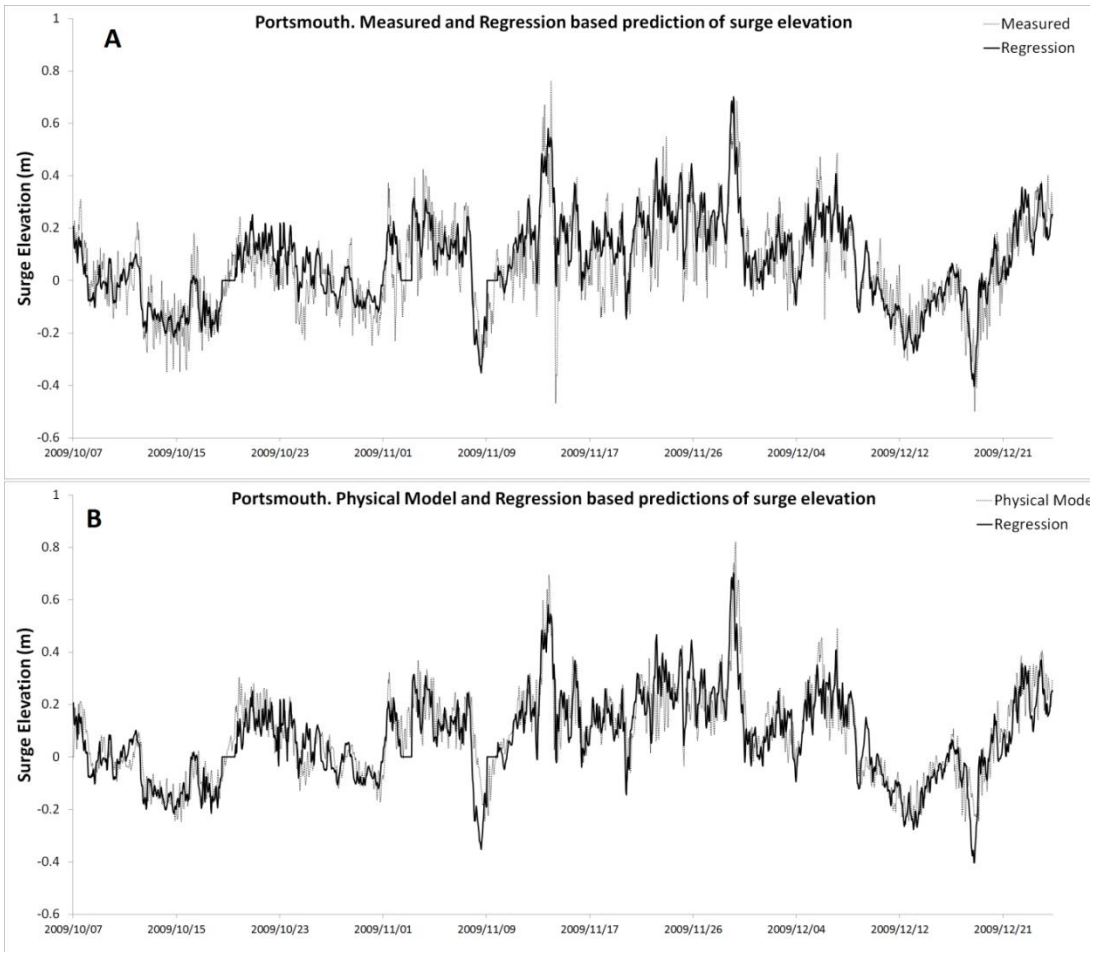

Fig. 6.3. Portsmouth surge elevations. A, measured and regression Oct–Dec 2009, B, physically-based model (MIKE-21) and regression Oct – Dec 2009.

The regression function was found to under-predict the peak amplitudes in many cases. Fig. 6.4 provides an example of the greater extent of under-prediction commonly found in the regression-based approach. The variability in peak water levels is often related to the timing of the surge rather than the peak, particularly as peak surge elevations often occur off the high tide (Horsburgh and Wilson, 2007). For this reason, the differences in the phase of the predicted surge, and the resulting influence upon the peak combined water levels (often referred to as the skew-surge) were also contrasted. Over the eight events the peak surge elevations predicted by the regression model lay within one hour of those predicted using MIKE-21, with a maximum shift of two hours seen during one event. The average absolute difference in peak water level accuracies from the two models (given as the difference between the model predictions and the measured state) was 0.04 m, with the MIKE-21 model providing the greater accuracies on average. These results were representative of the accuracies found elsewhere. For instance, peak water level errors during the two largest surges in November 2009 and an event on the 10th March 2008 were 0.11m

and 0.15m on average at the Lymington gauge in the MIKE-21 and regression models, respectively, while the skew-surge error was less than 0.13 m in both.

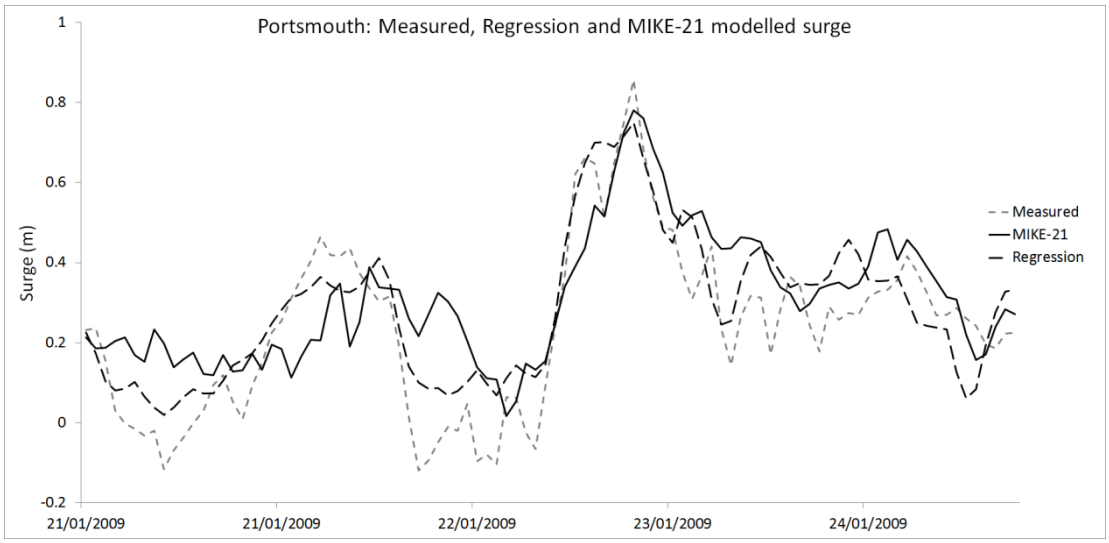

Fig. 6.4. Comparison of MIKE-21 and regression predictions of surge on the 23rd January 2009.

6.5.2.2. Waves

During the three month comparison, domain average T_z RMSE was 0.65 s and 0.64 s in the regression and MIKE-21 hindcasts, respectively, while Pbias in both was below 5%. Greater variance between the two models was present in the H_s model accuracies. In the deeper water regions, such as Hayling Island and Poole Bay, the regression and MIKE-21 H_s hindcasts contained similar RMSEs. Further inshore, particularly at Lymington, the regression function provided higher RMSE accuracies than those provided by MIKE-21. Correspondingly, the Pbias within the MIKE-21 hindcast was seven times larger, indicating a consistent over-prediction of the H_s in the nearshore region not present when using the regression function (Fig. 6.5).

Using the 'secondary' regression to provide a prediction surface, the regression-based predictions of the waves at the three EMU buoys were also examined. Regression accuracies closely resembled those given using the MIKE-21model, particularly in terms of H_s. However, the errors were generally larger than expected compared to the initial regressions at the permanent buoys. For instance, H_s Pbias at the Portsmouth EMU Buoy exceeds 70%, whereas no Pbias larger than 10% was found at the permanent gauges.

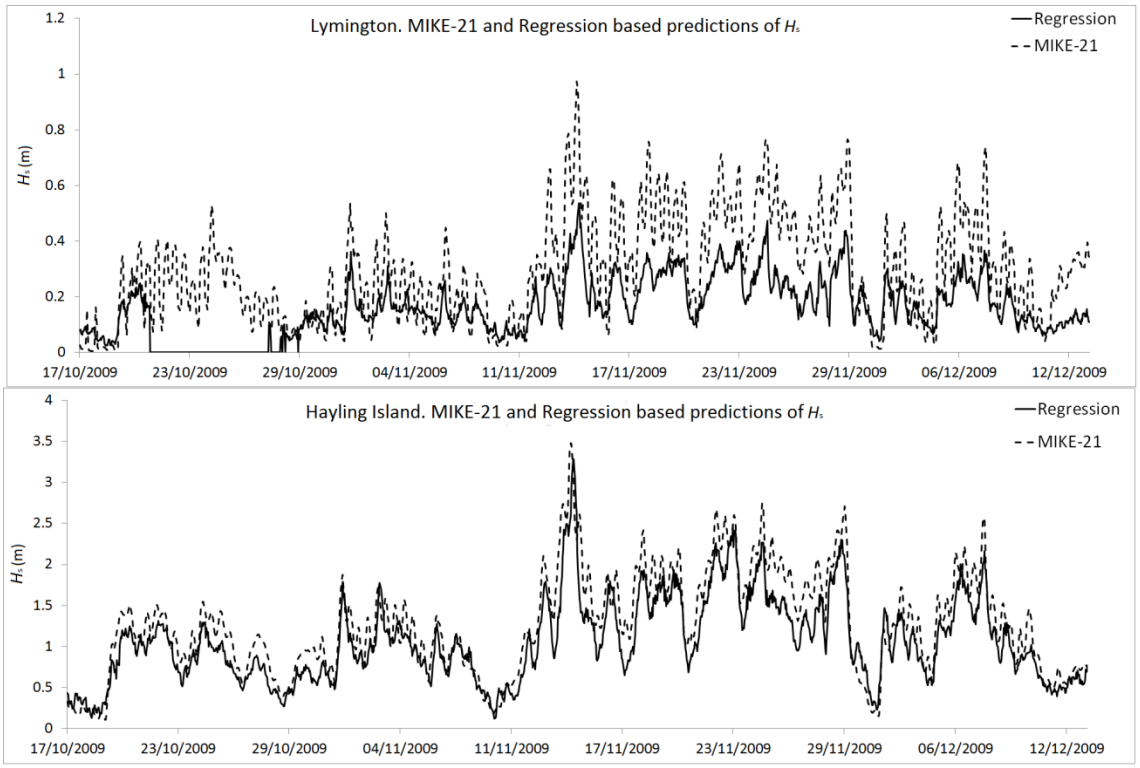

Fig. 6.5. Physically-based model (MIKE-21) and regression predictions of H_s at Lymington and Hayling Island.

During the eight storm events at the Hayling Island site, errors in the maximum H_s and the T_z relative to *in-situ* measurements were examined. The results indicated that the MIKE-21 model was able to more accurately recreate the peak H_s. The average error during all events was 0.19 m and 0.39 m using the MIKE-21 and regression models, respectively. Average normalised errors equated to 9.1% and 17.2% of the measured H_s peak values on average, respectively. T_z accuracies between the two models were more similar. Over the eight events the error in the predicted T_z was 0.65 s and 0.57 s in the MIKE-21 and regression model outputs, or 12% and 11.3% when given relative to the size of the measured T_z. Fig. 6.6 provides an example of the greater degree of under-prediction at the peaks commonly found in the regression-based approach. These results were shown throughout the domain, even in the nearshore regions where the regression reduced significant Pbias contained in the MIKE-21 model during the October to December comparisons. For instance, at Lymington, despite the significant reduction in the overall bias provided by the regression model, the consistent under-prediction of event peak amplitudes resulted in an under-prediction of the event on the 14th of November 2009 by 0.23 m, while the MIKE-21 prediction contained an over-prediction of 0.19 m.

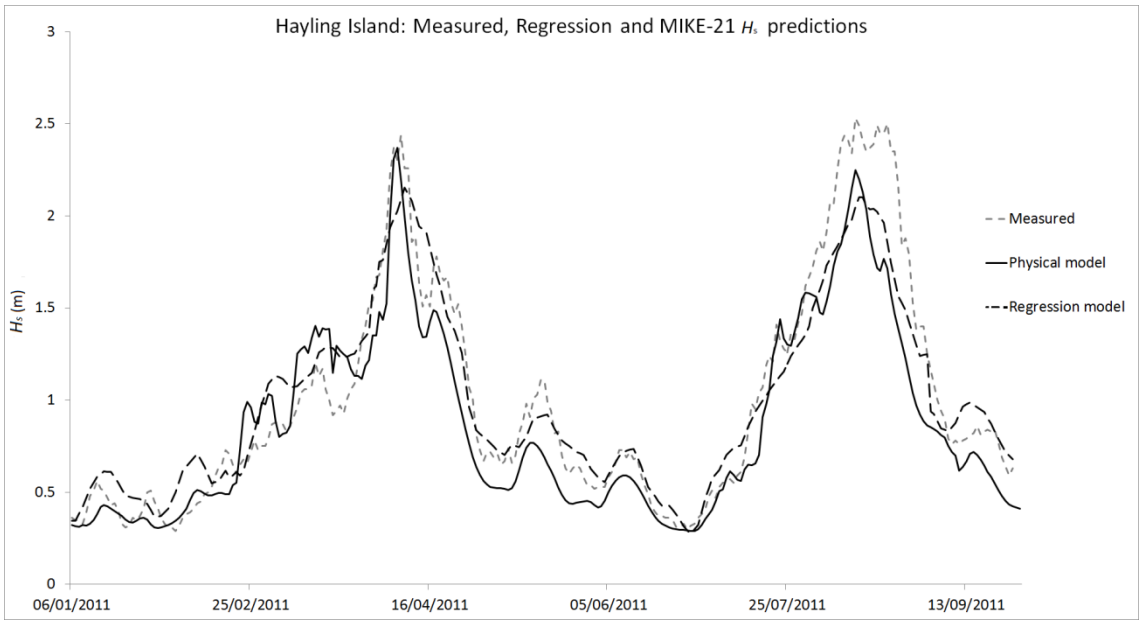

Fig. 6.6. Comparison of MIKE-21 and regression predictions of H_s on the 23rd January 2009.

6.5.3. Ensemble predictions

6.5.3.1. Uncertainty distributions and ensemble generation

The uncertainty distributions from which the ensemble perturbations were drawn (95 percentile upper and lower boundaries) and the size of the discretisation of the parameter distributions were given as:

- Tidal elevations – 0.1 m to -0.1 m at 0.01 m intervals.
- Boundary surge elevations (West) – 0.09 m to -0.14 m at 0.01 m intervals.
- Boundary surge elevations (East) – 0.14 m to -0.12 m at 0.01 m intervals.
- Wind speeds – 5.6 ms^{-1} to -4.6 ms^{-1} at 0.01 ms^{-1} intervals.
- Waves (H_s) – 0.13 m to -0.9 m at 0.01 m intervals.
- Waves (T_z) – 1.24 s to -1.21 s at 0.01 s intervals.

An ensemble size of 2000 members was chosen. It was possible to generate 2000 ensemble members at the four surge and five wave sites, as well as a spatial surface at 20,000 grid points (reproducing the MIKE-21 mesh), for 280 5 minute time steps (i.e. a 24 hour lead time), in under 40 minutes, using the computational resources available. With 2000 members, the ensemble means never varied by more than 0.02 m or 0.01 m in the surge or H_s heights at any time step.

6.5.3.2.. Surge predictions

Table 6.3 gives the RMSE of the mean of the ensemble relative to the *in-situ* measurements, the proportion of the measured values that lie within the ensemble bounds, and the RMSE in the ensemble spread associated with the surge and wave ensemble predictions. Examples of the rank histograms produced are given in Fig. 6.7.

Table 6.3. Ensemble surge and wave statistics.

	Portsmouth	Southampton	Sandown	Lymington	Hayling	Poole Bay	Milford
Ensemble mean RMSE							
Surge(m)	0.09	0.1	0.08	0.1	–	–	–
H_s (m)	–	–	0.15	0.04	0.18	0.22	0.19
T_z (s)	–	–	0.29	0.64	0.9	0.69	0.83
Ensemble mean Pbias (%)							
Surge	5.5	4.13	2.6	-3.9	–	–	–
H_s	–	–	2	6.6	6	4.4	4.9
T_z	–	–	<1	<1	<1	<1	<1
Measured points within ensemble spread (%)							
Surge	93	93.5	93	91	–	–	–
H_s	–	–	82.5	95	88.9	81.8	77.7
T_z	–	–	55	61	66	72	65
RMSE of the ensemble spread (from ensemble mean)							
Surge(m)	0.24	0.26	0.23	0.21	–	–	–
H_s (m)	–	–	0.05	0.03	0.08	0.09	0.07
T_z (s)	–	–	0.05	0.1	0.22	0.25	0.22

The ensemble mean represents the 'best guess' of the prediction. Across the four tide gauges, RMSE ranged from 0.08 m to 0.1 m, while Pbias was never greater than 5.5%. The high proportion of the measured points included within the ensemble spread (always greater than 90%) indicates that the uncertainty in the system was not under-predicted by the ensemble. However, Table 6.3 also indicates that the average RMSE in the ensemble spread was more than twice the RMSE when contrasting the ensemble mean against the measured time-series, indicating that the uncertainty attributed to the prediction was too large, on average, through the prediction period. The rank histogram of Portsmouth further indicates that the ensemble spread was too large as a clear dome form was produced. This was found at each site, with the exception of Lymington, where the distribution across the ensemble members was more level, indicating a lesser degree of over-prediction of the ensemble spread

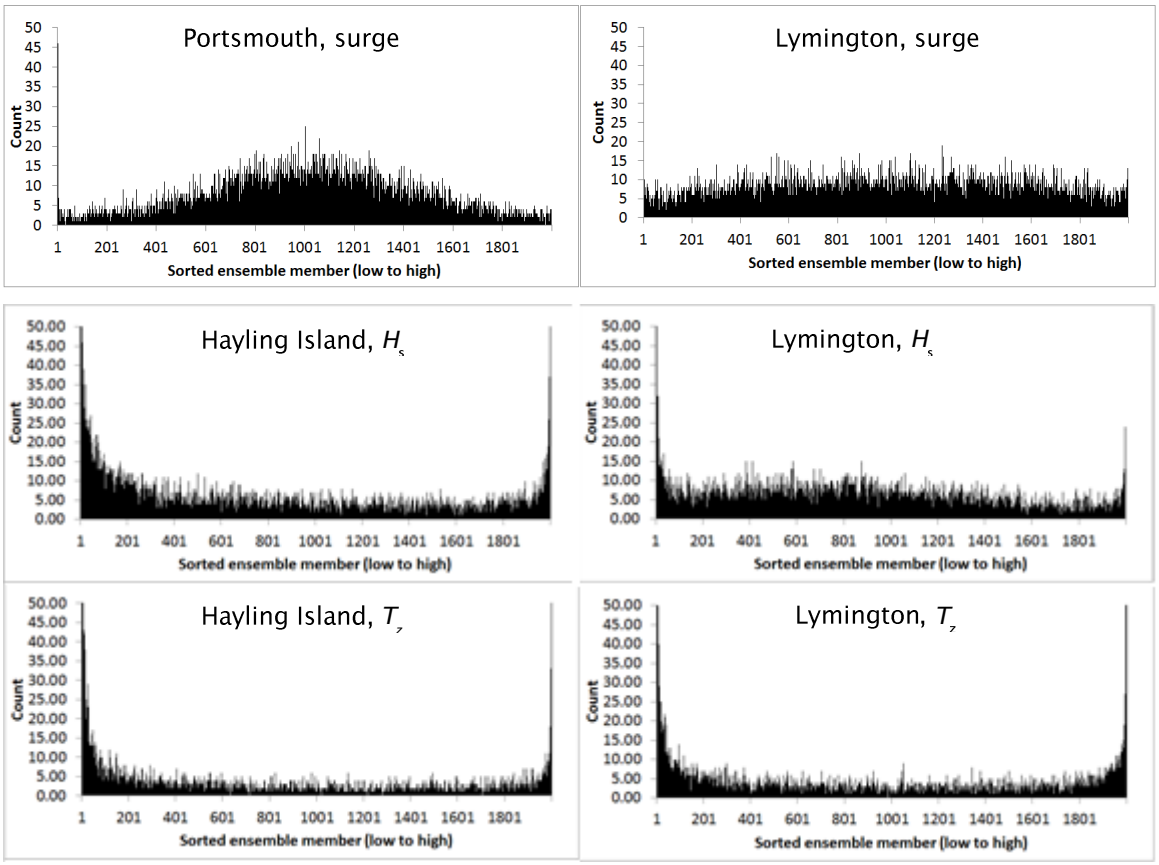

Fig. 6.7. Ensemble rank histograms of surge, H_s and T_z at selected sites. Note that the count axis has been truncated at 50 in order to provide a clearer image.

6.5.3.3. Wave predictions

Across the gauge sites considered, the RMSE in the ensemble mean ranged from 0.04 to 0.22 m and 0.29 to 0.9 s in the H_s and T_z predictions, respectively. Pbias was always less than 1% in the T_z predictions and less than 7% in the H_s. Significant proportions of the measured time-series were not contained within the ensemble spreads, particularly in terms of T_z, where proportions ranged from 55% to 72%. The RMSE of the ensemble spread was usually two to three times smaller than the RMSE of the mean, relative to the measured H_s, while the same comparison of the T_z ensemble demonstrated differences of up to six times the RMSE in the ensemble mean.

The rank histogram plots show an increase in counts at the extremes of the ensemble distribution, indicating that the ensemble spread was too small, confirming the indications given in Table 6.3. The rank histogram plots were similar across all gauges. The only exception was some reduction in the severity of the under-prediction in the Lymington H_s, as demonstrated by the slightly more level plot given in Fig. 6.7.

6.5.3.4. Updating the independent variables: a H_s example

Updating the independent variables with values derived from the Kalman filter estimation, provided a more accurate prediction (relative to the measured values) and

reduced the uncertainty (e.g. reduced the spread in the prediction ensemble). Fig. 6.8 (top) indicates the average error (relative to the measured data) and the average ensemble spread for the T_0 to T_{+12} time steps from each simulation. The results demonstrated that the impact of the Kalman filter updating was greatest within the first two hours, reaching a plateau approximately six hours from the update.

Fig. 6.8 (bottom) provides an example of the influence of the updating at two of the 12 update points in the time-series, the first, 12 hours prior to the peak, the second, 5 hours prior.

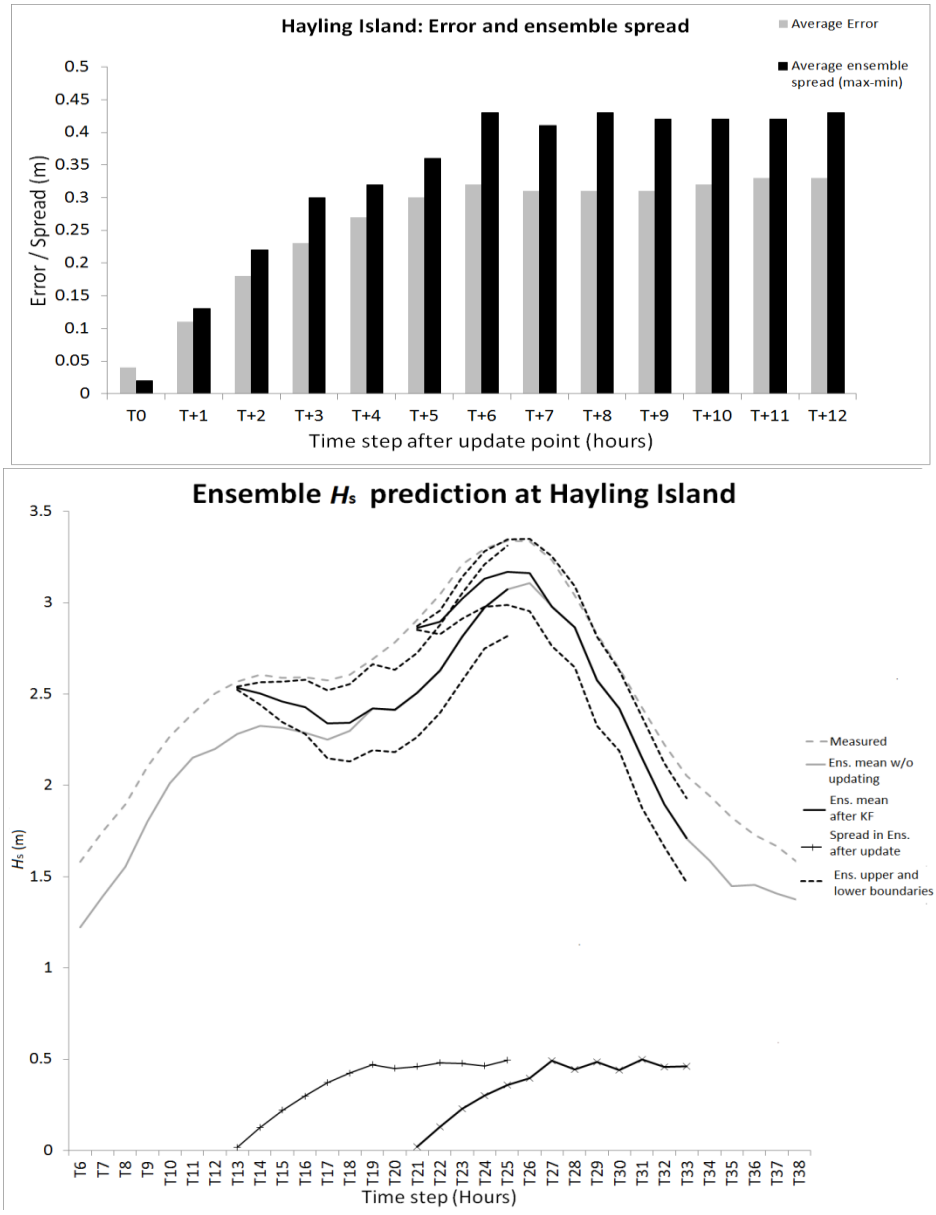

Fig. 6.8. The temporal variability in the Kalman filter update in terms of increase in accuracy and reduction to uncertainty (top), and the corresponding update at 12 hours and 5 hours prior to the event peak (bottom).

Fig. 6.8 demonstrates that the update to the ensemble mean was significantly biased towards the measured value (due to the relative uncertainties attributed to the modelled and measured states), and the increase in the error and uncertainty as one moves forward from the respective update point in the prediction. For example, the results indicated that the peak H_s, when the update was applied 12 hours prior to the event peak, contained an error of 0.23 m and the ensemble spread was 0.43 m. Updating six hours later (at six hours prior to the event peak) increased the accuracy of the forecast, resulting in an error at the peak of 0.22 m and a spread of 0.4 m, while values of 0.13 m and 0.28 m, respectively, were found when a subsequent update was applied three hours prior to the event peak.

6.6. Discussion

This research introduced a simple empirical model for the prediction of surge and wave states within the Solent and Southampton Waters estuarine system, contrasting the accuracies of its predictions with that from a physically-based numerical model. The addition of uncertainty to independent variables using a Monte Carlo approach, and the introduction of Kalman filter updating, was used to demonstrate the importance of probabilistic modelling and data assimilation strategies for coastal managers.

A multiple regression model was defined using the Matlab stepwise regression function, creating an empirical relationship between the input data (e.g. atmospheric and boundary conditions) and the measured values at a variety of nearshore gauges. The regression models for surge, H_s and T_z were used to predict the relevant states for a two year period. The results indicated that the regression models provided consistent predictions, containing little temporal or spatial variability when evaluated using normalised errors. For example, the average surge values across the gauges were always within 0.01 m of the average from all gauges, while the average variance between months at all gauges was also 0.01 m. The errors given in the surge and T_z predictions compared well with those expected from currently operational systems. At Portsmouth the regression contained an average error of 0.08 m while results available from POL (http://www.pol.ac.uk/ntslf/model.html) indicate that the operational storm surge model also contained an average RMSE of 0.08 m during 2008 and 2009. Similarly, operational reports generally state the errors in wave predictions as between 20 and 25% of the incident magnitude (NOAA Onlinehttp://polar.ncep.noaa.gov/waves/valid_wna.html; Bradbury *et al.*, 2004; Bidlot *et al.* 2007) which corresponds well the gauge average value of 16.9% from the regression model. The H_s prediction errors were in reasonable agreement, but slightly

larger than those expected, with a gauge average error of 31%, with the greatest accuracies found at Poole bay (23%).

The regression model predictions were also contrasted with those from the MIKE-21 model. Over the winter period between October and December 2009, the two models performed with similar accuracies in all three cases. For instance, gauge average RMSE in the surge was 0.1 m in both instances. Some variability was present, however. For example, the regression model was shown to provide lower Pbias values, particularly in terms of H_s, in the nearshore regions such as Lymington, where previous research has demonstrated a tendency for over-prediction using the MIKE-21 model, attributed, in part, to bathymetric uncertainty. Model predictions of H_s and surge elevations were also contrasted over a series of eight storm events. The results demonstrated that the MIKE-21 models predicted the peak H_s and surge magnitudes more accurately. The regression consistently under-predicted the peak magnitude of the events considered. For example, the MIKE-21 model was able to provide an 8% and 3% increase in accuracy in the prediction of the peak magnitudes in the H_s and surge, respectively. In terms of surge prediction, the ability to model the peak surge elevations and their timing, relative to the high tide, is of greatest influence to peak water levels, and therefore, of interest to coastal managers. The modelled surge peaks were found to diverge by one hour on average between the two predictions. To investigate the impacts that the changes to amplitude and timing of the surge had on the resulting peak water levels, the surge predictions were combined with harmonically-derived tidal predictions. The difference between the tide and the resulting water levels is termed the skew-surge. Comparison of the two time-series revealed that on average the prediction accuracies of the two models diverged by an absolute value of 0.04 m, while relative to the *in-situ* measurements on average, the MIKE-21 predictions were only 0.01 m more accurate than those given using the regression model.

These results indicate that, for storm events, the current regression model may be too simplistic and require further development before recommendation as a suitable alternative to the more accurate MIKE-21 system. However, as many surge peaks fall away from the high tide (Horsburgh and Wilson, 2007), the emphasis is often not on the peak, but on the elevation of the surge following or just prior to, the surge peak, during the high tide. In such circumstances, the regression model was shown to provide predictions with only slightly lower accuracy (0.01 m) than the MIKE-21 predictions.

The analysis of the 'secondary' regression points raised an important issue when contrasting the physical-based and regression models, particularly when considering the spatial interpolation of the wave predictions. The regression predictions at the 'secondary' gauges showed a strong correlation with MIKE-21 predictions, yet a significantly lower degree of accuracy than those at the primary

gauge sites. This was due to the 'secondary' spatial regression model being defined by the spatial correlations between the nodes in the MIKE-21 domain. Therefore, errors in the MIKE-21 model propagated to the regression model. In this instance, the MIKE-21 model was shown to over-predict H_s in some shallow regions, such as the EMU buoy sites, which previous research has highlighted was attributed, in part, to inaccuracies in the bathymetry datasets. This resulted in similar errors in the regression model. One way to address this connection might be to remove any requirement of a physical-based model, for instance, through increasing the complexity of the statistical model to account for variables such as bathymetry depths, in the expectation of such data adequately representing un-gauged sites. However, given the expectation that the errors in the MIKE-21 model were influenced by inaccurate bathymetry data, one would expect that the same errors would persist in such an updated regression, and this technique would only be applicable where uncertainty in the formulation of the physically-based model was the obstacle. The inclusion of additional *in-situ* measurement devices would be a way with which to direct a spatial regression without the need for a physically-based model. Research into the optimal location and number of such measurements required to fully represent the variability of conditions in complex nearshore regions could be useful for the development of empirical forecasting systems in regions such as the Solent. Extending the length of deployment of the EMU buoys to provide a reasonable dependent variable dataset for regression training, could aid in reducing uncertainties in the eastern Solent shallow water regions. Alternatively, in very complex regions, such as the Solent, the 'fusion' of the two methods may be the most appropriate approach. In this approach the physical-based model may be simulated once, providing the initial forecast of the ocean state across the region while the empirical model could then sample input uncertainty to define an ensemble, the spread of which could be applied to the original physically-based model prediction. This would allow the uncertainty in the predictions to be quantified without the requirement for vast computational resources, while retaining the ability to accurately represent the state of the system between *in-situ* measurement sites.

The inclusion of the physical-based model could alsoreduce uncertainty relating to the prediction capabilities of an empirical model to predicting extreme events where long measurement datasets are not available. In such cases there may not be a sufficient number or range of extreme events with which to train the empirical model, leading to uncertainty over its predictive capabilities, until such events take place. For instance, only a few years of data was available to train the empirical model in this research, therefore, extreme events larger than those contained in these datasets, or likely to occur in the future, can not been explicitly considered and may not necessarily be well represented in the current model. Although the inclusion of the March 10th 2008 event, one of the largest on record, did provide at least one event that

sampled from very extreme scenarios, more such events should ideally be included as they represent the conditions of most interest to coastal managers in the region. Physically-based models, on the other hand, are based upon formulations that are assumed to be represent the real-world physics of a system, therefore, once calibrated to a region, may be expected to more adequately predict a wide range of event types even if an event larger than found in the calibration period was to occur. Therefore, the use of a physically-based model to provide the baseline prediction, while the empirical model defines an ensemble range, may be the best option in such conditions.

A further alternative may be to utilise the physically-based model as the dependant variable. In such as way, once a physically-based model has been established for a region it aims to be emulated by the empirical model, thereby reducing computational demands to enable probabilistic forecasts to be made. This may be particularly useful in a situation where even a single baseline simulation of the physically-base d model may require a run-time that is unsuitable for a real-time forecasting system.

Using a single desktop computer with two 2.13 GHz processors and 4 GB of RAM, the regression model was able to provide a 280 step forecast (used as it represents a 24 hour forecast at five minute time steps) of surge, H_s and T_z at the same 20,000 points included in the MIKE-21 mesh, in under 40 minutes. This was considerably faster than the 3.5 hours required by the coupled MIKE-21 HD and SW model to provide the same output. This demonstrates the ability of the regression function to provide very large ensemble groups within time constraints that allow for regular updates (e.g., every one hour) that would be of interest for real-time flood forecasting.

The generation of probabilistic predictions was also considered, with uncertainty distributions generated based on the comparison of input datasets with *in-situ* measurements. The results demonstrate the importance of quantifying the uncertainty in the data used to drive a prediction and the increases in accuracy that can be made from a data assimilation step. Fig. 6.8 (bottom) was particularly useful in demonstrating how, through the correction of the independent variables forcing the prediction; the forecasts were able to be brought further in line with the 'measured' time-series. Fig. 6.8 (top) indicates that the benefits to both the accuracy of the prediction, as well as the uncertainty within it, were greatest in the short-term, with improvements largely negligible after six hours.

The ability of the regression model to create large ensembles, within a short enough run time to allow for the regular updating of the independent variables, was shown to be highly valuable to coastal managers. Given the H_s example where the Kalman filter was applied, for instance, the use of the ensemble was paramount in describing to the modeller the likelihood of a given event occurring, as well as how that likelihood changed as one approached the event peak. In the example given, six

hours prior to the event a modeller would predict a peak magnitude of 3.12 m, with a range of 0.4 m. However, updating a subsequent forecast with a start point three hours prior to the event, this prediction had changed to 3.21 m, with a range of only 0.28 m. Not only does this allow for increased accuracies and certainties as the event draws nearer, it also enables quantification of expected magnitudes at given confidence levels. For example, at three hours prior to the event peak, analysis of the ensemble would allow a modeller to indicate that 90% and 95% of the ensembles predicted a magnitude of 3.33 m and 3.35 m, respectively. The importance of the information from such techniques has been highlighted in other research. Flowerdew *et al*. (2007) discuss the development of pilot schemes to update the current operational forecasting systems in the UK from deterministic to probabilistic systems, for example, while the migration of data assimilation strategies, commonly used in atmospheric modelling, into the oceanographic sector, has been discussed increasingly over the last decade (Kalman, 1960; Lionello *et al*., 1995; Kantha and Clayson, 2000; Kobayashi and Yasuda, 2004; Neal, 2007).

Although the research has provided a useful example of how one can quantify uncertainty and increase accuracies in a forecasting system, it is also important to validate the ensemble provided. In this case, the ensemble spread was shown to be poor. Although the proportion of the measured values contained within the ensembles was generally high, particularly in terms of the surge, other statistics indicated that the spread was either too large (surge) or too small (waves) at each site. Various factors might explain the inadequacy of the ensemble estimations. First, the uncertainty associated with the models themselves was not considered. This can be an important source of uncertainty to consider as model formulations might be more applicable in one region than another. The ways in which the uncertainty distributions were estimated may also be at fault, particularly in the case of the surge boundaries. For example, model inputs supplied by the Previmer system were contrasted with surge datasets given at two gauges nearest to the domain boundaries. The nearest Previmer boundary point to each was used; however, some spatial displacement was present, which, considering the influence of nearshore bathymetry upon hydrodynamics, and the relatively large errors that can arise from small phase differences, may lead to significant discrepancies. Furthermore, only relatively short time-series were used in the comparisons of the datasets, and only a single value was used to represent the uncertainty in a given variable at all times, which in reality, may vary temporally.

The errors in the ensemble spread, and the larger errors in the regression model, relative to the MIKE-21 predictions, should not take away from the findings in this research, which still highlight key issues, such as the importance of probabilistic approaches to forecasting, the benefits of data assimilation, and the requirement to find computationally efficient replacements to allow for the production of sufficiently large ensembles. What the errors do highlight are areas in which future research could

provide better probabilistic systems. For instance, to more accurately quantify the uncertainty in the system, thereby increasing the ensemble spread, the Met Office's proposed ensemble forecasts of ocean and atmospheric states (see Flowerdew *et al.*, 2007) could be utilised. These datasets would enable the real-time updating of uncertainty distributions, based directly on the Met Office ensemble datasets at a given time, while data assimilation strategies could still be employed with the use of the Ensemble Kalman filter (Evensen, 1994; 2003) in which the forecast variance is defined from the ensemble. This could be particularly useful in acknowledging the temporal variability in uncertainty.

Further research could assess ways in which the relatively simple regression models defined here could be developed to provide more accurate predictions during extreme events, while still retaining their computational demand advantage over the complex models currently used operationally. A variety of empirical models have been demonstrated in previous research to provide low cost, high accuracy predictions, which may be useful in directing future refinement. For example, Deo and Naidu (1999) describe the use of an autoregressive function for the prediction of wave heights while Kobayashi and Yasuda (2004) provide an example of the use of multiple regressions, combined with Kalman filtering, for the transfer of offshore to nearshore wave states. Similarly, Prouty (2007), who also stressed the need for computationally inexpensive forecasting tools, found that they were able to provide accurate predictions of storm surge propagation in the North Sea utilising an artificial neural network and a series of gauges along the East coast of the UK. Similar approaches may be useful, particularly when forecasting large surge and wave events propagating from the Atlantic into the English Channel. Furthermore, in complex regions where oceanographic data is available and an accurate physically-based model can be developed, future research could examine the development of a 'fused' prediction system, retaining the advantages of both approaches, or, alternatively, where the physically-based model is extremely inefficient, assess an emulator-based approach.

The findings from this research will be of relevance to a wide modelling audience, particularly in light of the current trends toward probabilistic modelling and the application of data assimilation techniques. The application of an empirical-based approach will be of most interest to coastal managers working in computationally poor regions, where the feasibility of running high resolution, data intensive models is low.

6.7. Conclusion

A regional model for the transformation of mid-Channel surge and wave states to the nearshore, using a computationally inexpensive regression-based approach was contrasted with a physically-based numerical model of the Solent estuarine system.

The benefits of utilising a probabilistic forecast, including a data assimilation step, were also assessed. The research indicated that:

- The empirical model prediction accuracies were, on average, equal to those obtained from the physically-based model at all gauged sites, despite the variability in conditions between the sites considered. In some instances the empirical model out-performed the physically-based model.
- During a series of storm events, the physically-based model predictions were more accurate by 3% and 8% when hindcasting surge and H_s peaks, respectively, indicating an over-simplification in the empirical approach considered in the research that should be addressed in future research.
- The efficiency of the empirical model approach enabled the simulation of a large ensemble forecast and hourly data assimilation step, shown to both quantify uncertainty and reduce error in the short-term forecast.
- The choice of forecasting approach in an operational system will depend on the length of datasets available with which to train an empirical model and the complexity of the system one wishes to represent. This research suggests that due to the complexity of the Solent, a fusion of both approaches would be most suitable when making predictions over the whole region.

These findings provide a strong case for utilising empirical-based approaches to forecasting in coastal zones (either independently or in addition to physically-based approaches) due to the similarity in prediction accuracies with those obtained using physically-based approaches, as well as the quantification and reduction of uncertainty in the forecasts due to the ability to generate large ensembles and assimilate *in-situ* measurements in near real-time. The high computational efficiency of the regression model proposed will be of particular interest to coastal managers in regions where resources are limited, particularly where one wishes to quantify and reduce uncertainty in model forecasts; an area of interest in recent flood forecasting research.

Chapter 7: Discussion

The contextual aim of this research was to provide a regional tide-surge-wave model for the provision of real-time probabilistic forecasts through the transformation of Mid-Channel forecasts to the nearshore regions of the Solent. A series of specific research objectives (Section 1.2) were used to examine pertinent issues relating to this aim, such as; the spatial and temporal variability in the accuracy of the model predictions, the processes occurring in the domain of relevance to coastal flooding and the model sensitivity to them, the reduction in computational resource requirements that can be obtained using empirical-based modelling approaches, and the quantification of uncertainty and the increase in prediction accuracy that can be obtained through the implementation of probabilistic modelling and data assimilation.

The objectives provided in this research will be of interest to those involved in operational coastal flood forecasting. Through these objectives, this research attempted to provide information of value to coastal modellers with interests in, both, the physical processes in estuarine environments, quantification of uncertainty, and data assimilation in ocean state predictions.

The Solent-Southampton Water estuarine system was selected as the study site for this research. The complexity and wide range of environments contained within the region was particularly useful for the examination of the spatial variability in the processes (such as tide-surge-wave interactions) taking place, and the influence of the forcing datasets upon model predictions in the variety of conditions often found in complex estuarine regions. Such a setting is also of use for increasing the applicability of the research findings to other regions, due to the ability to draw broad conclusions relating to the conditions influencing aspects, such as, the degree to which tide-surge-wave interactions take place.

From an operational perspective, the study site also provided an example of a region that requires a relatively high resolution, regional nest, in order to adequately represent the variability in the nearshore conditions. Furthermore, previous research in the area has reported significant errors in the reproduction of tidal hydrodynamics (Levasseur, 2008), while it also contains environments where spectral wave models have been considered to be particularly uncertain (Ris *et al.*, 1999; Rogers *et al.*, 2002; Brown and Wolf, 2009). These conditions were valuable when examining spatial variability in prediction accuracies in estuarine environments, and examining the causes of the errors in regions containing relatively low prediction accuracies.

The presence of current operational forecasting capabilities in the English Channel, as well as the relatively dense network of *in-situ* measurements available in

and around the Solent, were essential in providing datasets with which to force the regional model and assess the accuracies of the predictions from it.

7.1. Accuracy of the regional model predictions

Predictions of the tide, surge and wave conditions in the Solent-Southampton Water region were simulated using the MIKE-21 software and datasets obtained from outputs in the English Channel, provided by a pre-operational forecasting system, Previmer. The accuracies of the predictions were assessed relative to *in-situ* measurements throughout the region in order to ascertain the locations and event characteristics during which the model provided relatively high and low accuracies.

Predicted tidal amplitudes were consistently under-predicted throughout the region, with errors in the semi-diurnal constituents of up to 18% at the Southampton tide gauge. However, the predictions of the tidal constituents were broadly consistent with previous attempts at modelling through the region. Levasseur (2008), utilising a 3D modelling package, also reported errors of up to 15% in the semi-diurnal amplitudes, while K_1 and some shallow water constituents (particularly $2MS_6$ and $2MN_6$) contained errors greater than 40%. Furthermore, Levasseur (2008) quotes errors in the MSR and MNR at Southampton, of 0.44 m and 0.39 m, respectively. These errors were similar to the 0.48 m and 0.44 m errors found in this research. The similarities in the tidal errors implied that the use of the 2D rather than 3D model was reasonable. Levasseur (2008) suggested that most of the error associated with diurnal and semi-diurnal constituents could be attributed to tidal inputs at the boundaries. Furthermore, issues relating to the accuracy of predicted tides from numerical models within complex nearshore regions have been noted in previous research, and for this reason, in operational forecasting systems, predicted tides are replaced with those defined from harmonic analysis at class A tide gauges (Flowerdew *et al.*, 2007; Hawkes *et al.*, 2009). The substitution of the modelled tide with those estimated from harmonic analysis was examined. The addition of the modelled surge to the substituted tide resulted in considerable reductions in the error of the predicted combined water level elevations, reducing the RMSE compared to the "normal" predicted water levels by around half.

The predicted surge elevation was given as the difference between the tidal elevations and the combined tide and surge elevations. During the three month assessment between October and December 2009, the average RMSE of the seven tide gauges was 0.09 m while absolute Pbias was 15.2%. Predicted surge accuracies from the regional model were comparable with those obtained from the operational storm surge model developed by POL (archives of accuracy assessments are available to download from http://www.pol.ac.uk/ntslf/model.html). Over the period between

October 2009 and December 2009, the accuracy of the operational storm surge model at Portsmouth was an average RMSE of 0.07 m. Data from the operational model was not available at other locations used in this research. Similarly, the prediction accuracies during the largest peaks in the modelled time-series suggested that the regional model was capable of reproducing large surge events with comparable accuracy to the operational model, based on the findings of Wortley *et al*. (2007), although a bias, indicating under-prediction of event peaks, was often present. Time-series plots indicated that much of the error was related to the smooth nature of the predicted surge relative to that extracted from the measured record. This may be related to the relatively coarse temporal resolution of the datasets used to force the model. Alternatively, previous research by Horsburgh and Wilson (2007) found that due to small errors in harmonically predicted tides, the surge elevations given at tide gauges could often contain tidal patterning. Bocquet *et al*. (2009) found similar discrepancies in the surge smoothness between predicted and measured surges. They suggested that the harmonic estimation of tidal elevations can contain a RMSE of up to 0.1 m and suggest accuracy assessments of surge predictions are likely to be penalised due to such uncertainty in the measured record.

The regional model provided predictions of H_s and T_z with a domain averaged RMSE of 0.32 m and 0.81 s, respectively. H_s Pbias was positive (indicating an over-prediction) throughout the domain, most likely due to uncertainty in the wind datasets used to force the model, which also consistently over-predicted wind speeds when contrasted with *in-situ* measurements. Pbias and normalised RMSE statistics indicated that the model performed most accurately at sites located in deeper waters (greater than approximately 10 m), where errors were comparable with RMSEs from three operational forecasting systems assessed by Bidlot *et al*. (2007). Similarly, normalised RMSEs were comparable with the 25% and 20% accuracies given by the NOAA online assessments of their system (http://polar.ncep.noaa.gov/waves/valid_wna.html) and by Bradbury *et al*. (2004). However, at gauge sites in some of the shallower regions, for instance Lymington and the EMU Portsmouth Buoy, H_s Pbias was greater than 50%, indicating a relatively large over-prediction. These errors were difficult to contrast with operational systems as many reports, for example, Bidlot *et al*. (2007) contrasted forecasting systems in deeper offshore sites only. Similarly, Bradbury *et al*. (2004) did not utilise *in-situ* measurements in areas such as Lymington due to the complex bathymetry and an insufficiently fine model spatial resolution with which to provide reasonable comparisons. However, previous research has described a tendency of wave models to over-predict H_s and under-predict T_z due to an over-prediction of the high frequency energy, particularly in shallow, short fetch areas (Ris *et al*., 1999; Rogers *et al*., 2002). Brown and Wolf (2009) highlight that forecasts from a coupled tide-surge-wave model had lower accuracies in water depths of 5 m or less. An assessment by

Moeini and Etemad-Shahidi (2007) found SI errors of up to 20% in both H_s and T_z when hindcasting in an enclosed basin despite using measured wind conditions, while Johnson and Kofoed-Hansen (2000) have indicated that the formulations used in MIKE-21 SW (after Janssen, 1989, 1991) may overestimate sea surface roughness in shallow water regions. Additional analysis indicated that RMSEs could be reduced in the regional model by altering the local bathymetry, for instance, at Lymington the alteration of the bathymetry reduced the H_s RMSE from 0.17 m to 0.09 m.

The examination of the accuracies in the model predictions provided information of value, both relating to the other experiments contained in this research, as well as to coastal modellers working in the Solent and similar environments. The ability of the model to recreate the measured states with comparable accuracy to existing operational systems provided an indication that the model set-up adequately represented the fundamental processes occurring in the domain. In doing so, it provides a tool with which subsequent analysis could be performed. Furthermore, the spatial variability in the accuracy of the model predictions, particularly relating to the tides and nearshore wave conditions, enabled conclusions to be drawn that will be of relevance to other coastal modellers. The relatively large errors contained in the predicted tides and waves, particularly in the western Solent, support previous research which has highlighted that model predictions can become increasingly uncertain in complex nearshore environments. The comparisons with harmonically derived tidal elevations revealed that in regions where a dense network of *in-situ* measurements are available, more accurate tidal predictions can be obtained using harmonic analysis of tide gauge time-series. Similarly, the improvements to the wave predictions obtained through local manipulation of the bathymetry provide an indication of the importance of high quality datasets, particularly in shallow coastal regions. These findings are of relevance In light of recent advances in data collection; for instance, coastal modellers now have the ability to sample bathymetries with very high (>2 m) resolution, using tools such as Lidar (e.g. the CCO now provides such datasets at a variety of locations along the south coast of England).

7.2. Accuracy of the Previmer products and the sensitivity of model outputs to them

The contribution of the local wind and boundary conditions to the regional model predictions was examined by conducting a series of simulations, systematically removing the dataset of interest and contrasting the resulting outputs with those obtained when the dataset was included. Furthermore, the boundary conditions and local wind datasets, supplied by Previmer were contrasted with those from a well-

established operational forecasting system in the UK. The influence of the divergence between the inputs, upon the model predictions, was examined.

This research was conducted in order to provide a more detailed understanding of the variables of greatest significance to nested model predictions in coastal regions. In addition, it aimed to assess the quality of the Previmer datasets, quantifying the error in the predictions that may be attributed to dataset selection.

The sensitivity of the model outputs to the local winds and boundary conditions varied spatially, temporally, and between the wave and surge variables. The exclusion of the local wind stress resulted in a domain averaged $RMSE_{h,h}$ and $Pbias_{h,h}$ of 0.03 m and 6.5%, respectively, when contrasting surge predictions with and without the inclusion of wind stresses during the October to December 2009 period. Reduction to the peak surge magnitudes reached 13.9% during the 10th March 2008 event, where wind stress was excluded. Spatial variability in the influence indicated that the sensitivity to wind-stress was smallest in the offshore Nab Buoy site and greatest at Southampton. The exclusion of the winds resulted in a decrease to peak water levels of up to 0.2 m, while the skew-surge was decreased by up to 15.6%. The influence of the boundary surge datasets upon the coastal surge prediction was greater than that of the wind stress. Its removal resulted in the reduction to peak storm surge heights of 73.0% on average.

The opposite trend was shown when contrasting the relative influence of the local winds and boundary conditions upon the wave predictions. Despite the local extent of the model domain, the wind was the most influential force upon the modelled waves. This was most clearly demonstrated when the boundary wave dataset was removed. During the event on the 14th November 2009, despite the removal of the boundary wave energy input, the predicted H_s peak was within 15% of that predicted with the boundary waves included at the EMU Nab Buoy site. Although spatial variability was present in the degree to which the boundary wave conditions influenced the model predictions (with the greatest sensitivity occurring the in most exposed sites, such as the EMU Nab Buoy), the local wind field was the most significant contributor to the model output in the domain. The removal of the local winds resulted in the H_s event peak decreasing by an average of 60%, while in the most sheltered regions, such as Southampton this value rose to 90% during the November 14th 2009 and March 10th 2008 events.

The results provided broad indications of the sensitivity of the model predictions to input forcing, providing conclusions which, although basic, were of value to modellers working in estuarine environments containing a variety of conditions such as those found in the Solent. The results indicate that both datasets were of significance to peak storm surge elevations, correlating with previous research. For instance, Wells *et al*. (2001), Wortley *et al*. (2007), and Davis *et al*. (2010) have also demonstrated that the local wind field provides an important energy contribution to the surge. Similarly,

the importance of accurately representing the surge state outside of the immediate model nest has been suggested to be particularly important in the English Channel, where the funnelling effect and long fetch conditions enable the continual build-up of a surge propagating south from the North Sea, providing a considerable influence upon the state of the surge reaching the coast (Smith and Ward, 1998). Alternatively, it has been demonstrated that the accurate representation of the local wind field was considerably more important than the quality of the boundary conditions, when predicting wave states at the coast, particularly where the fetch was relatively short. These findings are expected to be broadly representative of conditions in many coastal regions and, therefore, applicable to a wide variety of nested, coastal modelling applications.

The local winds and boundary conditions obtained from the Previmer system were contrasted with those from the operational system currently in use in the UK. The comparison of the datasets revealed that, on average, they were consistent with one another. Unsurprisingly, therefore, the model predictions made when substituting the Previmer datasets with those from the Met Office, provided accuracies that were consistent with those obtained when forcing the models with the Previmer products. On the surface, this provides an indication that the products from the Previmer system were a suitable replacement to those that could be purchased from the Met Office. Furthermore, when considering the wind fields, both datasets displayed errors, relative to *in-situ* measurements, which were significantly larger than those provided in previous research based in offshore locations (Bidlot *et al.*, 2007). This may highlight an uncertainty in atmospheric model predictions in coastal regions. Previous research, for instance Bradbury *et al.* (2004), has suggested that the English Channel itself is problematic for wind modelling due to difficulties representing the funnelling effect of shore parallel winds. In addition, the coarse temporal resolution of the input datasets may have contributed to the errors. In each of the datasets contrasted, the averaged time-series given from the two systems were broadly consistent; however short-term divergence in the magnitude and phase of the variable states, particularly during the storm conditions, was relatively large. The greatest divergence occurred during the event on the 14th November 2009. For instance, during this event the wind speed peak timing diverged by up to three hours, while the magnitude of the surge and H_s contained differences of more than 0.15 m and 1.3 m, respectively. The impact of the differences in the representations of this event upon the model predictions were more significant than those revealed when considering the averaged changes during the full comparison between October and December 2009. During this event, the use of the Met Office datasets increased the accuracy of the timing of the peak wind speed, surge and H_s events, relative to the predictions made using the Previmer data. Similarly, it also improved the accuracy of the magnitude of the peak surge elevation, more accurately recreating a secondary peak in the surge which was not contained in the

Previmer boundary conditions. Interestingly, the H_s peak magnitude was under-predicted, relative to *in-situ* measurements, when the Met Office datasets were used. In this case, the substitution of the Met Office datasets did not improve on the prediction accuracy relative to the Previmer-forced predictions. This may have been due to inaccuracies in the Met Office model boundary conditions. For instance, Bradbury *et al.* (2004) has also reported that the Met Office model under-predicted H_s when modelling conditions greater than 2.5 m at Hayling Island.

The evaluation of the Previmer datasets aided in establishing probable causes for some of the errors found in the regional model predictions. For instance, the under-prediction of the surge and wave peaks was likely to be partially attributed to the wind stress, which also under-predicted peaks in the time-series, relative to the Met Office datasets and *in-situ* measurements. The broad agreement between the datasets provides confidence in the Previmer system. However, the divergence during storm conditions is problematic due to the importance of these periods to coastal inundation. At present, the results suggest that the Met Office derived products provide a more accurate source of forcing for the regional model. The difference in temporal resolution, particularly in the wind and wave conditions (three hour and one hour in the Previmer and Met Office products, respectively), may have contributed to the lower accuracies in the Previmer datasets during storm events. The comparisons between the datasets have not only critiqued the Previmer products, they have also highlighted uncertainties in those supplied by the Met Office, such as the relatively large errors in the coastal wind predictions, and the under-prediction of the wave heights (corresponding well with previous research). Due to the importance of the shelf-scale model outputs to regional nested model predictions, these findings will be of relevance to those working in similar conditions, and those interested in the products available from the Previmer system.

7.3. Tide-surge-wave interactions

The influence of the tide-surge-wave interactions upon the model predictions was examined, with particular focus on the sensitivity of the wave and surge predictions to the tidal fluctuations. To quantify these interactions, simulations were conducted in which a variable of interest was excluded, and the resulting model output was contrasted to that obtained when the variable was included. Furthermore, the influence of the errors in the tidal amplitudes obtained from the regional model upon the surge and wave predictions were assessed by perturbing the tidal boundaries and examining the effects upon the model outputs.

This research was conducted for three reasons. Firstly, it enabled the quantification of local tide-surge-wave interactions in coastal environments, providing

broad insights to be made regarding the conditions which control the magnitudes of the interactions. Secondly, it quantified the degree to which errors in the modelled tidal elevations may propagate through the modelling system, due to tide-surge-wave interactions, despite their replacement, post-simulation, with harmonically derived tides. Finally, due to the relatively large proportion of the computational run-time dedicated to the wave component of the regional model, this research aimed to assess the importance of its inclusion by examining the contribution of the waves to the peak surge magnitudes.

During three events occurring on the 14th November 2009, the 29th November 2009, and the 10th March 2008, the tide-surge interaction resulted in alteration of the surge amplitude and timing. The largest changes to the peak surge conditions occurring at the Lymington and Southampton tide gauges during the event on 10th March 2008. Predicted peak surge elevations were altered by 9.9% and 11%, respectively, at the two tide gauges. The importance of the tide-surge interaction upon the combined water level elevations varied between the events considered. The most important factor was not just the change in the peak surge magnitude but also the alteration to the timing of the surge relative to the timing of the high tide. Tide-surge interactions induced alteration to the skew-surge and peak water level elevations by up to 30% and 10%, respectively, at the Southampton site. Brown and Wolf (2009) discussed the tide-surge interaction and its implications for coastal managers. They acknowledged that a combination of both magnitude and timing of the surge was important, and suggested that the skew-surge was a useful indicator of risk for coastal managers. The findings presented in this research demonstrated that accurate representation of the local tide-surge interaction can be essential in the provision of high quality flood warnings, particularly when the surge occurs on or near to the high tide. These results correspond with other studies indicating the importance of tide-surge interactions upon the magnitude and timing of surge events, including; Prandle and Wolf (1978), Wells *et al*. (2001), Horsburgh and Wilson (2007), Wolf (2009) and Brown *et al*. (2010).

The sensitivity of the wave predictions to the tidal input was greatest in the nearshore regions when the waves were at their highest. At the EMU Hayling Buoy, the peak H_s was altered by up to 16.3% due to the water level input. Where water levels increased, so too did the H_s and T_z, and *vice versa*. This corresponds with previous research by Chini *et al*. (2010) who found that the inclusion of tide-surge data was important in accurate prediction of H_s, as increased depths enabled waves to break later, resulting in larger wave heights in shallow regions. Alternatively, research has found that in depth-limited conditions waves will interact with the sea bed leading to linear and non-linear bottom dissipation mechanisms such as percolation, bed motion, shear stress, and scattering reducing the energy within the wave (Luo and Monbaliu,

1994; Padilla-Hernandez and Monbaliu, 2001; WISE group, 2002). The magnitude and variability in interaction corresponds with previous research in the southern North Sea (Tolman, 1991), and the English Channel and Irish Sea regions (Wu *et al.*, 1994). These studies found that that the inclusion of tides and currents had a relatively small influence upon mean wave parameters but that the effects were highly localised. The largest impacts were found in shallow regions during storm peaks in which changes of 10% were generally recorded, corresponding well with the 9.17% average change to the H_s event peak at the Emu Hayling Buoy.

Despite the relatively large influence of the exclusion of the tidal input upon the surge and wave predictions, the perturbations of the tide (representing the errors obtained in the regional model predictions) did not cause significant changes to the modelled states. For instance, the alteration to the tidal boundary during the 10th March 2008 event shifted the peak in the surge closest to the high tide by no more than 20 minutes, and did not change the skew-surge elevation by more than 4%. Similarly, the largest alteration to the peak wave H_s induced by the perturbation of the tidal elevations was 6%.

The sensitivity of the surge prediction to the influence of the state of the waves contained a high degree of spatial variability, with the largest changes to the surge peaks found at the gauges located in the eastern Solent and along the south west coast of the Isle of Wight, coinciding with the most extreme wave conditions. During the event on the 10th March 2008, the inclusion of the wave field led to an increase in predicted peak surge heights of up to 9.2% at the Emu Hayling Buoy, corresponding with previous research which has indicated that coupling of wave and hydrodynamic models can significantly alter the height of modelled surge elevations. Kim *et al.* (2010) found that extreme typhoon-induced surge events could not be modelled without the inclusion of wave radiation stresses which accounted for up to 40% of the surge elevation. The conditions of this particular event were extreme, with wave heights exceeding 18 m. Choi *et al.* (2003), Funakoshi *et al.* (2008) and Xie *et al.* (2008) reported changes to surge predictions of between 10 – 15% due to model coupling. In each case, the authors note that the influence of the waves upon the surge displayed high degrees of spatial variability. Mastenbroek *et al.* (1993) found both spatial and temporal variability in the change to the predicted surge, highlighting that in two of three independent events considered, the effect of the wave model was negligible, while in the third the increase to predicted surge heights was in the region of 5%. The spatial variability in the model sensitivity, correlating to the magnitude of the waves, as well as the 9.2% – 17% increase of peak surge heights at the Emu Hayling Buoy and along the south west coast of the Isle of Wight, are similar to those results given by Choi *et al.* (2003) under similar wave and surge conditions (e.g. H_s heights of 2.5–6 m and surge elevations of 1.5–2 m).

The results indicated that the tide-surge-wave interactions are of greatest relevance during storm events, while the influence can be highly localised. These findings correspond with previous research in other regions and will provide coastal modellers with indications regarding the contribution that the interactions will have upon model predictions, as well as highlighting the spatial and temporal variability in their magnitudes. The assessment of the sensitivity of the surge and wave predictions to the perturbations in the tidal elevations is relevant to current operational forecasts, in which it is common practice to replace modelled tides with those from harmonic analysis. This research has indicated that the errors from the tidal predictions will propagate through the system, due to tide-surge-wave interactions. However, these errors were shown to be relatively small, therefore, the current accuracy of the tidal models is not expected to be a limiting factor on the accuracy of the wave and surge predictions, even in complex estuarine systems such as the Solent. The results also indicated that the contribution of the waves upon the prediction of the surge is of greatest significance during storm events. This demonstrated that it would not be suitable to remove the wave model component from the regional prediction system in order to reduce computational run-time, even where wave damage to defence structures was considered to be insignificant. This was an important consideration to the latter stages of the research which attempted to provide probabilistic predictions. It will also be relevant to those working in regions experiencing low to medium exposure to waves, highlighting that the influence of HD-SW coupling may still provide significant contributions to surge elevation.

7.4. Empirical data-driven approaches to modelling, ensemble forecasts, and the Kalman filter

The application of an empirical data-driven approach to transforming offshore ocean states to the coastal regions of the Solent was examined. A regression model was utilised, the accuracies of which were assessed against *in-situ* measurements and predictions made using the MIKE-21-based regional model. Using the regression model, a probabilistic model forecast was described, randomly perturbing input datasets from pre-defined uncertainty distributions. The prediction also included a Kalman filter data assimilation step. An example event, with errors randomly distributed to the forcing datasets, was used to demonstrate the degree to which ensemble predictions and Kalman filtering could quantify uncertainty and improve the accuracy of the forecasts.

This portion of the research had two broad objectives. Firstly, previous literature has suggested that in some circumstances physically-based numerical models may not

be appropriate due to formulation uncertainty, in which case, data-driven approaches may provide more accurate predictions. Due to the complexity of the Solent, the application of a simple data-driven approach, such as regression, was of interest. Secondly, the use of probabilistic predictions to quantify uncertainty, and data assimilation to reduce it, are key research interests in operational oceanography. Therefore, this research attempted to describe a method by which ensemble predictions and a data assimilation step could be produced, within a time-frame suitable for short-term, real-time forecasting.

The regression models provided prediction accuracies containing little temporal or spatial variability during a two year assessment. The errors given in the surge and T_z predictions compared well with those expected from currently operational systems. At Portsmouth the regression contained an average error of 0.08 m while results available from POL (http://www.pol.ac.uk/ntslf/model.html) indicate that the operational storm surge model also contained an average RMSE of 0.08 m during the same period. Similarly, operational reports have stated that the the errors in wave predictions are commonly between 20 and 25% of the incident magnitude (NOAA Onlinehttp://polar.ncep.noaa.gov/waves/valid_wna.html; Bradbury *et al.*, 2004; Bidlot *et al.*, 2007), which corresponds well with the gauge average value of 16.9% from the regression model. The H_s prediction errors were in reasonable agreement, but slightly larger than those expected, with a gauge average error of 31%. The highest accuracies were found at Poole bay (23%).

The regression model predictions were similar to those obtained using the MIKE-21 model during the October and December 2009 period. For instance, gauge average RMSE in the surge was 0.1 m in both instances. At Lymington the regression predictions of H_s contained a lower Pbias than those obtained using the MIKE-21 model, indicating that the over-predictions (attributed in part to bathymetric uncertainty) could be reduced using the regression approach. However, the MIKE-21 models predicted a series of peak wave and surge magnitudes more accurately than the regression. These results indicated that for extreme events the current regression model may be too simplistic and require further development before recommendation as a suitable alternative to the MIKE-21-based model. On the other hand, the importance of the reduction in accuracies during storm events will depend on the application to which the models are assigned. For instance, the MIKE-21 model was able to provide an 8% and 3% increase in accuracy in the prediction of the peak magnitudes in the H_s and surge, respectively. Depending on the accuracy requirements of the forecasting system, the 3% difference in surge magnitudes may be acceptable. For instance, this indicates that during a 1 m surge event, the two model predictions, on average, would be expected to diverge by only 3 cm. Similarly, in regions where wave exposure is low, the 8% reduction in accuracy may also be acceptable.

The difference in computational demands between the two modelling approaches was considerable. For instance, using a single desktop computer with two 2.13 GHz processors and 4 GB of RAM, the regression model was able to provide a 24 hour forecast at 5 minute time steps, of surge, H_s and T_z at the same 20,000 points included in the MIKE-21 mesh, in less than 40 minutes. This was considerably faster than the 3.5 hours required by the coupled MIKE-21 HD and SW model to provide the same output.

The probabilistic predictions were created by drawing on uncertainty distributions representative of the errors in the input datasets, relative to *in-situ* measurements. The ability of the regression model to create large ensembles, within a short enough run time to allow for regular updating of the independent variables, is of valuable to coastal managers. In the example given, 6 hours prior to the event a modeller would predict a peak magnitude of 3.12 m, with a range of 0.4 m based upon the ensemble spread. However, updating a subsequent forecast with a start point 3 hours prior to the event, this prediction had changed to 3.21 m, with a range of only 0.28 m. Not only does this allow for increased accuracies and reduced ensemble spreads as the event draws nearer, it also enables quantification of expected magnitudes at given confidence levels. For example, at 3 hours prior to the event peak, analysis of the ensemble would allow a modeller to indicate that 90% and 95% of the ensembles predicted a magnitude of 3.33 m and 3.35 m respectively. The increase in the accuracy of the prediction, and the reduction to the uncertainty, was greatest in the short-term, with improvements largely negligible after 6 hours. The importance of the information from such techniques has been highlighted in other research. Flowerdew *et al*. (2007) discuss the development of a pilot scheme to update the current operational forecasting systems in the UK from deterministic to probabilistic systems, for example, while the migration of data assimilation strategies commonly used in atmospheric modelling into the oceanographic sector has been discussed increasingly over the last decade (Kalman, 1960; Lionello *et al*., 1995; Kantha and Clayson, 2000; Kobayashi and Yasuda, 2004; Neal, 2007).

The findings of these experiemnts have indicated that the use of a simple data-driven modelling approach could provide predictions of ocean state with comparable accuracies to those obtained using complex, computationally demanding models, in a fraction of the time. Furthermore, the benefits that could be obtained by utilising a computationally efficient forecast, for instance, the generation of large ensembles and the inclusion of data assimilation, at regular intervals (e.g. one hour), have been shown to provide valuable information to coastal managers interested in flood inundation. The relatively short duration of the reduction in prediction error obtained from data assimilation indicated that the techniques presented in this research will be of most use in the hours directly preceding a storm event. These findings will be of relevance to a wide modelling audience, particularly in the light of current trends towards

probabilistic modelling and the application of data assimilation techniques. The application of the computationally efficient empirical-based approach will be of most interest to coastal managers working in computationally poor regions, where the feasibility of running high resolution, data intensive models is low.

7.5. Limitations and future research

The research conducted in chapters three to six have enabled the aims set out in the introduction to be met. The findings revealed in the thesis are expected to be of particular interest to ocean modellers working in complex estuarine environments, and relate to current research interests in ocean forecasting. The errors in the modelled tidal elevations, the increase to accuracies derived using harmonic analysis, and the assessment of the significance of expected tidal errors upon surge and wave states, will indicate to modellers in similar conditions that the use of tidal substitution may often be best practice. Similarly, the findings related to the spatial variability in the model prediction accuracy, the influence of the input datasets, and the local coupling between the wave and water levels, is expected to provide valuable information to coastal modellers interested in the importance of input data uncertainty upon model predictions and the magnitudes of signal interactions expected in the variety of conditions found in coastal environments.

The evaluation of the Previmer data products, relative to those obtained from the operational forecasting system in the UK, and the expected uncertainty in the regional model predictions due to divergence between the datasets, will be of interest to those looking to use Previmer products, while the comparison of the empirical model predictions with those from the MIKE-21-based model will be of relevance to modellers working in regions where computational resources are limited. Furthermore, the demonstration of the ways in which probabilistic predictions and data assimilation strategies can quantify uncertainty and increase the accuracies of predictions, will support other research which has highlighted a recent desire to address uncertainty in model predictions using similar methods.

To expand upon the findings presented in this thesis, further research in three key areas could be conducted. Firstly, the time-series used could be extended. For instance, this research provided a comparison of Previmer and Met Office data products, and quantified the change to the model predictions that would result due to the divergence between them. Comparisons were made during a three month period between October and December 2009. The findings were able to demonstrate that on average the two systems provided broadly consistent datasets, indicating that during the period of interest in this research, the Previmer datasets were suitable for forcing the regional model. However, the greatest divergence occurred during storm

conditions. As only two significant events were present in the time-series considered, future research should extend the analysis presented in this thesis over longer time-series to assess if the two systems divergence consistently during storm events. This is particularly relevant to coastal flood forecasting where extreme ocean conditions are of most relevance. Furthermore, a 'dataset selection' uncertainty was used in this research, and although this provided a useful means of assessing the quality of the Previmer datasets, relative to those from a well-established system, it did not explicitly demonstrate which dataset was the most accurate; rather, it only implied the accuracy of one over the other by contrasting the predictions of the surge or waves (i.e. the dependant variable). Further analysis should not only extend the length of the analysis, but should also contrast both datasets against a measurement, prior to application to the model. However, this can be difficult as water level measurements are rarely located in offshore regions where the boundary conditions are supplied. The concept of 'dataset selection' uncertainty could also be extended in future work, perhaps considering a fusion of data inputs, in which an averaged input value based on a set of predictions from operational systems could be provided. Alternatively, where ensemble predictions are available, the inputs from both systems (and their ensemble distributions) could be used to define the boundary condition uncertainty distributions from which to draw upon.

Secondly, the presence of tide-surge, and HD-SW interaction was examined during a three month autumn period between October and December 2009 and during a relatively small set of storm events. The results indicated the magnitude and spatial variability of local signal interactions in the region, and provided evidence to suggest that current uncertainties in predicted tidal elevations were unlikely to lead to significant errors in wave and surge predictions. The largest interactions were shown to occur during storm periods, while significant variation between storm events was often found. Due to the variability between events, and the limited number of events considered, future research should apply the methodologies presented in this research to examine the interactions during a larger set of events. Furthermore, the regional model could be utilised, with a Monte Carlo approach, in which the relevant states (wave, surge and tidal elevations and phase) could be perturbed to create an ensemble of conditions in which the interactions could be examined, to more fully assess the interactions taking place, and their sensitivity to the relevant variables. Such research would not only validate the findings of this thesis, but would also be useful in predicting signal interactions in other regions where oceanographic conditions vary from those in the Solent.

Thirdly, in chapter six, a computationally efficient means of transforming offshore predictions to the nearshore regions was assessed in order to produce large ensembles of predictions for probabilistic forecasts, within time constraints suitable for real-time updating (e.g. one hour), where computational resources inhibited the

use of numerical models such as MIKE-21. This method was useful in removing the requirement for computationally demanding, high spatial resolution meshes in the nearshore region. However, this approach still required inputs provided by larger scale forecasting systems, such as Previmer, which may not be available to coastal managers in resource poor regions. Further research could examine the ways in which the requirement of the Previmer datasets could be removed. Establishing such an approach could be particularly useful to coastal managers without access to forecasts from systems such as Previmer. The work of Prouty (2007), in which an ANN was established utilising a series of *in-situ* tide gauges along the east coast of the UK, could be particularly relevant due to the relatively dense network of *in-situ* measurements along the south of the UK, and the common propagation of storm surges and waves through the English Channel from the North Atlantic, provided a substantial lead time could be obtained to enable warnings to be made and mitigation measures to be undertaken.

In a similar vein, this research highlighted that when one wishes to model throughout a complex region, such as the Solent, limitations may arise when using a point-based empirical model approach. Future research could examine this necessity in more detail, and expand the findings to a variety of coastal environments. For instance, when forecasting in a harbour in which an *in-situ* measurement in located (e.g. Portsmouth Harbour), it may be reasonable to assume that wave and surge conditions throughout the harbour are relatively constant. In such a situation the use of the empirical approach defined in this study may be suitable, particularly where large datasets (such as bathymetric surveys) are not available, limiting the development of suitable physically-based models. In such conditions, future research may wish to focus on increasing the accuracy of the empirical model predictions of storm events, shown in this research to be less accurate than those achieved using the physically-based model, likely due to the relatively simple nature of the liner regression approach used. The development of a more complex empirical model, while assessing the resulting alteration to computationally efficiency would be beneficial research to such regions. Alternatively, in complex regions such as the whole Solent-Southampton Water estuarine system, interpolation between point sources is unlikely to adequately represent the spatial variability in the system. In these instances, future research may be better off examining the best way to represent the spatial surface in the system, while minimising computational costs. In this research this limitation in the empirical model used was addressed by using the MIKE-21 model to inform of the spatial surface between gauged locations, due to the high degree of spatial variability in conditions throughout the region. However, this method contained inherent uncertainties relating to temporal variability in the spatial surface as it was defined as the relationship between each node and the four in-situ measurement sites was defined by the average during the event on the 14th November 2009 simulation, therefore assuming that the relationships between the nodes would be representative

at other times. However, this is likely to not always be the case. Research into the optimal way to represent variability in the spatial surface while retaining computational efficiency would be highly beneficial in this region. Future research may wish to examine this using a 'fusion' of the physical and empirical approaches in which the physically-based model may be simulated once, providing the initial forecast of the ocean state while a subsequent empirical model, such as the regression presented in this research, could then be used to define an ensemble, the spread of which could be applied to the original prediction. This would allow the user to sample from the uncertainty in the variables of interest (e.g. the boundary conditions), while retaining the benefits of using the physically-based model, without the vast computational requirements. Alternatively, the construction of an emulator of the physically-based model may achieve a similar goal by constructing relationships linking the physically-based model outputs throughout the domain with the independent input variables.

Future research into the development of a 'fused' modelling approach or emulator may also be of value in addressing the issues facing the empirical model when predicting very extreme events, particularly in the case where a wide range of such events are not available to train the empirical model. For instance, the data used to train the empirical surge model in this research contained only one event that would be considered very extreme (that occurring on the 10th March 2008). This can be problematic when attempting to predict events that lie beyond the limits of the training data, particularly in complex systems where the relationship between input and output variables may change as event magnitude increases. In the case of the surge, the empirical model defined in this research was predominantly based on events with magnitude between 0.5 and 0.8 m, and therefore, may become increasingly uncertain when making predictions beyond this range (due to known non-linearity, e.g. in the role of wind stress on the ocean surface) without further validation or re-training with a greater variety of more extreme events. To address this in the Solent future research should examine the accuracy of the current model to a larger number of very extreme events with further hindcasts, particularly at Portsmouth where long records exist. This would require the generation of Previmer datasets (as independent variables) for such periods, which was not available in the current research. In areas where long historical records are not available, the development of the 'fused' or emulator approaches may be preferable. Although a lack of extreme event datasets with which to train an empirical model will also hinder the validation of a physically-based model, the ability of the latter to represent the physics of the system, as well as validation of the formulations in other regions where such conditions may have been recorded, could provide more confidence when forecasting very extreme events. With concerns of increased storm magnitude in the future, due to global climate change, this is likely to be a particularly pertinent area of research.

Further research could also examine additional ways in which data assimilation could be implemented into such a system. In this research a relatively simple update was applied to the input datasets. Although this provided an effective short-term increase in accuracy, other techniques exist. For instance, the empirical model predictions of the state of the surge and waves in the Solent could be updated. A model could be established describing the covariance between the update time step and the subsequent time steps in the forecast. By doing so, an update applied at a given point could be applied to the remainder of the forecast, accounting for the likely reduction of the relevance of the measurement as temporal gap increases, in an attempt to increase the accuracy of the forecast.

Chapter 8: Conclusions

The research presented in this thesis has provided novel findings that will be of interest to coastal modellers working in a variety of regions, and from which further research can build upon. The key findings (detailed further in previous chapters) include:

- Previmer derived datasets were of comparable accuracy to those obtained from the Met Office, providing a valuable tool to future coastal modellers requiring forcing datasets. However, to more accurately define peak storm events, an increase in the temporal resolution beyond the 3 hours available in the research is required.
- HD model predictions become increasingly uncertain in the some of the shallowest regions of the domain. In such conditions the substitution of the modelled tides with those derived from harmonic analysis was shown to be best practice for operational forecasts of extreme water levels.
- Errors in the wave predictions, particularly in regions such as Lymington, were reduced partly through the alteration of the local bathymetry, while a consistent bias throughout the domain was correlated to errors in the wind field datasets. These results highlight the importance of high quality (accuracy and spatial resolution) atmospheric and bathymetric datasets, particularly in coastal regions, while also supporting previous research suggesting that current 3rd generation wave model formulations may be inaccurate in some very nearshore applications.
- Tide-surge-wave interactions were most significant during extreme storm events, clearly demonstrating that coupling of all three processes is vital in the provision of accurate model predictions. However, the propagation of the error in the system, due to the expected errors in the modelled tides upon the local tide-surge-wave interactions, was relatively small, indicating that current tidal prediction accuracy is unlikely to be a significant limiting factor on storm tide level and wave predictions in the region (assuming harmonic tidal substitution).
- A simple empirical model was shown to provide accuracies that were comparable with those obtained from the MIKE-21 regional model on average, although model development is required to address lower accuracies when modelling extreme events, while application suitability in other areas will be highly dependant upon the complexity of the region and the data available.
- The vastly reduced computational requirements associated with the empirical model allowed for the simulation of probabilistic forecasts with a near real-time data assimilation step. This was found to quantify and reduce uncertainty in short term forecasts.

The analysis conducted in this research has enabled the objectives established in the introduction to be met. In doing so, this work has provided information that will be of value to those working within the Solent region specifically, although many of the findings are applicable to other coastal environments and be of relevance to a wide modelling audience.

The findings provide two clear directions for future research. First, extension of the number of storm events examined would enable more robust conclusions, applicable in a wider variety of conditions, to be made when contrasting: the datasets provided by the Previmer and Met Office systems; the accuracy of the empirical model; and when examining the significance of the tide-surge-wave interactions in the region. In particular a Monte Carlo approach could be used to more fully sample the sensitivity of model outputs and the degree of tide-surge-wave interaction occurring during a wide range of storm conditions. Second, the utilisation of empirical approaches to forecasting in a variety of environments could be further developed. In broadly homogenous regions, such as harbours, where the use of a single *in-situ* measurement site is of value, further research could aim to increase the accuracy of the empirical model during storm events through the development of more complex empirical approaches than the linear regression used in this research, while also assessing the computational burden associated with additional complexity. Alternatively, in complex regions such as the Solent, where a physically-based model is required to adequately represent the spatial variability in ocean conditions, future research would be best focussed on finding the optimum method by which an emulator, or model 'fusion' could be devleoped in order to represent the spatial variability in the system and retain prediction accuracy during extreme events (particularly those not yet experienced in the region) while enabling the simulation of large ensembles without requiring excessive computational resources.

Appendix

A simple example of the Kalman filter update, after Neal (2007): The bucket of water

A television forecast says that rainfall will occur overnight to the amount of 4 cm, therefore $X_f = 4$.
The variance (V_f) associated with the forecast is 1.5 cm.
The bucket is placed outside overnight and is estimated the next morning by eye to contain 5 cm. Therefore, $X_o = 5$ cm.
With no other means to accurately measure this, the variance of this estimate is assumed to be 1 cm. Therefore, $V_o = 1$ cm.
The combination of both estimates is used to get the most accurate estimation using the Kalman filter:

$$K = P^f H^T (H P^f H^T + P^o)^{-1}$$

$$X^a = X^f + K(X^o - HX^f)$$

Where P_f is the error covariance matrix associated with the forecasted state vector, H is the measurement operator, ^{T} signifies a transpose of a matrix, P_o is a measurement noise covariance matrix describing covariance of the measurement errors, X_a is the analysed ('best guess') state, X_f is the forecasted state, K is the Kalman gain, X_o is the state measurement.

When considering only a single point case then the operator (H) equals 1 as the measure maps directly onto the model state. This means that the innovation matrix ($X_o - HX_f$) equals the difference between the measured and simulated state (which equates to $X_o - X_f = 1$).
For a point model K simplifies to $K = V_f / V_f + V_o$ (i.e. 1.5 / (1.5+1)) = 0.6.
The analysed estimate of X can then be given as:

$$X_a = X_f + K1$$

$$X_a = 4 + 0.6*1$$

$$X_a = 4.6$$

The variance of the analysed state estimate can also be calculated:

$$P_a = (I - KH) P_f (I - KH)^T + K P_o K^T$$

When applied to a single point bucket example this simplifies to:

$$V_a = V_f - K V_f$$

$$V_a = 1.5 - 0.6*1.5$$

$$V_a = 0.6$$

References

Allard, R., Dykes, J., Hsu, Y., Kaihatu, J., Conley, D., 2008. A real-time nearshore wave and current prediction system. Journal of Marine Systems. 69, 37-58.

Bacon, S., Carter, D., 1991. Wave climate changes in the North Atlantic and North Sea. International Journal of Climatology. 11, 545-558.

Bates, D., Watts, D., 1988. Nonlinear regression analysis and its applications. Wiley, New York.

Battjes, J., 2006. Developments in coastal engineering research. Coastal Engineering, 53, 121-132.

Battjes, J. and Gerritsen, H., 2002. Coastal modelling for flood defence. Philosophical Transactions of the Royal Society A: 360, 1461-1475.

Battjes, J.A., Janssen, J.P.F.M., 1978. Energy loss and set-up due to breaking of random waves. Proceedings of the 16th International Conference of Coastal Engineering, ASCE, 569-587.

Bazartseren, B., Hilderbrandt, G., Holz, K., 2003. Short-term water level prediction using neural networks and neuro-fuzzy approach. Neurocomputing, 55, 3-4, 439-450.

Bernier, N., Thompson, K., 2007. Tide-surge interaction off the east coast of Canada and northeastern United States. Journal of Geophysical Research, 112, C6, C06008, DOI: 10.1029/2006JC003793.

Beven, K.J., Binley, A.M., 1992. The future of distributed models: model calibration and uncertainty prediction. Hydrological Processes, 6, 279-298.

Bidlot, J., Li, J., Wittmann, P., Fauchon, M., Chen, H., Lefèvre, J., Bruns, T., Greenslade, D., Ardhuin, F., Kohno, N., Park, S., Gomez, M., 2007. Intercomparison of operational wave forecasting systems. 10th International workshop on wave hindcasting and forecasting and coastal hazard symposium, North Shore, Oahu, Hawaii, 11-16 Nov, 2007.

Bocquet, F., Flowerdew, J., Hawkes, P., Pullen, T., and Tozer, N., 2009. Probabilistic coastal flood forecasting: forecast demonstration and evaluation. Environment Agency

Report, SC050089, available online: http://publications.environment-agency.gov.uk. Last accessed: 15/11/2011.

Bolanos, R., and Sanchez-Arcilla, A., 2006. A note on nearshore wave features: Implications for wave generation. Progress in Oceanography, 70, 168-180.

Booij, N., Ris, R., Holthuijsen, L., 1999. A third-generation wave model for coastal regions: 1. Model description and validation. Journal of Geophysical Research, 104(C4), 7649-7666.

Boon, J., 2004. Secrets of the tide. Horwood Publishing, Chichester.

Bowden, K., 1983. Physical oceanography of coastal waters. Ellis Horwood Limited, Chichester.

Bradbury, A., Mason, T., Holt, M., 2004. Comparison of the performance of the Met Office UK-Waters Wave Model with a network of shallow water moored buoy data. 8th International Workshop on Wave Hindcasting and Forecasting, North Shore, Oahu, Hawaii, Nov 14-19 2004.

Brown, J., Wolf, J., 2009. Coupled wave and surge modelling for the eastern Irish Sea and implications for model wind-stress. Continental Shelf Research, 29, 1329 – 1342.

Brown, J., Souza, A., and Wolf, J., 2010. An 11-year validation of wave-surge modelling in the Irish Sea, using a nested POLCOMS-WAM modelling system. Ocean Modelling, 33, 1-2, 118-128.

Brown, J., Bolanos, R., Wolf, J., 2011. Impact assessment of advanced coupling features in a tide-surge-wave model, POLCOMS-WAM, in a shallow water application. Journal of Marine Systems, 87, 1, 13-24.

Butler, T., Altaf, M., Dawson, C., Hoteit, I., Luo, X., Mayo, T., 2012. Data assimilation within the Advanced Cireculation (ADCIRC) modelling framework for hurricane storm surge forecasting. Monthly Weather Review, 140, 7, 2215-2231.

Campbell, J., 2002. Introduction to remote sensing (3rd). Taylor and Francis: London.

Cañizares, R., Heemink, A., Vested, H., 1998. Application of advanced data assimilation methods for the initialisation of storm surge models. Journal of Hydraulic Research, 36, 4, 655-674.

Cañizares, R., Madsen, H., Jensen, H., Vested, H., 2001. Developments in operational shelf sea modelling in Danish Waters. Estuarine Coastal and Shelf Science. 53, 595-605.

Cheung, K., Phadke, A., Wei, Y., Rojas, R., Douyere, Y., Martino, C., Houston, S., Liu, P., Lynett, P., Dodd, N., Liao, S., and Nakazki, E., 2003. Modelling of storm induced coastal flooding for emergency management. Ocean Engineering, 30, 1353-1386.

Chini, N., Stansby, P., Leake, J., Wolf, J., Roberts-Jones, J., Lowe, J., 2010. The Impact of Sea Level Rise and Climate Change on Inshore Wave Climate: A Case Study for East Anglia (UK). Coastal Engineering, 57, 973 – 984.

Choi, B., Eum, H., and Woo, S., 2003. A synchronously coupled tide-wave-surge model of the Yellow Sea. *Coastal Engineering*, 47, 381-398.

Collins, J.I., 1972. Prediction of shallow water spectra. Journal of Geophysical Research, 102, C11, 25035-25046.

Conti, S., Gosling, J., Oakley, J., O'Hagan, A., 2009. Gaussian process emulation of dynamic computer codes. Biomerika, 96, 3, 663-676.

Conti, S., O'Hagan, A., 2010. Bayesian emulation of complex multi-output and dynamic computer models. Journal of Statistical Planning and Inference, 140, 640-651.

Cooper, N.J., 2005. Wave dissipation across intertidal surfaces in the Wash tidal inlet, eastern England. Journal of Coastal Research, 21, 1, 28-40.

Cox, D., Tissot, P., Michaud, P., 2002. Water level observations and short-term predictions including meteorological events for entrance of Galveston Bay, Texas. Journal of Waterway Port Coastal and Ocean Engineering, 128, 1, 21-29.

Crapolicchio, R., De Chiara, G., Elyouncha, A., Lecomte, P., Neyt, X., Paciucci, A., Talone, M., 2012. ERS-2 Scatterometer: Mission performance and current reprocessing achievements. IEEE Transactions on Geoscience and Remote Sensing, 50, 7, 2427-2448.

Davis, J., Paramygin, V., Forrest, D., and Sheng, Y., 2010. Toward the probabilistic simulation of storm surge and inundation in a limited resource environment. Monthly Weather Review, 138, 2953-2974.

Davies, A., Lawrence, J., 1994. Examining the influence of wind and wind-wave turbulence on tidal currents, using a 3-dimensional hydrodynamic model including wave-current interaction. Journal of Physical Oceanography, 24, 12, 2441-2460.

DEFRA, 2004. National assessment of defence needs and costs for flood and coastal erosion management (NADNAC): Summary report. Available online: http://www.defra.gov.uk/environ/fcd/policy/nadnac0604.pdf. Last accessed: 24/06/2008.

Delft University, 2008. SWAN Technical Documentation. Available online: http://www.fluidmechanics.tudelft.nl/swan/index.htm. Last accessed: 01/08/2008.

Deo, M., Naidu, C., 1999. Real time wave forecasting using neural networks. Ocean Engineering, 26, 3, 191-203.

DHI., 2009(a). MIKE-21 Flow model FM hydrodynamic model user guide. Document available online from: *http://www.mikebydhi.com/Download*

DHI., 2009(b). MIKE-21 and MIKE 3 Flow Model FM, Hydrodynamic and transport module scientific documentation. Document available online from: *http://www.mikebydhi.com/Download*

DHI., 2009(c). MIKE-21 Spectral wave module, scientific documentation. Document available online from: *http://www.mikebydhi.com/Download*

Dix, J., Lambkin, D., Cazenave, P., 2007. Development of a regional sediment mobility model for submerged archaeological sites. English Heritage ALSF project no.5524. School of Ocean and Earth Science. University of Southampton, U.K. 156ppLevasuer 2008).

Doodson, A., 1922. The harmonic development of the tide-generating potential. Proc. Roy. Soc. London, Ser. A 100, 305-329.

Ducarne, B., Venedikov, A., Arnoso, J., and Vieria, R., 2006. Analysis and prediction of ocean tides by the computer program VAV. *Journal of Geodynamics*, 41, 119-127.

Dunlop, E., Olsen, R., Wilson, L., De Margerie, S., and Lalbeharry, R., 1998. The effect of assimilating ERS-1 fast delivery wave data into the North Atlantic WAM model. Journal of Geophysical Research, 103, 7901-7915.

Dyke, P., 1996. Modelling marine processes. Prentice Hall: Hertfordshire

Eldeberky, Y., Battjes, J.A., 1995. Parameterization of triad interactions in wave energy models. Paper presented at Coastal Dynamics Conference, ASCE, Poland.

Eldeberky, Y., Battjes, J.A., 1996. Spectral modelling of wave breaking. Application to Boussinesq equations. Journal of Geophysical Research, 101, C1, 1253-1264.

Environment Agency, 2007. Building and maintaining river and coastal flood defences in England. The Stationary Office, London.

Environment Agency, 2009a. Investing for the future. Flood and coastal risk management in England: A long-term investment strategy. Available for download online at: http://www.environment-agency.gov.uk/research/library/publications/108673.aspx.

Environment Agency., 2009b. UK Coastal Monitoring and Forecasting (UKCMF) Service – Strategy for 2009 to 2019. Available to download online at: *http://publications.environment-agency.gov.uk/pdf/GEH01009BRFE-e-e.pdf.*

Evans, E., 2004. Foresight : Scientific summary. Volume ii, managing future risks. Office of Science and Technology, London.

Evans, D., Alpers, W., Cazenave, A., Elachi, C., Farr, T., Glackin, D., Holt, B., Jones, L., Liu, T., McCandless, W., Menard, Y., Moore, R., Njoku, E., 2005. Seasat – a 25-year legacy of success. Remote Sensing of Environment, 94, 3, 384-404.

Evensen, G., 1994. Sequential data assimilation with a nonlinear quasi-geostrophic model using Monte Carlo methods to forecast error statistics. Journal of Geophysical Research, 99 (C5), 10143-10162.

Evensen, G., 2002. Sequential data assimilation for nonlinear dynamics: The Ensemble Kalman Filter. In: Pinardi, N., and Woods, J., Eds. Ocean Forecasting: conceptual basis and applications. Springer: Berlin.

Evensen, G., 2003. The Ensemble Kalman Filter: theoretical formulation and practical implementation. *Ocean Dynamics*, 53, 343-367.

FEMA., 2001. MIKE-21 modelling System. Document available online from FEMA at: *http://www.fema.gov/pdf/fhm/frm_mike.pdf.* Last accessed: 25/11/2010.

Flather, R., 1994. A storm surge prediction model for the Northern Bay of Bengal with application to the cyclone disaster in April 1991. Journal of Physical Oceanography, 24(1), 172-190.

Flather, R., 2000. Existing operational oceanography. Coastal Engineering. 41, 13-40.

Fletcher, S., Johnson, D., Hewett, T., 2007. Coastal management in the Solent: An introduction. Marine Policy. 31, 585-590.

Flowerdew, J., Hawkes, P., Mylne, K., Pullen, T., Saulter, A., Tozer, N., 2007. Coastal flood forecasting: model development and evaluation. Available online: http://publications.environment-agency.gov.uk. Last accessed: 10/12/2011.

Foreman, S., Holt, M., and Kelsall, S., 1994. Preliminary assessment and use of the ERS-1 altimeter wave data. Journal of Atmospheric and Ocean Technology, 11, 1370-1380.

Foresight, 2004. Future flooding: executive summary. Available online: http://www.foresight.gov.uk/Flood%20and%20Coastal%20Defence/executive_summary.pdf. Last accessed: 14/07/2008.

Fu, L., Christensen, E., Yamarone, C., Lefebvre, M., Menard, Y., Dorrer, M., Escudier, P., 1994. TOPEX/ POSEIDON mission overview. Journal of Geophysical Research, 99, C12, 24369-81.

Funakoshi, Y., Hagan, S., Bocopoulos, P., 2008. Coupling of hydrodynamic and wave models: case study for Hurricane Floyd (1999) Hindcast. Journal Waterw. Port Coast. Ocean Eng. Doi:10.1061/(ASCE)0733-950x(2008)134:6(321)

Gerritsen, H., 2005. What happened in 1953? The big flood in the Netherlands in retrospect. Philosophical Transactions of the Royal Society, A. 363, 1271-1291.

Graber, H., Cardone, V., Jensen, R., Slinn, D., hagen, S., Cox, A., Powell, M., Grassl, C., 2006. Coastal forecasts and storm surge predictions for tropical cyclones: a timely partnership program. Oceanography, 19, 1, 130-141.

Greenslade, D., 2001. The assimilation of ERS-2 significant wave height data in the Australian region. Journal of Marine Systems, 28, 141-160.

Haigh, I., Butcher, P., Harris, J., Cooper, N., Trip, I., 2004. Developing an improved understanding of storm surges in the Solent. In 39th DEFRA flood and coastal management conference, York, UK.

Haigh, I., Nicholls, R., Wells, N., 2009. Mean sea levels around the English Channel over the 20th Century and their wider context. Continental Shelf Research 29. 2083-2098.

Haigh, I., Nicholls, R., Wells, N., 2010. Assessing changes in extreme sea levels: Application to the English Channel, 1900 – 2006. Continental Shelf Research, 30, 1042-1055.

Haigh, I., Nicholls, R., and Wells, N., 2011. Rising sea levels in the English Channel 1900 to 2100. Proceedings of the ICE Maritime Engineering, 164, 2, 81-92.

Hall, P., Sayers, P., Walkden, M., Panzeri, M., 2006. Impacts of climate change on coastal flood risk in England and Wales: 2030-2100. Philosophical Transactions of the Royal Society A. 364, 1027-1049.

Hamill, T., 2001. Interpretation of rank histograms for verifying ensemble forecasts. Monthly Weather Review, 129, 550- 560.

Hammersley, J., Handscomb, D., 1964. Monte Carlo methods. London: Methuen and Co ltd.

Hampshire County Council, 2006. The Hampshire Coast. Available Online: http://www3.hants.gov.uk/coastpage/facts-figures.htm. Last accessed: 20/03/2012.

Hasselmann, K., 1962. On the nonlinear energy transfer in a gravity-wave spectrum, Part 1, General theory. Journal of Fluid Mechanics, 12, 481-500.

Hasselmann, K., Barnett, T.P., Bouws, E., Carlson, H., Cartwright, D.E., Enke, K., Ewing, J.A., Gienapp, H., Hasselmann, D.E., Krusemann, P., Meerburg, A., Muller, P., Olbers, D.J., Richter, K., Sell, W., Walsen, H., 1973. Measurements of wind-wave growth and swell decay during the Joint North Sea Wave Project (JONSWAP). Deutsches Hydrographisches Institut. Available online: http://repository.tudelft.nl/view/hydro/uuid%3Af204e188-13b9-49d8-a6dc-4fb7c20562fc/. Accessed 04/04/2013.

Hasselmann, K., 1974. On the spectral dissipation of ocean waves due to whitecapping. Boundary Layer Meteorology, 6, 107-127.

Hasselmann, S., Hasselmann, K., 1985a. Computation and parameterizations of non-linear energy transfer in a gravity-wave spectrum, Part 1: A new method for efficient computations of the exact non-linear transfer integral. Journal of Physical Oceanography, 15, 1369-1377.

Hasselmann, S., K. Hasselmann, J. H. Allender and T. P. Barnett, 1985b. Computations and parameterizations of the non-linear energy transfer in a gravity-wave spectrum. Part II: Parameterizations of the non-linear energy transfer for application in wave models. Journal of Physical Oceaonography, 15, 1378-1391.

Hasselmann, S., Hasselmann, K., Bauer, E., Janssen, P., Komen, G., 1988. The WAM mode – a third generation ocean wave prediction model. Journal of Physical Oceanography, 18, 12, 1775 – 1810.

Hawkes, P., Tozer, N., Pullen, T., Scott, A., Flowerdew, J., Mylne, K., Xavier – Bocquet, F., Horsburgh, K., 2009. Probabilistic coastal flood forecasting. Paper presented at 44th Defra flood and coastal management conference, Telford, UK.

de las Heras, M.de las., Burgers, G., and Janssen, P., 1995. Wave data assimilation in the WAM wave model. Journal of Marine Systems, 6, 77-85.

Herzfeld, M., Waring, J., Parslow, J., Margvelashvili, N., Sakov, P., Andrewartha, J., 2002. MECO: model for estuaries and coastal oceans, scientific manual. CSIRO Marine Research.

Hodur, R., 1997. The naval research laboratory's coupled ocean / atmosphere mesoscale prediction system (COAMPS). Monthly Weather Review, 125, 1414-1430.

Holt, J.T., and James, I.D., 2001. An s coordinate density evolving model of the northwest European continental shelf: 1, model description and density structure. Journal of Geophysical Research, 106, 14015-14034.

Horsburgh, K., Wilson, C., 2007. Tide-surge interaction and its role in the distribution of surge residuals in the North Sea. Journal of Geophysical Research. 112, C08003, doi:10.1029/2006JC004033.

Houghton, J., 2005. Global Warming. Reports on progress in physics, 68, 1343-1403.

House of Commons- committee of public accounts, 2007. Environmental Agency: building and maintaining river and coastal flood defences in England. The Stationary Office: London. Available online: http://www.parliament.the-stationery-office.co.uk/pa/cm200708/cmselect/cmpubacc/175/175.pdf. Last accessed: 14/07/2008.

Hsiao, S.V., Shemdin, O.H., 1978. Bottom dissipation in finite-depth water waves. Proceedings of the 16th International Conference of Coastal Engineering, ASCE, 434-448.

Hsu, T., Ou, S., and Liau, J., 2005. Hindcasting nearshore wind waves using a FEM code for SWAN. Coastal Engineering, 52, 177-195.

Huang, W., Murray, C., Kraus, N., Rosati, J., 2003. Development of a regional neural network for coastal water level predictions. Ocean Engineering, 30, 17, 2275-2295.

Hunt, J., 2005. Inland and coastal flooding: developments in prediction and prevention. Philosophical Transactions of the Royal Society A. 363, 1475-1491.

Inter-Agency Committee on Marine Science and Technology, 2004. UK marine waters 2004: Marine Processes and Climate. Available online at: http://www.oceannet.org/library/publications/documents/marine_processes_and_climate.pdf. Last accessed: 25/10/2010.

Isle of Wight Council., 2005. A case study documenting the UK south-east regional strategic coastal monitoring programme. Available online: http://www.interreg-messina.org/documents/Component%202/MESSINA%20-%20Component%202%20-%20Case-Study%20-%20Strategic%20Monitoring.pdf. Last Accessed: 01/08/2011.

Janssen, P.A.E.M., 1989. Wave induced stress and the drag of airflow over sea waves. Journal of Physical Oceanography, 19, 745-754.

Janssen, P.A.E.M., 1991. Quasi-linear theory of wind wave generation applied to wave forecasting. Journal of Physical Oceanography, 21, 1631-1642.

Janssen, P., 2004. The Interaction of Ocean Waves and Wind. Cambridge University Press: Cambridge.

Janssen, P., 2008. Progress in ocean wave forecasting. Journal of Computational Physics, 227, 3572-3594.

Johnson, H., Kofoed-Hansen, H., 2000. Influence of Bottom Friction on Sea Surface Roughness and its Impact on Shallow Water Wind Wave Modelling. Journal of Physical Oceanography, 30, 1743 - 1756.

Jones, J., Davies, A., 2007a. On the sensitivity of tidal residuals off the west coast of Britain to mesh resolution. Continental Shelf Research. 27, 64-81.

Jones, J., and Davies, A., 2007b. A high resolution finite element model of the M2, M4, M6, S2, N2, K1 and O1 tides off the west coast of Britain. Ocean Modelling, 19, 70-100.

Jones, I.S.F., Toba, Y., 2001. Wind stress over the ocean. Cambridge University Press.

Jonsson, I.G., Carlsen, N.A., 1976. Experimental and theoretical investigations in an oscillatory turbulent boundary layer. Journal of Hydraulic Research, 14, 1, 45-60.

Kalman, R., 1960. A new approach to linear filtering and prediction problems. *Transactions of the ASME- Journal of Basic Engineering* 82D, 35-45.

Kantha, L., Clayson, C., 2000. Numerical models of oceans and oceanic processes. Academic Press: San Diego.

Kennedy, M., O'Hagan, A., 2000. Predicting the output from a complex computer code when fast approximations are available. Biometrika, 87, 1, 1-13.

Kim, S., Yasuda, T., Mase, H., 2010. Wave set-up in the store surge along open coasts during Typhoon Anita. Coastal Engineering, 57, 631-642.

Kinsman, B., 1965. Wind waves: their generation and propagation on the ocean surface. Prentice-Hall: Englewood.

Knauss, J., 1996. Introduction to physical oceanography (2nd). Pearson: New Jersey.

Ko, D., Martin, P., Rowley, C and Preller, R., 2008. A real time ocean prediction experiment for MREA04. Journal of Marine Systems, 69, 17-28.

Kobayashi, T., Yasuda, T., 2004. Nearshore wave prediction by coupling a wave model and statistical methods. Coastal Engineering, 51, 297-308.

Komen, G.J., Cavaleri, L., Donelan, M., Hasselmann, K., Hasselmann, S., Janssen, P.A.E.M., 1994. Dynamics and modelling of ocean waves. Cambridge University Press.

Krogstad, H., and Barstow, S., 1999. Satellite wave measurements for coastal engineering applications. Coastal Engineering, 37, 283-307.

Lam, N., 1983. Spatial interpolation methods: a review. The American Cartographer, 10(2), 129-150.

Lamb, H., 1932. Hydrodynamics. Cambridge University Press: New York.

Law, C., 1975. Storm surges in the English Channel. Hydrographic Journal, 2, 30-34.

Lazure, P., and Dumas, F., 2008. An external-internal mode coupling for a 3D hydrodynamical model for applications at regional scale (MARS). Water Resources, 31, 233-250.

Levasseur, A., 2008. Observations and modelling of the variability of the Solent-Southampton Water estuarine system. Thesis for the degree of Doctor of Philosophy. School of Ocean and Earth Science. University of Southampton. Available online: http://eprints.soton.ac.uk/63761/01/Levasseur_2008_PHD.pdf.

Lin, W., Sanford, L., Suttles, S., 2002. Wave measurement and modeling in Chesapeake Bay. Continental Shelf Research, 22, 18-19, 2673-2686.

Lionello, P., Gunther, H., Hansen, B., 1995. A sequential assimilation scheme applied to global wave analysis and prediction. Journal of Marine Systems, 6, 87-107.

Liu, P., Schwab, D., and Jensen, R., 2002. Has wind wave modelling reached it limit? Ocean Engineering, 29, 81-98.

Logemann, K., Backhaus, J., Harms, I., 2004. SNAC: a statistical emulator of the north-east Atlantic circulation. Ocean Modelling, 7, 1-2, 97-110.

Longley, P., Goodchild, M., Maguire, D., and Rhind, D., 2005. Geographic Information Systems and Science (2nd). Wiley and Sons: Chichester.

Luettich, R., Westerink, J., 2004. Formulation and numerical implementation of the 2D/3D ADCIRC finite element model version 44.X. Available Online: http://adcirc.org/adcirc_theory_2004_12_08.pdf. Last accessed: 23/08/2012.

Luo, W. and Monbaliu, J., 1994. Effects of the bottom friction formulation on the energy balance for gravity waves in shallow water. Journal of Geophysical Research, 99, C9, 18501 – 18511.

Madsen, O.S., Poon, Y.K., Graber, H.C., 1988. Spectral wave attenuation by bottom friction: Theory. Proceedings of the 21st International Conference of Coastal Engineering, ASCE, 492-504.

Madsen, H., and Canizares, R., 1999. Comparison of extended and ensemble Kalman Filters for data assimilation in coastal area modelling. International Journal for Numerical Methods in Fluids, 31, 961-981.

Madsen, H., Jakobsen, F., 2004. Cyclone induced storm surge and flood forecasting in the northern Bay of Bengal. Coastal Engineering. 5, 277-296.

Marchuk, G., and Kagan, B., 1984. Ocean tides: mathematical models and numerical experiments. Pergamon Press: Oxford.

Mason, R., Gunst, R., Hess, J., 2003. Statistical Design and Analysis of Experiments. Wiley- Interscience, New Jersey.

Mastenbroek, C., Burgers, G., Janssen, P., 1993. The dynamical coupling of a wave model and a storm-surge model through the atmospheric boundary-layer. Journal of Physical Oceanography, 23, 8, 1856-1866.

Mattocks, C., and Forbes, C., 2008. A real-time, event-triggered storm surge forecasting system for the state of North Carolina. Ocean Modelling, 25, 95-119.

Maybeck, P., 1979. Stochastic models, estimation and control, Volume 1. Academic Press: New York

McLaughlin, D., 2002. An integrated approach to hydrologic data assimilation: interpolation, smoothing, and filtering. Advances in Water Resources, 25, 1275-1286.

Miles, J., 1957. On the generation of surface waves by shear flows. Journal of Fluid Mechanics, 3, 185-204.

Miller, R., 1985. Optimal estimation and the Kalman Filter for numerical ocean forecast modelling. In: Gulf Stream Workshop Proceedings. University of Rhode Island. Watts, D., Ed.

Moeini, M., Etemad-Shahidi, A., 2007. Application of two numerical models for wave hindcasting in Lake Erie. Applied Ocean Research, 29(3), 137-145.

Möller, I., Spencer, T., French, J.R., Leggett, D.J., Dixon, M., 1999. Wave transformation over salt marshes: A field and numerical modelling study from North Norfolk, England. Estuarine, Coastal and Shelf Science, 49, 411-426.

Moon, I.J., Kwon, J.I., Lee, J.C., Shim, J.S., Kang, S.K., Oh, I.S., Kwon, S.J., 2009. Effect of the surface wind stress parameterization on the storm surge modelling. Ocean Modelling, 29, 115 – 127.

Moulinec, C., Denis, C., Pham, C.T., Rouge, D., Hervouet, J.M., Razafindrakoto, E., Barber, R.W., Emerson, D.R., Gu, X.J., 2011. TELEMAC: An efficient hydrodynamic suite for mqassively parallel architectures. Computers and Fluids, 51, 30-34.

Neal, J., 2007. Flood forecasting and adaptive sampling with spatially distributed dynamic depth sensors. PhD Thesis, University of Southampton, UK.

Oakley, J., O'Hagan, A., 2004. Probabilistic sensitivity analysis of complex models: a Bayesian approach. Journal of the Royal Statistics Society, Series B (Statistical Methodology), 66, 3, 751-769.

O'Hagan, A., 2006. Bayesian analysis of computer code outputs: A tutorial. Reliability Engineering and System Safety, 91, 10-11, 1290-1300.

Open University, 1989. Waves, tides and shallow-water processes. Open University: Milton Keynes.

Padilla-Hernández, R. and Monbaliu, J., 2001. Energy balance of wind waves as a function of the bottom friction formulation. Coastal Engineering 43, 131-148.

Palmer, T., 2011. Energetic swell waves in the English Channel. Thesis for the degree of Doctor of Philosophy. School of Civil Engineering and the Environment, University of Southampton, UK.

Pawlowicz, R., Beardsley, B., Lentz, S., 2002. Classical tidal harmonic analysis including error estimation in Matlab using T_TIDE. Computers and Geosciences, 28, 929-937.

Peng, S., Xie, L., and Pietrafessa, L., 2007. Correcting the errors in the initial conditions and wind stress in storm surge simulation using an adjoint optimal technique. Ocean Modelling, 18, 175-193.

Penning-Rowsell, E., Johnson, C., Tunstall, S., 2006. Signals from pre-crisis discourse: lessons from UK flooding for global environmental policy change. Global Environmental Change. 16, 323-339.

Persson, A., Grazzini, F., 2007. User guide to ECMWF forecast products. Available online: http://www.ecmwf.int/products/forecasts/guide/index.html. Accessed: 24/08/2012.

Phillips, O., 1957. On the generation of waves by turbulent wind. Journal of Fluid Mechanics, 2, 417-445.

Prandle, D., 2000. Introduction: Operational oceanography in coastal waters. Coastal Engineering, 41, 3-12.

Prandle, D., Wolf, J., 1978. Surge-tide interaction in the southern North Sea. In: Nihaul, J., ed. Hydrodynamics of Estuaries and Fjords. Proceedings of the 9th International Liege Colloquium on Ocean Hydrodynamics. Elsevier.

Prouty, D., 2007. Using artificial neural networks to predict storm surge in the North Sea and the Thames Estuary. PhD Thesis, University of Southampton, UK.

Pugh, D., 1987. Tides, surges and mean sea-level: a handbook for engineers and scientists. Wiley, Chichester, 472pp.

Pugh, D., 2006. Changing sea levels. Cambridge University Press: UK

Rantzen, M., 1969. English Channel tides. Adlord Coles Ltd, London.

Ris, R.C., 1997. Spectral modelling of wind waves in coastal areas. PhD. Thesis, Delft University, 1997.

Ris, R., Holthuijsen, L., Booij, N., 1999. A Third Generation Wave Model for Coastal Regions, 2: Verification. Journal of Geophysical Research. 104, C4, 7667 – 7681.

Rogers, E., Hwang, P., Wang, D., 2002. Investigation of wave growth and decay in the SWAN model: three regional-scale applications. Journal of Physical Oceanography, 33, 366-389.

Rossiter, J., 1961. Interaction between tide and surge in the Thames. Geophysical Journal of the Royal Astronomical Society, 6, 1, 29-53.

Royston, S., Horburgh, K., Lawry, J., 2012. Application of rule based methods to predicting storm surge. Continental Shelf Research, 37, 79-91.

Rugbjerg, M., Sørensen, O.R., Jacobsen, V., 2006. Wave forecasting for offshore wind farms (MIKE 21 SW). Paper presented at the 9th International Workshop on Wave Hindcasting and Forecasting, Victoria, b.C., Canada, 24-29.

Ruocco, A., Nicholls, R., Haigh, I., Wadey, M., 2011. Reconstructing coastal flood occurance combining sea level and media sources: a case study of the Solent, UK since 1935. Natural hazards, 59, 3, 1773-1796.

Saulter, A., 2007. Met Office and National Centre for Ocean Forecasting capability statement: wave forecast and consulting services. Available online: www.ncof.co.uk/documents.htm?parents=106. Last accessed: 10/01/2012.

Sfetsos, A., 2002. A novel approach for the forecasting of mean hourly wind speed time series. Renewable Energy, 27, 2, 163-174.

Shennan, I., Milne, G., Bradley, S., 2012. Late Holocene vertical land motion and relative sea-level change: lessons from the British Isles. Journal of Quaternary Science, 27(1), 64-70.

Siddons, L., Wyatt, L., and Wolf, J., 2008. Assimilation of HF radar data into the SWAN wave model. Journal of Marine Systems, doi:10.1016/j.jmarsys.2007.12.017.

Siek, M., Solomatine, D., 2011. Real-time data assimilation for chaotic storm surge model using NARX neural network. Journal of Coastal Research, 64, 1189-1194.

Sleath, J.F.A., 1984. Sea bed mechanics. John Wiley and Sons, New York.

Smagorinsky, J., 1963. General circulation experiment with primitive equations. Monthly Weather Review, 91, 3, 99-164.

Smith, K., Ward, R., 1998. Floods: Physical Processes and Human Impacts. John Wiley and Sons, Chichester.

Snyder, R., Dobson, F., Elliot, J., and Long, R., 1981. Array measurements of atmospheric pressure fluctuations above surface gravity waves. Journal of Fluid Mechanics, 102, 1-59.

Sørensen, O., Schaffer, H., and Sørensen, L. 2004. Boussinesq-Type Modelling using an Unstructured Finite Element Technique. Coastal Engineering, 50, 181-198.

Sørensen, O., Kofoed-Hansen, H., Rugbjerg, M., and Sørensen, L.S., 2004. A Third-generation spectral wave model (MIKE 21 SW) using an unstructured finite volume techniwue. In Proceedings of the 29th International Conference on Coastal Engineering.

Sørensen, O., Kofoed-Hansen, H., and Jones, O., 2006. Numerical Modelling of Wave-current Interaction in Tidal Areas using an Unstructured Finite Volume Technique (MIKE 21 SW). Paper presented at ICCE 2006.

Spencer, T., and French, J., 1993. Coastal flooding: transient and permanent. Geography, 78, 179-182.

Steabs, C., and Bauer, E., 1998. Statistical comparison of global significant wave heights from Topex and ERS-1 altimeter and from operational wave model WAM. Phys. Chem. Earth, 23(5), 581-585.

Steidley, C., Sadovski, A., Tissot, P., Bachnak, R., Bowles, Z., 2003. Using an artificial neural network to improve predictions of water levels where tide charts fail. Innovations in Applied Artificial Intelligence, Lecture notes in Artificial Intelligence, 3533, 599-608.

Stern, N., 2007. The economics of climate change: the Stern review. New York: Cambridge University Press. Also available online: http://www.hm-treasury.gov.uk./independent_reviews/stern_review_economics_climate_change/stern_review_report.cfm. Last accessed: 24/04/2011.

Thurman, H.V., 1988. Introductory Oceanography. Merrill Publishing Company.

Tilburg, C., Garvine, R., 2004. A simple model for coastal sea level prediction. Weather and Forecasting, 19, 3, 511-519.

Tolman, H., 1990. The influence of unsteady depths and currents of tides on wind-wave propagation in shelf seas. Journal of Physical Oceanography, 20, 8, 1166-1174.

Tolman, H,. 1991. Effects of tides and storm surges on North Sea wind waves. Journal of Physical Oceanography, 21, 6, 766 - 781.

Tolman, H., 2009. User manual and system documentation of WAVEWATCH III version 3.14. NOAA/NWS/NCEP/MMAB Technical Note 276, 194 pp. Available online: http://polar.ncep.noaa.gov/waves/wavewatch/wavewatch.shtml. Accessed: 24/08/2012.

Tozer, N., Saulter A. and Hawkes, P., 2007. Coastal flood forecasting. 42nd DEFRA Flood and Coastal Management Conference, University of York, 3rd to 5th July.

Tucker, M., 1991. Waves in Ocean Engineering: measurement, analysis, interpretation. Ellis Horwood Limited: Chichester.

Vatvani, D. K., Gerritsen, H., Stelling, G. S. and Krishna Rao, A. V. R. 2002 Cyclone-induced storm surge and flood forecasting system for India. In Proc. Int. Conf. Solutions to Coastal Disasters, San Diego, February 2002, pp. 473–487. Reston, VA: ASCE

Velegrakis, A., 2000. Geology, geomorphology and sediments of the Solent system, In: Collins, M., and Ansell, K., (Ed.) 2000. Solent science: a review, Proceedings in Marine Science, 1, 21–43.

Vilsmeier, R., and Hänel, D., 1995. Adaptive solutions for unsteady laminar flows on unstructured grids, Int. J. Numer. Meth. Fluids, Vol 22, 85–101.

Voorrips, A., 1999. Spectral wave data assimilation for the prediction of waves in the North Sea. Coastal Engineering, 37, 455–469.

Wadey. M., Nicholls, R., Hutton, C., 2012. Coastal flooding in the Solent: An integrated analysis of defences and inundation. Water, 4, 430–459.

Warren, I. and Bach, H., 1992. MIKE 21: a modelling system for estuaries, coastal waters and seas. Environmental Software, 7, 4, 229–40.

Weber, S.L., 1991. Bottom friction for wind sea and swell in extreme depth-limited situations. Journal of Physical Oceanography, 10, 1712,1733.

Wells, N., Baldwin, D., Wang, J., Collins, M., 2001. Modelling of extreme storm surge in the English Channel for the period 14–18 December 1989. The Global Atmosphere and Ocean System. 7, 4, 275–294.

Williams, J., Wilson, C., Horsburgh, K., 2008. Data assimilation tests using NISE10 storm surge model. POL Internal document, 188. Available online: http://nora.nerc.ac.uk/5428/1/id188.pdf. Accessed: 24/08/2012.

Williams, J., Horsburgh, K., 2006. The operational storm surge model: Maintenance, performance and development, April 2005 – March 2006. POL internal document, No 178, 49pp.

WISE group: Cavaleri, L., Alves, J., Ardhuin, F., Babnin, A., Banner, M., Belibassakis, K., Benoit, M., Donelan, M., Groeneweg, J., Herbers, T., Hwang, P., Janssen, P., Janssen, T., Lavrenov, I., Magne, R., Monbaliu, J., Onorato, M., Polnikov, V., Resio, D., Rogers, W., Sheremet, A., McKee Smith, J., Tolman, H., van Vledder, G., Wolf, J. and Young, I., 2007. Wave modelling- the state of the art. Progress in Oceanography, 75, 603-674.

Wolf, J., 1981. Surge-tide interaction in the North Sea and River Thames. In: D, Peregrine, ed. 1981. Floods due to high winds and tides. New York, Elsevier, pp. 75-94.

Wolf, J., 2008. Coupled wave and surge modelling and implications for coastal flooding. Advances in Geosciences, 17, 19-22.

Wolf, J., 2009. Coastal flooding: impacts of coupled wave-surge-tide models. Natural Hazards, 49, 2, 241-260.

Wolf, J., Hargreaves, J., Flather, R., 2002. Application of the SWAN shallow water wave model to some UK coastal sites. POL Report, No.57, N100.5/c/57, 51pp.

Wolf, J., Flather, R., 2005. Modelling wind and surges during the 1953 storm. Philosophical Transactions of the Royal Society A. 363, 1359-1375.

Wolf, J., Woolf, D.K., 2006. Waves and climate change in the north-east Atlantic. Geophysical Research Letters, 33, L06604, doi: 10.1029/2005GL025113.

Wortley, S., Crompton, E., Orrell, R., Smith, D., Horsburgh, K., Williams, J., 2007. Storm tide forecasting service operational report to the Environmental Agency for the period 1st June 2006 to 31st May 2007. Met Office, UK.

Wu, J., 1980. Wind-stress Coefficicents over sea surface and near neutral conditions- A revisit. Journal of Physical Oceanography, 10, 727-740.

Wu, J., 1982. Wind-stress coefficients over sea surface from breeze to hurricane. Journal of Geophysical Research, 87, 9704-9706.

Wu, J., 1994. The sea surface is aerodynamically rough even under light winds. Boundary Layer Meteorology, 69, 149-158.

Wu, X., Flather, R., Wolf, J., 1994. A third generation wave model of European continental shelf seas with depth and current refraction due to tides and surges and its validation using GEOSAT and buoy measurements. POL Report 33. Available online: http://nora.nerc.ac.uk/3896/. Accessed: 24/08/2012.

Wu, J., Hamada, M., 2002. Experiments: Planning, Analysis and Parameter Design Optimization. John Wiley and Sons, Singapore.

Xie, L., Liu, H., and Peng, M., 2008. The effect of wave-current interactions on the storm surge and inundation in Charleston Harbour during Hurricane Hugo 1989. Ocean Modelling, 20, 252-269

Young, I., 1999. Wind generated ocean waves. Elsevier Science ltd: Oxford .

Zang, Y., Tooley, M., 2003. A historical record of coastal floods in Britain: frequencies and associated storm tracks. Natural Hazards. 29, 13-36.

Zhang, W., Shi, F., Hong, H., Shang, S., Kirby, J., 2010. Tide-surge interaction intensified by the Taiwan Strait. Journal of Geophysical Research, 115, C06012, DOI: 10.1029/2009JC005762.